Université de Toulouse

THÈSE

En vue de l'obtention du

DOCTORAT DE L'UNIVERSITÉ DE TOULOUSE

Délivré par :

Université Toulouse 3 Paul Sabatier (UT3 Paul Sabatier)

Présentée et soutenue par :
PANDEY Rajesh Kumar
le vendredi 29 novembre 2013

Titre :

Etude des Bassins Fluviaux en Inde par Télédétection
(Study of River Basins in India by remote Sensing)

École doctorale et discipline ou spécialité :
ED SDU2E : Hydrologie, Hydrochimie, Sol, Environnement

Unité de recherche :
Laboratoire d'Etudes en Géophysique et Océanographie Spatiales (LEGOS)

Directeur(s) de Thèse :

Dr. CALMANT Stéphane
Dr. CRETAUX Jean-François

Jury :

Prof. CHAUZY Serge, Président du Jury
Prof. SHUM C.K., Rapporteur
Dr. (Mme) SEYLER Frédérique, Rapporteur
Dr. TIWARI Virendra, Examinateur
Dr. CALMANT Stéphane, Directeur de Thèse
Dr. CRETAUX Jean-François, co-Directeur de Thèse

Acknowledgement

I sincerely express my humble gratitude to all the peoples who assisted me and without whom I would not have been able to complete my dissertation work.

First, I would like to acknowledge my supervisors, Dr. Stéphane Calmant and Dr. Jean-François Crétaux for their extensive guidance in order of conducting my work. I extend my sincere thanks to them for their inspiring guidance, constant interest, suggestions, and encouragement throughout the course of work.

I sincerely acknowledge Dr. Virendra Mani Tiwari for providing me the opportunity to take-up this work and his inspiration, encouragement and guidance throughout the course of this work. I am very thankful to Dr. (Mme) Marie-Claude Gennero for her help to learn altimetry and its application. I am very thankful to Dr. Fabrice Papa for his support and suggestions to carry out this thesis work.

I am immensely grateful to the Directors of LEGOS Toulouse, Dr Y. Penhout and Dr Y. Morel, for providing the infrastructure to carry out this dissertation work. I am also grateful to the Directors of NGRI Hyderabad, Dr V. P. Dimari and Dr Mrinal Sen, for providing me the opportunity to conduct the work under Indo-French project.

I am thankful to Indo-French Centre for the Promotion of Advance Research (IFCPAR) and Centre National de la Recherche Scientifique (CNRS) for their financial support to stay in France.

I am thankful to staff of Laboratoire d'Etudes en Géophysique et Océanographie Spatiales (LEGOS) for their help and co-operation without whom it would not be easier to carry out my work comfortably. I am, also,

thankful to Mme Catherine Stasiulis and Mme Marie-Claude Cathala for their help and co-operation.

I owe my deep sense of gratitude to my parents, family, brother and friends for their love, encouragement and affection.

I am thankful to all the peoples who are directly or indirectly helped me during this work.

LEGOS/UPS (UT-III) (Rajesh Kumar Pandey)

Toulouse

Content Table

Acknowledgement ..... i - ii

Content Table ..... iii – vii

List of Figures ..... viii - xii

List of Tables xiii

Introduction (in English) ..... 15 - 17

Introduction (in French) ..... 18 - 20

1. Continental Hydrology and Remote Sensing ..... 21 - 28

Introduction..... 21

1.1. Terrestrial Water 22

1.2. Application of Satellite Based Observations..... 24

1.2.1. Radar Altimetry 24

1.2.1.1. Inland Sea and Lakes 26

1.2.1.2. River and Flood Plains 26

1.2.2. Imagery 27

2. Satellite Remote Sensing 29- 61

Introduction..... 29

2.1. Satellite Altimetry 30

2.1.1. Satellite Altimetry Principle..... 33

2.2. Principle of Radar Altimetry 35

2.2.1. Pulse Reflection 35

2.2.2. Waveform Characteristics..... 36

2.2.2.1. Tracking and Retracking 38

2.2.2.2. Waveform over Continent..... 39

2.2.3. Altimetry Orbit Precision 40

2.3. Corrections Applied in Altimetry Measurements 41

2.3.1. Atmospheric Corrections 43

2.3.1.1. Ionospheric Correction 43
2.3.1.2. Dry Tropospheric Correction 43
2.3.1.3. Wet tropospheric Correction 44
2.3.2. Geophysical Range Corrections..... 45
2.3.2.1. Pole Tide Correction 45
2.3.2.2. Solid Earth Tide Correction..... 45
2.4. Satellite Altimetry Missions 45
2.4.1. TOPEX/POSEIDON (T/P) 45
2.4.2. JASON 1 and JASON 2 46
2.4.3. ERS 1 and ERS 2 47
2.4.4. ENVISAT 47
2.5. Limitations of Altimetry over Land 49
2.5.1. Retracking Algorithm..... 49
2.5.2. Data Sampling..... 50
2.5.2.1. Tracking Windows..... 50
2.5.2.2. Temporal resolution..... 50
2.5.2.3. Reflector Mispointing (Hooking Effect) 51
2.6. Satellite Imagery 52
2.6.1. Spectral Reflectance Signature 52
2.6.2. Characteristics of Image..... 54
2.6.2.1. Picture Elements (Pixels) 55
2.6.2.2. Spatial Resolution 55
2.6.3. Processing of Imagery..... 56
2.7. Gravimetry 56
2.7.1. GRACE Mission 57
2.7.2. GRACE Data and Hydrology 59
2.7.3. Errors in GRACE Solutions..... 60
3. Study Area: River Basins in India 62-77
Introduction..... 62
3.1. Water Resources of India..... 63
3.2. Indian Monsoon 66
3.2.1. Seasonal Rainfall Distribution 66

3.2.2. Rainfall Variation 67
3.3. River System in India 67
3.3.1. Himalayan Rivers 69
3.3.2. Ganga- Brahmaputra Basin 69
3.3.2.1. Ganga Basin 70
3.3.2.2. Hydrology of Ganga Basin 71
3.3.2.3. Kosi Basin 73
3.3.3. Krishna Basin 74
3.3.4. Godavari Basin 76
3.4. Study Region 77
4. Data and Methodology 78–89
Introduction 78
4.1. Altimetry Data 79
4.1.1. Datasets 79
4.1.2. Altimetry Data Processing 80
4.1.3. Altimetry Time Series 81
4.2. Imagery Data 84
4.2.1. Processing of Imagery 85
4.2.2. Land Cover Classification 85
4.3. GRACE Data 87
4.4. Precipitation Data 88
5. Altimetry Derived Water Level 90-115
Introduction 90
5.1. Altimetry Derived Water Stage over Ganga 90
5.1.1. Water Level in Ganga Post Confluence with Yamuna and Ghaghara 93
5.1.2. Longitudinal Profile of Ganga 95
5.2. Water Level in Krishna and Godavari 98
5.2.1. Water Level in Krishna River 98
5.2.2. Water Level in Godavari River 100
5.2.3. Longitudinal Profile of Krishna and Godavari 102
5.3. Altimeter Derived Discharge for Ganga-Brahmaputra River System 104
5.3.1. Datasets to Calculate Water Discharge 104

5.3.2. JASON 2 - derived Water Level over Ganga and Brahmaputra 107
5.3.3. JASON 2-derived Discharge of Ganga and Brahmaputra 108
5.3.3.1. Rating Curve 108
5.3.3.2. JASON 2 – derived Discharge..... 110
5.3.4. Long-term Ganga- Brahmaputra Monthly Discharge Update 112
5.3.4.1. Application of Altimeter-derived Discharge of G+B 114
Conclusion 115
6. Surface Water Analysis..... 116-129
Introduction 116
6.1. Method for Estimating Surface Water Extent 117
6.2. Land Cover Classification in Lower Ganga 117
6.3. Flood in Kosi sub-basin 120
6.4. Kosi Flood in 2008 122
6.4.1. Study Area and Methodology 122
6.4.2. Datasets 122
6.4.2.1. Altimetry Data 122
6.4.2.2. MODIS Data 124
6.4.2.3. SPOT-Vegetation Data..... 126
6.4.2.4. Precipitation Data 127
6.4.3. Surface Water Extension and Water Height Evaluation 127
Conclusion 132
7. GRACE Data Analysis 133-138
Introduction 133
7.1. Spatio-Temporal Evaluation of Total Water Storage (TWS) 134
7.2. TWS variation in Indian Subcontinent 135
7.2.1. Dataset and Methodology 135
7.2.2. TWS variation in Ganga Basin..... 135
7.3. Precipitation Variation in Ganga Basin 139
7.3.1. TRMM Rainfall Data 139
7.3.2. Analysis of TRMM Rainfall Data 139
Conclusion (in English) 142-144

Conclusion (in French)..... 145-147

Appendices 148-160

References 161-184

Abstract (in English) 185

Abstract (in French) 187

List of Figure

Figure 1.1: Worldwide distribution and evolution of river discharge measuring stations (http://www.bafg.de/cln_033/nn_266918/GRDC/EN) 22

Figure1.2:Worldwide operating gauging stations from WMO-GRDC (red, Fekete, 1999) and UNESCO/UNH RivDIS v1.0 dataset (green, Vörösmarty et al, 1996) 23

Figure 1.3: JASON-2 derived water height (red) and in situ river water height (black) variation over Ganga River [Papa et al., 2012] 27

Figure 1.4: Inundated area in lower Ganga basin from MODIS/Terra images .....…. 28

Figure 2.1: Global coverage of T/P and JASON missions (Frappart, 2006) 32

Figure 2.2: Principle of radar altimetry (Credits: CNES) 33

Figure 2.3: Footprint size and echoes of altimetry signal for ideal (left) and distorted (right) reflecting surface (Credits: CNES) 36

Figure 2.4: Individual (left) and averaged (right) signal transmitted to ground from satellite (Radar Altimetry tutorial) 37

Figure 2.5: Geophysical information from radar echoes (credit: AVISO document) ... 37

Figure 2.6: Typical waveform shapes over inland water bodies (Berry et al., 2005) ... 39

Figure 2.7: Development in orbit precision of altimetry missions. (Credit: AVISO) ... 41

Figure 2.8: Geometry of hooking effect [Calmant et al., 2008] 51

Figure 2.9: Ideal spectrum for vegetation, water and dry soil [Lillesand and Kiefer, 1987] 53

Figure 2.10: Schematics of GRACE data acquisition [Tapley and Chris, 2003] 58

Figure 2.11: Schematic view of observation of TWS from GRACE (Cazenave and Chen, 2010] 59

Figure 3.1: Long term average rainfall distribution during June-September in India (IMD-India) 62

Figure 3.2: River basins in India (CWC Report, 2008) 68

Figure 3.3: Line diagram of Ganga and its major tributaries with average annual flow (million cubic meters) [Jain et al, 2007; Status report MOEF, 2009] 71

Figure 3.4: Flow variation in Ganga River at gauging stations [Status report MOEF, 2009] 72
Figure 3.5: Krishna river basin highlighting major reservoirs (Source: IWMI) 75
Figure 4.1: Virtual Station: red rectangle is selection window, red line is flow direction and green line is satellite pass 82
Figure 4.2: JASON 2 derived water level time series with error bars (i.e. Standard deviation in median value) for track 231 over Brahmaputra River 83
Figure 4.3: Flow chart of the Algorithm used for flood mapping from MODIS images and altimetry derived water height over the Region of Interest (ROI) which is the water covered area in this study .....……..... 86
Figure 4.4: Land cover classification as open water (deep blue), island (light blue) with yellow as background representing either dry land or vegetation from MOD09A1 data in lower Ganga Basin 87
Figure 5.1: Location of virtual stations across the Ganga River in India 91
Figure 5.2: Water level variations over Ganga River for ascending tracks of ENVISAT 92
Figure 5.3. The Ganga and the Yamuna conflunce at Allahabad, India (blue dot-point). Blue lines represent ENVISAT tracks.Track 496 intersects both rivers before confluence whereas track 767 passes just after the conflunce 93
Figure 5.4: Altimeter derived water height variation in Ganga and Yamuna for ENVISAT mission. Red and blue lines represent water height variation in Yamuna and Ganga respectively for track 496 before their confluence. Green line presents the water height variation after the confluence for track 767..... 94
Figure 5.5: Water level variation in Ganga and Ghaghara before and after their confluence from ENVISAT. Green and Blue lines present water level for track 234 over Ghaghara and Ganga respectively before their confluence. Red line is water level variation after their confluence for track 782 95
Figure 5.6: Longitudinal profile of high and low water in Ganga River 96
Figure 5.7: Virtual Stations over Krishna and Godavari rivers for ENVISAT mission 98
Figure 5.8: Water level variation in Krishna River from ENVISAT mission 99
Figure 5.9: Water level time series in Godavari River for Envisat mission 101

Figure 5.10: Longitudinal profile of high water (blue line) and low water (red line) of the Krishna and the Godavari River 103
Figure 5.11: Schematic map of region of interest. Locations of the two in-situ gauging stations in Bangladesh: Hardinge (G) and Bahadurabad (B) are displayed with red dots. JASON 2 intersections are presented by yellow dots. The inset map shows the Ganga (yellow) and the Brahmaputra (green) rivers catchments [Papa et al., 2010a] 105
Figure 5.12: Time series of in-situ discharge: (a) discharge of Ganga River at Hardinge station and (b) discharge of Brahmaputra River at Bahadurabad station. Solid lines present in-situ discharge derived from water level whereas dotted lines are direct measured discharge [Papa et al. 2012] 106
Figure 5.13: (a) Comparison of in-situ river level measurements (black line) at Hardinge Bridge with JASON 2 derived river level over Ganga River (red line). (b) Scatter plot of JASON 2 derived river heights versus the in situ river height over the Ganga. The linear correlation coefficient (R) and the number of points (N) are indicated. The solid line shows the linear regression between both variables. (c) and (d) are analogue as (a) and (b) for the Brahmaputra River (Bahadurabad) [Papa et al, 2012] .....……..... 107
Figure 5.14: Rating curve at Hardinge over Ganga and Bahadurabad station over Brahmaputra. (a) and (c) present stage-discharge relationship from in-situ river height and in-situ discharge. (b) and (d) present scatter-plot of in-situ discharge vs. JASON 2 derived water stage [Papa et al., 2012] .....…... 110
Figure 5.15: Comparison of altimeter-derived discharges and in-situ observed discharge. (a). River discharge estimate from JASON 2 using in-situ rating curve (green line) and discharge estimates from altimeter–derived rating curve compared with in-situ discharge observations (red plus, solid line). Blue line represents discharge estimate from ENVISAT [Papa et al., 2010a, 2012] .....……..... 111
Figure 5.16: Altimeter derived monthly discharge time series. Discharge derived from T/P, ERS-2 and ENVISAT (black line) [Papa et al., 2010a] and discharge estimate from JASON 2 (green line) compared with in-situ observed discharge (red line) for Ganga (a), Brahmaputra (b) and combination of the two (c). The blue curve shows

the residual i.e. the difference between altimeter derived and in-situ discharge [Papa et al., 2012] 113
Figure 5.17: Climatology of Ganga-Brahmaputra river system. (a) Altimeter derived monthly discharge (black lines) of Ganga and Brahmaputra with standard deviation shown by vertical bars which shows monthly evolution of interannual variability; blue line present in-situ monthly discharge (1993–2001 and 2008–2010); red line is discharge estimate by Fekete et al. [2000]; the green line is the same as the black line, after applying a scaling factor of 120.5%. (b) Scaled-altimeter-derived discharge (black line) and discharge estimated by Fekete et al. [2000] (red lines), blue line is residual discharge (difference of 19 year mean monthly value from individual months) for altimeter derived results 114
Figure 6.1: Land cover classification in lower Ganga basin from MODIS data 118
Figure 6.2: Land cover classifican: Open Water (dark blue) and island (light blue) with background in yellow color ……..... 119
Figure 6.3: Flood on Kosi in 2008 within red rectangular box: open water (dark blue) and land covered by water (light blue) with yellow background …… 120
Figure 6.4: Flood in Kosi region: upper row is representing the flood in 2007 whereas the lower is same in year 2008. Blue colour is open water and light blue colour is land area covered by water, yellow colour is the background .....…… 121
Figure 6.5: Schematic location map of study region: Area within red rectangle, in inset, is the study area. Blue shaded area approximately represents lower Kosi Basin. District boundary is presented by Black lines; Green lines represent ENVISAT ground tracks whereas red line represents T/P or JASON track. Point T1 and T2 for track 967 and T3 and T4 for track 696 are the crossing point (VS) of ground tracks over Kosi River (thick blue line) where water levels are calculated ...……..... 123
Figure 6.6: Altimetry derived water stage (with ref. to EGM2008) for track number 696 and 967 of ENVISAT. Red points highlight the ENVISAT measurements acquired after the breach of the upper Kosi levee in 2008. ……..... 124
Figure 6.7: Progression and regression of flood water in lower Kosi Basin. Water spillage starts after breach in levee on 20th August. Maximum spillage is around 2900 km^2 on 28 August .....……..... 125

Figure 6.8. Inundation area variation from MODIS obeservations in the lower Kosi basin (a). Water covered area during flood period (b). Monthly variations of inundated area. Red line represents the 2008 flood event. Blue line represents average of inundated surface in past decade, with standard deviation error bars. 126
Figure 6.9: Snow covered area in upper catchment of Kosi basin laying in Himalayan 127
Figure 6.10: Monthly average precipitation in the upper-Kosi Basin in 2008 (green line) compared with average precipitation for 2005-2010 (red line). Comparison shows there are no significant changes in precipitation pattern in 2008 compared to average precipitation in last five years ….....……..... 128
Figure 6.11: Average monthly in-situ precipitations for 2006-2011 in different districts (fully or partly lying in study area) of Bihar. Red dotted and red solid lines represent precipitation in study area (weighted area for partly lying in study region). Average precipitation for study area in 2008 is slightly (~10%) higher than average precipitation during 2006-2011 .....…… 129
Figure 6.12: Daily mean-precipitation in lower Kosi Basin. Daily average precipitation for 2005-2010 (red line) compared with 2008 daily precipitation (green line) ... 130
Figure 6.13: Interpolations of MODIS data along the ENVISAT track 967 during the flood period in 2008. Blue colour represents open water pixel, light blue is pixel covered by mix of water and dry land and yellow is non water pixel 131
Figure 7.1: Interchange of water between continent, ocean and atmosphere [Credit: USGS] 133
Figure 7.2: TWS in Ganga basin. Black line is TWS variation without considering the seasonal signal and red curve after removing the seasonal signal 136
Figure 7.3: Spatial trend of TWS and residual TWS in Ganga basin. ……..... 137
Figure 7.4: Decomposition of residual TWS (1st three modes) in Ganga basin by EOFs 138
Figure 7.5: Spatial trend of rainfall in Ganga basin from TRMM data ……..... 140
Figure 7.6: Mann-Kendall test for significance tendency of TRMM data …….……. 140
Figure 7.7: EOF analysis of TRMM rainfall data in Ganga Basin …….…..... 141

List of Tables

Table 2.1: A taxonomy of remote sensing (WG Rees, 2001) 30

Table 2.2: Satellite altimetry missions since 1978 to till date and future missions (Credit: AVISO) 31

Table 2.3: Microwave bands used for radar altimetry (Credit: AVISO) ……..…… 35

Table 2.4: Operational and research satellites for earth surface study 55

Table 3.1: Yearly total rainfall in India [CWC, 2010] 63

Table 3.2: Water resources of India [Gupta et al., 2004] 64

Table 3.3: Groundwater resource of India [Kumar et al., 2005] in Km^3/year 65

Table 3.4: Basinwise average flow and utilizable water in BCM [CWC website] 65

Table 3.5: Hydrological parameters of Ganga River in India [Report NIH, 1998-99] 73

Table 4.1: Summary of altimetry mission characteristics 79

Table 4.2: Parameters description which are extracted for ENVISAT mission 80

Table 4.3: Parameters description which are extracted for JASON 2 81

Table 5.1: Number of Vitual Stations where water level variations are estimated 90

Table 5.2: Slope of Ganga derived from altimeter observation..... 97

Introduction

The continental water represents only a fraction of water on the Earth (~ 0.025%) but it has a very vital role in life on Earth and in climate dynamics. The continental water is stored in different reservoirs as snow and ice in mountains, ice-sheets and glaciers, surface water in rivers and lakes, subsurface water in form of soil moisture (or root zone water) located in first few meters of surface, underground water, manmade reservoirs and canals and wetlands. The continental water participates in exchange with the atmosphere and oceans through the horizontal and vertical mass flux (evaporation, transpiration, and runoff).

The spatio-temporal distribution of fresh water is not uniform which compels the mankind to colonize at a particular region for their livelihood. Many fold increase of world's population raise the usage of fresh water for agriculture and industrial purpose which highly impacts the climate system. Unfortunately, the continental hydrological cycle is not well known. Many catchments in the world are sparsely gauged and the available measurements in these regions are often uncertain, scarce, intermittent or non-concomitant. This condition jeopardizes the construction of hydrological models that are needed, in short terms, to predict droughts, floods and availability of water and in the long term, the effects of changes in the land cover or change of the climate.

In this context, remote sensing is providing the best alternative for measuring the hydrological parameters for example rainfall, evaporation, radiation, soil moisture to assist study of continental hydrology. At present, the satellite remote sensing observations are successfully applied in the monitoring of flood, drought and land cover classification from imagery, variation of water level estimation in rivers and lakes from radar altimetry and estimation of water stock from space Gravimetry missions. The combined use of hydrological models, in-situ observations and satellite measurements, which have comprehensive geographic coverage and significant temporal repeatability that is necessary for the analysis of groundwater and surface water variations, improve

understanding of hydrological processes at work in large river basins, their influence on climate variability, geodynamics and their socioeconomic implications.

The present thesis discusses the use of various satellite data for analysis of hydrology in Indian River basins. The datasets in use are comprised of satellite altimeter observations from ENVISAT, TOPEX/POSEIDON (T/P) and JASON 2 missions, images from MODIS, gravity measurement from Gravity Recovery And Climate Experiment (GRACE) and precipitation data from satellite and in-situ measurements. This whole manuscript is divided into seven chapters. Chapter 1 presents the basic information about the continental hydrology and the use of remote sensing data in its study. Chapter 2 describes the different remote sensing missions which observations are used in this study. This chapter discusses the general principle and other aspects of measurement of satellite altimetry, imagery and Gravimetry. Chapter 3 discusses about water resources in India. The important river systems and the water conditions, source and utilization, in these river systems is presented in this chapter. Chapter 4 presents the data sets, tools and methodology used in this study.

Chapter 5 and 6 presents the results from different remote sensing datasets for surface water analysis. The results of altimetry data analysis are presented in chapter 5. The water level variations in Indian rivers mainly Ganga, Krishna, Godavari and at few locations of their major tributaries are calculated from the ENVISAT, T/P and JASON 2 missions. The water level variations are produced from these satellite missions at about 150 locations. The altimeter derived water level is used for calculation of discharge of Ganga and Brahmaputra rivers. The chapter 6 presents the results from the analysis TERRA / MODIS images. The MODIS images are used for classification of land cover and mapping of inundations. Inundation mapping along with altimetry data from ENVISAT together is used to calculate the water height and volume in flooded region of Kosi, a sub-basin of Ganga basin,.

Chapter 7 is devoted to the application of space gravity measurements from GRACE mission that has been used to estimate the changes in total water stocks at scale of basin to globe. Local variations of the gravity field reflect redistribution of water bodies in the envelope of the Earth. The variation of total water storage in Ganga river basins is discussed in this chapter.

In a short summary, present thesis work presents the use of the various remote observations for studying the hydrology of Indian River basins, especially in Ganga river basin. The river water level variations are produced from altimeter observations, surface water spillage is estimated from satellite imagery and water volume is estimated by using altimeter and imagery data together over flooded areas. The variations in total water storage from GRACE at basin level are also presented in this study.

Introduction (in French)

L'eau continentale ne représente qu'une fraction de l'eau sur Terre (~ 0,025%), mais elle a un rôle très important dans la vie sur Terre et dans la dynamique du climat. L'eau continentale est stockée dans différents réservoirs tels que la neige et la glace dans les montagnes et les glaciers, l'eau de surface dans les rivières et les lacs, l'humidité du sol (zone racinaire) située dans les premiers mètres sous la surface, les eaux souterraines, les réservoirs artificiels, des canaux artificiels et des zones humides. L'eau continentale participe à des échanges avec l'atmosphère et les océans à travers les flux de masse horizontaux et verticaux (évaporation, transpiration et eaux de ruissellement).

La répartition spatio-temporelle de l'eau douce n'est pas uniforme ce qui contraint l'humanité à coloniser des régions particulières pour sa subsistance. La croissance exponentielle de la population humaine augmente de même que l'utilisation de l'eau douce pour l'agriculture ou l'industrie, ce qui a un fort impact sur le système climatique. Malheureusement, le cycle hydrologique continental n'est pas bien connu. Beaucoup de bassins versants dans le monde sont peu calibrés et les mesures disponibles dans ces régions sont souvent incertaines, rares, intermittentes ou non concomitantes. Cette condition rend difficile la construction de modèles hydrologiques qui sont nécessaires, pour prévoir, à court terme les sécheresses, les inondations et la disponibilité de l'eau, et, à long terme, les effets des changements de couvert végétal ou le changement climatique.

Dans ce contexte, la télédétection offre une bonne alternative pour la mesure des paramètres hydrologiques, tels que les précipitations, l'évaporation, le rayonnement, l'humidité du sol nécessaire à l'étude de l'hydrologie continentale. À l'heure actuelle, les observations de télédétection par satellite sont appliquées avec succès pour la surveillance des inondations, la sécheresse et la classification de la couverture terrestre par imagerie, la variation de l'estimation du niveau d'eau dans les rivières par altimétrie radar et l'estimation du stock d'eau par des missions de gravimétrie spatiale. L'utilisation combinée de modèles hydrologiques d'observations in situ et de mesures satellites, qui ont une couverture géographique complète et une répétitivité temporelle importante

nécessaire pour l'analyse des eaux souterraines et des variations d'eau de surface, offre en outre la possibilité d'améliorer la compréhension des processus hydrologiques à l'oeuvre dans les grands bassins fluviaux, leur influence sur la variabilité du climat, la géodynamique et leurs implications socio-économiques.

La présente thèse traite de l'utilisation de diverses données satellitaires dans l'analyse de l'hydrologie des bassins indiens. Les données utilisées sont constituées de données altimétriques fournies par les missions ENVISAT, TOPEX / POSEIDON (T/P) et JASON 2, des images de l'instrument MODIS du satellite TERRA, la mesure de la gravité par la mission Gravity Recovery And Climate Experiment (GRACE), des données sur les précipitations obtenues par satellites et des mesures in situ. Ce manuscrit est divisé en sept chapitres. Le chapitre 1 présente les informations de base sur l'hydrologie continentale et l'utilisation de données de télédétection dans l'étude. Le chapitre 2 décrit les différentes missions de télédétection dont les observations sont utilisées dans cette étude. Ce chapitre traite du principe général et d'autres aspects des mesures d'altimétrie, de l'imagerie et de la gravimétrie par satellite. Le chapitre 3 traite des ressources en eau en Inde. Les systèmes fluviaux importants, ainsi que les sources et de l'utilisation de l'eau de ces systèmes fluviaux sont présentés dans ce chapitre. Le chapitre 4 présente les ensembles de données, les outils et la méthodologie utilisés dans cette étude.

Les Chapitres 5 et 6 présentent les résultats de différents ensembles de données de télédétection pour l'analyse des eaux de surface. Les résultats de l'analyse des données altimétriques sont présentés dans le chapitre 5. Les variations du niveau d'eau dans les rivières indiennes principalement Ganga, Krishna et Godavari sont calculées à partir des missions ENVISAT, T/P et JASON 2. Les variations de niveau d'eau sur environ 150 intersections des traces des satellites avec les rivières sont obtenues à partir de ces missions. Le niveau d'eau déduit des mesures altimétriques est utilisé pour le calcul du débit du Gange et du Brahmapoutre. Le chapitre 6 présente les résultats de l'analyse des images TERRA / MODIS. Les images MODIS sont utilisées pour la classification de la couverture terrestre et la cartographie des inondations. La cartographie des inondations ainsi que des données altimétriques ENVISAT sont utilisées conjointement, dans le sous - bassin Kosi du bassin du Gange, pour calculer la hauteur, l'étendue et le volume d'eau dans la région inondée.

Le chapitre 7 est consacré à l'application des mesures de gravimétrie spatiale par la mission GRACE qui a été utilisée pour estimer les variations des stocks d'eau à travers le monde. Les variations locales du champ de pesanteur reflètent la redistribution des masses d'eau dans l'enveloppe de la Terre. La variation de la capacité totale de stockage de l'eau dans les grands bassins fluviaux du sous-continent indien est discutée dans ce chapitre.

Dans un bref résumé, le présent travail de thèse présente l'utilisation des différentes observations à distance pour étudier l'hydrologie des bassins versants indiens, en particulier dans le bassin de la rivière Ganga. Les variations du niveau d'eau des rivières sont obtenues à partir des observations altimétriques, l'étendue d'eau de surface est estimée à partir d'images satellite, et le volume d'eau est estimé en utilisant les données d'imagerie et d'altimètre conjointement sur des zones inondées. Les variations des stocks de l'eau au niveau des bassins sont également présentées dans cette étude.

Chapter 1

Continental Hydrology and Remote Sensing

Introduction

The hydrological cycle, an important component of the Earth system, is a continuous process of exchange of water mass between ocean, continent and atmosphere. Its interactions with climate have paramount importance in the context of global warming. The inland water participates in water cycle in exchange with atmosphere and ocean by horizontal (e.g. river flow, runoff) and vertical (e.g. evaporation, transpiration) mass flow. About 1350 million km^3 of water are available in the biosphere. Distribution of water on the Earth's surface is very uneven. Majority of it lies in ocean (97.5%), a very small fraction of it contributes to atmosphere (0.001%) and rest (2.5%), termed as fresh water, lies in continental domain in form of snow, ice, running water and ground water. More than 99% of the available fresh water is confined in rocks, lakes, rivers, root zones, inland seas and in other small water bodies. Easily available water resources for all kind of life are less than 1%. However, these water resources are often scar in vast areas of continental biosphere and subject to climate change that might lead to aridity, deforestation, or high canopy development.

The water plays a central role in all kind of lives available on the earth. The water is required for agriculture, industry and day-to-day activities. These various human activities (and its ambience) are highly depending on surface water and ground water. To fulfil the demand of growing population of the world, the demand of water is increasing continuously. The World consumption of fresh water reached 54% of the total water stock in 1995 and is likely to equate the fresh water resource available by 2025 in North Africa and South Asia when Asia will be using ten times more water than the rest of the world **(**World Resources Institute, http://www.wri.org/wri/wr2000). Also, the climate change has a severe impact on the water resources in many parts of the globe. Therefore, it is necessary to understand the continental hydrology in context of

climate and its impact on variation in river water level, surface water and ground water reserves to have proper management and its sustainable use.

1.1 Terrestrial Water

The continental water system is very complex from storage capacity to morphology at both global and regional scale. Thus the understanding of continental water system, even at basin scale, it requires gathering of many hydrological parameters, for example rainfall, water levels in rivers and lakes and surface runoff, to estimate water resources distribution. Further to study inter-annual variability, it requires a long-time continuous observations of others parameters in terms of anthropogenic influence on hydrological regimes. The monitoring of these parameters at global scale requires a huge hydrological network and high manpower or sophisticated instrumentation to have continuous monitoring for the changes. A huge number of in-situ networks, mostly available at regional scale, have been established for gathering various hydrological parameters (Figure 1.1).

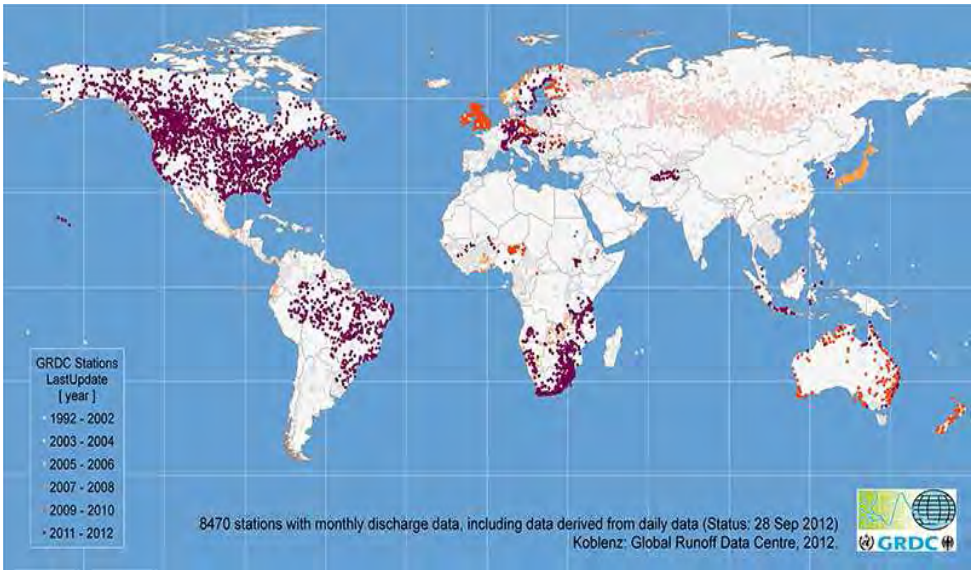

Figure 1.1: Worldwide distribution and evolution of river discharge measuring stations (http://www.bafg.de/cln_033/nn_266918/GRDC/EN).

The installation and maintenance of these networks are very expensive. Therefore, this kind of extensive program is only possible by international cooperation and can sustain in many developing and economically stressed countries. The monitor of terrestrial water using the traditional discharge gauging stations is continuously

decreasing worldwide. The decline in hydro-meteorological monitoring stations [WMO/UNESCO, 1991; Rodda et al., 1993; Vörösmarty et al., 1996; Ad Hoc Work Group on Global Water Datasets, 2001] in last decades is shown in Figure (1.2). Decline is found all over the world, even in well monitored countries like US and Canada [Lanfear and Hirsch, 1999; Shiklomanov et al., 2002]. Therefore it is necessary to develop some alternatives which are consistent and durable to supplement the in-situ data for collecting and distributing the water levels, flow rates and other hydrological parameter in large watersheds with regular updates.

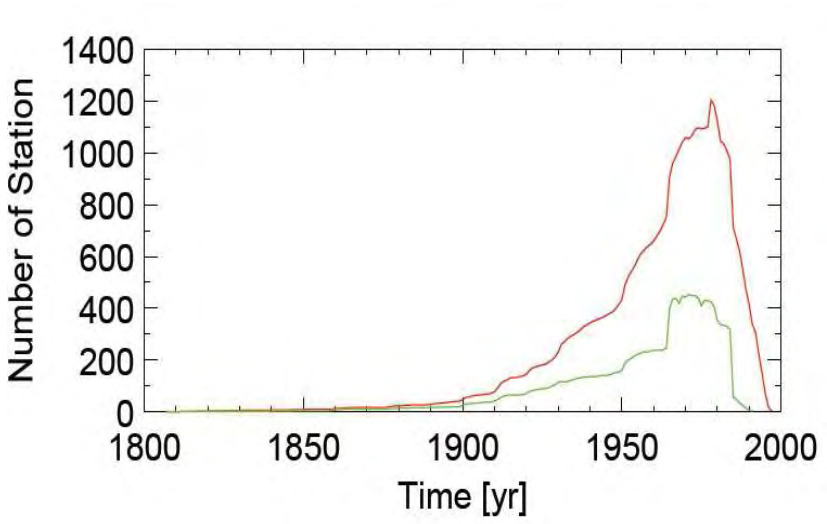

Figure 1.2: Worldwide operating gauging stations from WMO- GRDC(Red line, Fekete, 1999) and UNESCO/UNH RivDIS V1.0 datasets (green line, Vörösmarty et al., 1996).

In this context, Space-borne observations provide an alternative for understanding the hydrological processes and management of surface and ground water. Presently, several domains of hydrological sphere are studied from remote sensing. For example, the delimitation of flood by satellite imagery, tracking changes in water level of rivers and flood zones by radar interferometry and altimetry, estimates of stock of water on continents from space Gravimetry and the measurement of soil moisture using passive microwave. In addition to in-situ observations and hydrological modelling, Satellite remote sensing provides the opportunity to improve the understanding of hydrological processes in large river basins, their influence on climate variability, geodynamics and their socio-economic implications. The combined use of hydrological models, in-situ observations and satellite measurements provide global coverage and repetitive temporal observation to describe the variations of groundwater and surface water.

Alsdorf et al. [2003] pointed that satellite remote sensing with homogeneous and highly temporal repetitiveness can be an alternative for monitoring the inland waters.

1.2 Application of Satellite Based Observations

At present, space-borne observations are very successfully applied for study of various hydrological processes in continental hydrology. Various studies across the different continents have shown ability of remote sensing in monitoring flood events from imagery [Pandey et al., 2014; Frappart et al., 2005; Frazier et al., 2003; Hess et al., 2003], evaluating water level variation in rivers, lakes and flood regions [Abarca-Del-Rio et al., 2012; Birkett, 1998; Calmant et al., 2008; Crtaux et al, 2011b; Crétaux and Birkett, 2006] from radar altimetry. The synthetic aperture radar (SAR) observations are used to map flood zones of large river basins [Hess et al., 1995; Hess et al. 2003; Wang et al., 1995; Saatchi et al., 2000; Siqueira et al., 2003]. The SAR interferometry techniques, which involve heights inferred from measuring the phase coherence of two SAR images measured at different times, have been used for estimation of changes in water level in the flooded forests in the Amazon basin [Alsdorf et al., 2001]. MODIS/Terra images have been successfully used for flood mapping [Pandey et al, 2014; Crétaux et al., 2011a; Toshihiro et al, 2007] and classification of land cover [Zhan et al., 2002].

The space Gravimetry data from Gravity Recovery And Climate Experiment (GRACE) mission is used to study the variation and water storage based on the concept of variation in Earth's gravitational field [Rodell and Famiglietti, 1999; Wahr et al., 1998]. Soil moisture estimation is carried out by using the observations from passive (microwave) remote sensing [Schmugge and Jackson, 1994; Jackson et al, 1989]. Schmugge et al. [2002] has summarized the various application of remote sensing in hydrology.

1.2.1 Radar Altimetry

Radar altimetry onboard various satellites, which were initially developed for study of ocean, have been adopted for the study of continental hydrology. Nowadays, the radar altimetry data is commonly used in the study of continental hydrology particularly because of its dense spatial coverage (Quasi-global) and easy availability. It provide

huge amount of data which are used in monitoring of inland waters, lakes, large rivers, and flood plains. The altimetry data has brought many areas for hydrological study which was previously inaccessible. Various studies in 80's have discussed the potential of satellite Radar Altimeters for estimation of water level data for inland water bodies [Alsdorf et al., 2001; Rapley et al., 1987; Guzkowska et al., 1986; Mason et al., 1985].

Birkett et al. [2002] pointed a discrepancy of RMS (root mean square) average 1.1 m (with 0.4-0.6 m) in height resolution of radar altimetry and in-situ measurements over the Amazon Basin from T/P measurements during 1992-1999. A part of it is attributed by the uncertainties of in-situ records but mostly due to poor modelling of the orbit. Orbit errors are decreasing with the new generations of satellite missions, for example, the uncertainty in the radial component of satellite orbits is now estimated to 15 cm for ERS-1 and 3 cm for T/P [Le Traon et al. 1995] compared to 50 cm for GEOSAT [Koblinsky et al., 1993]. The better orbit precision and advancement in Radar Altimetry retracking algorithms improve the water level estimate with an accuracies of 3- 4 cm RMS over the river and in order of few decimetres over large rivers [Santos da Silva et al., 2010; Frappart et al., 2006a; Crétaux et al., 2005; Birkett et al., 2002; Birkett, 1998]. Therefore, satellite radar altimeter-derived water level variations are precise enough to monitor the water levels of large rivers, lakes, wetlands and floodplains.

At present there are various databases that provide the water stages in major river basins of the world. They are broadly classified in two categories namely River and Lakes Hydrology product (RLH), designed for hydrologist who has no prior knowledge of altimetry, and River Lake Altimetry (RLA) for altimetry experts. HYDROWEB, hosted by LEGOS (Laboratoire d'Etudes en Géophysique et Océanographie Spatiales) Toulouse, France, provides the water stages over major rivers around the world from T/P, JASON 1, ENVISAT, GFO, and JASON 2 missions (http://www.legos.obs-mip.fr/soa/hydrologie/hydroweb/) [Crétaux et al., 2011]. Rivers and Lakes database from ESA (European Space Agency) provides real time data for ENVISAT and JASON 2 missions (http://tethys.eaprs.cse.dmu.ac.uk/RiverLake/shared/main). Another database is maintained by US Department of Agriculture which provide time series over lakes for T/P and JASON suite (http://www.pecad.fas.usda.gov/cropexplorer/global_reservoir/).

The global altimetry dataset has now more than two decade long lifetime and is intended to be continuously updated in the coming decade with current altimetry

missions (JASON 2 and ALTIKA) and proposed future missions (Sentinel-3A and JASON 3 among many others).

1.2.1.1 Inland Sea and Lakes

The condition of altimetry data acquisition over the inland seas and large lakes are similar to ocean surface. Use of radar altimetry in monitoring of inland water bodies was started in late 80s and in early 90s [Koblinsky et al., 1993; Guzkowska et al., 1990; Rémy et al., 1989; Ridley and Partington, 1988; Rapley et al., 1987]. The application fields of satellite altimetry were quickly extended in study of polar ice caps [Legrésy and Rémy, 1997; Legrésy et al., 2005] and other continental water bodies such as lakes, major rivers and flood plain [Zhang et al., 2011; Lee et al. 2011; Crétaux and Birkett, 2006; Koblinsky et al., 1993].

The first use of altimetry data was carried out on the Great Lakes of North America using Geosat observation [Morris and Gill, 1994a, 1994b] and T/P [Morris and Gill, 1994a; Birkett, 1995], where conditions were similar to observations in the ocean. Thereafter this technique is successfully used in the study of inland seas [Crétaux et al. 2005; Aladin et al., 2005; Cazenave et al., 1997], lakes [Abarca et al., 2012; Kouraev et al. 2011; Kuoa and Kaoa, 2011; Birkett, 2000; Birkett, 1998; Birkett et al., 1995]. Numerous studies showed that the altimetry data have been accurate enough to monitor the large inland water bodies with accuracy of few centimetres. The bibliography of study over rivers and flood plains using remote sensing is presented in section (1.2.1.2).

1.2.1.2 Rivers and Flood Plains

The application of satellite altimetry methods for the study of large river basins were initiated by Birkett [1998, 1995] in the Amazon basin which opened the new prospect for continental hydrology. Soon, this technique was adopted for extensive study of major rivers of the world [Kosuth et al., 2006; Maheu and Cazenave, 2003; Campos De Oliveira et al., 2001; Mercier, 2001]. The satellite altimetry provides access to changes in water level of the rivers, on the flood zones and many other areas which were inaccessible earlier by conventional in-situ measurements. Among the various applications of altimetry, most commonly it is used for large scale monitoring of continental water cycle, analysis of hydraulic phenomenon (e.g. calculating the slopes,

flood propagation, etc…), water stage monitoring [Calmant and Seyler, 2006] and support for hydrodynamic modelling. Figure (1.3) shows the comparison of in-situ water level variations at Hardinge bridge over the Ganga river and the water level variation derived from JASON 2 for a period of 2008-2012 [Papa et al., 2012; 2010a]. A standard error of 14 cm is reported in this study which is more or less similar to the errors for other major rivers in the world.

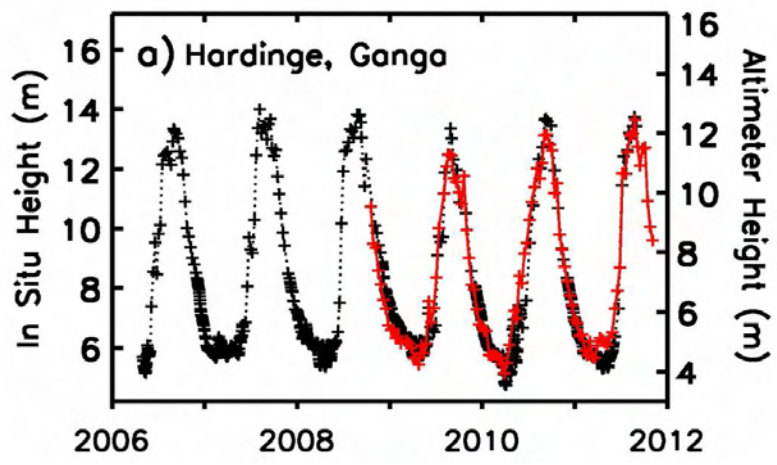

Fig 1.3: JASON 2 derived water height (red) and in situ river water height (black) variation over Ganga River [Papa et al., 2012].

1.2.2 Imagery

Numerous studies have been carried out for surface water extent mapping from remote sensing observations. Surface water extent can be measured with variety of visible band sensors, onboard Landsat, MODIS (Moderate-Resolution Imaging Spectroradiometer) or SPOT (Satellite Pour l'Observation de la Terre) with different repeat frequencies and by Synthetic Aperture Radar (SAR) imagery (e.g. RADARSAT, JERS-1 and ERS) [Papa et al., 2006; Mertes, 2002; Prigent et al., 2001; Smith, 1997]. A combination of RADARSAT and SPOT images were used to study the extent of water in wetlands and produced time series of flooded regions in the Peace-Athabasca delta in Canada with high spatial resolution [Töyrä et al., 2005; 2001]. Frappart et al. [2006a, 2005] have combined radar altimetry with SAR images onboard the Japanese Earth Resources Satellites (JERS-1) or visible images of the Vegetation instrument onboard the SPOT satellites in order to study floods over the Rio Negro (Amazon) and Mekong basins. The ASAR observations have been used to detect flooded areas [Henry et al.,

2006] and fresh water ecosystem in Siberia [Bartsch et al., 2008] for cloud cover regions with high spatial resolution.

Multi-spectral imagery from MODIS have been used to monitor the extent and water level of flood region [Pandey et al, 2014; Abarca-Del-Rio et al, 2012; Crétaux et al., 2011a; Sakamoto et al., 2007; Peng et al, 2005]. From MODIS images, weekly time series of inundation (Figure 1.4) have been produced in different river basins. The SAR Interferometry [Alsdorf et al, 2007; Alsdorf and Lettenmaier, 2003] and passive and active microwave observations [Prigent et al., 2001] also offer important information on land surface waters, such as changing area extent of large wetlands. A common problem in remote sensing of wetland inundation is the detection of water under aquatic vegetation. Leblanc et al. [2011] used Meteosat thermal images to derive monthly flood maps of Lake Chad that has captured the water under aquatic vegetation and adequately reconstructed the drying of Lake Chad since the 1980's.

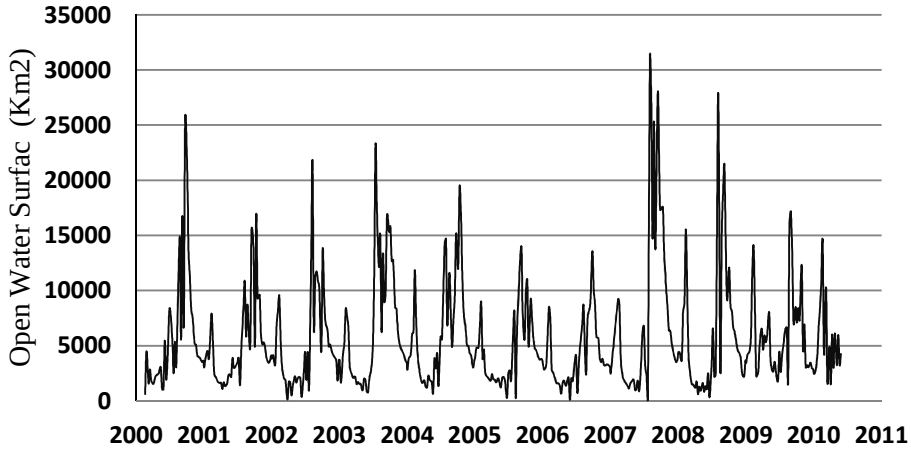

Figure 1.4: Inundated area in lower Ganga basin from MODIS/Terra images.

Chapter 2

Satellite Remote Sensing

Introduction

Remote sensing is the process of acquiring information about the Earth's surface from measurements of either the reflected or emitted electromagnetic radiations from surface. Emitted radiations fall in both thermal infrared (TIR) and microwave range of spectrum bands whereas the reflected radiations fall across the various spectrum bands. The measurements are carried out in both active and passive mode within different spectrum range. Remote sensing systems which measure naturally available energy are called passive sensors. Sun is the major source for passive sensors. Active sensors use their own source of energy. These sensors emit radiations which are directed towards target in investigation. Remote sensors collect and record energy reflected or emitted from target or the sensors, can be onboard a balloon, an aircraft within the Earth's atmosphere, on a spacecraft or (artificial) satellite outside the Earth's atmosphere. Table (2.1) summarises the development in remote sensing for various spectrum bands [Çizmeli and San, 2008; WG Rees, 2001].

Remote sensing is applied for a wide range of applications broadly categorized as 'environmental'. In the atmosphere, it measures temperature, precipitation, distribution and type of clouds, wind velocities and concentration of various gases (e.g. water vapour, CO_2, O_3). Over the land surface, tectonic motions, topography, temperature, albedo (reflectance) and soil moisture are measured. These observations are utilized to identify the land cover and other hydrological studies. Over ocean surfaces, we measure temperature, wind speed, topography and colour (often related to study of plankton). They are used for studying the distribution or dynamic behaviour of snow, sea ice, icebergs, glaciers and ice sheets.

Table 2.1: A taxonomy of remote sensing [WG Rees, 2001]

	Passive systems			Active Systems	
	Reflected Sunlight	Thermal Emission			
		Infrared	Microwave	Visible / IR	Microwave
Non-Imaging		Thermal Infrared Radiometry	Passive microwave radiometry	Laser profiling	Radar Altimetry Microwave Scatterometer
Imaging	Aerial photography Visible/IR imaging	Thermal Infrared Imaging			Real Aperture Radar Synthetic Aperture Radar
Sounding	UV backscatter sounding	Thermal Infrared Sounding	Passive microwave sounding	LIDAR	

Today, satellite remote sensing is commonly used to study various aspects of the Earth's surface. Satellite missions, based on their capability and objectives, can be geostationary or near polar-orbit (sun-synchronous). Geostationary satellites, placed approximately at an altitude of 36000 kilometres, revolve with same speed as of Earth's rotation and hence they seem stationary. The sensors onboard these satellites provide the information over a specific area. Weather and communication satellites are the classic examples of geostationary satellites. The low altitude satellites in conjunction with the Earth's surface are near polar satellites. The orbit of these satellites passes close to poles and covers almost entire Earth's surface. A sun-synchronous satellite is a near polar satellite. Altitude and inclination for this kind of satellites are combined in such a way that they pass every location at same local mean solar time.

2.1 Satellite Altimetry

In last few decades, Radar Altimetry has a strong presence in study of sea level variation and other applications in oceanography over time and space domain. Radar altimetry journey begins with altimeter onboard satellite Skylab (1973) with measurements of undulations in marine geoid. This study had highlighted the importance of satellite altimetry in geodetic study. Seasat, launched by NASA in June

1978, was designed for oceanographic studies and had onboard the first space-borne synthetic radar aperture (SAR) along with other instrument such as altimeter, laser reflector, a transit beacon and scatterometer. Seasat observations were used to map oceanic geoid. Geosat was launched in March 1985 (mission ended in January 1990) by the U.S. Navy with primary objective as measuring marine geoid. It also provided measurements of sea state and winds. Since then a number of dedicated altimetry satellite missions (T/P, ERS 1/2, GFO, ENVISAT, JASON 1/2, Cryosat-2, HY-2A and recently launched Altika/SARAL) have been launched by various space agencies such as NASA, CNES, ESA, NSAOS (China's National Satellite Ocean Application Service) and ISRO (Indian Space Research Organization) for tracking the oceanic and non-oceanic surfaces and successfully applied in studies of these surfaces. T/P and JASON series has the highest repeatability period of 10 days among the various altimetry missions till date. A summary of measurement and orbit precision of the individual missions from past, present and likely future satellite missions are given in Table (2.2).

Table 2.2: Satellite altimetry missions since 1978 to till date and future missions (Credit: AVISO)

Satellite Missions	**Operation Period**	**Repeat Period**	**Measurement Precision (cm)**	**Orbit Precision (cm)**
Seasat	July, 1978 – October, 1978	17	5	~100
Geosat	March, 1985 – January, 1990	17	4	30-50
ERS-1*	July, 1991 – May, 1996	3, 35, 168	3	8-15
T/P	October, 1992 – January, 2006	10	2	2-3
ERS-2	April, 1995 – July, 2011	35	3	7-8
GFO	February, 1998 – November, 2008	17		
JASON 1	December, 2001 – October, 2007	10	2	5
ENVISAT	March, 2002 – May, 2012	35	3	5
JASON 2	June, 2008 – present	10	2	5
Cryosat-2	April l, 2010 – present	369	2	5
HY-2A	August, 2011 - present	14, 168		
Altika/SARAL	February, 2013 -present	35	2	5
Sentinel-3	Launch in 2014	27		
JASON 3	Launch in 2014	10		
JASON-CS	Launch in 2017	10		

* A 3-day period for calibration and sea ice observation (12/28/1991 to 03/30/1992 and 12/24/1993 to 04/10/1994), a 168-day period for geodetic applications (04/10/1994 to 09/28/1994 and 09/28/1994 to 03/21/1995) and a 35-day period for multi-disciplinary ocean observations.

Several studies have explored the use of satellite altimetry in study of continental hydrology to evaluate water level variations of rivers, change in water volume in lakes and large scale river basins. Various studies under the different projects like 'River and Lakes', 'CASH' or 'Hydroweb' had been taken up across the globe to evaluate inland water bodies form altimetry observations from different missions. These studies show that altimetry can be widely used for various hydrological studies within an acceptable range of uncertainties. Further development of methodology and algorithm can improve the measurement accuracy over the water bodies from altimetry. A dense and homogeneous coverage of Earth's surface from the altimetry missions (Figure 2.1) allows the investigation of hydrological systems globally.

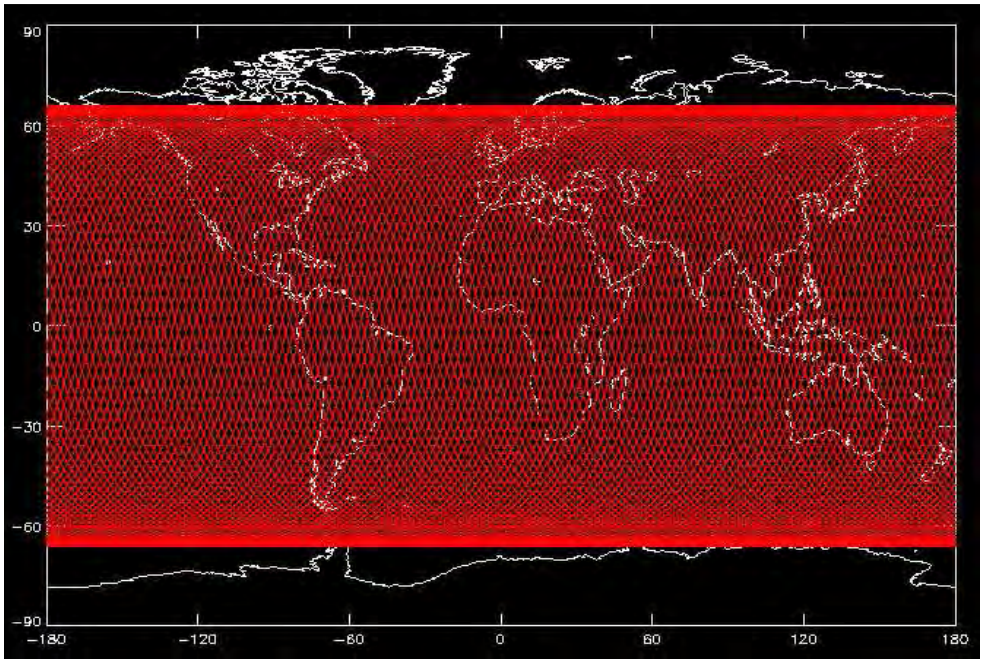

Figure 2.1: Global coverage of T/P and JASON missions (Frappart, 2006).

Satellite altimetry was initially designed to measure the sea surface height, ocean circulation and sea level variations but it has been used to monitor water stage variations over lakes, rivers and flood plains [Cretraux and Birkett, 2006; Calmant and Seyler, 2006; Birkett et al., 2002; Birkett, 1998]. The altimeters onboard ERS-1, ERS-2, ENVISAT and more recently Altika/SARAL missions are engineered to collect data from varying topographic surfaces in addition with their primary mission of open ocean measurements. These observations allowed extraction of long time series over inland water bodies. T/P and JASON 2 have also retrieved data over inland water. The inclusion of JASON 2 near Real Time capability allows generation of data every 10

days over applicable targets. Recently launched Altika/SARAL mission extends the monitoring of inland water bodies. Future missions like Sentinel-3 and JASON 3 will further improve and extend the measurements.

2.1.1 Satellite Altimetry Principle

Satellite altimeters basically evaluate the distance from the satellite to a target surface by measuring the satellite-to-surface round-trip travel time of electromagnetic pulses emitted from altimeters. Surface height or water level variations on water bodies is difference between satellite's positions in orbit with respect to an arbitrary reference surface i.e. reference ellipsoid. The general principle of Radar Altimetry is shown in Figure (2.2).

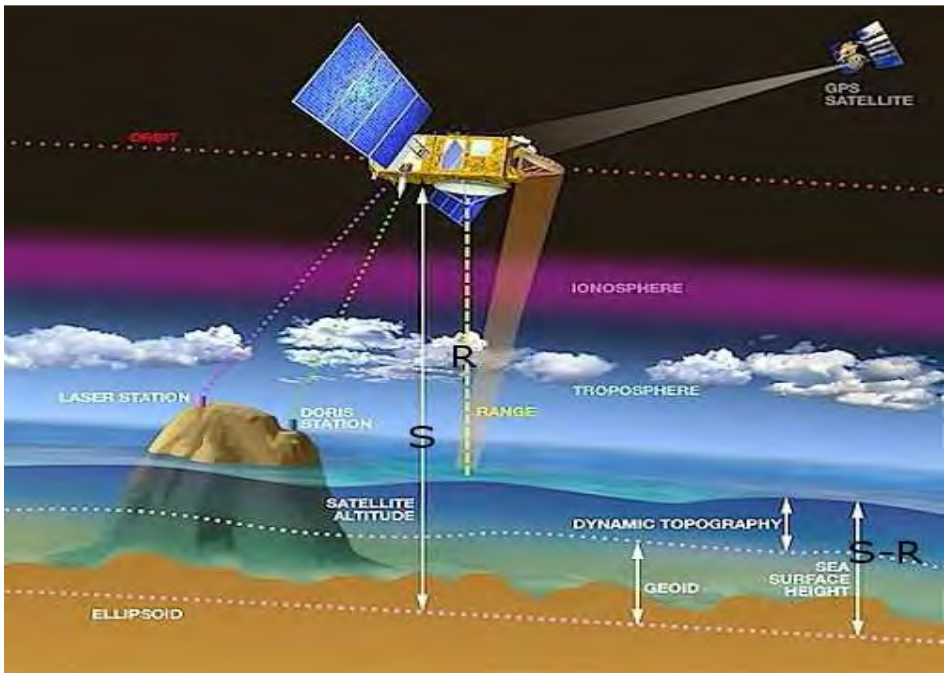

Figure2.2: Principle of radar altimetry (Credits: CNES)

The radar altimeter measures the two-way transit time of reflected pulse from the Earth's surface back to the instruments. One way distance from satellite-to-surface travelled by electromagnetic pulses is called 'Range'. The range is proportional to the transit time of electromagnetic pulse. Assuming that the radar pulse travels with speed of light (c), the (uncorrected) altimeter range (R) can be estimated from the transit time (t). The relation is presented by equation (2.1).

$$R = \frac{ct}{2} \qquad \text{Eq. (2.1)}$$

This formulation is based on free propagation of radar pulses but radar pulses face obstacle by ions, dry gases, water vapour and other particles present in atmosphere. These obstacles correspond to a false estimate of satellite-to-surface distance obtained from equation (2.1). A number of corrections are applied to determine the precise range which is discussed in section (2.3).

Satellite orbit trajectory determination is another important aspect in precise determination of sea surface height or water level variation over inland water bodies. There is various ways to accurately track the satellite orbit. The satellite altitude (S) with respect to reference ellipsoid is calculated with accuracy of 2-3 cm using the satellite's orbital parameters and precise positioning instruments. These two measurements, range estimated by equation (2.1) and satellite altitude, are together used to derive sea-surface height (SSH) with respect to reference ellipsoid. The sea level variation is simply the difference between the satellite altitude and the altimetry range.

$$SSH = S - R \qquad \text{Eq. (2.2)}$$

The investigations over continental hydrology follow the same principle and water level variations over water inland bodies are calculated using the equation (2.1) and equation (2.2). Considering various corrections, see section (2.3), arises due to obstacle in propagation, imperfection in instrumentation and due to geophysical effect, equation (2.2) along with correction terms over the continental water bodies can be written as:

$$H = S - R + C_{ion} + C_{dry} + C_{wet} + C_S + C_p \qquad \text{Eq. (2.3)}$$

Where C_{ion} is ionospheric correction, C_{dry} is dry tropospheric correction, C_{wet} is wet tropospheric correction. These corrections are necessary to reduce the delay in propagation time due to obstacles in ionosphere and atmosphere. C_s and C_p are the corrections applied for adjusting the effect of shape and rotation of Earth.

2.2 Principle of Radar Altimetry

Radar altimetry (RA) measures transit time and backscatter power of individual transmitted pulses. The frequencies used for radar altimetry measurement spreads in microwave range (Table 2.3). Single band or combinations of bands are used for altimeter measurement in a proposed mission. For example, RA-2 onboard ENVISAT mission is operating at main nominal frequency of 13.575 GHz (Ku band) and secondary frequency of 3.2 GHz (S band). S-band provides the range delay due to ionosphere. RA-2 operates autonomously in three different resolution modes to provide better coverage in difficult terrains. The magnitude and shape of the returned echo provide the characteristics of the reflecting surface.

Table2.3: Microwave bands used for radar altimetry (credit: AVISO)

Band	Frequencies (GHz)	Wavelengths (cm)
P	0.3-1	30 - 100
L	1 – 2	15 - 30
S	2 – 4	7.5 - 15
C	4 – 8	3.75 - 7.5
X	8 – 12	2.4 - 3.75
Ku	12 – 18	1.67 - 2.4
K	18 - 26.5	1.1 - 2.4
Ka	26.5 – 40	0.75 - 1.1

2.2.1 Pulse Reflection

Microwave pulses, emitted from instrument onboard satellite are sent at regular intervals defined by Pulse Repetition Frequency (PFR) towards nadir of satellite to surface of the Earth with a very high frequency), for example 1795 Hz for ENVISAT. After reflection from the surface illuminated, a portion of the signal is returned to the satellite. The magnitude and shape of the echoes (waveform) contains the information about the characteristics of target surface which caused the reflection. The duration of time elapsed from transmission of pulse to the reception of its echo measure the altitude of satellite. The interaction of wave pulses with water surface and distorted surface (e.g. land surface) and its corresponding returned echoes are shown in Figure (2.3).

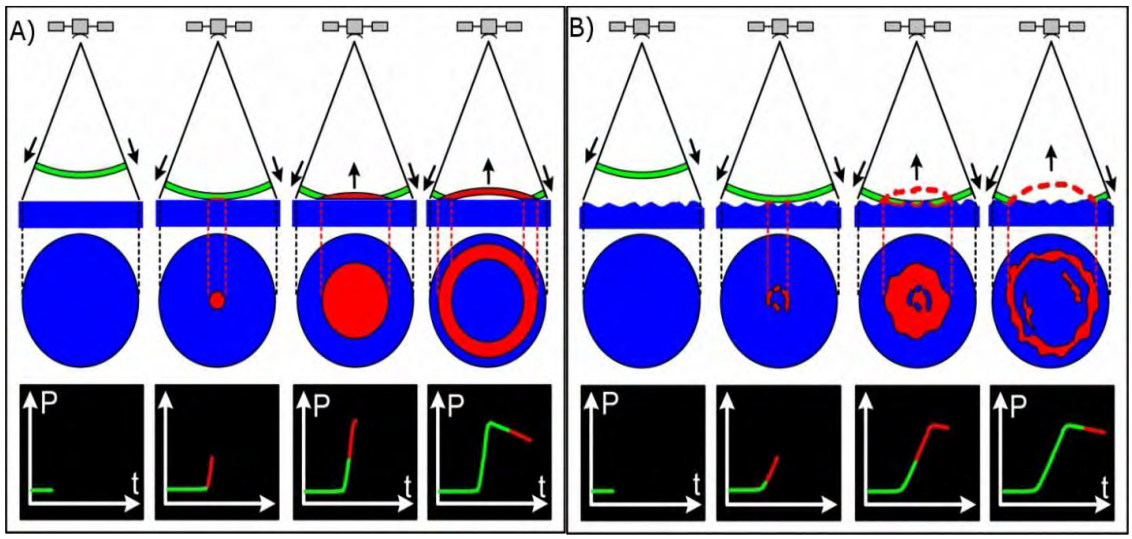

Figure 2.3: Footprint size and echoes of altimetry signal for ideal (left) and distorted (right) reflecting surface. (Credits: CNES)

The area illuminated by the wave is represented by the intersection of the surface and the spherical shell passing sequentially from one point to a disc. The illuminated area reaches its maximum size in form of a disk, known as ‘pulse limited footprint’. Then it becomes a ring of constant area and its diameter keeps increasing until it reaches the limits of beam known as ‘limited beam footprint’ according to characteristics of instrument. This representation of the received power by the altimeter as function of time is called ‘waveform’. Returned waveform (power signal) depends upon: (a) Surface (target surface) scattering character (b) two-way atmospheric attenuation and (c) radar system parameters.

The left side in Figure (2.3) presents reception of waveform for ideal case where the surface is flat and horizontal. In practice, the observed surfaces are more or less away from the ideal case where the amplitude of reflected wave increases more gradually. From this reflected wave ocean wave height can be derived as the slope of the curve representing its amplitude over time is proportional to the wave height.

2.2.2 Waveform Characteristics

The received individual waveforms from each footprint interaction are noisy and they are averaged (typically 50 ms) on board to reduce the statistical fluctuations and to perform time tracking. Treatment of these received waveforms, which is performed on board the satellite or some times on the ground, using sophisticated algorithms to

extract the geographical information such as satellite altitude and land use classification among many others. To increase the signal-to-noise ratio, the individual echoes are averaged by 50 (ERS 1/2) or by 90 (T/P and JASON 1) to make elementary waveforms and then they are transmitted to ground (Figure 2.4).

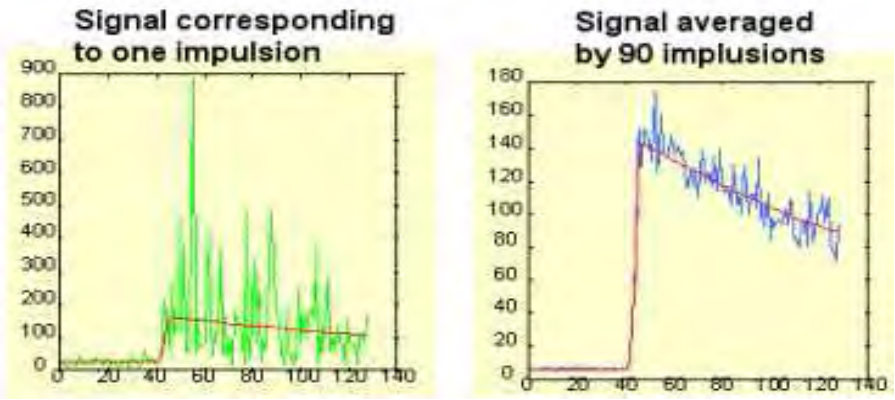

Figure 2.4: Individual (left) and averaged (right) signal transmitted to ground from satellite (Radar Altimetry tutorial)

The most common use of altimeter measurements is the calculation of sea surface height and water level variations over inland sea, flood region, river and lakes. There are several other information which can be derived from treatment of altimeter signals (Figure 2.5). The treatment of the echoes, based on the theoretical waveform given by Brown model (Brown, 1977), extracts a number of information about the target surface.

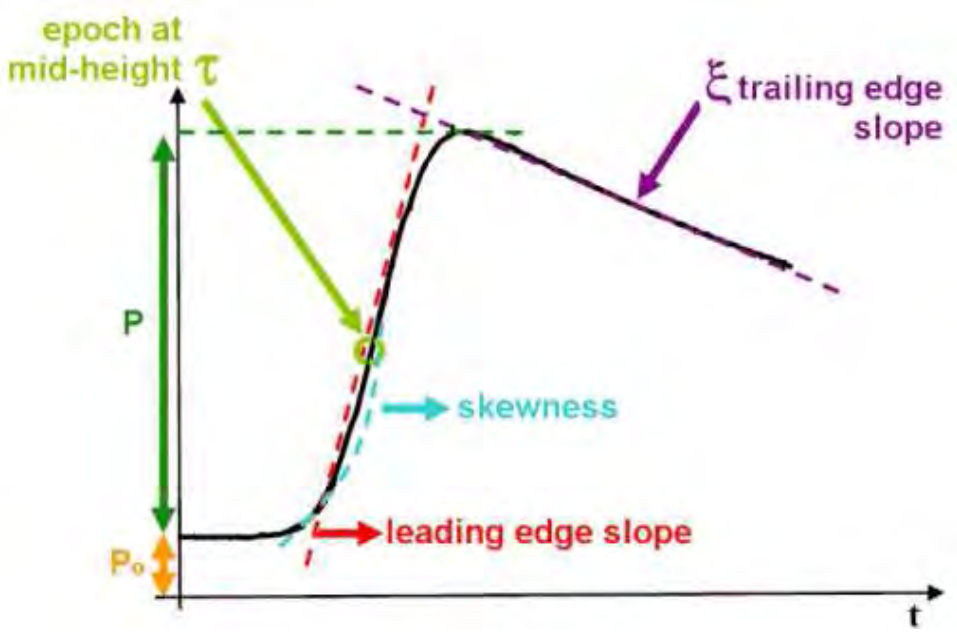

Figure 2.5: Geophysical information from radar echoes (credit: AVISO document)

- **Range:** The midpoint of epoch of waveform determines the time delay for returned signal. The time delay is the time which radar pulse took to propagate to the satellite-surface distance (i.e. range).
- **Backscatter Coefficient (σ_0):** The power amplitude (P) with respect to the emission power amplitude is the total energy received by altimeter. The backscatter coefficient describes the characteristics of reflecting surface. The coefficient varies with the nature of reflecting surface. It is low for mountain regions and high for the flat surfaces. For ideal reflecting surface (Figure 2.3A), σ_0 is about 40 dB which is often recorded over oceanic surfaces. Mercier [2001] has suggested that the σ_0 value over continent should be considered within the range of 12-50 dB because of the great terrain diversity in time and space.
- **Leading and trailing edge:** The leading slopes are related to significant wave height whereas the trailing edge tells about the deviation of nadir point for antenna.

2.2.2.1Tracking and Retracking

It is necessary to keep the leading edge of returned signal within processing windows under varying surface condition and range from altimetry at nadir to extract information from the waveforms. This treatment is known as onboard tracking. These waveform sample are telemetered to ground receiving stations where they are reprocessed using the algorithms to extract the more precise information such as range, backscatter coefficient, significant wave height along with off-nadir antenna pointing angle and skewness of the surface height distribution. This operation is called 'reprocessing or retracking'. At present, four retracking algorithms named as *Ice-1, Ice-2, Ocean* and *Sea-Ice* are used for reprocessing of waveforms depending on the surface type.

- Ice-1 was developed to study Polar ice caps and in more general continental surface. This algorithm is based on estimating waveform-amplitude which reduces signal-to-noise ratio with increase in number of sampling points and is insensitive to changes in wave shape [Wingham et al., 1986]. This method is known as *Thresh-holding Methods*.

- Main objective behind the development of Ice-2 algorithm [Legrésy and Rémy, 1997] was to study Polar ice caps of Antarctica and Greenland. Development of this algorithm was based on objective to match shape of measured wave with theoretical radar wave models defined by Brown [Brown, 1977].
- Sea-Ice algorithm [Laxon, 1994] is used to study the waveforms form sea-ice. This algorithm is similar to Ice-1 algorithm.
- Ocean retracking algorithm is widely used to study of ocean surfaces [Brown, 1977].

Frappart et al. [2006a] have presented the different types of algorithms available for retracking operations and developed for study of inland water bodies in detail. These algorithms are used in the chain reprocessing of ENVISAT and JASON 2 altimeters. Other algorithm adopted for waveforms having two peaks [Brenner et al., 1997] is less frequently used due to the complexity of its implementation.

2.2.2.2 Waveforms over Continent

Over ocean the waveform consists of three main parts: the leading edge, the max peak, and the trailing edge (figure 2.5). Over ocean, most returned waveforms are Quasi-Brown waveforms with a sharp and stable narrow peak (Figure 2.6a).

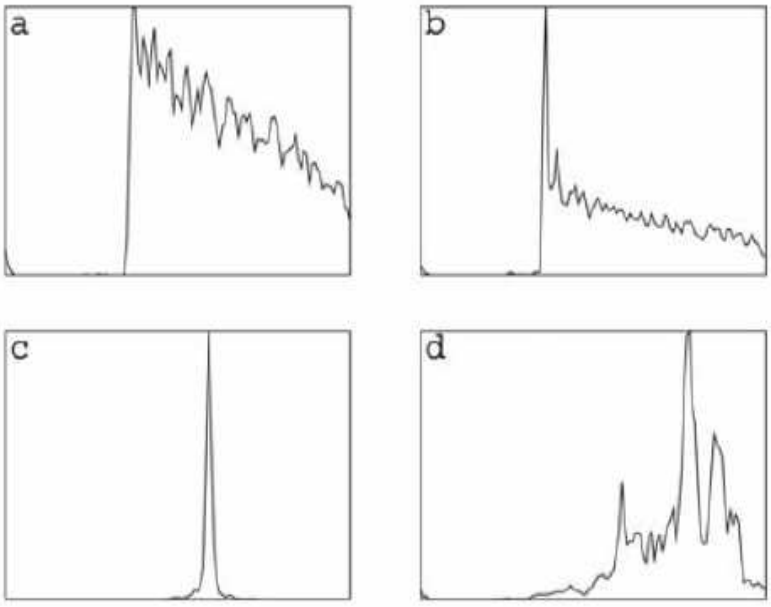

Figure 2.6: Typical waveform shapes over inland water bodies (Berry et al., 2005).

Over inland water bodies, the waveforms are more complex and related to slope and roughness within footprint and consequently the waveforms shape change with different inland water surfaces. These waveforms are classified in four categories [Guzkowska et al., 1990; 1986]: *Quasi-Brown model* (Figure 2.6a)), *broad peak* (Figure 2.6b), *Quasi-Specular* (Figure 2.6c) and *multiple peak* (Figure 2.6d) waveforms. Figure 2.6 shows the four typical kinds of waveforms from ENVISAT over various inland water surface [Berry et al., 2005].

- Quasi-Brown mode waveforms are characterized by leading edge with wide plateau descending slowly. These kinds of waveform are produced over the large lakes, Wide River or flood plains.
- Quasi-specular waveforms have the sharp vertical leading edge with rapid decrease of trailing edge. This kind of waveforms is produced at narrow rivers.
- Broad peak waveforms are characterized with slow descending trailing edge compared to quasi specular waveforms. This kind of waveform is formed by the water bodies surrounded by low reflecting surfaces.
- Double/multiple peak waveforms are found over the close river channels. Each peak corresponds to the reflection from respective river channel.

2.2.3 Altimetry Orbit Precision

Geo-location, along with precise location of centre of mass of spacecraft and its velocity in 3D within a well-defined ITRF with accuracy of few cm RMS, of satellite orbit is one of the most important aspects for the space derived height estimation. For radar altimetry at nadir, precise knowledge of orbit of altimeters is essential. The uncertainty in vertical positioning of altimeter introduces errors in altimeter measurements. The orbit path estimation is subject to consideration of various factors such as instruments specification coupled with satellite, motion of satellite in gravitational field, atmospheric pressure drag, solar radiation and effect of attraction because of the moon and sun among the various others.

The progressive improvements in knowledge of gravitational field and other perturbation have subsequently improved the accuracy in satellite orbit estimation. At present, various positioning systems such as GPS, satellite laser ranging and DORIS are

used for altimetry missions, which are highly accurate within a few centimetres (Table 2.2). The Figure (2.7) shows the development of orbit accuracy for various past and present altimeter missions.

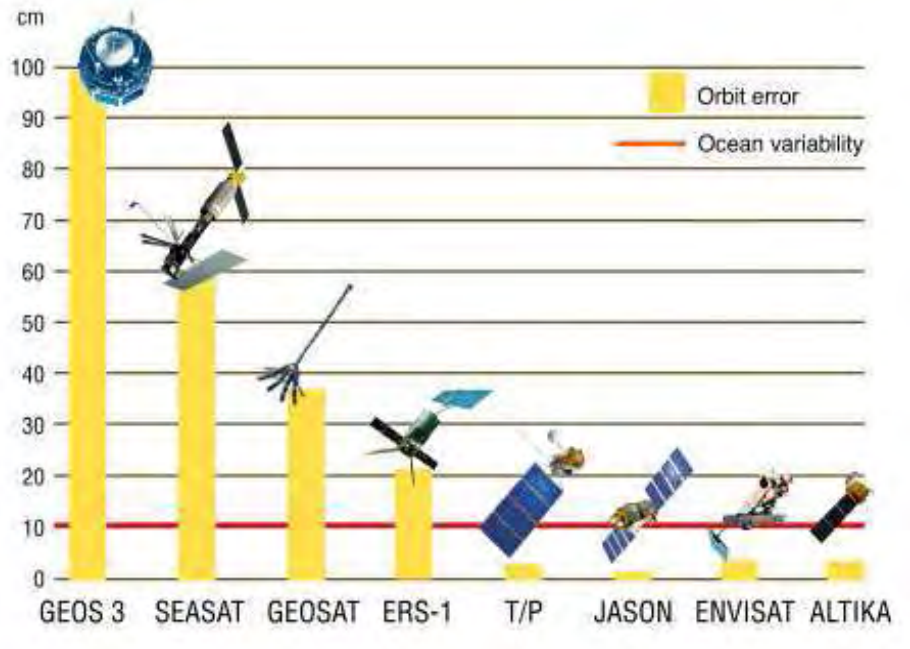

Figure 2.7: Development in orbit precision for altimetry missions (Credit: AVISO)

The DORIS (Doppler Orbitography and Radio-positioning Integrated by Satellite) beacon/satellite receiver system, satellite laser ranging, and/or GPS (global positioning system) are used for high precision in orbit determination for modern altimetry missions. The accuracy of orbit determination is in order of 2-3 cm for T/P and about 5 cm for JASON 1/2. The orbit accuracy for ERS and ENVISAT mission is less than 5 cm (Table 2.2).

2.3 Corrections Applied in Altimetry Measurements

During propagation, radar signals pass through a medium that is not empty and subsequently speed of signals are checked by electrons present in upper atmosphere, dry gases, water vapour and liquid water in lower atmosphere. These obstacles in path of propagation slowdown the velocity of the electromagnetic pulses emitted from the antenna onboard radar altimetry and returned after reflection. These phenomena may lead to an overestimation of the range, using equation (2.1), of about 2.5 m (Mercier, 2001). Further, the estimated range is subject to scrutiny of the effect of Solid Earth

tides, ocean tides and pole tides which arise due to deformation of the solid Earth, effect of the attraction of the Moon and Sun. These tides effect must be nullified for accurate static height determination over water bodies. Therefore, to obtain the precision in measurement it is necessary to identify, estimate and remove them. Some of corrections (i.e. Doppler correction, time delay flight correction and time delay ground correction) are considered directly by specific instruments installed on board the satellites whereas the other corrections are applied by using climate models and other observations.

Sensor Data Records (SDRs) are followed by the corrective treatments at the reception and evaluation of data by ground receiving stations in order to transform the data into Level 1 and Level 2 data, called Interim Geophysical Data Records (IGDRs), expressed in appropriate units with controls of data quality. Level 2 data is subject to scrutiny of instrumental errors and others raised during the course of propagation through the atmosphere and relative position to reference ellipsoid. These various corrections applied on SDR to Level 2. The various corrections during the analysis of altimeter observations are summarized as below.

- **Instrumental Range Correction** = Doppler correction + Time Delay Flight Correction + Time Delay Ground Correction
- **Atmospheric Corrections** = Ionospheric + Wet Tropospheric + Dry Tropospheric
- **Geophysical Range Corrections** = Inverse Barometer + Sea State Bias + Ocean Tide + Polar Tide + Earth Tide

The instrumental corrections are applied because of the imperfection in the instruments. These corrections are already incorporated and they are not provided to the user community. These corrections are based on Doppler correction, time delay flight calibration and time delay ground calibration. The various instrumental corrections and geophysical corrections have been discussed in details by Chelton et al. [1989] and can be found in the handbook of Satellite Altimetry and Remote sciences [ed. by Fu and Cazenave, 2001]. Brief introduction of some geophysical corrections applied in analysis in continental water bodies are discussed in this section.

2.3.1 Atmospheric Corrections

The atmospheric corrections are required to mitigate the delay in transit time introduced by the interaction of radar waves with atmospheric layers. The presence of water vapour, dry gases and free electrons in the atmosphere reduces the propagation speed of radar waves and subsequently leads to overestimate of range from equation (2.1). The estimation of the delay from individual constituents affecting the radar pulse is essential. These various atmospheric corrections are briefly given in below sub-sections.

2.3.1.1 Ionospheric Correction

The slowdown of radar waves in the ionosphere is caused by the presence of free electrons in upper atmosphere released by ionization of atoms in presence of sun light. Since ionosphere is dispersive medium therefore the slowdown also depends upon frequency of electromagnetic waves used in radar altimetry. Also, ionospheric ranges vary for different latitude values. Prior to the launch of T/P mission, the ionospheric range correction was based upon semi-empirical model estimates of the vertically integrated electron density. For T/P mission, the dual frequency, Ku and C band, altimeter was adopted to estimate the ionospheric range correction. Post T/P mission, dual frequency altimeters are more common. Now, DORIS and Global positioning System (GPS) are providing more accurate ionospheric range correction.

2.3.1.2 Dry Tropospheric Correction

The propagation of the radar pulses are affected by the presence of dry gases, mainly due to Oxygen and Nitrogen, in the lower atmosphere (0 - 15 km). These dry gases change the refractive index of the air.

The dry tropospheric range correction in units of cm is given by

$$\Delta R_{dry} = 0.2277\, P_0\,(1 + 0.0026\cos 2\psi) \qquad \text{(Eq. 2.4)}$$

From equation (2.4), it is evident that dry tropospheric correction is proportional to pressure (P_0) and latitude (ψ). This correction cannot be measured by instrument onboard the satellites. It is estimated from weather models. The dry tropospheric

correction for T/P, ERS 1/2, ENVISAT and JASON 1/2 is obtained from ECMWF (European Centre for Medium-range Weather Forecast) model.

2.3.1.3 Wet Tropospheric Correction

The wet tropospheric correction (WTC) includes the propagation delay of radar waves caused by water vapour and cloud liquid droplet present in troposphere. Height from altimetry increases from few millimetres for cold-to-dry air with few tens of cm for hot-to-humid air in evaluation of Seasat altimeter data [Tapley et al., 1982]. For oceanographic study, the observation of water vapour and liquid water from onboard radiometer is used to derive the wet tropospheric correction. The radiometer measurement is not appropriate in case of continental surface [Mercier and Zanife, 2006] and this observation is not utilized to derive the correction. Therefore, the wet tropospheric correction over the continent is derived from the outputs of meteorological models such as ECMWF and NCEP (National Centre for Environmental Prediction) using the below equation [Frappart, 2006a].

$$\Delta R_{humid} = -(1+0.0026\cos(2\psi))\{1.116454*10^{-3}\int_{Psat}^{Psurf} q\,dp + 17.66543928\int_{Psat}^{Psurf}\frac{q}{T}\,dp\}$$

Eq. (2.5)

Where ΔR_{humid} is wet tropospheric correction, ψ is latitude and $P_{surf,}$ P_{sat}, q and T are meteorological model derived parameters. This formulation is valid for Ku band.

CLS (Collecte Localisation par Satellite) calculates the wet tropospheric correction from the meteorological data at altitude of the Earth surface instead of sea level which provides a better fit to the troposphere for high altitude places (Mercier and Zanife, 2006). Crétaux et al. [2009] has compared the radiometer measured WTC with the WTC from metrological data taken from GDR and calculated at CLS. They have argued that the WTC from CLS model and radiometer observation is in range of 1- 2 cm for T/P and ~3 cm for JASON 1 and ENVISAT over the Issyk-Kul Lake in central Asia.

2.3.2 Geophysical Range Corrections

Here we will briefly discuss the solid Earth and Pole tide corrections. Inverse barometer correction and ocean tide corrections are not discussed because they are not required for inland water bodies.

2.3.2.1 Pole Tide Correction

The centrifugal force, associated with the rotation of the Earth, causes the Earth to deform. Any variations of the Earth's instantaneous rotation vector are accompanied by variations of the associated centrifugal force, which then leads to variations of the deformations. Pole tide is the response to the variation of both the solid Earth and the oceans to the centrifugal potential that is generated by small perturbations to the Earth's rotation axis. The polar tidal ranges up to few cm and is well computed from observed polar motions [Wahr, 1985].

2.3.2.2 Solid Earth Tide Correction

The solid Earth tide is the response of the solid Earth to gravitational forces of Sun and the Moon. These gravitational forces are causing the periodic movement of the Earth's crust and the tidal elevation is proportional to tidal potential that is determined by Love numbers. The magnitude of this tide often reaches +20cm, and can exceed 30 cm too.

2.4 Satellite Altimetry Missions

2.4.1 TOPEX/POSEIDON (T/P)

T/P mission, launched in August 1992, mission is collaboration between CNES, the French space Agency, and NASA, the US space agency, with an objective of 'observing and understanding the ocean circulation'. The satellite was placed in an orbit inclined 66 ° at an altitude of 1336 km. The spatio-temporal distance of T/ P is characterized by an inter-trace of 315 km at the equator and has a repetition time of 10 days, covering almost entire Earth's surface (Figure 2.1). The choice of orbital parameters was dictated by the initial scientific objectives. High altitude makes the satellite trajectory less

sensitive to gravitational perturbations and friction effects of the atmosphere, allowing a very precise calculation of the orbit of the inclination with the requirements of a spatio-temporal sampling suitable for the observation of the mean ocean circulation, in particular well suited for de-aliasing the tides.

- **NASA Radar Altimeter (NRA):** A dual-frequency radar altimeter operating, 90% of the flight, time in Ku-band (13.6 GHz) and C-band (5.3 GHz). This dual-frequency system has been designed to calculate the ionospheric correction over the oceans.
- **Poseidon (SSALT: Solid State Altimeter):** An experimental altimeter, lightweight and with low power consumption, operating in the Ku band has been developed by Alcatel Space. Sharing the same antenna of NRA, it is active only for 10% of the observation time.
- **TOPEX Microwave Radiometer (TMR):** A triple-frequency (18, 21, and 37 GHz) microwave radiometer measuring brightness temperatures to calculate the water vapour and liquid water contain in the atmosphere. These measurements are used to calculate the wet troposphere correction over the oceans.
- **DORIS, GPSDR (**Global positioning system demonstration receiver) and **LRA** (Laser retroreflector array) systems are used for precise orbit determination of the satellite.

2.4.2 JASON 1 and JASON 2

JASON 1, jointly developed by NASA and CNES, a follow-up of T/P mission was launched in December 2001 with same orbital parameters and similar payload onboard.

- **Poseidon-2 Altimeter:** A single dual-frequency altimeter which is built on the legacy of Poseidon-1, operating in Ku and C bands and is used for measurements of ocean topography.
- JMR Radiometer: JASON 1 Microwave Radiometer measures the radiation from earth's surface at three frequencies (18.7, 23.8 and 34.0GHz) to determine atmospheric water vapour and liquid water content.

- **DORIS, LRA and TRSR** (Turbo Rouge Space Receiver)**:** These instruments are used for precise orbit determination of the satellite.
- JASON 2, launched in June 2008, is next in series of T/P mission with next generation of Poseidon Altimeter, Poseidon-3, and better surface radiation measuring instrument, advanced microwave radiometer (AMR) and orbit determination instruments.

2.4.3 ERS-1and ERS-2

ERS-1 and ERS-2 (European Remote Satellite) have been designed and developed by the European Space Agency (ESA) with the primary mission of Earth observation using radar techniques. They are placed in an orbit at 800 km altitude and inclined at 97.8 ° with a spatial coverage of 82.2 ° S latitude 82.2 °N latitude. ERS-1, launched in July 1991 and completed its operation in 1999. ERS-2, launched in 1995, provided high-resolution, wide-swath imaging radar producing high quality images of the oceans, coastal zones, polar ice and land regions, irrespective of weather conditions and cloud coverage or whether it is day or night. Both satellites have similar on board payloads:

- **Radar Altimeter (RA):** A single frequency radar altimeter operating in Ku-band (13.6 GHz)
- **Active Microwave Instrument (AMI):** An instrument combining the functions of radar synthetic aperture (SAR) and a Wind Scatterometer (SCATT).
- **Along-Track Scanning Radiometer (ATSR):** The ATSR operating in the infrared and provides the detailed maps of the temperature at ocean surface with an accuracy in order of 0.5 degrees Celsius. It also measures cloud top temperatures, cloud cover and land surface temperatures.
- **Global Ozone Monitoring Experiment (GOME):** This ultraviolet and visible light spectrometer, onboard ERS-2, provides information on ozone, CFCs and trace gas levels.

2.4.4 ENVISAT

ENVISAT was ESA's successor to ERS and it was launched in 2002 with 10 instruments aboard is the largest civilian Earth observation mission. It was designed to

provide measurements of the atmosphere, ocean, land and ice over a five-year period [Wehr and Attenna, 2001]. After a successful journey of 10 years, it completed its operation in April 2012.

- **Advanced Synthetic Aperture Radar (ASAR)** operates at C-band. ASAR ensures continuity with the image mode (SAR) and the wave mode of the ERS-1/2 AMI.
- **MERIS (medium-spectral resolution)** imaging spectrometer operates in the solar reflective spectral range.
- **Advanced Along Track Scanning Radiometer (AATSR)** measures the precise sea surface temperature (SST) with accuracy of 0.3 K.
- **Radar Altimeter 2 (RA-2)** is an instrument for determining the two-way delay of the radar echo from the Earth's surface to a very high precision of less than a nanosecond. It also measures the power and the shape of the reflected radar pulses.
- **Microwave radiometer (MWR)** measures the integrated atmospheric water vapour column and cloud liquid water content and also the surface emissivity and soil moisture over land.
- **GOMOS** measures atmospheric constituents by spectral analysis of the spectral bands (250 nm to 675 nm, 756 nm to 773 nm, and 926 nm to 952 nm). Additionally, two photometers operate in two spectral channels; between 470 nm to 520 nm and 650 nm to 700 nm, respectively.
- **Michelson Interferometer for Passive Atmospheric Sounding (MIPAS)** is a Fourier transform spectrometer for the measurement of high-resolution gaseous emission spectra at the Earth's limb.
- **SCIAMACHY** is an imaging spectrometer which performs global measurements of trace gases in the troposphere and in the stratosphere.
- **Doppler Orbitography and Radio-positioning Integrated by Satellite (DORIS)** is a microwave tracking system that is utilized to determine the precise location of the ENVISAT satellite.

- **LRR** is a passive device which is used as a reflector by ground-based SLR stations using high-power pulsed lasers.

2.5 Limitations of Altimetry over Land

The altimetry datasets from various missions (e.g. T/P, GFO, ERS 1/2, JASON ½, ENVISAT and Altika) used so far over continental water investigation were primarily designed for Oceanic surface or ice cap where altimetry beams are several kilometres wide. Therefore these data used for inland water investigations, where river width is hardly wider than few kilometres, can be erroneous. Second problem is echoes from inland water bodies, which are far from waveform over the ocean surface, received by the antenna. Another major issue is mispointing of reflecting that, too, raises the error in water stage calculation for inland water bodies [Calmant et al., 2008; Calmant and Seyler, 2006]. These problems are raised either because of variation in topography, change of reflecting properties or the size of target surfaces and are discussed in this section.

2.5.1 Retracking Algorithm

The reflected waveforms over inland water bodies are different from the oceanic surface [Calmant et al., 2008; Calmant and Seyler, 2006] and retrieval of ranges over continental waters is difficult because the onboard trackers were designed for typical ocean waveforms [Smith, 1997]. First time ENVISAT data was retracked with four algorithms and then ERS 1&2, GFO, T/P, and JASON mission were retract with new algorithms too. These retracking algorithms are intended for ocean, ice and icebergs. Also none of these algorithms has been calibrated and validated specifically for monitoring of continental water bodies. The algorithms developed in River and Lakes Project was applied by Berry et al. (2005) in several lakes and rivers globally. Frappart et al. [2006a] has shown that the Ice-1 algorithm, which seeks the centre of gravity of waveform, is robust enough for monitoring the continental water. Santos da Silva et al. [2010] has explored the application of altimetry data from ENVISAT and ERS missions and retracked byIce-1and Ice-2 algorithms in Amazon basin. Frappart et al. [2006a] and Santos da Silva et al. [2010] have been shown that Ice-1 and Ice-2 are the best suit altimetric measurements in continental hydrology even if they have not been ideally designed for application in continental hydrology.

2.5.2 Data Sampling

2.5.2.1 Tracking Windows

The tracking gate onboard altimeter allows a better fit to the echoes of their parameters to be received after reflection from the surface. It anticipates adjustments of echo in time following from the processing of echoes obtained at the present time and in earlier times. These adjustments relate to position and amplitude of the registration window. This window, a temporal amplitude constant, is cantered on the expected time of return of the signal and its height, calibrated for power provided so that the echo reflected occupies the most of this window. This character of anticipation is particularly adapted to homogeneous surfaces, both in terms of elevation as the backscatter. If medium is not uniform then the altimeter is disturbed by topographical contrasts within a track imaged. This arises because tracking algorithm onboard is unable to adapt their parameters, for varying condition of imaged surface, is known as locking window. Once locking window is lost, it takes few seconds (1-3seconds for T/P) to recapture the locking window for imaging the surface [Fu and Cazenave, 2001]. Within this few seconds the satellite has travelled several kilometres which lost several small water bodies or crossing rivers.

This problem hampers the operation of Poseidon-2, onboard JASON 1, radar altimeter on continents leads to loss of a large amount of data. To remedy it, the reception windows were enlarged for ENVISAT by 4-16 times. A new tracking system, developed by CNES, has been adapted to tackle these problems in Poseidon-3 altimeter onboard JASON 2, Altika/SARAL and future missions. The new tracking system is designed to maintain the receiving echoes by adjusting itself based on the priori height estimate from digital terrain model (DTM) interpolation along the trace of the orbit on the ground, through altimetric measurements obtained by T/P and ENVISAT missions.

2.5.2.2 Temporal resolution

The temporal resolution (i.e. revisit time) depends on the characteristics of the satellite orbit (Table 1.1). This low temporal resolution limits the applications of altimetric studies for hydrological processes, for example flood, that require monitoring in short time alert. The sampling rate for space derived data is much lower than the time

step of in-situ measurements usually collected once or twice a day, or even much more often, every 15 min in automated networks of developed countries. Bercher et al. [2006] evaluated the amount of information lost due to this under-sampling. Also, the life span of particular satellite mission is not large. Considering these facts, Calmant et al. (2008) has proposed multi-mission series as an alternative to monitor the large lakes and inland seas where the water level is not varying on daily basis. Over the rivers the situation is more critical because there are few points of intersection of the orbits of satellites that intercept a watercourse. In very small cases, the creation of multiple mission VS is possible for rivers. To obtain daily basis time series, an alternative approach using interpolation of gauged data with altimetry data has been adopted by Roux et al. [2008].

2.5.3 Reflector Mispointing (Hooking Effect)

Over smaller water bodies and short width and braided river channels, the received reflected energy is corrupted by reflections from riverbanks or islets [Calmant et al, 2008]. The strong reflections from the edge of water body are overridden over the reflection from nadir within footprint which leads to error in estimation of magnitude. This is known as hooking effect (Figure 2.8) and its principle has been discussed by Frappart et al. [2005].

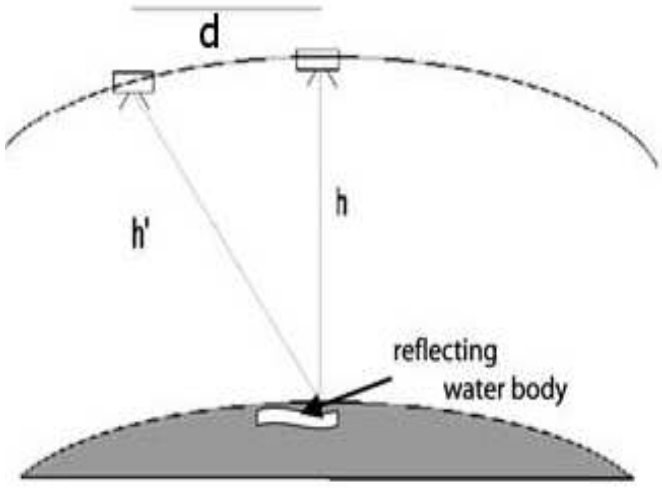

Figure 2.8: Geometry of hooking effect [Calmant et al., 2008].

Parabolic fit of altimeter profiling over such water bodies has been taken in account for correction in range estimation. The error estimation caused by hooking effect is given by equation (2.6).

$$\Delta h = h' - h = h\left(\sqrt{1 + \left(\frac{d}{h}\right)^2} - 1\right) \quad \text{Eq. (2.6)}$$

Where $\Delta h \approx \frac{d}{2h}^2$, given that $\frac{d}{h} \ll 1$

2.6 Satellite Imagery

Accessing and monitoring the state of earth surface helps in management of natural resources for all living beings [Committee on Global Change Research, National research Council, 1999, Xiao et al, 2004, Schmugge et al., 2002] monitoring of floods and in determination of other hydrological parameter [Alsdorf et al., 2002; Wang et al., 1995;]. There are numerous international programs/projects that have been made to classify land cover such as Global land cover characterization based on 1-km AVHRR (Advanced Very High Resolution Radiometer, http://edc2.usgs.gov/glcc/glcc.php). Another similar project, the Global Land Cover 2000 (GLC2000), with 1-Km SPOT4-Vegetation data has been carried out in collaboration of many research teams around the world to map the global land cover. The data acquired from EROS, MODIS, ERS 1/2 and RADARSAT have extended this classification with high resolution on regional and global scale [Xie et al., 2008; Papa et al., 2006; Prigent et al., 2001; Smith, 1997; Mertes et al., 1995]. Over the past half century, remote sensing imagery has been acquired by a range of airborne and space-borne sensors from multispectral sensors to hyper-spectral sensors with wavelengths ranging from visible to microwave at different spatial resolution ranging from sub-meter to kilometres.

2.6.1 Spectral Reflectance Signature

When the solar radiation hits the target surface, it may be reflected, transmitted or absorbed. The reflectivity, transitivity or absorption of different material varies at different wavelengths. In principle, spectral reflectance signature (i.e. a plot of reflected radiation as a function of incident wavelength) of material is unique and they are applied to distinguish from each other. A reflectance spectrum of different kind of land cover such as water, dry bare soil and vegetation is shown in Figure (2.9).

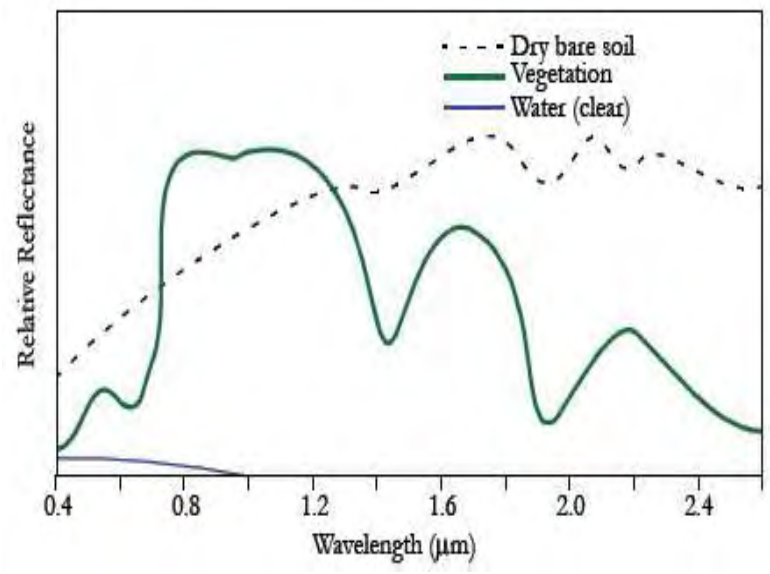

Figure 2.9: Ideal spectrum for vegetation, water and dry soil [Lillesand et al., 2007].

The reflectance signature is used to identify the target surface. The reflectance of band 5 value of MODIS in between 100 and 1200 in unit of MODIS observations, for example, is referring the open water. Further the combination of reflectance from different spectrum range in order to define vegetation indices is used to identify the land cover.

Vegetation Indices (VI)

Vegetation indices can be calculated by rationing, differencing, rationing differences and sums and by forming linear combination of spectral band data. Jackson and Huete [1991] have discussed the empirical and theoretical view on the effective and interpretation of vegetation indices. The ration vegetation index (RVI), defined as ration of Near Infrared (NIR) and red radiance, and was used to derive the leaf area index for a forest canopy [Tucker, 1979; Jordan, 1969]. Deering [1978] has proposed Normalized Difference Vegetation Index (NDVI) by combine use of NIR and Red spectral band (R). Jackson and Huete [1991] has studied the sensitivity of these tow indices and argued that the NDVI is more sensitive to sparse vegetation densities than the RVI, but is less sensitive to high vegetation densities.

$$\mathrm{NDVI} = \frac{\mathrm{NIR}-\mathrm{R}}{\mathrm{NIR}+\mathrm{R}} \qquad \text{Eq. (2.7)}$$

The enhanced vegetation index (EVI) [Jiang et al., 2008] is an 'optimized' index designed to enhance the vegetation signal with improved sensitivity in high biomass regions and improved vegetation monitoring through a de-coupling of canopy background signal and a reduction in atmosphere influences. EVI is computed by following equation:

$$\mathrm{EVI} = 2.5 * \frac{(\mathrm{NIR}-\mathrm{RED})}{(\mathrm{NIR}+\mathrm{C1}*\mathrm{RED}-\mathrm{C2}*\mathrm{BLUE}+\mathrm{L})} \qquad \text{Eq. (2.8)}$$

where NIR/red/blue are atmospherically-corrected or partially atmosphere corrected (Rayleigh and ozone absorption) surface reflectance, L is the canopy background adjustment that addresses non-linear, differential NIR and red radiant transfer through a canopy, and C1, C2 are the coefficients of the aerosol resistance term, which uses the blue band to correct for aerosol influences in the red band. The coefficients adopted in the MODIS-EVI algorithm are; L=1, C1 = 6, C2 = 7.5, and G (gain factor) = 2.5. Jiang et al. [2008] has proposed the calculation EVI without using the Blue band value for generation of long term EVI time series when atmospheric effects are insignificant and data quality is good.

2.6.2 Characteristics of Image

The satellite-sensor platforms are characterized by wavelength used for image acquisition, spatial resolution of the sensor, coverage area and temporal coverage. Spatial resolution of the satellite imagery are classified as low resolution (~1km or more), medium resolution (100 m to 1 km), high resolution (5 m to 100 m) and very high resolution (5 m or less). Table (2.4) presents the application of different bands for acquiring the data in different resolution and repeat period.

Based on the spectral regions used in data acquisition, the satellite imaging system is classified into: Optical imaging system (visible, near infrared and shortwave infrared), Thermal imaging system and Synthetic Aperture Radar (SAR) imaging systems. The data acquisition in optical and thermal imaging system is carried out by single or combination of spectral bands. Similarly, SAR systems use single frequency (L, C or X band), multiple frequencies (combination of two or more) or polarization of frequencies. Data (i.e. image) acquired by remote sensing represent a piece of earth

surface as seen from space can be analogue (aerial photograph) or digital (data acquired by satellite sensors).

Table 2.4: Operational and research satellites for earth surface study.

Platform	**Sensor**	**Bands**	**Spectral**	**IFOV**	**Repeat time**	**Country**
Landsat*	MSS	4	VIS/NIR	80m	16d	USA
	TM 4, 5	7	VIS/NIR/TIR	30/120m	16d	USA
	TM 6	8	VIS/NIR/TIR	20/30/120m	16d	USA
NOAA	AVHRR	5	VIS/NIR/TIR	1-4 km	12h	USA
GOES	VISSR	2	VIS/TIR	0.9/8 km	12h	USA
NIMBUS	CZCS	1	VIS	10 km	27d	USA
HCMM	HCMR	2	VIS/TIR	500m/600m	16d	USA
Shuttle	LFC	Film	VIS/NIR	10-20m		USA
	SIR-A, B	1	Radar	17-58 m		USA
	SIR-C	2	Radar	10-60m		USA
EOS-A	HIRIS	192	VIS/TIR	30 m	4d	
	MODIS-N	35+	VIS/TIR	250-1000m	2d	
	MODIS-T	64	VIS/TIR	1km	2d	
SPOT**	HRV-P	1	VIS	10m	2.5d	France
	HRV-XS	3	VIS/NIR	20m	2.5d	
MOS/LOS	MESSR	4	VIS/NIR	50m	17d	Japan
	VTIR	4	VIS/TIR	1-3 km	17d	
	MSR	1	MSR	25 m	17d	
ERS-1	AMI	1	Radar	30 m	3d	EEC
	ASTR	3	TIR	1 km	3d	
Radarsat	SAR	1	Radar	30 m	3d	Canada

* Landsat 7 was launched in 1999 with additional sensor operating at 15m panchromatic band

** SPOT 4 launched in 1998 with change in panchromatic band range 0.61-0.68

2.6.2.1 Picture Element (Pixels)

A digital image comprises of a two dimensional array of small rectangular (or square) area on the earth surface is called picture elements (pixel) which is function of the sensor i.e. Instantaneous Field of View (IFOV). A pixel has an intensity and location address in the two dimensional images. Intensity of individual pixel represents the characteristics of the reflecting surface. Location addresses of pixels provide the geographical information of target surface.

2.6.2.2 Spatial Resolution

Spatial Resolution is the size of smallest object that can be identified by remote sensors. In digital image, the resolution is limited by pixel footprint represented on

earth. Pixel footprint size is the detector's resolution (footprint of AVHRR visual channel is approximately 1.1 km). A high resolution image refers to the delectability of smaller object.

2.6.3 Processing of Imagery

The land cover mapping is comprised of data acquisition, pre-processing, analysis/classification and documentation. Digital Image processing is basically the process of image restoration, image enhancement, image classification and image transformation. A review of the problem, prospects of images classification and current state of art has been discussed by Lu and Weng [2005].

- Pre-processing (image restoration), in general, is way of the presentation of data in a format from where most information can be extracted. At this stage, Registration, Mosaicking and Georeferencing are applied to the data depending on the need for further analysis.
- Image enhancement is the modifications of image for better visualization by contrast stretch composite generation or digital filtering.
- Image classification is based on the detection of spectral signature of land cover classes in terms of supervised and unsupervised.
- Image transformation is used for extracting the land surface cover detection. Most widely used transformation method is defining the vegetation indices [Jackson and Huete, 1991] and principle component defining.

2.7 Gravimetry

The Earth's gravitational potential, V, is represented by a spherical harmonics expansion. High resolution global gravity field model has been inferred from combine use of satellite tracking measurement and surface gravity data [Gruber et al., 2000a; 2000b; Lemoine et al,. 1998].

$$V = \frac{GM}{r} \sum_{l=0}^{\infty N_{max}} \left(\frac{a_e}{r}\right)^l \sum_{m=0}^{l} P_{l,m}(\sin\varphi)\left[C_{l,m}\cos m\lambda + S_{l,m}\sin m\lambda\right]$$

Eq. (2.10)

Where G-universal gravitational constant, M - mass of Earth, a - semi major axis of earth's reference ellipsoid, r - satellite distance, φ - latitude, λ - longitude, $S_{l,m}$, $C_{l,m}$ spherical harmonic coefficients of degree *l* and order *m*, and $P_{l,m}$, are Associated Legendre Functions of degree l and order m. Though the spherical harmonic expansion of geopotential requires an infinite series of harmonics nut it is limited to maximum degree $N_{max.}$

Gravity is an integral of mass; the spatio-temporal gravity variation is representation of the horizontal mass redistribution. On a time scale from months to decades, mass redistribution occurs because of change in water stock largely in oceans, ice caps and continental reservoirs [Ramillien et al. 2005; Rodell and Famiglietti, 1999; Chao and O'Connor, 1988]. The water stock variation affects water cycle and ultimately the climate. Measurements of the water stock variation at global and regional scale are essential for its proper management and hydrological related studies. Gravity Recovery And Climate Experiment (GRACE) mission was launched with primary objective to monitor the spatio-temporal changes in storage of snow, soil and underground water globally.

2.7.1 GRACE Mission

The GRACE mission was launched on March 17, 2002 for an intended lifetime of 5 years but it is still in service in an extended mission. This mission was jointly designed by NASA and DLR (Deutsches Zentrum für Luft und Raumfahrt). The main application of GRACE is to quantify terrestrial hydrological cycle by measurements of vertically-integrated water mass changes inside aquifers, soil, surface reservoirs and snow pack, with a precision of a few millimetres in terms of water height and a spatial resolution of ~ 400 km [Tapley et al., 2004]. The measurement of mass redistribution from GRACE observation is used for validating and improving the existing hydrological models more precisely which describe the hydrological cycle and impacts

of climate and environmental changes. This information can assist in determining ground residual basin-scale estimates of evaporation [Ramillien et al., 2006; Rodell et al., 2004], multi-objective calibration of large-scale hydrological models [Werth et al., 2009; Güntner, 2008] or validation of hydrological models [Klees et al., 2007; Tapley et al., 2004; Wahr et al., 2004] and ice melt [Velicogna and Wahr, 2006].

The GRACE mission consists of two identical satellites in near-circular orbits at ~500 km altitude and 89.5º inclination. These two satellites are separated from each other by approximately 220 km along-track. The distance between them is measured by a highly accurate inter-satellite, K-Band microwave ranging system (Figure 2.10).

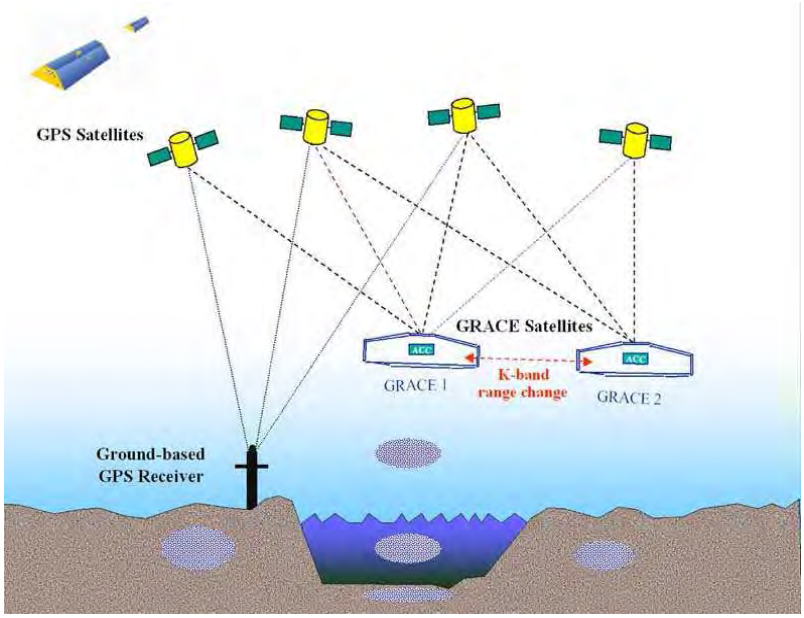

Figure 2.10: Schematics of GRACE data acquisition [Tapley and Chris, 2003].

Each satellite, in addition to the inter-satellite ranging system, also carries Global Positioning System (GPS) receivers and attitude sensors [Dunn et al., 2003] and high precision accelerometers [Touboul, 2001] to measures the effects of non-gravitational forces, namely, the solar pressure, friction air and other non-modelled [Touboul et al., 1999] phenomena. Ward et al. [2002] shows that this procedure provides an error of about 2 cm in derived geoid models. For the purely gravitational component related to mass distribution within the Earth, the effects of non-gravitational forces, measured by the accelerometers are removed from the observed signal. GPS receivers present on each satellite provide accurate locations used to infer changes in the distance between satellites and get the absolute positions of the satellites.

The GRACE data distributed to the scientific community consists of a set of coefficients (and their uncertainties). These coefficients are calculated from the orbital parameters, i.e. position, speed and accelerations, of twin satellites the GRACE mission by three teams: to a CSR (Centre for Space Research) at the University of Texas at Austin (USA), the GFZ (GeoForschungs Zentrum) Potsdam in Germany and the GRGS (Research Group in Space Geodesy), the Observatoire Midi-Pyrénées. The CNES (Centre National d'Etudes Spatiales) and the Department of Earth Observation and Space Systems (DEOS), Delft, University of Technology, are creating their own solutions from the raw data.

2.7.2 GRACE Data and Hydrology

The terrestrial water, stored at the surface (ice, rivers, lakes, and small closed water bodies), subsurface (soil moisture, root zone water), underground aquifers or in atmosphere (direct evaporation and transpiration from vegetation). These components of terrestrial water participate in hydrological cycle and play an important role in climate variability [Zeng et al., 2008]. There are several studies linking impact of this water storage to the climatic variability but still there is a lack of significant knowledge of influence of the climatic factors on the terrestrial hydrological variables. The changes in total water storage can be presented as the vertical sum of these components (Figure 2.11).

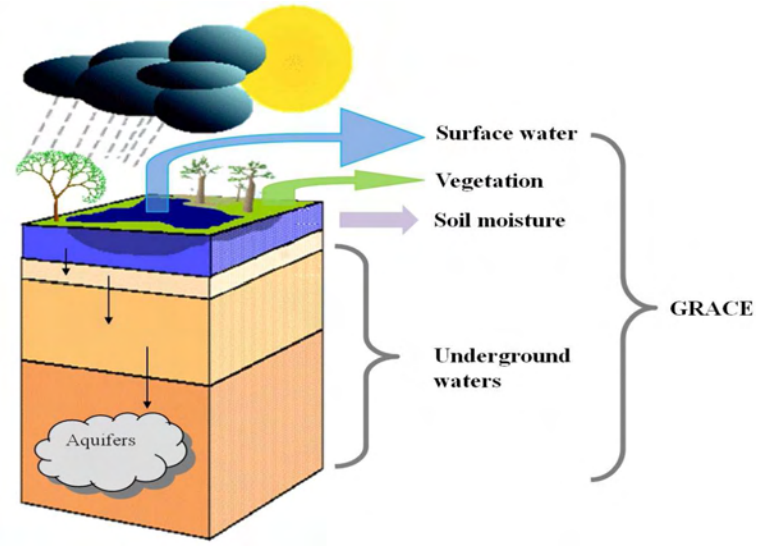

Figure 2.11: Schematic view of observation of TWS from GRACE [Cazenave and Chen, 2010].

The total water storage (TWS) variation is obtained from the water budget equation given in equation (2.11).

$$\frac{d(TWS)}{dt} = P - ET - R \qquad \text{Eq. (2.11)}$$

Where P is precipitation, ET is evapotranspiration and R is surface runoff.

The TWS is an important constituent in global hydrological cycle and has high intake in climate system. Accurately quantified TWS change (with respect to the mean TWS over a certain period of time) provides a key measure of the continental water cycle and available water resources in a given region or river basin. However, there is lacuna in TWS estimation because of the lack of observation and systematic monitoring of in-situ measurement. The availability of other constituent of TWS such as ground water data, evapotranspiration, and soil moisture are often inadequate or insufficient. The advancement in remote sensing has filled this gap with alternative source of many of these components of the TWS. The imagery and altimetry has its application limited to surface water which is discussed in earlier part of this chapter.

Before the launch of GRACE, it was not possible to have the direct measurement of time varying storage of snow, soil and underground water at global scale. At this time, the spatio-temporal variation of terrestrial water storage (TWS) was estimated from global land surface models. The validation and accuracy of these models are limited to certain hydrological parameters and regions. The GRACE mission provides an alternative source of monitoring the variations in TWS. A schematic view of TWS observation from GRACE is shown in Figure (2.10). The studies of Wahr et al. [2004], Ramillien et al. [2008, 2005], Bruinsma et al. [2010] and Tiwari et al. [2011, 2009] among others have discussed the use of GRACE observations along with other hydrological parameter observations in determination of the TWS at regional and global scale.

2.7.3 Errors in GRACE Solutions

The GRACE twin satellites do not have a fixed orbit, like many polar orbiting satellites but their orbit is determined by gravitational forces. Therefore, GRACE orbits (or overpass tracks) are irregularly spaced in time and have limited overpass frequency.

The GRACE measurements are sensitive mainly to variations along the ground-tracks, which limits the sampling of east-west oriented mass redistributions [Schmidt et al., 2008; Wahr et al., 2006; 2004; Chen et al., 2006a; 2006b]. Further the error is introduced in monthly GRACE solutions due to measurement of noise, propagation of errors in the background models and consequently the aliasing of high frequency mass variations (for example, oceanic tides and atmospheric mass redistribution). Post processing, for example spatial smoothing, also introduces inaccuracy in monthly GRACE gravity field solutions [Han et al., 2005; Swenson and Wahr, 2006, 2002]. At small spatial scale, the nearby changes in mass redistribution influence the amplitude of signal which is known as leakage.

Chapter 3

Study Area: River Basins in India

Introduction

There are more than a dozen major rivers with several tributaries across the India but their geographical presence is not uniform. Many of them are perennial and some are seasonal. The perennial rivers systems such as Ganga, Brahmaputra and Indus originate in Himalayas and carry water throughout the year. These river systems are fed as result of melting of ice and snow and monsoon precipitation. Similarly, the melting of ice and snow in Himalayas and rainfall are the source of water in tributaries of the major rivers in India which contribute around 50% of water resource [Lal, 2001]. The non-perennial rivers flow during the monsoon period and receive the water form precipitation in their respective catchment.

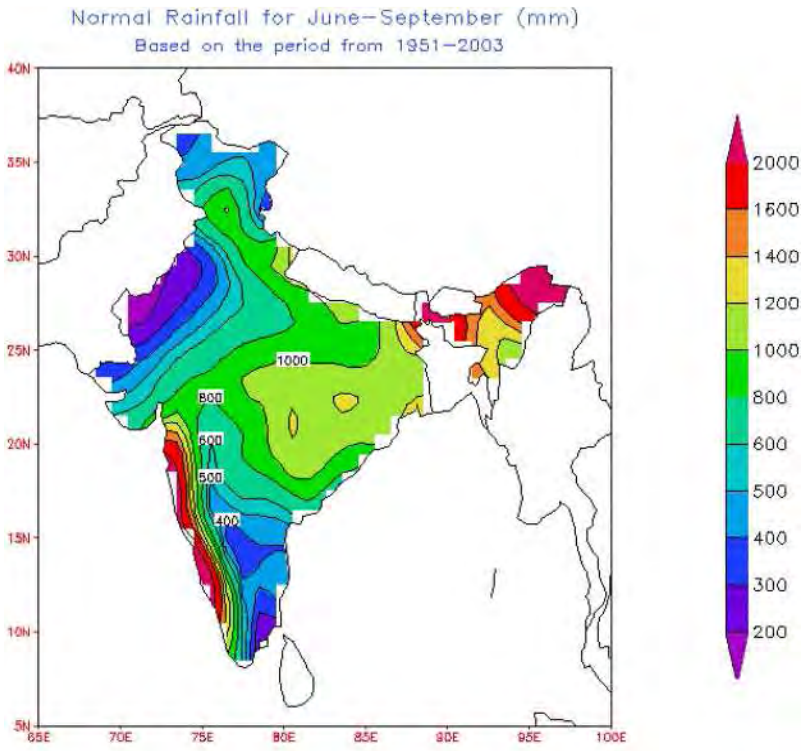

Figure 3.1: Long term average rainfall distribution during June-September in India (IMD-India)

India receives an annual precipitation of around 4000 km^3 including snowfall and rainfall during the monsoon period [Gupta and Deshpande, 2004]. About 75% of annual rainfall in India is contributed by southwest monsoon between June-September. A long term average rainfall during southwest monsoon over India is shown in Figure (3.1). There are very heavy rainfall in all parts of Assam and west coast of peninsula amounting to 200 cm annually. The southern slopes of the Khasi Hills, the Brahmaputra valley and narrow slopes of the west coast strips (11°N to 13°N) receive more than 400 cm of annual rainfall. On contrary, the western Rajasthan receives 40 cm and some part of country receives even less [Jagannathan, 1968]. Because of uneven distribution of rainfall, part of country is under acute flood when some part is facing the drought. A summary of rainfall in the country for past 9 years, from 2001 to 2009, has been given in Table (3.1).

Table 3.1: Yearly total rainfall in India [CWC, 2010]

Year	**2001**	**2002**	**2003**	**2004**	**2005**	**2006**	**2007**	**2008**	**2009**
Total Rainfall (mm)	1110	930	1234	1086	1215	1161	1181	1117	954
Rainfall Total Vol. (BCM)	3648	3200	4057	3570	3996	3819	3882	3674	3136

3.1 Water Resources of India

India is endowed with rich water resources with approximately 45000 km long riverine systems across the country. The geographical area of India is 3.29 million Km^2 which is 2.4% of the world's land area but it holds 15% of world's population. The state of India holds about $1/6^{th}$ of world population and $1/25^{th}$ of world's water resources [Kumar et al, 2005]. A gross annual assessment of available water resources of India [MOWR, 1999; Gupta et al., 2004] is given in Table (3.2). The surface water and ground water resources of India and its utilization by various sections have been discussed by Kumar et al. [2005]. According the National Commission for Integrated Water Resources Development (NCIWRD) of India, the utilizable annual surface water within country is 690 km^3 whereas the estimated average annual flow in Indian River systems is 1953 km^3 [Kumar et al., 2005]. India has been agriculture based economy and surface water resources are widely used for agriculture purposes. As it is well

known that though there are many rivers in India but they are not having their uniform presence across the country hence groundwater is also used extensively.

The river water is widely used for irrigation, hydro power generation, agro-industries and other non-agricultural industries. The hydrological cycles in most of the river basins of India has been modified quantitatively and qualitatively by construction of dams and reservoirs, changes in land use of its catchment and other man made activities over river channel. Apart from the water available in various rivers, the ground water is also an important source for drinking, irrigation, industrial uses etc. There are many reports from the different agency [CGWB, 2006] and various studies [Tiwari et al., 2011, 2009; Rodell et al. 2009; Amarasinghe et al., 2007; Kumar et al., 2005] stating that there is decrease in ground water resources in India especially in north India.

Table 3.2: Water resources of India [Gupta et al., 2004].

Water Resources	**Quantity**	**Precipitation (%)**
Annual precipitation (including snowfall)	4000 km^3	100
Evaporation + groundwater	2131 km^3	53.3
Average annual potential flow in rivers	1869 km^3	46.7
Per capita water availability (1997)	1967 m^3	--
Estimated water availability	1122 km^3	28.1
Surface water	690 km^3	17.3
Replenishable ground water*	432 km^3	10.8

*Natural recharge from rainfall (~ 342.4 km3) + potential due to augmentation from canal irrigation system (~ 89.5 km3). Source: Ministry of Water Resources-India, 1999.

The surface water distribution varies largely. Both in term of available surface water and average monsoon runoff of Ganga and Brahmaputra are two largest river basins followed by Godavari, Krishna, Indus and Mahanadi [Gupta et al, 2004]. A basin wise surface water resources in India are shown Table (3.4). The Ganga basin has the largest amount of surface water (~250 km^3 / year) and hence its large alluvial aquifers facilitate a huge contribution to replenishable groundwater (~170 km^3 / year). The annual potential natural groundwater recharge from rainfall in India is about 342.4 km^3 /

year. The estimates by Central Ground Water Board (CGWB) of total replenishable groundwater and its different utilization are shown in Table (3.3).

Table 3.3: Groundwater resource of India [Kumar et al., 2005] in Km^3/year

1	Total replenishable groundwater	432
2	Provision for domestic, industrial and other uses	71
3	Available groundwater for irrigation	361
4	Utilizable groundwater for irrigation (90% of sl. n° 3)	325
5	Total utilizable groundwater (sum of sl. n° 2 and 4)	396

Table 3.4: Basin-wise average flow and utilizable water in BCM [CWC website]

Sl. No.	**Name of the River Basins**	**Avg. Annual Potential in the River**	**Estim.Utilisable Flow (excluding Ground Water)**
1	Indus (up to Border)	73.31	46.00
2	a) Ganga	525.02	250.00
	b) Brahmaputra, Barak and others	585.60	24.00
3	Godavari	110.54	76.30
4	Krishna	78.12	58.00
5	Cauvery	21.36	19.00
6	Pennar	6.32	6.86
7	East flowing Rivers between Mahanadi & Pennar	22.52	13.11
8	East flowing Rivers between Pennar and Kanayakumari	16.46	16.73
9	Mahanadi	66.88	49.99
10	Brahmani & Baitarni	28.48	18.30
11	Subarnarekha	13.37	6.81
12	Sabarmati	3.81	1.93
13	Mahi	11.02	3.10
14	West flowing Rivers of Kutch, Saurashtra including Luni	15.10	14.98
15	Narmada	45.64	34.50
16	Tapi	14.88	14.50
17	West Flowing Rivers from Tapi to Tadri	87.41	11.94
18	West flowing rivers from Tadri to Kanayakumari	113.53	24.27
19	Area of Island drainage in Rajasthan Desert	Neg.	-
20	Minor River Basins drainage to Bangladesh & Myanmar	31.00	-
	Total	**1869.35**	**690.32**

3.2 Indian Monsoon

The Arabic root word ‘Mausam’ literal meaning is ‘season’. In meteorology the monsoon (i.e. Mausam) means the seasonal reversal of wind and in that sense the term has been used to describe such changes even in higher latitude and stratospheric winds [Rao, 1976]. Broadly, a year in India can be classified into four seasons [Jagannathan, 1968]: (i) Winter season (January and February), (ii) Hot weather season (March to May), (iii) Southwest monsoon (June to September) and (iv) Post Monsoon season (October to December). The classification of weather in India is discussed in detail by Jagannathan [1968].

3.2.1 Seasonal Rainfall Distribution

Winter season is the driest season for the country as a whole but Jammu and Kashmir, southeast Peninsula and certain other part of country receives considerably good amount of rainfall. During winter season, the western disturbances result as the rainfall across the North India. During the hot weather season, a wide area roughly comprising Maharashtra, Madhya Pradesh, Chhattisgarh, Utter Pradesh, Rajasthan, and Gujarat receive rainfall of around 5cm while other part of the country receive rainfall between 20cm to 80cm. Rainfall during hot weather season is in form of thunderstorm. This season is characterized by tropical storm, developed between 10°N to 15°N, over the ocean areas.

The southwest monsoon is the dominating rainfall period in India which contributes over 75% of annual precipitation. During this period, a heavy rainfall is received by different regions in India. For example, 200 cm to 400 cm in Assam, 200 cm to 300 cm in West Coast and its adjoining Ghats, 120 cm to 140cm over Bihar plateau and 100 cm to 120 cm in Uttar Pradesh and some central part of India. Other part of the country, for example Southern region in India, receives the rainfall in range of 30 cm to 50 cm. The distribution of southwest average rainfall over India for 1951 to 2003 is shown in Figure (3.1). The amount and distribution of rainfall post monsoon differs significantly from the same in the southwest monsoon. The high rainfall recipient areas spread from Assam through the coast of Andhra Pradesh, Tamil Nadu, and Kerala which receive around 20 cm of rainfall. This period is also known as northeast monsoon.

3.2.2 Rainfall Variation

The variation of average rainfall and its seasonal distribution over the different part of the country has been discussed in previous section. The long-term mean annual precipitation is 116 cm [Lal, 2001]. The highest recorded rainfall is of about 1169 cm at Mousinram near Cherapunji in Meghalaya-India. The intensity of rainfall over the country in general is a maximum during the southwest monsoon and varies geographically. A maximum intensity of 2-3 cm is found over the Western Ghats and adjoining coastal plains. Over plain region, the intensity varies between 1.5 - 2cm. Large part of India receive the excessive rainfall in heavy downpours caused by cyclonic storms and depressions. Locally heavy rainfall caused by depression varies from 7 to 20 cm in many parts of India. In hilly area, the rainfall in a day has been recorded in range of 25 to 35cm [Jagannathan, 1968].

In view of the highly variable nature of rainfall, it is very important to understand the day-to-day precipitation and distribution when the large amount of agriculture and other sectors affecting the human need is depending on it. This uneven temporal distribution of rainfall creates hazards flood situation over plain area in India. This flood situation is amplified by the water carried by rivers flowing in the respective region.

3.3 River Systems in India

Inland water resources of a country can be classified as rivers, canals, reservoirs, tanks, ponds, and oxbow lakes. Except the rivers and canals, other water systems are small in area of about 7M-ha. Broadly for the hydrological investigation, the India is divided in 20 major river basins. Figure (3.2) shows the drainage of the river systems in India [CWC Report, 2008].

The size, type, nature and number of water resources bodies are varying significantly within the country. Many States viz. Uttar Pradesh, Uttaranchal, Jammu and Kashmir and Madhya Pradesh have maximum number of rivers. Southern states like Andhra Pradesh, Karnataka and Tamil Nadu are dominated by tanks and ponds. A detailed description of rivers systems in India has been discussed by Jain et al. [2007]. Amarsinghe et al. [2005] discussed the spatial variation in supply and demand of water across the river basins of India.

Figure 3.2: River Basins in India (CWC Report, 2008)

Based upon the topography and location, the river systems of India are classified into four groups: (i) Himalayan Rivers, (ii) Deccan Rivers, (iii) Coastal Rivers and (iv) Rivers of the inland drainage basin. The major Indian River systems are shown in Figure (3.2).The Deccan Rivers have very little flow because they are rain fed and most of them are non-perennial. Most of the coastal rivers, especially on the west coast, have small catchment areas and are naturally small in length. Many of the coastal rivers are non-perennial. Kumar et al. [2005] discussed the utilization of various water resources in India. The availability and management of various water resources in future was discussed in detail by Gupta et al. [2004]. For interlinking the different rivers systems, National River Linking Plan (NRLP) have been designed and various studies have been conducted to understand the feasibility of India for interlinking of rivers [Shah, 2008; Jain et al., 2005; Gupta et al., 2004].

3.3.1 Himalayan Rivers

The Himalayan Rivers are fed by rainfall as well as the snowmelt and hence they are perennial by nature. During the southwest monsoon, these rivers receive maximum volume of water from snow melt as well as the rainfall and carry about 80% of annual flow [Jain et al, 2007]. The main Himalayan Rivers are the Ganga, the Brahmaputra, the Meghna and the Indus. The Indus, a trans-boundary river, rises near Mansarovar in Tibet, flows through Kashmir (India) and Pakistan before discharging its water in Arabian Sea near Karachi (Pakistan). Important tributaries of Indus are Sutlej, Beas, Ravi, Chenab and Jhelum. The Ganga (also known as Ganges) is the largest river in India, flowing through many states (Uttaranchal, Uttar Pradesh, Bihar and West Bengal) of India and Bangladesh. The important tributaries of Ganga are the Yamuna, the Ramganga, the Ghaghara, the Gandak, the Kosi and the Sone. The Brahmaputra rises in Tibet where it is known by the name Tsangpo. It enters in India in Arunachal Pradesh and after traversing Assam, it enters Bangladesh. Major tributaries of Brahmaputra are the Dibang, the Lohit, the Subansiri, the Manas and the Teesta. The Barak River, the head stream of Meghna rises in the hills in Manipur. The Meghna is part of Ganga-Brahmaputra-Meghna-System. The combined Ganga-Brahmaputra River meets Meghna in Bangladesh and their huge volume of water flows into the Bay of Bengal.

3.3.2 Ganga-Brahmaputra Basin

The Ganga and Brahmaputra, after flowing through large part of Indian soil, join each other in Bangladesh. Thereafter it flows by the name of Padma which further joined by Meghna river system. The combined basin of the Ganga, Brahmaputra and Meghna spread in India, Nepal and Bangladesh is known by the name of Greater Ganga Basin (GGB). The GGB has vast variation in terms of altitude, cropping pattern, climate, population density, social and cultural life etc. The combine basin has largest fertile area of the world and provides waters to almost 500 million peoples. The average annual discharge of the Ganga, the Brahmaputra and the Meghna rivers is 16,650 m3/s, 19,820 m3/s, and 5,100 m3/s, respectively [Jain et al, 2007]. The maximum discharge in these rivers is observed post southwest monsoon period.

The Ganga River flows in total of 2525 km while the Brahmaputra stretches approximately 2900 km. The Meghna River, having flown in a south-westerly direction draining north-eastern Bangladesh and several states in eastern India, joins the Padma River, the conglomeration of the Ganges and Brahmaputra, at Chandpur, then flows 160 km and empties into the Bay of Bengal.

3.3.2.1 Ganga Basin

Ganga basin is the largest river basin in India by both catchment-wise and population wise. The two main rivers Bhagirathi and Alakhnanda originate in Himalaya and joined by many other small rivers. These two rivers join together at Devprayag and thereafter flow with name of Ganga. The Ganga enters into plains near Haridwar and from there it flows in south/south-easterly direction. Yamuna is the most important tributary of the Ganga that joins on its right bank at Allahabad. After confluence with Yamuna, the Ganga River flows in an eastward direction and is joined by a number of tributaries from both sides. The principal tributaries joining the Ganga River through its long course are the Tons, the Yamuna, the Ramganga, the Ghaghra, the Gandak, the Kosi, the Mahananda, the Pun-Pun, the Kiul, the Burhi Gandak and the Sone. Some of tributaries are also joined by sub-tributaries like Chambal and Betwa, which are the two important sub-tributaries of the Yamuna.

The Ganga basin extends over an area of 1,086,000 km^2. The basin lies between longitudes 73°30E to 89°0E and latitudes 22°30N to 31°30N extending over India, Nepal, and Bangladesh. It is the largest basin in India and has a catchment area of 861404 km^2 in India, covering 26% of the country and hosts about 43% population as per 2001 census of India [Status report MOEF –India, 2009]. About 79% of Ganga basin lies across 11 Indian states namely Uttarakhand, Utter Pradesh, Madhya Pradesh, Rajasthan, Haryana, Himachal Pradesh, Chhattisgarh, Jharkhand, Bihar, West Bengal and Delhi. A line diagram of Ganga and its major tributaries with average annual flow at various gauging stations is shown in Figure (3.3).

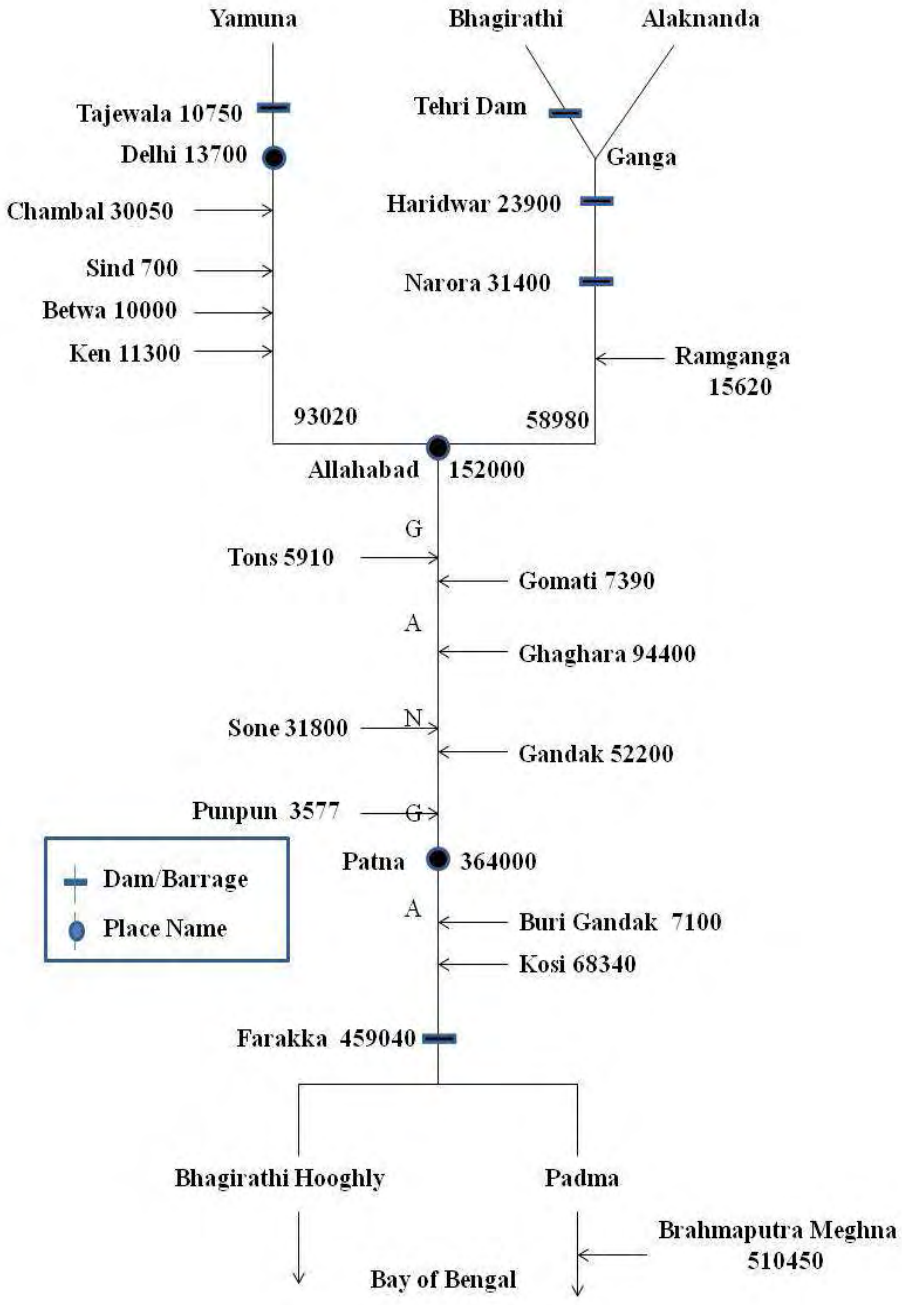

Figure 3.3: Line diagram of Ganga and its major tributaries with average annual flow (million cubic meters) [Jain et al, 2007; Status report MOEF, 2009].

3.3.2.2 Hydrology of Ganga Basin

The hydrological cycle in the Ganges basin is largely governed by the Southwest monsoon. The average annual precipitation in the basin varies from 35 cm in the western end to nearly 200cm near the delta with an average of 110 cm. Snow and

glacier melt during the summer (March to June) which provides large flows to Ganga and its tributaries. A large temporal variation in precipitation in the course of river during the year also generates large fluctuation in flow of the rivers (Figure 3.4). Basin suffers abundant water during monsoon period whereas there is water stress for non-monsoon period [Biswas and Uitto, 2001]. The Ganga has average annual (1949-1973) flow rate of 12105 m^3/sec and a flow of 382 billion cubic meters (BCM). During June-October the average flow is 24526 m3/sec /but for January - May it is 2199 m^3/sec [Rahman, 2005a].

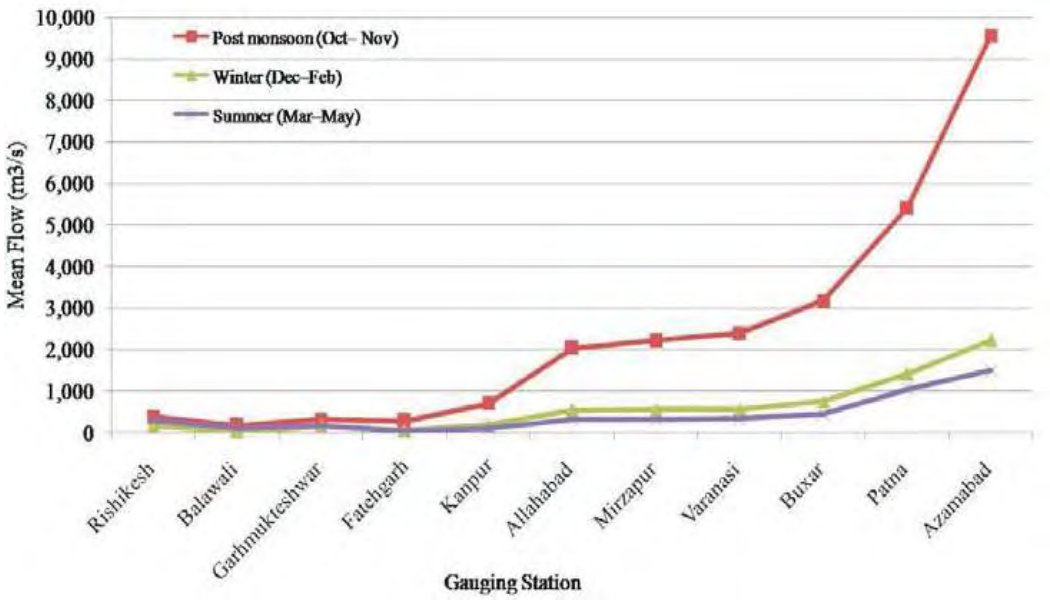

Figure 3.4: Flow variation in Ganga River at gauging stations [Status report MOEF, 2009].

The potential of surface water resource in the Ganga and its tributaries in India has been estimated to 525 billion m^3 out of which 250 billion m^3 is considered to be utilizable (Table 3.4). According the 1991 census, per capita water availability in the basin was 1471 m^3/ year. The Ganga River carries about 1451 million metric tons of sediment per year which is among the world's highest sediment load. Hydrological parameters across the River Ganga at various places from its source to the outfall into the Bay of Bengal (BOB) in India are shown in Table (3.5) [Report NIH, 1998-99]. There is very lean flow till Allahabad and after pouring the Yamuna and other tributaries further downstream, the flow increases. During post monsoon period, there is vertical increase in flow after the Varanasi. During the lean season, the discharge of Ganga at Narora (Uttar Pradesh) is lowest (321 m^3/s). Further downstream the river

discharge is 1542 m^3/s at Kannauj and 1679 m^3/s at Kanpur. At Allahabad at the confluence with Yamuna, the recorded flow is 1870 m^3/s during lean season whereas at Varanasi it is 4120 m^3/s. Further downstream, at Patna the flow is 5693 m^3/s.

Table 3.5: Hydrological parameters of Ganga River in India [Report NIH, 1998-99].

Station Name	**Distance from Source (km)**	**Elevation from MSL (m)**	**Average slope of land**	**Avg. mean annual flow (m3/sec)**	**Mean annual flow range (m3/sec)**
Rishikesh	250	350	1 in 67	856	1305-21631
Kanpur	800	138	-	1184	910-30763
Allahabad	1050	95	From Rishikesh to Allahabad 1 in 4100	4226	2987-112206
Varanasi	1295	80		4106	2793-112206
Buxer	1430	60		4436	3438-192625
Patna	1600	50		7626	6341-192625
Farraka	2055		From Allahabad to Farraka 1 in 13500	10159	
Calcutta		19	-	1056	
Nawadwip	2285	12		1314	1107-18666
Outfall to BOB	2425		1 in 24000		

3.3.2.3 Kosi Basin

Kosi is a major tributary of the Ganga River, often referred as sorrow of Bihar, originates at an altitude of 7 km in the Himalayas and drains through the foothills in Nepal and the alluvial plain in north Bihar - India before it confluence with Ganga. It is a perennial stream whose three main tributaries, Sun Kosi from the west, Arun from the north, and Tamur from the east meet at Tribeni to form the Sapt Kosi. The Arun Kosi is the biggest of the three streams. The total drainage area of the Kosi River is 74500 km^2 out of which 11000 km^2 lie in India. The Kosi basin lies between 85°E to 89°E longitudes and 25° 20'N to 29°N latitudes.

The river, upstream Tribeni in Nepal and about 11 km downstream, flows in deep gorge in mountains before entering into Gangetic plain (Gole and Chintale, 1966). Further downstream Kosi is joined by a number of small tributaries. The plain of North Bihar is one the most susceptible area in India which is very prone to flood. The floods

of the Kosi and Gandak rivers in the plain of North Bihar has been responsible for the extensive and frequent loss of human life and properties in past several decades. A review of flood events (Kale, 1997) occurred in this region indicates that the Bihar region had suffered the highest number of flood event in recent past.

The Kosi catchment is divided into two distinct parts, one lying in Tibet across the Himalayan range (upper Kosi) and second in the low lying areas of Nepal and Bihar in India (lower Kosi). All the peaks and valleys above 4.9 km are always covered with snow except the ridges. A very large part of catchment of Kosi, nearly 80%, lies in Nepal and Tibet. The area within India has flat topography which is confined in Bihar. In the plains Kosi forms the world's largest, 180 km long and 150 km wide, flat alluvial fan (Agarwal and Bhoj, 1992) of conical shape. It has a general slope from north to south and west to east, being steeper in the north and flatter in the south. The total catchment area of Kosi basin is 95,156 sq. km of which 20,376 sq. km lies in India.

Kosi river system is migratory in nature and is described as avulsive shift. A westward migration of 150 km in two centuries, before the embankment on both sides of the river in 1956, is well recorded in historical literatures (Arogyaswamy, 1971). Gole and Chintale (1966) described the river system as inland delta formed by sedimentation which leads to migration of river channel. A number of other possible causes such as regional tilting, tectonic activity, Corriolis effect and auto-cyclic mechanism are suggested for unidirectional shifting (Agarwal and Bhoj, 1992; Arogyaswamy, 1971; Wells and Dorr, 1987). The presence of a number of paleochannels in the satellite image in lower Kosi basin also establishes the migratory nature of the river (Sinha et al., 2008).

3.3.3 Krishna Basin

The Krishna River rises at Mahabaleswar in Maharashtra and drains into Bay of Bengal. The main stream of the Krishna River has two major tributaries: the Bhima River from the north and the Tungabhadra River from the south. Other tributaries of Krishna are the Malaprabha, the Ghataprabha, the Koyna, the Vasna and the Panchganga. There are many dams constructed over the Krishna. The Krishna basin (Figure 3.6) is India's 5th largest river basin in terms of annual discharge (~70 km^3/year) covering 258948 km^2 of southern India, spreading in three states Maharashtra (113271

km^2), Karnataka (69425 km^2) and Andhra Pradesh (113271 km^2) [Kumar et al, 2005; Biggs, et al., 2007].

Figure 3.5: Krishna River Basin highlighting major reservoirs (Source: IWMI)

The river basin is relatively flat, except for the Western Ghats and some forested hills in the centre and northeast. The basin is almost a closed basin and it lies mostly on granites and basalts with low groundwater potential, with some deep alluvium in the delta with high groundwater potential. The geology of the Krishna basin is dominated in the northwest by the Deccan Traps, in the central part by unclassified crystalline, and in the east by the Cuddapah Group. The Dharwars (southwest central) and the Vindhian (east central) form a significant part of the outcrops within the unclassified crystalline. The Krishna Delta occurs on deep alluvial sediments that have aquifers with higher potential. The major part of basin is covered with agricultural land accounting to 75.86% of the total area and 4.07% of the basin is covered by water bodies.

The Krishna basin receives rainfall from both, southwest and northeast monsoon. The rainfall decreases gradually away from coastal area in basin: from 85 - 100 cm in Krishna delta to 30 - 40 cm in northeast. The average rainfall in the basin is 84 cm, of

which approximately 90% occurs during the monsoon from June to October. The climate of the Krishna basin is predominantly semi-arid with potential evaporation (1.457 mm/year on average) exceeding the rainfall in all but three months of the year during the peak of monsoon. A number of reservoirs across the basin is constructed to protect the severe drought and expand the irrigation land. The Nagarjuna Sagar project, for example, was designed along protective lines to irrigate large areas of both paddy and field crops during the rainy season [Venot et al., 2008].

3.3.4 Godavari Basin

Godavari River rises in Trimbakeshwar, in Nasik district of Maharashtra about 80 km from the Arabian Sea at an elevation of 1067 m and flows for a length of about 1465 km before out falling into the Bay of Bengal. Its principle tributaries joining from right are the Pravara and the Manjra whereas the Purna, the Penganga, the Wardha, the Wainganga, the Indravati and the Kolab joins from left. There are more than 800 small and large dams over the Godavari [India-WRIS wiki].

The Godavari basin is surrounded by the Satmala hills in the north, the Ajanta range and the Mahadeo hills in the south, the Eastern Ghats in the east and the Western Ghats in the west. The upper stretches of the Godavari drainage basin are occupied by the Deccan Traps. The downstream part of the middle basin is occupied mainly by the Cuddapah and Vindhyan meta-sediments and rocks of the Gondwana group. The entire drainage basin of the river comprises a series of ridges and valleys interspersed with low hill ranges except for the hills forming the watershed around the basin.

The Godavari basin receives major part of its rainfall during the Southwest monsoon period. The contribution of Northeast monsoon is about 16% of the total annual rainfall in the Godavari basin. The annual rainfall of Godavari basin varies from 300 cm to 60 cm. The basin lies between latitudes 16^0 16’ 0” N and 23^0 43` N longitudes 73^0 26’ E and 83^0 07’ E. Godavari Basin extends over an area of 312813 km^2, which is nearly 10% of the total geographical area of the country. The basin lies in the states of Maharashtra (152199 km^2), Andhra Pradesh (73201 km^2), Chhattisgarh (33434 km^2), Madhya Pradesh (31821 km^2), Orissa (17752 km^2) and Karnataka (4,406 km^2).

3.4 Study Region

The Ganga River along with its tributaries has very important role in socio-economics of large fertile plain in India. Therefore, the present thesis work is focused on the hydrology of Ganga River Basin especially in the lower Ganga basin. Although main emphasis is on the Ganga basin but in the study, various datasets have been analysed for other river basins (i.e. Krishna, Godavari and Brahmaputra) also in India. The Ganga basin (and other basins) is studied with the spatial observation from various satellite missions.

Chapter 4

Data and Methodology

Introduction

The hydrology of continental water bodies depends upon various factors such as geography, geology, hydraulics and climate of the concern region. These informations are gathered by conventional way but there are many regions which are inaccessible by conventional methods. The best alternative is space borne observations and this technique is successfully utilized for monitoring surface water, subsurface water, precipitation and other constituents spatially and temporally. For example, the altimeter onboard satellites provide the substantial hydrological information for water bodies beyond the reach of in-situ measurement.

From various past and current altimetry missions, there are huge numbers of intersections of altimetry tracks with inland water bodies where water level variations are estimated. These altimeter derived water stages, at the intersection points over the river, can be used to derive the hydrological profile of rivers. Satellite imagery is used in determination of land cover type, surface runoff and/or inundation. Observations from many other satellite missions provide information about the soil moisture, evapotranspiration and precipitation in both spatial and temporal domain.

In this chapter, a brief discussion of tools and methodologies used to analyse various datasets (Altimeter data, Imagery data, GRACE data, precipitation data and others) in the study of hydrological behaviour of rivers and river basins is presented. Firstly, the characteristics of altimetry missions, ENVISAT, T/P and JASON 2, in terms of their spatial and temporal coverage, orbital parameters and its processing steps are discussed. In latter part of this chapter, the characteristics and processing of Imagery data and GRACE data is presented.

4.1 Altimetry Data

4.1.1 Datasets

The first step of radar altimetry data processing to derive the water stage time series is extraction of data. In this thesis, altimeter measurement from ENVISAT, T/P, and JASON 2 mission are utilized. Table (4.1) presents a summary of characteristics of these altimetry missions. These extracted data have been processed on board the satellite (tracking) and at the ground segment (retracking). The altimetry data used in this study were extracted from the database of Centre de Topographie des Oceans et de l'hydrosphere (CTOH) hosted by the Laboratoire d'Etudes en Géophysique Océanographie et Spatiales (LEGOS; http://ctoh.legos.obs-mip.fr/). In this study, the considered data for water stage calculation are cycle 10 to 90 for ENVISAT mission whereas for JASON 2 and T/P mission the cycles are 10 to 103 and 11 to 359 respectively.

Table 4.1: Summary of altimetry mission characteristics.

	T/P	**ENVISAT**	**JASON 2**
Objective	Ocean surface study	Environmental, ocean and ice surface study	Ocean and climate study
Altitude	1336 km	800 km	1336 km
Orbit Inclination	66°	98.55°	66°
Inter-track distance at Equator	315 km	80 km	315 km
Algorithms for radar echo treatment	Ocean, Ice1, Ice2, Sea Ice	Ocean, Ice1, Ice2, Sea Ice	Ocean,Ice1, Ice2, Sea Ice
Frequency/ground coverage	10 Hz /580m	20 Hz/350 m	20 Hz/350 m
Repeat period	10 days	35 days	10 days

A high frequency (20Hz) altimetry data retracked by ICE-1algorithm for ENVISAT and JASON 2 missions is considered whereas for T/P mission, the CASH

(Contribution of Sspatial Altimetry to Hydrology) [Seyler et al, 2006] project data has been used. Frappart et al. [2006a] and Santos da Silva et al. [2010] have shown that ranges derived from the use of the ICE-1 re-tracking (other re-trackers are ICE-2, Ocean and Sea-Ice) algorithms are more appropriate for water level time series in rivers. The extracted parameters for ENVISAT and JASON 2 missions have been shown in Table (4.2) and extracted parameters for T/P mission is given in Table (4.3).

Table 4.2: Parameters description which are extracted for ENVISAT mission

Parameters	**Descriptions**
dsr_time_day	Time (day)
dsr_time_sec	Time (seconds of a day)
dsr_time_microsec	Time (microseconds of seconds)
lat	latitude
lon	longitude
alt_cog_ellip	Altitude of CoG above reference ellipsoid
hz18_diff_1hz_alt	18 Hz altitude difference from 1 Hz altitude
ku_band_ocean_range	range measured by Ku band with Ocean retracking algorithms
hz18_ku_band_ocean_range	Range measured in Ku band at 18 Hz by Ocean retracking algorithms
hz18_ku_ice1	Range measured in Ku band at 18 Hz by Ice1 retracking algorithms
hz18_ku_ice2	Range measured in Ku band at 18 Hz by Ice2 retracking algorithms
mod_dry_tropo_corr	Dry tropospheric correction from model
wet_tropo_cls	Wet atmospheric correction derived at CLS
ion_corr_doris_ku	Ionospheric correction from DORIS on Ku-band
solid_earth_tide_ht	Solid earth tide height
geocen_pole_tide_ht	Geocentric pole tide height
hz18_diff_1hz_lat	18 Hz slope-corrected latitude difference from 1 Hz latitude
hz18_diff_1hz_ lon	18 Hz slope corrected longitude difference from 1 Hz longitude

4.1.2 Altimetry Data Processing

Altimetry observation for intersection point of satellite ground track with water bodies (i.e. river, lakes etc.) are used to calculate the water level. The intersection point

is called Virtual Station (VS) which is a small area on water bodies from where reflections are considered for stage calculation. This study uses VALS (Virtual Altimetry Station Software v1.06, www.mpl.ird.fr/hybam/outils/logiciels_test.php) along with Google-Earth to define the VS and calculate water stage [Santos da Silva et al., 2010]. VALS was developed to interactively select altimetry data for defined VS and apply the corrections individually to satellite pass or parts of passes. A detail discussion on functionality of VALS is discussed by Santos da Silva et al. [2010]. The utilization of VALS to calculate water stage is briefly discussed in this section.

Table 4.3: Parameters description which are extracted for JASON 2

Parameters	Descriptions
alt	Altitude above the reference ellipsoid
alt_20hz	Altitude above the ref. ellipsoid measured at 20 Hz
ice_range_20hz_ku	Range measured at 20 Hz in Ku band by ice1 algorithm
iono_corr_gim_ku	GIM ionospheric correction on Ku band
lat	Latitude
lat_20hz	Latitude measured at 20 Hz
lon	Longitude
lon_20hz	Longitude measured at 20 Hz
model_dry_tropo_corr	Dry tropospheric correction from model
model_wet_tropo_corr	Wet tropospheric correction from model
pole_tide	Pole tide correction
range_20hz_ku	Range measured at 20 Hz in Ku band
range_ku	Range measured in Ku band
sig0_20hz_ku	20 Hz Ku band corrected backscatter coefficient
sig0_ku	Ku band corrected AGC
solid_earth_tide	Solid Earth tide correction value
Time	Time
time_20hz	Time measured 20 Hz

4.1.3 Altimetry Time Series

The first step consists of rough selection of the region using imagery from satellite. In this regard, a local database is defined that is used during the course of processing of altimetric measurement to calculate the water stage. The VS is defined by selecting a rectangular/square area and flow direction (in case of river). The ICE-1 algorithm derived altimeter measurements, parameters given in Table (4.2, 43), are extracted into

VALS. The extracted data for range estimation is of high frequency (e.g. 20Hz for ENVISAT and JASON 2) which gives a spatial measurement at every 350 m.

The second step is refining the selection in cross-sectional view. Since the rectangular area is defined in a way that it accounts all the reflections even during the maximum cross-section of river during the wet period. This results as a large number of measurements from non-water surface within the rectangular window. In this step, the reflection from the surface of waterbed is selected. But, sometimes the returned signals are contaminated by the reflections at river banks, islands or riparian vegetation. This contamination is removed by applying the hooking effect [Santos Da Silva et al, 2010]. The width of river limits the number of reflections within VS; therefore there are few measurements per pass within the rectangular window for the defined VS (Figure 4.1) which is considered for water stage estimation.

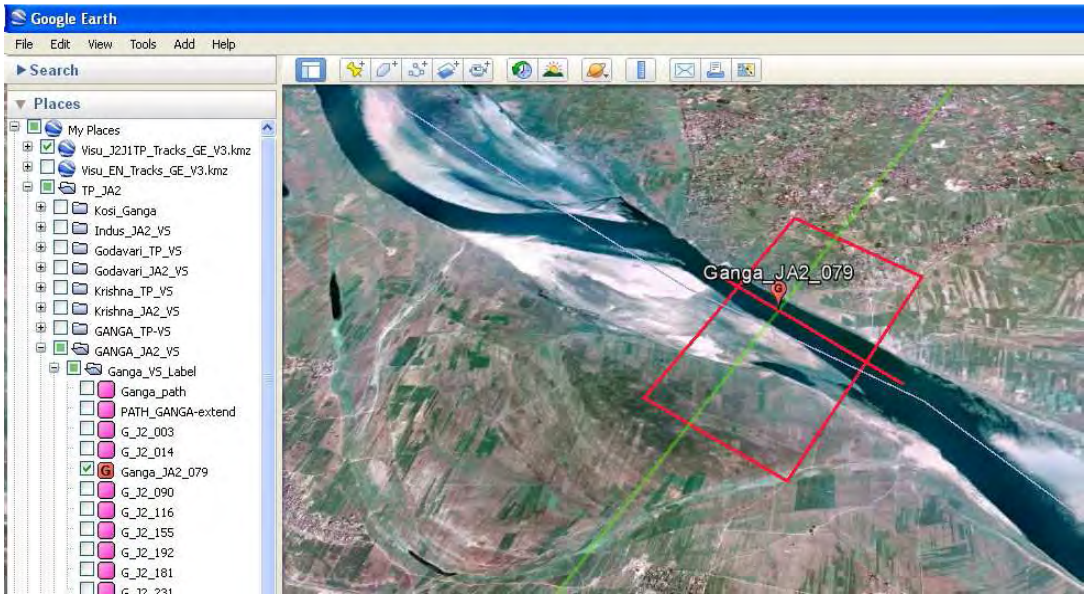

Figure 4.1: Virtual Station: red rectangle is selection window, red line is flow direction and green line is satellite pass.

The final step in the data processing is computation of master point per pass for selected measurements where the water stage is calculated. Frappart et al [2006a] and Santos da Silva [2010] had concluded that the median value is most suitable instead of mean value for continental study to calculate the water height for each individual VS. Therefore for every pass, the median value for the data subset selected in second step is calculated which defines the water height at VS at particular time (i.e. the time of

satellite pass). The median value is determined for every pass for a given track which together forms the water stage time series at the defined VS. Since the measurements per pass are spread over an area therefore at each point of time series, the standard deviation error is calculated using equation (4.1) to measure the quality of calculated time series.

$$\delta_h = \frac{1}{N-1}\sum_{i=1}^{N}|\mathrm{h_i} - \mathrm{h_{med}}| \qquad \text{Eq. (4.1)}$$

Where δ_h is standard deviation in derived median height h_i, N is number of observations par pass, h_{med} is individual height at reflecting surface.

The statistics mean and median is qualitative indicator of presence of contamination. When the data set is well selected then these statistical values are approximately similar. The derived water stage time series is referenced to the Earth Gravitational Model 2008 (EGM2008) developed up to harmonic degree 2159 [Pavlis et al., 2012]. A water stage time series with standard deviation over Brahmaputra from JASON 2 mission is shown in Figure (4.2).

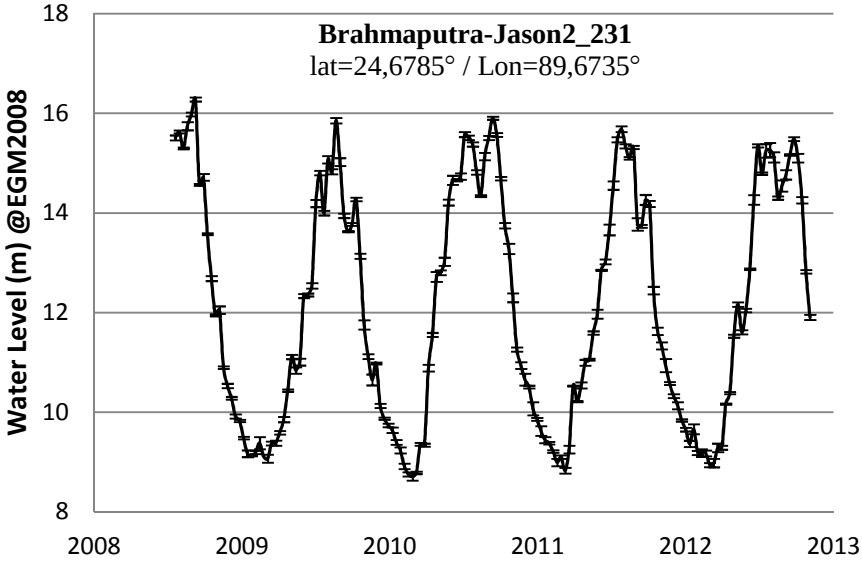

Figure 4.2: JASON 2 derived water level time series with error bars (i.e. Standard deviation in median value) for track 231 over Brahmaputra River.

The altimeter observation based estimated water level over the Ganga, Krishna Godavari and over their important tributaries and the application of derived water stage for calculating the river discharge are presented in chapter 5.

4.2 Imagery Data

The Moderate Resolution Imaging Spectroradiometer (MODIS) is a multispectral imaging system, onboard Terra and Aqua spacecraft at sun-synchronous near polar orbit at an altitude of 705 km, which covers almost entire earth surface every day. Onboard sensors operate in 36 spectral bands spanning into four spectral regions; visible (VIS) (0.412 to 0.551µm), near infrared (NIR) (0.650 to 0.940 µm), short/medium wavelength infrared (SWIR/MWIR) (1.240 to 4.565 µm), and long wavelength infrared (LWIR) (6.715 to 14.235 µm) at nadir. It acquires data in three spatial resolutions: 250m, 500m and 1000m. The MODIS derived products are classified into atmospheric, land and Oceanic based study. A number of land products are delivered by MODIS land (MODLAND) science team [Justice et al, 1998]. Justice et al. [2002] had discussed the various aspects of MODIS data over land. The MODIS products, in Hierarchical Data format (HDF), are distributed by the NASA Land Processes Distributed Active Archive Centre (LP DAAC, https://lpdaac.usgs.gov/).

The data level defines the additional information merged with raw data (i.e. level 0 data). Level 1 data is radometrically calibrated without any other alteration in raw data. Level 2 data is atmospherically corrected. Merging of map projection and gridding of data is, applied to level 2 data, allowed producing the level 3 data. In level 3 and higher level data, each swath is divided into small segments, called granules, for convenience in processing and distribution [Vermote et al, 2007, 2011]. The MODIS data is divided into non-overlapping 460 granules of dimension approximately 10°x10°. Individual granules are identified as $\mathbf{h_xV_y}$. Where x is granule location along longitude (h) and y is location of latitude (V). For example, the data for granule h25v06 and h26v06 are extracted in the present study.

We used the atmospherically corrected 8 days surface reflectance level-3 product MOD09A1 and daily surface reflectance level 2 product MOD09GHK of TERRA / MODIS mission. The MODIS product MOD09A1 provides the surface reflectance at 500m for band 1 to band 7 whereas the MOD09GHK provides surface reflectance at 250m resolution for band 1and band 2 and 500m for bands 3 to band 7. Though the band resolution is commonly referred as 250 and 500 m but the actual resolution at equator is 236m and 472m. The TERRA orbital configuration and MODIS viewing

geometry produces full global coverage every day except the equatorial zone where the repeat frequency is approximately 1.2 days [Zhan et al., 2002].

Details of MODIS product MOD09A1 can be found in MODIS surface reflectance user's guide from website of MODIS (https://modis-sr.ltdri.org). The digital images for MODIS are obtained for January, 2000 to May, 2010 in HDF format.

4.2.1 Processing of Imagery

First of all, the images and geographical information are merged together. In order to prepare geo-referenced images, the MODIS Reprojection Tool (MRT) [MRT Manual, 2002] is used. At this stage the projection system, re-sampling and datum conversion are defined specifically along with other parameters that are spectral sub-setting, spatial sub-setting, and output pixel size. Individual band value informations are saved in separate files in GeoTIFF format. These files are rearranged in order to generate the georeferenced images. Further, in some cases the region of interest may extend from digital image therefore combining two or more images are required. This process is done through the mosaicking of georeferenced images. The unproductive pixels are defined for a threshold value to ignore them at the time of combining the images.

During this study, no atmospheric correction was applied to the MODIS - MOD09A1 images because these corrections are already applied to every pixel with consideration that there is no cloud at time of data acquisition to minimize the impacts of absorbing gas molecules and aerosol dispersed in the atmosphere (Vermote et al. 2007, 2011). The integrated sinusoidal (ISIN) projection of the original data was converted into a geographic projection with datum as WGS84 using bilinear sampling.

4.2.2 Land cover Classification

Land cover is important variable that significantly affects the climate and hydrological process [Wang et al., 1995]. The result of the image processing, discussed in previous section, is used for land cover classification. The land cover classification is carried out from combination of NDVI, calculated using equation (2.7), and Medium Infrared (MIR) band value. The land cover is classified into five categories: open water

(inundated area), aquatic vegetation, vegetation and island (bare soil exposed within water) and dry land. A threshold value for MIR and NDVI together are used for such land cover classification [Pandey et al, 2014; Crétaux et al., 2011a].

MODIS - MOD09A1 product in the 500 m resolution is used to derive the land cover classification. The lower Ganga basin is covered in two granules h25v06 and h26v06. Therefore, we have performed the mosaicking of these granules after georeferencing following the steps discussed in previous section and also summarised in Figure (4.3). The threshold value to ignore unproductive pixels during the mosaicking is set to -28672 which are defined in product user guide.

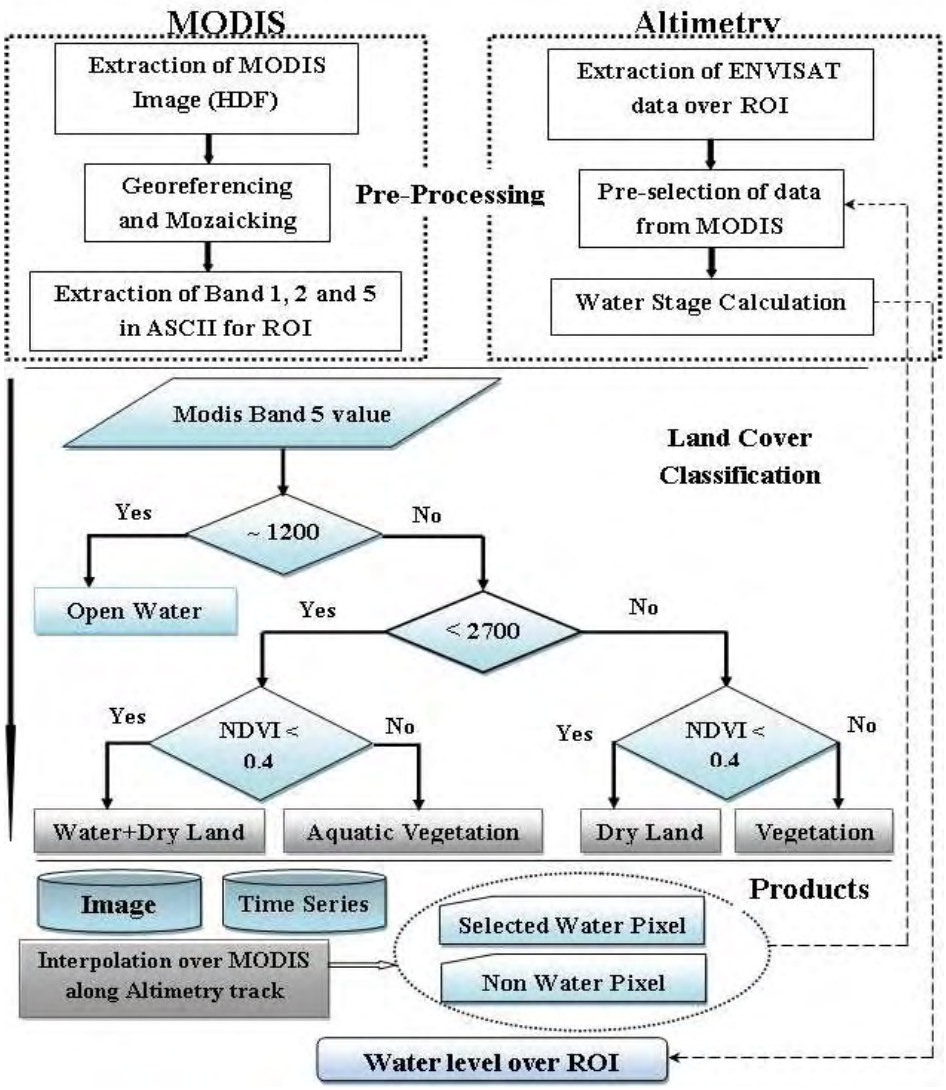

Figure 4.3: Flow chart of the Algorithm used for flood mapping from MODIS images and altimetry derived water height over the Region of Interest (ROI) which is the water covered area in this study.

The land cover is classified using the MIR band (band 5 in MODIS data acquisition) and NDVI. The NDVI is calculated from band 1 and band 2 of MODIS product MOD09A1. A threshold value of 1200 (in unit of MODIS band value) is used to identify the open water (Figure 4.4). The MIR band value above this threshold value along with NDVI defines the other classes of land cover. This algorithm also performs the water level (and subsequently water volume) calculation over the inundated area, along the altimetry track, identified by MODIS data analysis. Using this algorithm with data from MODIS and Altimetry the inundation extent and water level over the flooded region is calculated [Pandey et al., 2014]. A detailed analysis is discussed in chapter 6.

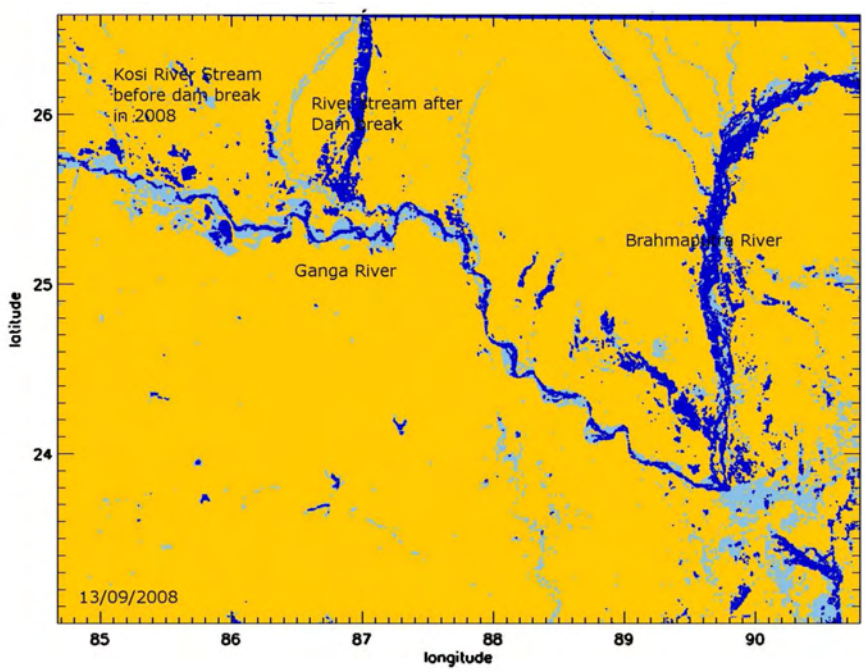

Figure 4.4: Land cover classification as open water (deep blue), island (light blue) with yellow as background representing either dry land or vegetation from MOD09A1 data in lower Ganga Basin.

4.3 GRACE Data

The GRACE Science Data System uses range and range-rate data to estimate variation in gravity field every month or every 10 days [Bruinsma et al. 2010; Schmidt et al. 2008; Bettadpur, 2007; Lemoine et al,. 2007]. Centre for Space Research (CSR) at the University of Texas in Austin, the Geo Forschungs Zentrum (GFZ) in Potsdam and NASA Jet Propulsion Laboratory (JPL) provide the GRACE global gravity solutions. The GRACE solutions are also distributed by NASA PODAAC (http://podaac-

www.jpl.nasa.gov/grace/), Goddard Space Flight Centre [Rowlands et al., 2002], the Delft Institute of Earth Observation and Space Systems [DEOS; Klees et al., 2008], the Groupe de Recherche de Geodesie Spatiale (GRGS) [Lemoine et al., 2007] and the Institute of Theoretical Geodesy (ITG) at the University of Bonn [Eicker, 2008].

The monthly gravity field solutions are produced by GFZ and CSR by adopting the dynamic least-square orbit adjustment and subsequent parameter recovery that estimate corrections to a background gravity model [Schmidt et al. 2008]. At high temporal scale, 10 days GRACE gravity solutions have been computed by GRGS. GRACE temporal solutions are generally expressed in the form of spherical harmonics coefficients of geoid between 60 and 100 corresponding to surface spatial resolution of ~400 to 700 km [Bruinsma et al., 2010]. The distributed GRACE solutions are corrected for atmospheric and oceanic mass distribution and tidal effects [Bettadpur, 2007].

The considered datasets, for analysis of total water storage variation from GRACE observation, are Release-02 (RL02) EWH solutions from CNES/GRGS [Bruinsma et al., 2010]. The data is available at every 10 days in 1 x 1 grids over land. The EWH product is expressed in term of equivalent water heights differences (in meters). The data is extracted for July 29th 2002 to December 23rd 2010. During this period there are fourteen 10-days periods data gap in RL02 from CNES/GRGS. These gaps are from 26th November 2002 to 23rd February 2003 (total 9 time series), 25th May 2003 to 3rd July 2003 (total 4 time series) and 20th January 2004 to 29th January 2004 (one time series). No smoothing or filtering is required as it has been stabilized during the calculation. Every 10-days data files have the TWH value at 1x1 degree grid starting from longitude -179.5 and latitude 89.5.

4.4 Precipitation Data

This study uses the precipitation data from Tropical Rainfall Measuring Mission (TRMM) which is a joint US-Japan satellite mission. The mission objective was to monitor the tropical and subtropical (40°S - 40°N) precipitations and to estimate their associated latent heating. The accurate measurement of the spatial and temporal variations of tropical rainfall around the globe remains one of the critical unsolved problems of meteorology. The TRMM satellite carries three rain measuring instruments: TRMM Microwave Imager (TMI), the Visible Infrared Scanner (VIRS), and the

Precipitation Radar (PR). TRMM has provided some of the first detailed and comprehensive dataset on the four dimensional distribution of rainfall and latent heat over vast oceanic and tropical continental regimes.

The TRMM precipitation data used in this study is monthly average, expressed in cm/month from 1998 to 2010. The present work also uses the results from the daily TRMM precipitation (product name: 3B42 v7 derived) data during the analysis of flood in lower Kosi basin. The analysis of the daily TRMM precipitation data is performed using web based analysis tool TOVAS (TRMM Online Visualization and Analysis System) from Giovanni application which is developed and maintained by Data and Information Services Centre of Goddard Earth Sciences of NASA (http://disc.sci.gsfc.nasa.gov/precipitation/tovas/).

Monthly-mean district-wise in-situ rainfall observations are also used to compliment the study of lower Ganga Basin during the flood period. These in-situ monthly mean precipitation data are obtained from India Metrological Department (IMD, http://www.imd.gov.in/section/hydro/distrainfall/bihar.html). These in-situ data are arithmetic average of precipitation from a number of rain gauges available in respective districts. This data set is not very consistent throughout the year but it is available for June to October.

Chapter 5

Altimetry Derived Water Level

Introduction

For a given spatial coverage of the altimetry missions, there are a large number of intersections (i.e. VS) of ground track with river system in India. The number of VS for different missions, discussed in Chapter 2, is given in Table (5.1). The water stage is calculated at all the possible intersection points across the Ganga, Krishna and Brahmaputra rivers and at some intersections on their tributaries. For defined intersections, the ICE-1 algorithm retracked altimetry datasets are processed using VALS software to estimate the water level variations. The estimated water level is used to develop the water level profile along rivers (Figure 5.2), estimate the water discharge from rivers (section 5.3) and map the water covered surface and water volume in flooding zone (Chapter 6).

Table 5.1 Number of Vitual Stations where water level variations are estimated.

S. No.	Mission/ River	ENVISAT	JASON 2	T/P	Total
1	Ganga	39	11	7	57
	Tributoriesof Ganga (Yamuna, Ghaghara and Kosi)	10	--	--	10
2	Krishna	23	6	2	31
3	Godavari	17	5	2	24
4	Brahmaputra	15	5	5	25
5	Indus	7	2	2	11

5.1. Altimeter Derived Water Stage over Ganga

The river width at the VS varies from few hundred of metres to few km from wet to dry period during the year. The VALS utility provides a fair analysis of altimeter data for calculation of water level variation even for river width of about 100 m (Santos da

Silva, 2010). In the present study, geoid from EGM2008 is used as reference level to present the altimeter derived water level variations. A spatial distribution of VS at intersection of Ganga with different altimetry missions is shown in Figure (5.1) where the water variations are estimated.

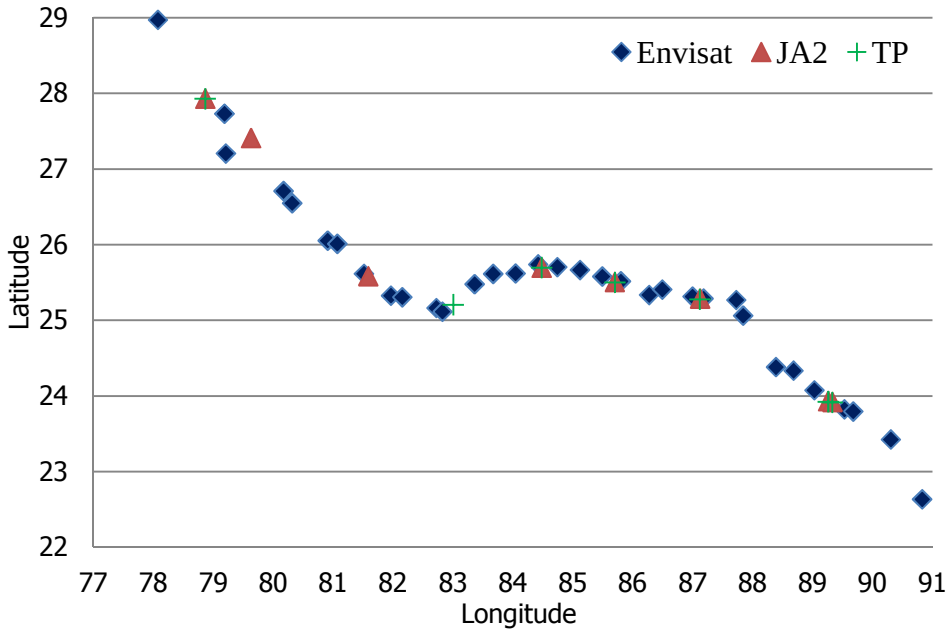

Figure 5.1. Location of Virtual Stations over the Ganga River in India.

The Ganga River originates in Himalaya, at the height of 3892 m above the mean sea level, and discharges into the Bay of Bengal after flowing through large part of plain area in India and Bangladesh. Snow melting on Himalaya and rainfall is the source of the river water. During the course of flow, it receives the water from many tributaries (a schematic representation of the water discharged from its tributaries is shown in Figure 3.4). The dams and artificially created water reservoir across the river control the free flow of water. These factors lead to an uneven water level variation across the river.

The water level variations have been calculated from high frequency (20 Hz) data acquired by RA2 altimeter onboard ENVISAT mission, for cycles between 9 and 90 for a period of August 2002 to July 2010. Similarly, high frequency observations from JASON 2 and T/P missions are adopted to estimate water level variation in the rivers. The Figure (5.2) presents the derived water level across the Ganga River for ascending tracks of ENVISAT mission.

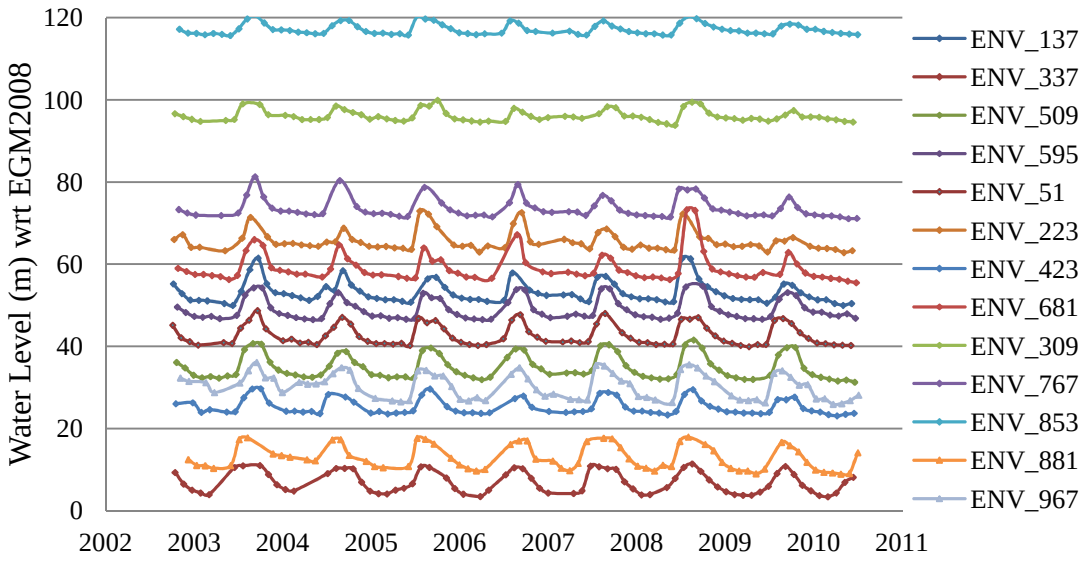

Figure 5.2.Water level variation over Ganga River for ascending tracks of ENVISAT.

ENVISAT derived water level variation time series shows a good agreement and have a similar behaviour in peak-to-peak height variation. A similar trend is observed for the descending tracks over the river. The water stage time series at individual VS are shown in appendix A1. The water level analysis shows that the maximum water in the river is found during the mid of summer monsoon (i.e. in mid-August or early September) whereas the minimum is observed in the month of May – June. The water level deviation from wet period to dry period within the year is not uniform and varies within the range of~7m to ~10m from place to place in the river.

Although the derived water level variation show good agreement at the different places along the river but still the validation of these time series with independent observations is required. At the time of water level derivation, one must be aware that river flow may be altered by various means for example, controls of discharge from the dam at different places in the river or geological setup of the river. The comparisons with in-situ measurements are best option to validate the derived product but due to lack of access to the in-situ measurements it is not carried out extensively. However, Papa et al. [2010a, 2012] has shown a good agreement between the water level variations at Hardinge station over Ganga for ENVISAT and JASON 2 data with in-situ measurement. A comparison of JASON 2 derived water level and in-situ observation at Hardinge station is discussed in section (5.3.2).

5.1.1 Water level in Ganga Post Confluence with Yamuna and Ghaghara

The flow from tributaries into Ganga is an important factor among many others which affects the flow and water level in river. The average annual discharge from important tributaries into Ganga is shown in figure (3.3). The Yamuna and the Ghaghara are two major contributors to the water of Ganga. Yamuna carries more water (93020 million cubic meters (MCM) / year) than Ganga (58980 MCM / year) and meet together at Allahabad in Utter Pradesh, India and hereafter they flow with the name of Ganga. Ghaghara (94400 MCM / year) joins the Ganga downstream in the state of Bihar, India. Further downstream, the Ganga is joined by the Brahmaputra and the Meghna river system. Figure (5.3) presents a schematic location map of the confluence of the Ganga with the Yamuna at Allahabad (marked by blue dot). An effect of flow of the Yamuna and the Ghaghara into Ganga is discussed in this section.

Figure 5.3. The Ganga and the Yamuna conflunce at Allahabad, India (blue dot-point). Blue lines represent ENVISAT tracks.Track 496 intersects both rivers before confluence whereas track 767 passes just after the conflunce.

ENVISAT track 496 passes over the Ganga and Yamuna before their confluence at Allahabad whereas the track 767 intersects after the confluence of these two. Along river distance between the VS before and after confluence is about 70 km for both the rivers. The altimeter derived water stage variation for Ganga and Yamuna rivers just before and after the confluence point is shown in Figure (5.4).

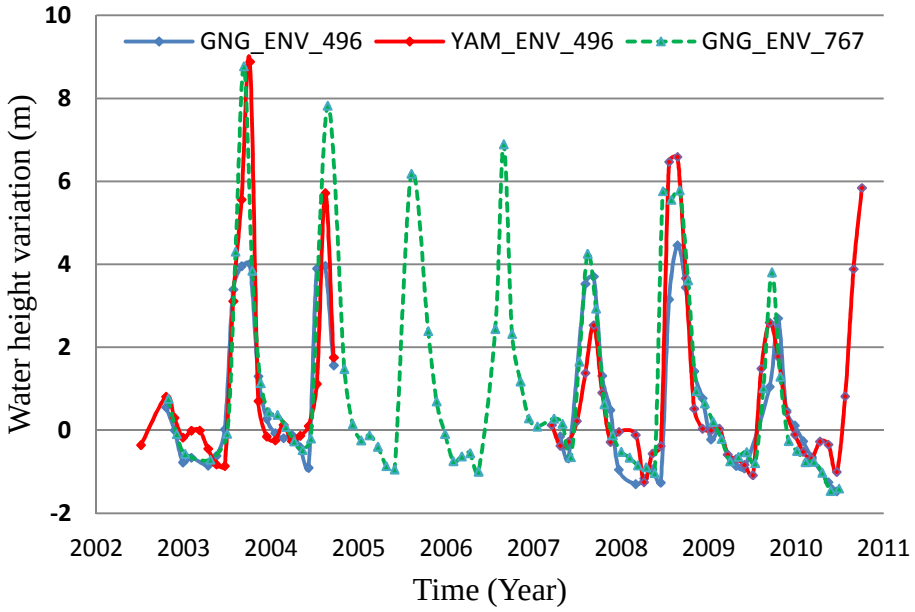

Figure 5.4: Altimeter derived water height variation in Ganga and Yamuna for ENVISAT mission. Red and blue lines represent water height variation in Yamuna and Ganga respectively for track 496 before their confluence. Green line presents the water height variation after the confluence for track 767.

Altimeter derived water level for ENVISAT track 496 and 767 shows that there is large variation in water level of the Ganga before and after the confluence compared with water level variation in Yamuna (Figure 5.4). High water level after the confluence in Ganga is in order of the high water level in Yamuna before the confluence. But low water level at all the three locations is in same order. It can be interpreted that the high water level in Ganga post confluence is dominated by the flow of huge amount of water discharged at confluence point.

For a period of mid-2004 to beginning of 2007, instrument on board the ENVISAT was used for calibration over the Tibetan Plateau descending tracks. The internal instrumental calibration raised a data gap which is reflected in the water level variation time series for track 496. Water level time series also shows that year 2003 and 2008 were exceptional in term of high amplitude of water level. These two years have received high rainfall which can be a probable reason of high amplitude at local VS.

The water level height variation for confluence of Ganga and Ghaghara, before and after the confluence for ENVISAT mission, is shown in Figure (5.5). The water level time series does not show any abrupt variation in water stage after the discharge from

Ghaghara into Ganga. This can be explained by considering that the water discharge from Ghaghara is less (see line diagram of Ganga and its tributaries, Figure 3.4) compared with water carried by Ganga. The water level variations across the Ganga for JASON 2 and T/P missions also have the similar peak to peak pattern. The JASON 2 derived water level in Ganga and Brahmaputra River are used to calculate the discharge from these rivers into the Bay of Bengal (see section 5.3). The time series for these missions are presented in Appendix A1.

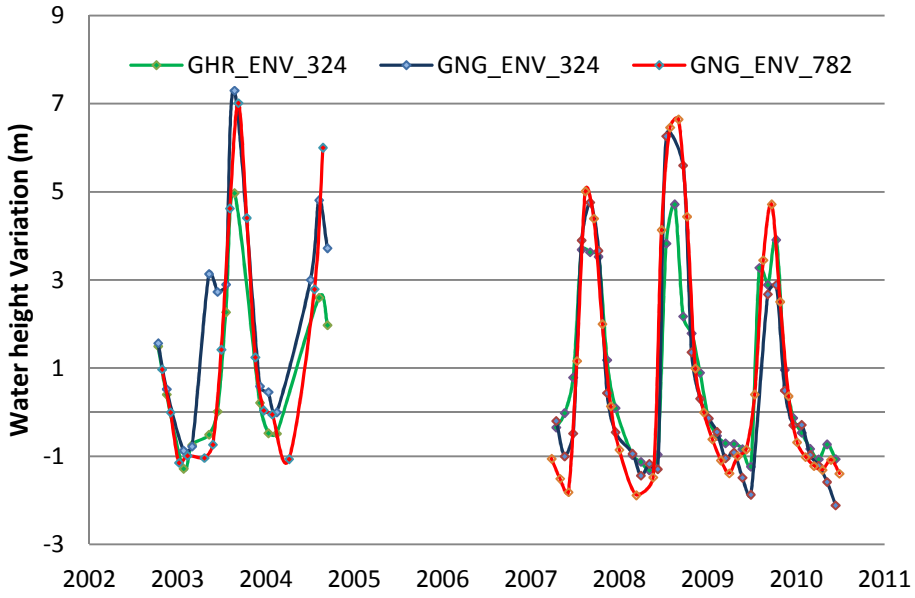

Figure 5.5: Water level variation in Ganga and Ghaghara before and after their confluence from ENVISAT. Green and Blue lines present water level for track 234 over Ghaghara and Ganga respectively before their confluence. Red line is water level variation after their confluence for track 782.

5.1.2 Longitudinal Profile of Ganga

Knowledge of longitudinal (along axis)/hydrological profile of a river is an important parameter for regional or local hydrological studies. The longitudinal profile, defined as channel elevation with respect to the distance to the river mouth, is concave which can be a result of tectonic, sedimentary and climatic effect. Climate change may lead to increasing erosion of the river bed, changing sediment supply and therefore consequence as changes in longitudinal profiles of rivers. Zaprowski [2005] has studied the effect of climate on concavity of river profile. Sinha and Parker [1996] have outlined the possible causes of concavity of longitudinal profile. Slope of the river (S)

can be derived from the longitudinal profile and used to estimate flow rate or discharge of river using Manning equation (Eq. 5.1).

The Manning equation, in terms of discharge (Q), can be expressed as:

$$Q = \frac{1}{n} W z^{5/3} S^{1/2} \qquad \text{Eq. (5.1)}$$

where 'z' is water height in river, 'S' is surface water slope, 'W' is width of river and 'n' is Manning coefficient. This equation is based on the assumption that river width is much larger than water height.

Since the perennial river beds contain water throughout the year therefore it is difficult to estimate the exact water height in reference with river bed from the altimeter observations but a part of water height (i.e. difference of high water and low water) can be obtained from the altimeter measurements. Using the altimeter derived water level, river surface waterslope, an important parameter for estimation of discharge using Manning Equation, can be determined by drawing the longitudinal profile of river.

The longitudinal profile of Ganga between the river mouth (i.e. Bay of Bengal) and Haridwar (Uttarakhand - India) is obtained using the elevation data estimated from the ENVISAT mission. The longitudinal profile of the Ganga is shown in Figure (5.6).

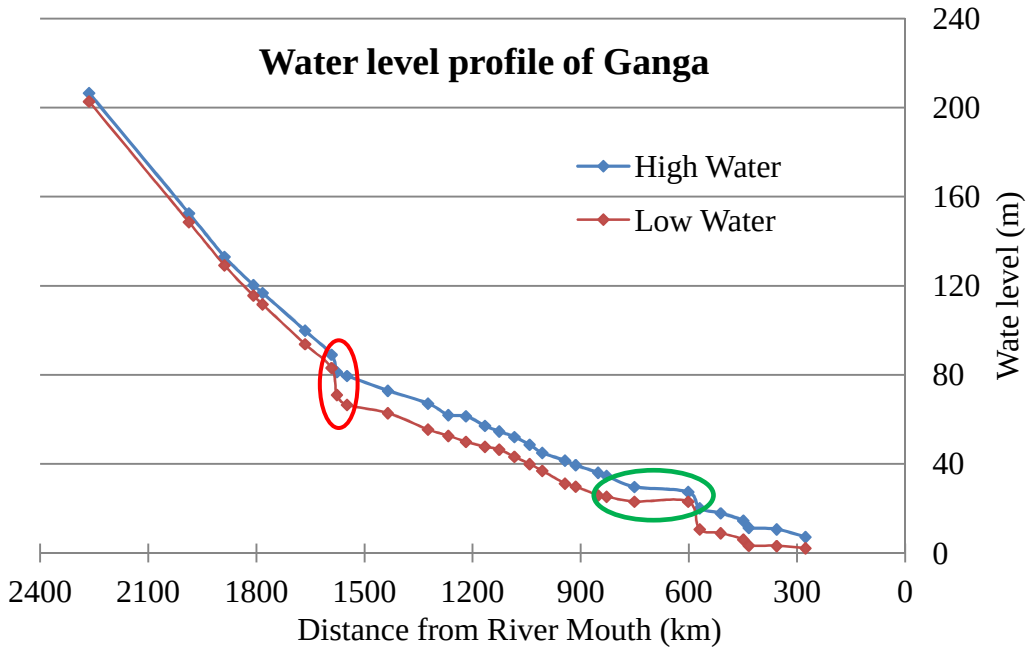

Figure 5.6: Longitudinal profile of high and low water in Ganga River.

The profile presents the high water (blue line) and low water (red line) across the river. At two locations, one at the Fatehgarh in Uttar Pradesh (UP) and other near the Farraka dam that are marked by red circle and green circle respectively on the profile, shows a shift in river bed slope. From the longitudinal profile it can be noted that the river upstream at Fatehgarh, marked by vertically elongated red circle, shows less variation in water surface height compared with downstream. In lower reach of river near the Farraka dam, marked by horizontally elongated green circle, it is observed that there is almost null slope which highlights the effect of water reservoir. Downstream the Farraka, the slope of river decreases further. The reason for shift of slope at Fatehgarh is certainly due to a succession of waterfalls. The waterfalls may be either due to change in geological terrain or structural faults.

Slope of river at different stretch of river is calculated from altimetry observations, for both high and low water level, and is presented in Table (5.2). The water level profiles present the decreasing trend of river water surface. Low water level profile has slightly larger slope compared to high water. The decreasing slope of river water surface corresponds to increase of flow.

Table 5.2: Slope of Ganga derived from altimeter observation

River Stretch	**Slope (m/km)**	
	High Water	Low Water
Upstream Fatehgargh (UP*)	0.17	0.18
Fatehgargh (UP) - Chhapara (BH)	0.06	0.05
Chhapara (BH) - Near Bhagalpur (BH)	0.07	0.07
Downstream Farakka	0.04	0.03

* UP-Uttar Pradesh, BH- Bihar

5.2 Water Level in Krishna and Godavari

The VS over the Krishna and the Godavari, at which the water level is calculated from altimetry data, are shown in Figure (5.7). The blue points represent the VS across the Godavari River and red colour points are across the Krishna river. These two rivers are joined by many tributories (see section 3.3.3 and 3.3.4) on their way to Bay of Bengal and have many dams across the rivers that control the natural flow of river which affect the water level and discharge. Further the water from these rivers is pumped out artificially for the purpose of irrigation. Other human interventions also lead to un-common variation in water level variations. The altimeter derived water level in these two rivers reflect the same behavior.

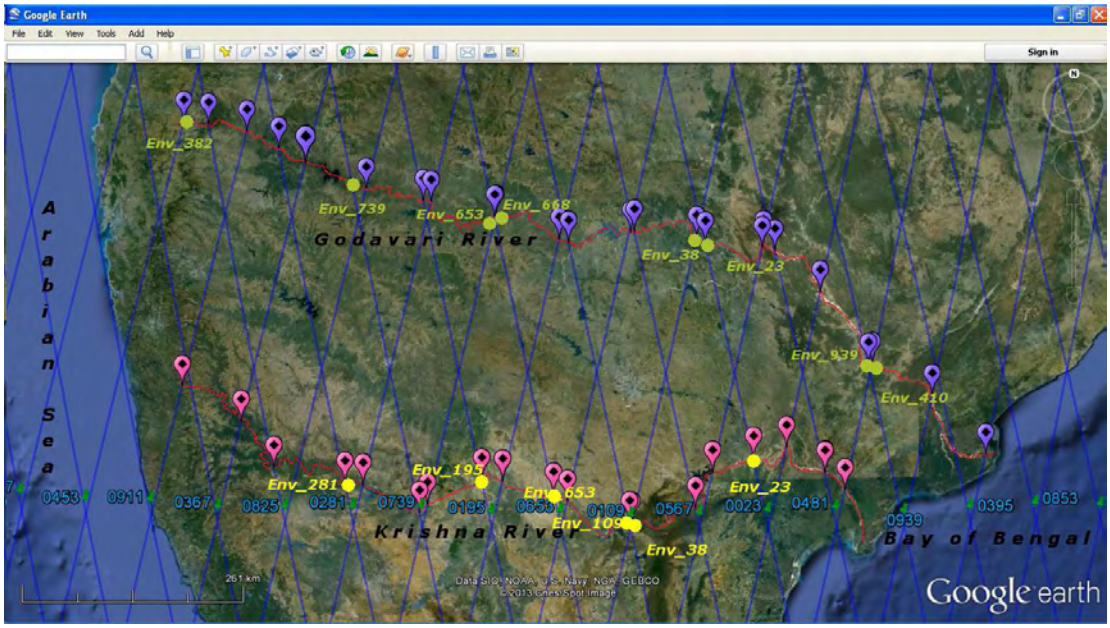

Figure 5.7: Virtual Stations over Krishna and Godavari rivers for ENVISAT mission.

5.2.1 Water Level in Krishna River

Figure (5.8) shows the altimeter derived water level variations at few locations, either close to dam or over the dam, in Krishna River, marked by yellow points in Figure (5.7). These time series show that the water level variations are not uniform through out the river. The VS that are significantly away from the dams show similar peak to peak pattern. However the water level variation across the river shows a corelation with southwest monsoon.

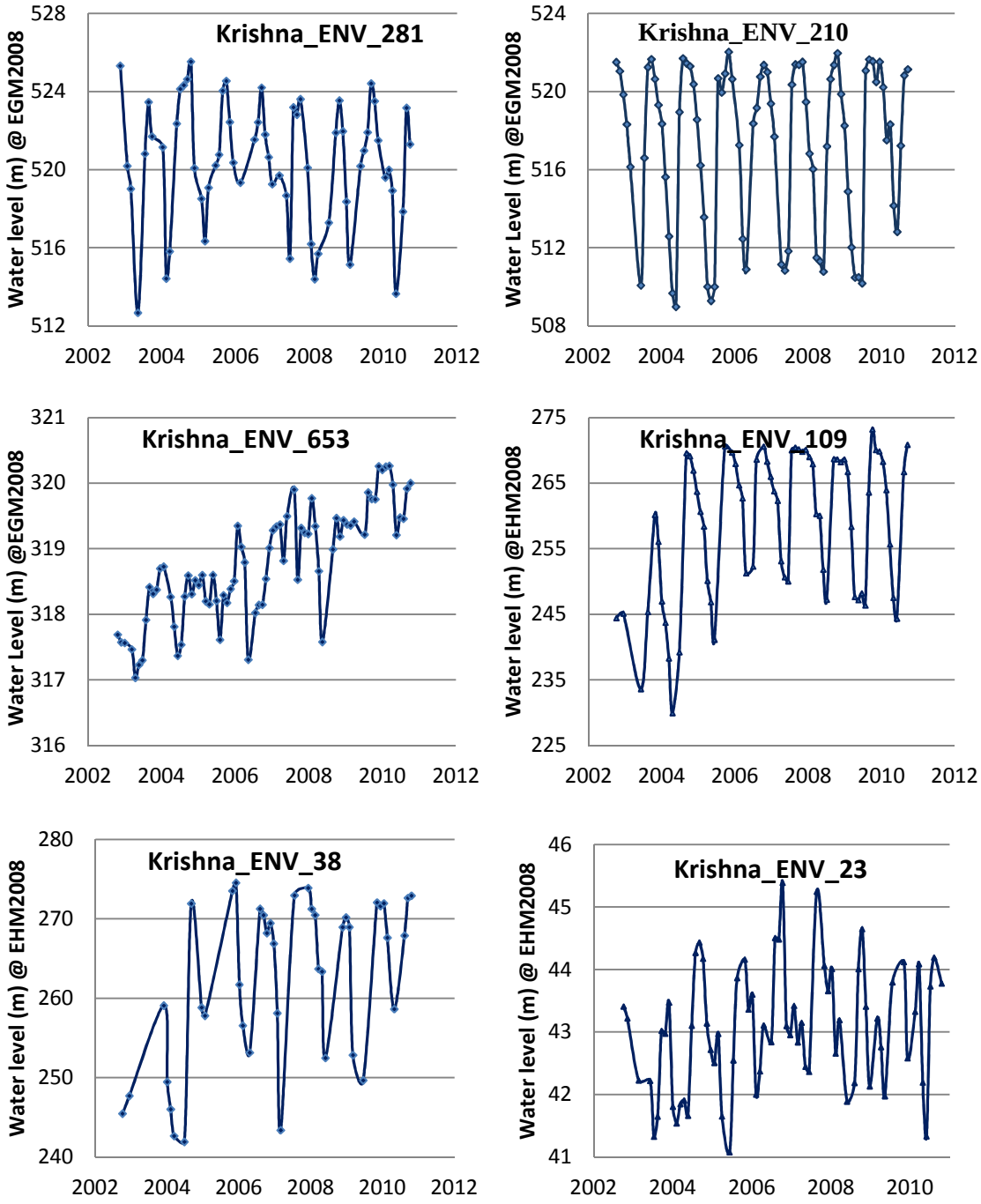

Figure 5.8: Water level variation in Krishna River from ENVISAT mission.

The ENVISAT track 281 and 210 cross the Krishna river before the Almati dam in Karnataka. The amplitude of the seasonal water level fluctuations is about 8 m at these locations. The track 210 is close to dam and the associated time series (Krishna_ENV_210) shows a good agrrement with water level variation from year to year. The time series for track 281 (Krishna_ENV_281) over the river also shows similar pattern but between 2004-2007.

The VS, Krishna_ENV_653, lay over the reservoir (1 km long). The reservoir was constructed in 1996 with primary objective to diminish the water scaracity in Mahabubnagar disctrict of Hydrabad under the Jurala project (India-WRIS Wiki). The water from this dam is used for drinking, irrigation and hydropower generation. At this location the water level variation is in order of 2 m but the low water level shows a increasing trend which can be intrepreted as increase in base flow. The Srisailam reservoir (built in 1980) stands about 100 km downstream to the Jural station. Before the Srisailam dam, the Krishna river is joined by one of its major tributary namely the Tungabhadra river. Many small tributaries join the Krishna river in between the Srisailam reservoir as it is spread over a long stretch of river.

The ENVISAT tracks 109, 38, and 567 cross the Krishna over the Srisailam reservoir before the Nagarjunsagar dam. The water level variation over these locations (for track 567, time series in appendix A1) show that the high water level is not affected but the low water level has increased post 2005. The water level variations for track 109 and 38 are shown in Figure (5.8). Sarna et al. [2010] has presented that the rainfall in Andhra Pradesh-India, which is the lower part of Krishna basin, is much below the normal rain during the year 1996 to 2005. They have also shown that post 2005 the region has received the normal or higher rainfall. A similar pattern in water level variation in time series for track 23 (Krishna_ENV_23) and track 954 (not shown in Figure) is also observed. These locations are downstream the Nagarjuna Sagar dam. The time series for track 23 seems to have less effected of water discharge, if any, from the dam and shows a more or less natural water stage variation.

5.2.2 Water level in Godavari River

The water level variation in Godavari river, marked by green circles in Figure (5.7) are shown in Figure (5.9). The time series are organized from upstream to downstream. The water level variation across the Godavari River show peak to peak similarity in amplitude for most of the cases but the water level variations are not uniform across the river. The non-uniform variation of water level in river can be argued that the water level at different locations in the river are affected due to variation of the river section.

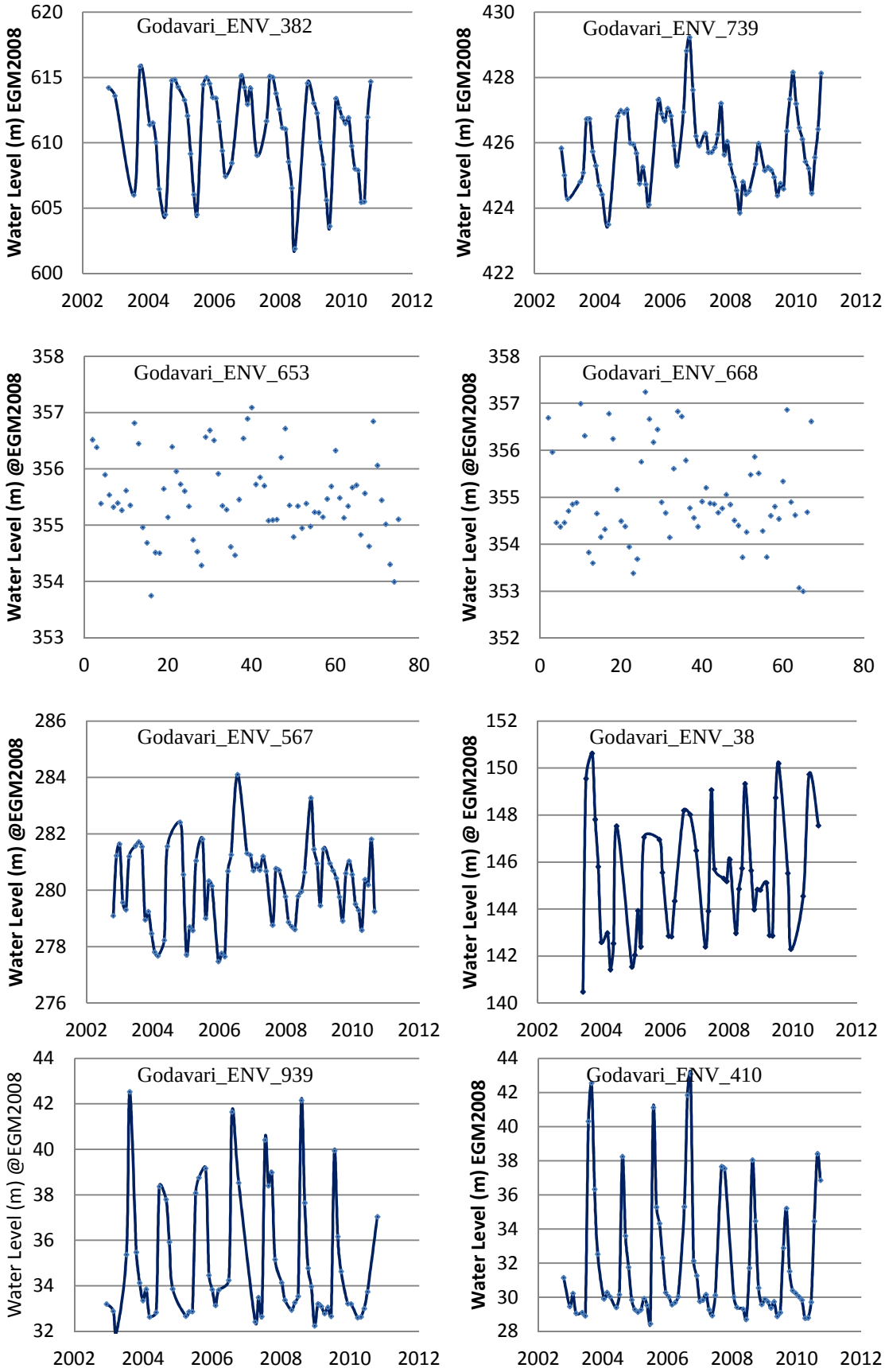

Figure 5.9 Water level time series in Godavari River from ENVISAT mission.

The ENVISAT track 382 crosses the Godavari river over the dam, constucted in 1965, in Gangapur town in Nasik District in Maharastra. The water stage time series over the dam is shown in Figure (5.9). The seasonal water level variation over this location is about 12m. The track 739 (Godavari_ENV_739) crosses the river about 22 km downstream the Nathsagar dam in Paithan in Maharatra. The wet to dry periods water level at location is 4m with a high event in year 2007. The track 653 (Godavari_ENV_653) and 668 (Godavari_ENV_653) cross the river further downstream in Maharastra and the inter-track distance between two is about 1 km. Before track 668, a small water channel joins the river. The altimeter derived water level show similar interannual variations across the river.

Further downstream of river in Andhra Pradesh, ENVISAT tracks 567 (Godavari_ENV_567) and 38 (Godavari_ENV_38) in vicinity of Ramsagar dam across the river. The water level varitions at the virtual satation close to dam has seasonal variation of 3-4 m whereas the water stage variation at comparatively distant VS is larger. The interannual water level variation in lower reach of river is in range of 6-8 m. The time series at track 939 (Godavari_ENV_939) and 410 (Godavari_ENV_410), intertrack distance is about 5 km, shows the good peak-to-peak amplitude variation in water stage. From above analysis, it is clear that water level variation in the Godavari river varies largely from place to place.

5.2.3 Longitudinal Profile of the Krishna and Godavari

Similar to the Ganga river, the longitudinal profile of the Krishna and the Godavari is drawn from the maximum and minimum water level derived from altimeter observation. The longitudinal profile of these rivers from the river mouth are presented in Figure (5.10). The blue line represents the high water in river whereas the red line indicates low water.

The profile shows a good similarity in high and low water level for Godavari compared to Krishna river bed. The differences between high and low water reflect the hydrological characteristics of the river. The geology of these river basins is affected by Deccan traps, and foothills of Vindhiyan, Dhrwar, Satmala and many other similar formations subsequently have an effect on the flow of river and subsequently the water level.

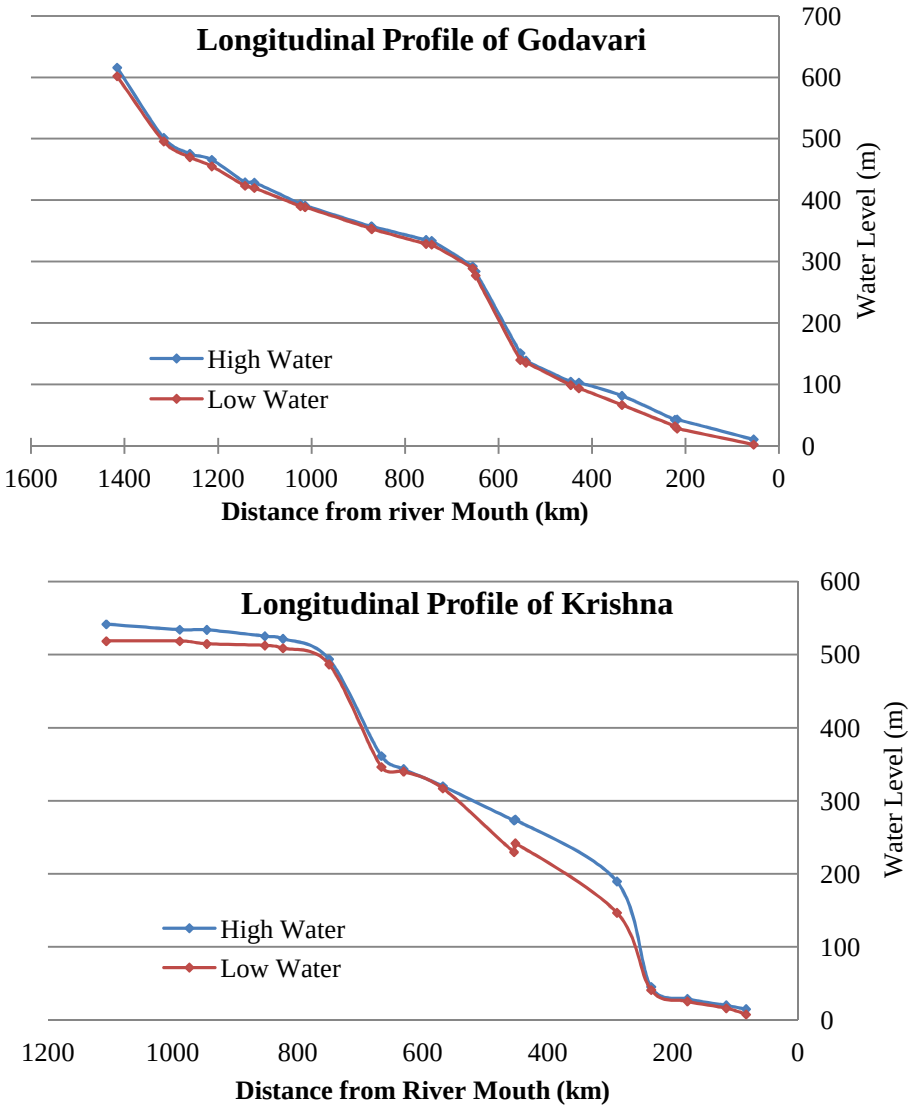

Figure 5.10: Longitudinal profile of high water (blue line) and low water (red line) of the Krishna and the Godavari River.

5.3 Altimeter Derived Discharge for Ganga - Brahmaputra River System

The Bay of Bengal is located in the tropical monsoon belt. Many major rivers e.g. the Ganga, the Brahmaputra, the Meghna, the Mahanadi, the Godavari, and the Krishna introduce large quantities of freshwater and silt into the Bay, especially during the monsoon season, from July to September. The discharge of Ganga and Brahmaputra is the third largest freshwater source to the world ocean, after the Amazon and the Congo [Dai et al., 2009]. The Ganga-Brahmaputra river system alone contributes about 40% of total discharge into Bay of Bengal [Sengutpa et al, 2006]. The available real time discharge data in this area is the coarse estimates of river runoff into the Bay of Bengal from hydrological models [Dai and Trenberth, 2002]. Dai et al. [2009] has estimated the stream flow for world's 925 largest rivers, using the combination of observations from in-situ gauges and simulations including the discharge of Ganga-Brahmaputra river system in Bay of Bengal till 2004.

Another approach to study the river discharge in several other regions in the world from using the remote sensing technique has been adopted by other workers over the Ob River in Siberia [Kouraev et al., 2004], the Amazon [Zakharova et al., 2006; Leon et al., 2006] or in Chari - Ouham confluence near the Lake Chad [Coe and Birkett, 2004]. Papa et al. (2010a) has used the altimeter data from T/P, ERS-2 and ENVISAT to derive the river discharge from Ganga and Brahmaputra for 1993-2008.

In the present study, JASON 2 data is used to extend the altimeter derived discharge for mid-2008 to 2011 using the approach adopted by Papa et al [2010a]. The JASON 2 data and other in-situ hydrological measurement are analyzed to derive the discharge from the outlet of Ganga and Brahmaputra in the Bay of Bengal. The work discussed here is taken from the article:

5.3.1 Datasets to Calculate Water Discharge

The in-situ hydrological observation in the Ganga-Brahmaputra Rivers in Bangladesh is obtained from Bangladesh Water Development Board (BWDB, http://www.bwdb.gov.bd/). These data sets are measured at Hardinge (hereafter G,

24.07_N; 89.03_E) over Ganga and at Bahadurabad (hereafter B, 25.15_N; 89.70_E) over Brahmaputra before they meet as shown in Figure (5.11).

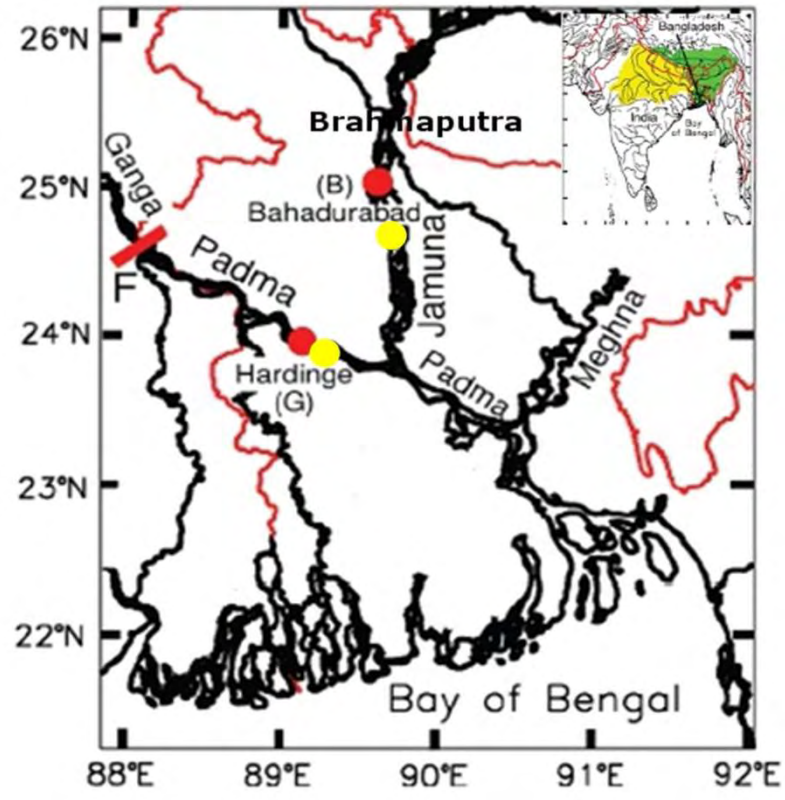

Figure 5.11: Schematic map of region of interest. Locations of the two in-situ gauging stations in Bangladesh: Hardinge (G) and Bahadurabad (B) are displayed with red dots. JASON 2 intersections are presented by yellow dots. The inset map shows the Ganga (yellow) and the Brahmaputra (green) rivers catchments [Papa et al., 2010a].

In-situ measurement comprises of:

In-situ Discharge: The Ganga-Brahmaputra discharge data is derived from the water level at both stations using stage-discharge relationships. Stage-discharge relationship is known as rating curve. The discharge data derived from rating curve obtained from measured stage and discharge value; hereafter we refer this data as "in-situ discharge" and are shown in Figure (5.12). This data has been available from 1993 to mid-2002 for Ganga with gap in early 2000, 2001 and 1993 to 2004 for Brahmaputra with gap of few days in October and November of 2003 and in September 2004. This data set is successfully used by Papa et al. [2010a] for deriving the monthly discharge from these rivers for a period of 2003 to 2008.

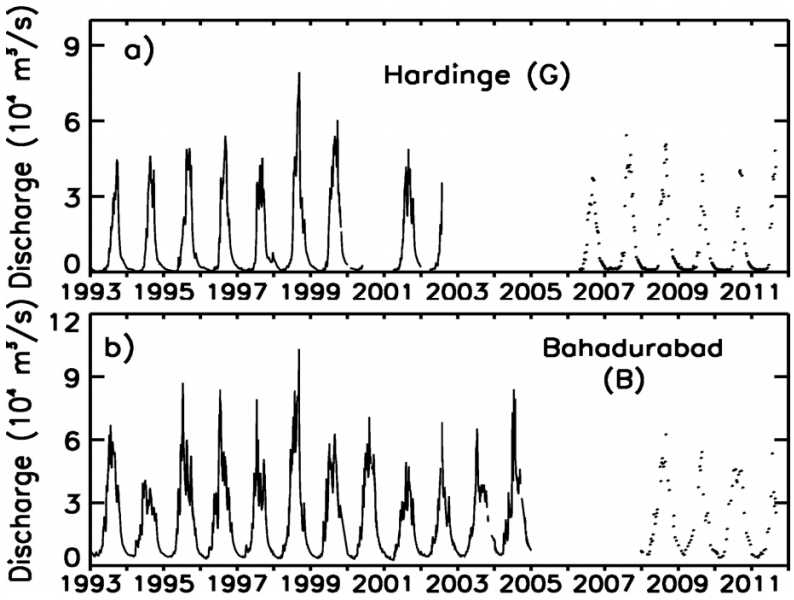

Figure 5.12: Time series of in-situ discharge: (a) discharge of Ganga River at Hardinge station and (b) discharge of Brahmaputra River at Bahadurabad station. Solid lines present in-situ discharge derived from water level whereas dotted lines are direct measured discharge [Papa et al. 2012].

(a) In-situ river water level: A large amount of in-situ water level measurement for gauging stations (858 measurements for the Ganga from May 2006 to August 2011 and 102 measurements for the Brahmaputra from January 2008 to August 2011) have been accessed during the study which are recorded at different time intervals. Papa et al. [2010a] has shown that for year 2007, 9 out 152 direct measurements coincide with ENVISAT and the comparison between these observations with a correction of 0.96 and a standard error of 0.26m that is much smaller than the variation of ~7m. The comparison of the in-situ measured water level and JASON 2 derived water level for year 2006 to 2011 shows better correlation between them. The comparison is shown in Figure (5.13).

(b) Direct discharge measurement: A direct measurement of river discharge coincident with in-situ water level measurement is also used in this study. These measurements are shown in Figure (5.12) by dotted lines.

The accuracy of these in-situ measurements is unknown. The difficulty in measurement of depth and velocity of stream further leads to an erroneous estimate of

the discharge from Ganga and Brahmaputra [Chowdhary and Ward, 2004]. The widely accepted accuracy for discharge estimation by community is in range of 10% to 20%.

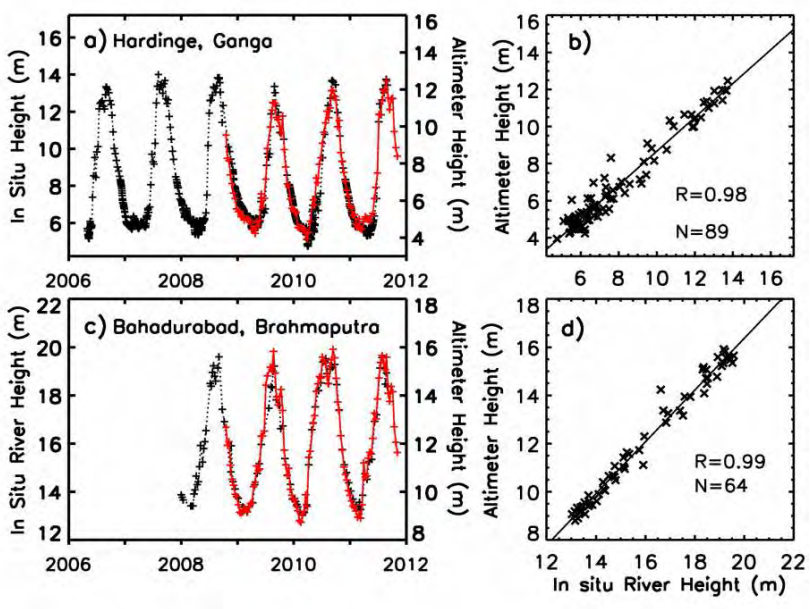

Figure 5.13: (a) Comparison of in-situ river level measurements (black line) at Hardinge Bridge with JASON 2 derived river level over Ganga River (red line). (b) Scatter plot of JASON 2 derived river heights versus the in situ river height over the Ganga. The linear correlation coefficient (R) and the number of points (N) are indicated. The solid line shows the linear regression between both variables. Figure (c) and (d) are analogue as Figure (a) and (b) for the Brahmaputra River (Bahadurabad Station) [Papa et al, 2012].

5.3.2 JASON 2-derived Water Level over Ganga and Brahmaputra

The JASON 2 derived water level time series at G and B are expressed with respect to reference level EGM2008. For comparison with in-situ measurement a simple statistics is carried out, i.e. the difference in absolute values, for the altimeter derived. The comparisons of these two data sets, shown in Figure (5.12), show good agreement and have similar peak to peak height variation. The water level in river at G and B are consistent with the seasonal cycle in Figure (5.13).

At Hardinge on the Ganga River from 2008 to 2011, there are 89 dates where in-situ measurements are coincident, within plus or minus two days apart, with altimeter derived water height. Similarly, for the Brahmaputra, there are 64 measurements simultaneously available for altimeter derived water height and in-situ

from 2008 to 2011 at Bahadurabad. The relationship between the satellite-derived river height and the in situ observations, shown in Figures (5.13b) and (5.13d), confirms a good agreement between the two data sets with a correlation of 0.98 and 0.99 for G and B, respectively. The estimated standard error is 28 cm for G and 19cm for H, typically in the range of accuracy of altimetric observations over large rivers (10–20 cm for instance over the Amazon [Frappart et al., 2006a; Birkett et al., 2002] or similar to the 26 cm found using ENVISAT over the Ganga in work by Papa et al. [2010a].

It is important to note that this accuracy strongly depends, among other factors, on the width of the river and on the morphology of the riverbanks. At VS G and H, the width of the river channel is always larger for the Brahmaputra than for the Ganga, which might partially explain the better accuracy of the river height measurements over the Brahmaputra than over the Ganga. Moreover, the gauging station and VS are not at same location but are apart from each other therefore it is not possible to have a perfect fit of these two data sets. The regression analysis between these two data sets is given by the below equations:

$$H_{JA2/Ganga} = H_{insitu/Ganga} * 1.04 + 0.86 \quad \text{Eq. (5.2)}$$

$$H_{JA2/Bhramputra} = H_{insitu/Bhramputra} * 0.94 + 4.97 \quad \text{Eq. (5.3)}$$

5.3.3 JASON2-derived Discharge of Ganga and Brahmaputra

5.3.3.1 Rating Curve

In hydrology, the river discharge is often estimated from river height using a one-to-one stage-discharge relationship [Rantz et al., 1982]. The relationship is known as stage-discharge rating or rating curve. This relationship is specific to each gauging station and its development is regulated by different national and international standards. Recently, Kouraev et al. [2004] have shown that there could be several relationships corresponding to different hydrological regimes such as low and high water stages or to rising and falling flooding periods for one gauging station. For instance, if the level-discharge relation shows highly scattered values then it is required to have a detailed analysis of the relation by splitting the data into subseries for different seasons and/or different level ranges. However, over large rivers e.g. the Amazon, it has

been demonstrated that the uncertainties resulting from the use of a single rating curve are smaller than the other sources of errors [Callède et al., 2001].

Further there are several factors which influence the estimation of discharge from water level which can alter the rating curve equation gradually or abruptly. These factors include the dynamics of river bed itself, various anthropogenic factors such as land use change, withdrawal of water. Therefore, it is necessary to update or recalibrate the rating curve time to time. This is particularly necessary for rivers such as the Ganga and the Brahmaputra which carry large volumes of flood water and sediments and may experience morphological changes. However, the study of Mirza [2003] on the evolution of the rating curves at G and H, for 1966 to 1992 period, conclude that the Ganga and Brahmaputra Rivers were in dynamic equilibrium during this period and the rating curves previously developed in 1966 were still valid till at least 1992.

Normally, the official rating curve is used to estimate the river discharge from satellite derived water stage but, in general, it is difficult to access the official rating curve or long term in-situ water level time series. In the study, a direct relationship between the available in-situ stage measurement and altimeter derived stage is established. This approach is also adopted for study over the Ob River in Siberia [Kouraev et al., 2004], the Amazon [Zakharova et al., 2006] and Ganga-Brahmaputra discharge in Bay of Bengal [Papa et al., 2010a].

The rating curve calculated from in-situ river discharge and simultaneous measured in-situ water stage at G and B is shown in Figure (5.14a) and Figure (5.14c) respectively. Similarly, the altimeter derived stage and in-situ discharge relation is shown in Figure (5.14b) and Figure (5.14d) for G and B respectively. There are 89 in-situ measurements at Hardinge during the period of 2006-2011 and 64 measurements at Bahadurabad for the period of 2008-2011. Both the rating curves at individual station show the similar pattern. Prior to the launch of JASON 2, there is anomalous discharge during the monsoon period in 2007 and 2008 (Figure 5.12) which is not accounted in the altimeter derived stage and discharge relationship. This kind of extreme event can raise high uncertainty in estimation of altimeter derived discharge beyond the range of measurement. There is high dispersion in scatter plot at Bahadurabad station which is argued as the difficulties in measurement of in-situ discharge in large and mighty river. This high dispersion leads to high uncertainty in discharge calculation. Following the

conclusion of Calléde et al. [2001], single rating curve is used to calculate the river discharge despite the high dispersion in scatter plot at B over Brahmaputra.

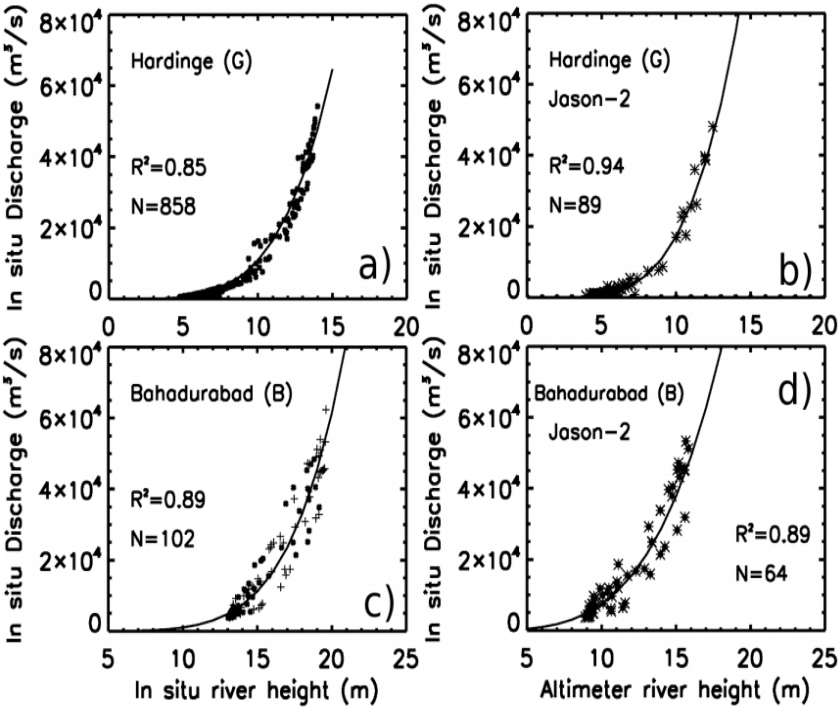

Figure 5.14: Rating curve at Hardinge over Ganga and Bahadurabad station over Brahmaputra. (a) and (c) present stage-discharge relationship from in-situ river height and in-situ discharge. (b) and (d) present scatter-plot of in-situ discharge vs. JASON 2 derived water stage [Papa et al., 2012].

5.3.3.2 JASON 2 Derived Discharge

Using the stage-discharge relationship, calculated from in-situ and altimeter derived stages verses in-situ discharge at G and B, the discharge time series is calculated at every 10-days for the period of 2008-2012. In the process of calculation of river discharge, the satellite derived water stage at both the stations G and H is adjusted using the regression analysis given in equation (5.1) and equation (5.2) with assumption of the conservation of flow at both the locations. The river discharge estimates using the various rating curve discussed in section (5.3.3.1) at G and B is shown in Figure (5.15). JASON 2 derived river discharge estimate for Ganga (Figure 5.15a) and Brahmaputra (Figure 5.15b) using in-situ rating curve (green line with plus sign) whereas same using altimeter derived rating curve (black line). The in-situ discharge is marked by red line. Blue line represents T/P, ERS-1, and ENVISAT derived river discharge [Papa et al.,

2010a]. The residuals (expressed as per cent of in situ discharge) at individual stations is calculated as the difference between altimetry derived discharge and simultaneous in situ discharges.

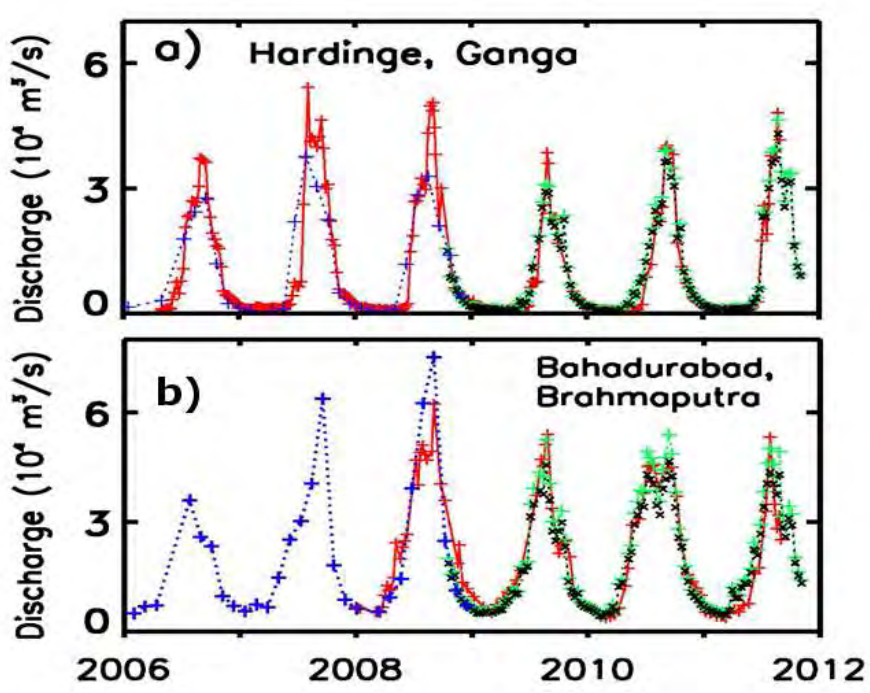

Figure 5.15: Comparison of altimeter-derived discharges and in-situ observed discharge. (a). River discharge estimate from JASON 2 using in-situ rating curve (green line) and discharge estimates from altimeter–derived rating curve compared with in-situ discharge observations (red plus, solid line). Blue line represents discharge estimate from ENVISAT [Papa et al., 2010a, 2012].

The river discharges obtained from the various sources at both the stations have an excellent similarity in terms of seasonal variation depicting the clear high and low discharge. The correlation of the derived discharges using the in-situ rating curve and altimeter derived rating curve with in-situ discharge at Hardinge over Ganga is 0.99 and 0.97 respectively. Similarly, the correction value between the derived discharge and in-situ discharge are 0.99 and 0.97 respectively. Though the comparison is made for short period (3 years), the year to year variation in derived discharge shows similarity with in-situ measurement. Double peak in 2010 for Brahmaputra is well recorded by both derived discharge as it is visible in in-situ measurement. The RMSD (root mean square difference) between JASON 2 derived discharge using in-situ rating curve and in-situ measured discharge is 1458 m^3/s while the RMSD between JASON 2 derived

discharges using altimeter-derived rating curve is 1652 m^3/s at Hardinge over Ganga. For Brahmaputra, the RMSD between the altimeter derived discharge using in-situ rating curve and altimeter derived rating curve with in-situ discharges are 2180 m^3/s and 2431 m^3/s respectively. The residual error in individual discharge at G and B (Figure 5.14b and 5.14d) is less than (+/-) 25 of in-situ discharge [Papa et al, 2012]. The mean error in different derived discharge (13%, and 14% for Ganga and 6.5% and 7.5% for Brahmaputra) using the altimeter derived rating curve and in-situ rating curve is well within the accepted range (10-20%) in discharge estimation. The estimated discharge for JASON 2 is better than discharge obtained by Papa et al (2010a) from T/P over Brahmaputra for period 1993-2001 and ERS-2 over Ganga for period 1995-2002.

Figure (5.14b) and Figure (5.14d) present the difference between altimeter-derived discharges using two rating curves as discussed in section (5.3.3.1). The error analysis shows that the residual of discharges derived using the stage-discharge relation is always smaller compared to the same obtained from in-situ derived stage-discharge relation, with a mean absolute difference of ~6% for Ganga and ~10% for Brahmaputra. The detailed statistical analysis of the work is presented in Papa et al. [2012].

5.3.4 Long-term Ganga-Brahmaputra Monthly Discharge Update

The JASON 2 derived river discharge at G and B is used to construct the long term, for period of 1993 to 2011, discharge time series which is an extension of the time series presented by Papa et al. [2010a]. The previous monthly discharge time series for period of 1993-2008 is combination of T-P–derived discharges for 1993–2001, ERS-2–derived discharges for 2002 and ENVISAT-derived discharges for 2003–2008. Since the JASON 2 derived discharge is estimated at every 10 days therefore for updating the long term monthly discharge time series, the JASON 2 derived discharge is averaged. The monthly mean discharge is obtained by averaging all the discharge, at every 10-days interval, within a month. The total river discharge for Ganga-Brahmaputra river system is calculated by summing the discharge for individual rivers. The updated monthly discharge with JASON 2 derived discharge of Ganga, Brahmaputra and combine discharge of the two are shown in Figure (5.16).

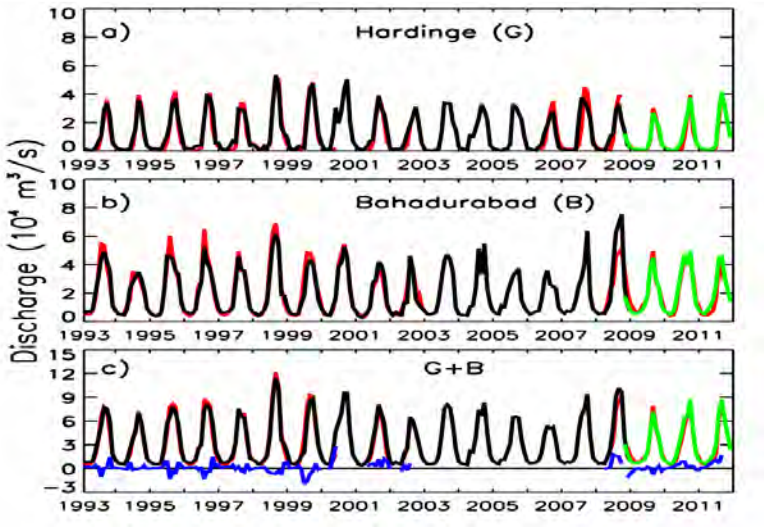

Figure 5.16: Altimeter derived monthly discharge time series. Discharge derived from T/P, ERS-2 and ENVISAT (black line) [Papa et al., 2010a] and discharge estimate from JASON 2 (green line) compared with in-situ observed discharge (red line) for Ganga (a), Brahmaputra (b) and combination of the two (c). The blue curve shows the residual i.e. the difference between altimeter derived and in-situ discharge [Papa et al., 2012].

The long term altimeter derived monthly discharges at G and B, along with updated one, have the similar seasonal and the interannual variations. The total river discharge of the Ganga-Brahmaputra river system (Figure 5.16c) has a similarity with dominant monsoon in the region with peak in August/September and shows large year-to-year variations in the magnitude of the peak. For the period 1993–2011 the mean aggregate discharge is ~32000 m^3/s with standard deviation of ~28000 m3/s. The annual maximum monthly discharge has a mean value of ~82000 m^3/s and a standard deviation ~14000 m^3/s for 1993–2011. Over the full-length record, the largest yearly peak of combined discharge in August and September of 1998 is ~115000 m^3/s (~120000 m3/s from in-situ observations) and the lowest occurs in 2006 with ~54000 m^3/s (no in-situ data to compare with).

For 2009–2011, more than 85% of the total discharges of Ganga-Brahmaputra river system are within 15% of in-situ total discharges of Ganga-Brahmaputra river system with standard deviation of the residuals (blue curve) is ~2900 m^3/s (~2700 m^3/s for 1993–2001). The mean error (defined as the mean of absolute value of the residuals) of monthly JASON 2 derived discharges of Ganga-Brahmaputra river system is 16% for 2009–2011 (~17% for 1993–2011) which is within the acceptable accuracy (15–20%).

5.3.4.1 Application of altimeter derived discharge of G+B

The accurate estimation of continent-to-ocean discharge has a key role in ocean related studies for example, sea salinity or sea surface temperature. Durand et al. [2007] and Vinayachandran and Kurian [2007] have studied the Ganga-Brahmaputra river system discharge by using the available runoff climatology [Dai and Trenberth, 2002; Fekete et al., 2000; Vörösmarty et al., 1996], a combination of climate-driven water balance model and in-situ discharge, when available. In order to estimate the flow at river mouth, the altimeter derived data set (black lines in Figure 5.17a) is adjusted to climatology from Fekete et al. [1999; 2000] (red line in Figure 5.17a).

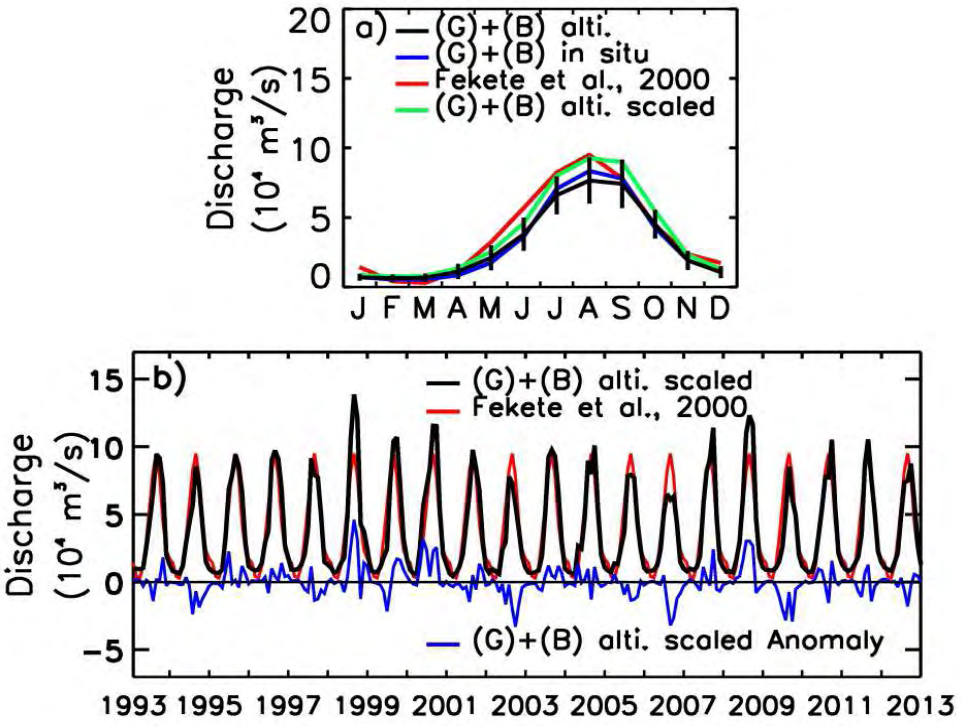

Figure 5.17: Climatology of Ganga-Brahmaputra river system. (a) Altimeter derived monthly discharge (black lines) of Ganga and Brahmaputra with standard deviation shown by vertical bars which shows monthly evolution of interannual variability; blue line present in-situ monthly discharge (1993–2001 and 2008–2010); red line is discharge estimate by Fekete et al. [2000]; the green line is the same as the black line, after applying a scaling factor of 120.5%. (b) Scaled-altimeter-derived discharge (black line) and discharge estimated by Fekete et al. [2000] (red lines), blue line is residual discharge (difference of 19 year mean monthly value from individual months) for altimeter derived results.

Although they have similar pattern, but the altimeter derived discharge is lower than the estimate of Fekete et al. [1996; 2000]. The difference can be explained by the fact that the latter integrates the entire Ganga and Brahmaputra watersheds and includes the contribution of local tributaries and precipitation downstream of Hardinge and Bahadurabad.

Conclusion

This chapter has presented derivation of water stage from the altimeter observations onboard the various satellite missions. The water level derived from the altimetry data has an advantage of giving the water level with respect to a common reference, e.g. ellipsoid or geoid, compared to conventional in-situ measurement. This data, over almost two decades, has free access for scientific community which is another advantage. But the disadvantage of altimeter derived water stage is that it does not provide the daily estimate of water level. This information can be used to estimate the discharge, longitudinal profile and slope of the river with certain uncertainties because of larger time interval, which is mission temporal coverage dependent. The altimeter derived water height can also be used for estimating the discharge. Therefore, it can be concluded that altimeter derived river height provides a supplementary input for different hydrological studies for unconventionally accessible region and the region where data is not easily available.

Chapter 6

Surface Water Analysis

Introduction

Inundations along the major rivers play a significant role in their hydrological [Alsdorf et al, 2001; Richey et al, 1989]. They affect not only the transport of water and sediments but also have an impact on the socio-economics of the region, for example, the loss of standing seasonal crops, human lives etc. [Hamilton et al, 2002]. During inundation, the water is not only delayed in its flow towards sea but exposed for high evapotranspiration too. The flooded regions are temporarily or permanently connected by the rivers and the water carried by the rivers determines the potential water volume in flooded areas. Other hydrological inputs such as rain and inflow from nearby catchment add flood water volume.

The determination of spatial and temporal variation of stored water volume in floodplains of the large river basins has great importance in hydrological studies. The measurements of the hydrological inputs by the conventional methods are quite difficult in such condition. Therefore, in the light of all these factors, the dynamics of the flood and the water level of main river channels, tributaries and associated floodplain are important for hydrological studies [Alsdorf et al., 2000]. Remote sensing observations have been successfully used as complimentary for hydrological inputs in hydrological studies [Frappart et al., 2005; Hess et al., 2003; Frazier et al., 2003; Töyrä et al., 2001; Smith, 1997; Mertes et al., 1995]. The spatial and temporal patterns of inundation areas can be indentified from multi-temporal satellite images: visible/infrared (IR) or Synthetic Aperture Radar (SAR) sensors are used to delineate floodplains. The capability and applicability of radar altimetry for monitoring the water stage over various water bodies has been demonstrated [Crétaux et al., 2011c; 2005; Crétaux and Birkett, 2006; Birkett et al. 2002; Birkett, 1998].

India is an agriculture based country and a large part of the country is covered by vegetations: seasonal crops like wheat, maze, paddy and annual crop like sugarcane. There are many regions in India covered by dense vegetation and very often

are affected by flood almost every year. The northern part of India, especially Bihar is one such flood prone region which is drained by many mighty rivers i.e. the Ganga, the Kosi, and the Gandak. In the southern part of country, a large area is under threat of reoccurring flood within the Krishna and the Godavari catchment.

In this chapter, an analysis of remote sensing imagery data is presented to identify surface water extent and study of flood dynamics. The datasets used to carry out this work comprise of:

- MODIS image for Land cover classification and identifying the inundation
- Altimeter measurements from ENVISAT
- In-situ precipitation measurement, especially in Kosi basin and TRMM precipitation
- VEGEATATION/SPOT data for snow cover analysis

6.1 Method for Estimating Surface Water Extent

Land cover classification is important factor in analysis of continental hydrology. Smith [1997] has discussed the use of remote sensing for mapping the inundation. NDVI based classification is most widely used for land cover classification among several methods (i.e. K-mean, maximum likelihood classification (MLC), etc.). Using the combined use of NDVI and band 5 of MODIS, the land cover is classified into five categories namely, open water, surrounded by water (Hereafter Island), dry land, aquatic vegetation and vegetation.

6.2 Land Covers Classification in lower Ganga

The MODIS images are processed to monitor the variation of land cover in lower catchment of Ganga: 23°N to 26.6°N latitude and 84.7°E to 90.8°E longitude for a period from February, 2002 to May, 2010. This region receives the water from Ganga, its tributaries and Brahmaputra in India and the Meghna and the Jamuna in Bangladesh. During the South-West monsoon, these rivers carried huge amount of water and spill in the low lying area along these rivers. The spillage of water along with high rainfall in respective area creates desolation in region.

The variations of different land cover in the lower catchment of Ganga are shown in Figure (6.1). The amplitude of land cover variations is similar in all the land cover classes except for vegetation at different time. This is one of the most fertile regions in India and two or three crops are produced each year. Therefore, the crop covered area

(vegetation) varies from year to year and within a year too. The main crop in the region is sugar cane, wheat, paddy among many other that are cultivated at different time period of a year. The sugar cane is cultivated annually whereas the paddy (mostly in June/July to November/December) and wheat (October/November to March/April) are seasonal one.

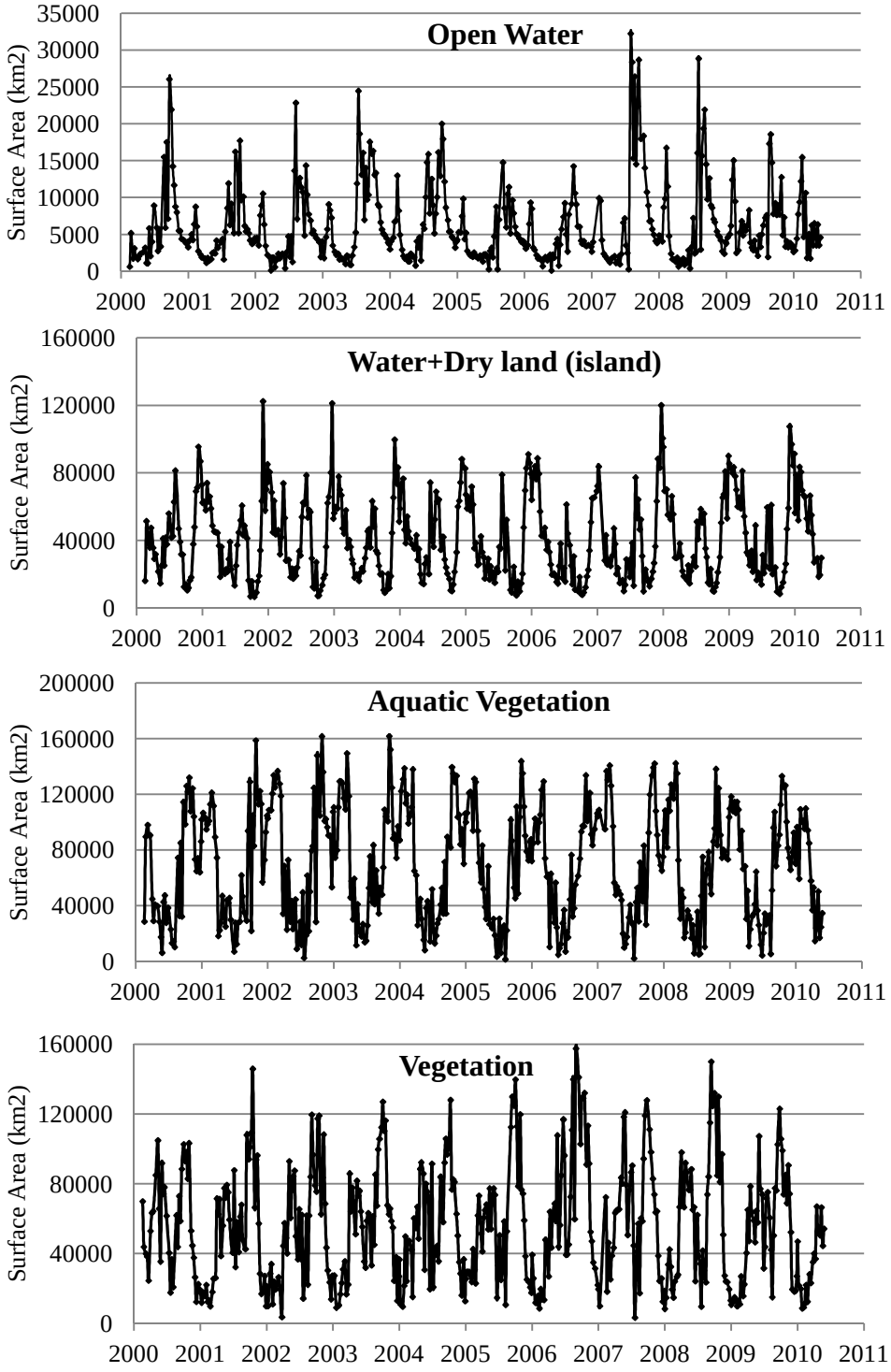

Figure 6.1: Land cover classification in Lower Ganga basin from MODIS data.

The total surface covered by open water, wet land or aquatic vegetation depend upon water carried by river or rainfall especially during monsoon. The land cover classification shows that year 2007 has been an exceptional year and large part of study region, almost double from previous year, is covered by open water. The analysis also reveals that large part of study region is under water logging in period of July to August which is the period when there is high rainfall in the region. During the dry period of a year, in months of May-June, the water covered part of study region is negligible but not zero because still there is water in the river bed. The aquatic vegetation covered surface and island area have a more similar year to year pattern. In the beginning of year 2008, a large part of area is identified as island which can be argued as the extension of regression of flood in the region.

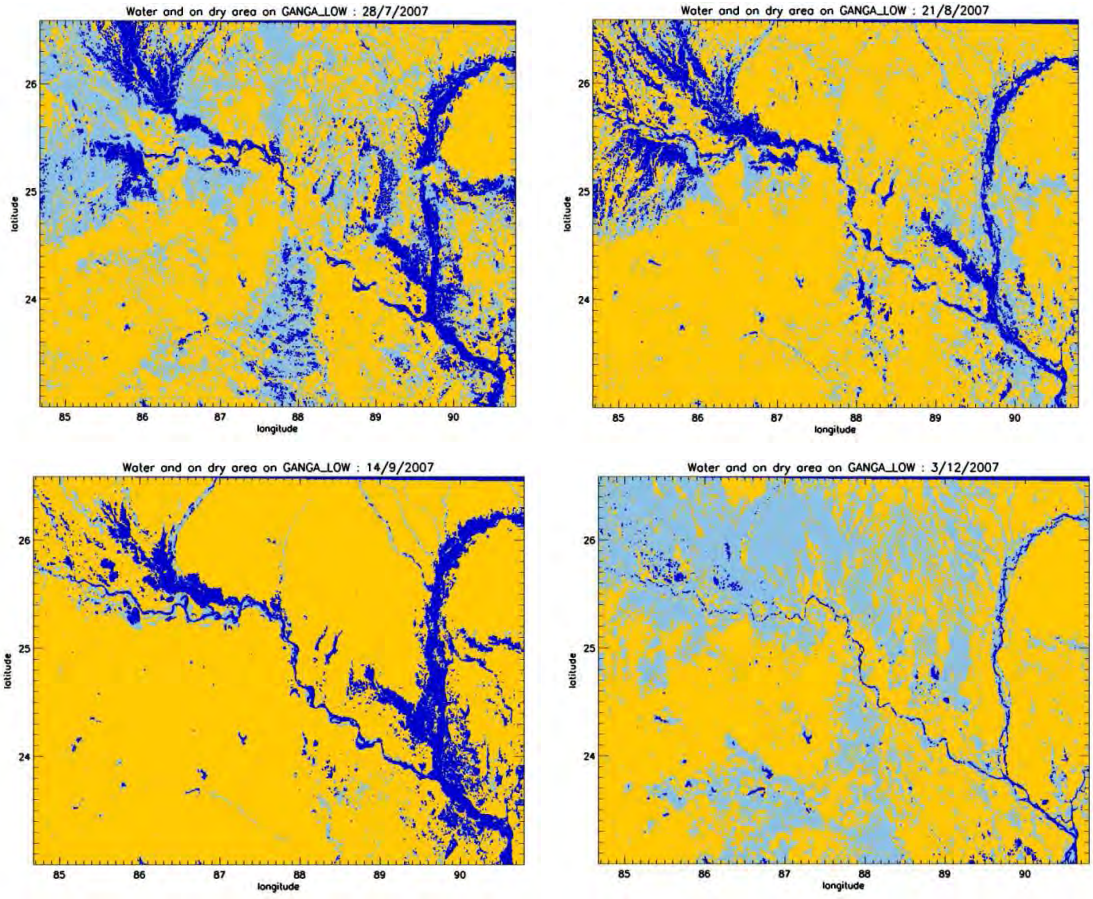

Figure 6.2: Land cover classifican: Open Water (dark blue) and island (light blue) with background in yellow color

Virtually all the rivers of the Indian sub-continent have long histories of floods along with its coast. Most commonly floods occur from heavy monsoon precipitation between June to September when natural watercourses do not have the capacity to

accommodate and carry excess water. The analyses of MODIS images show that different part in the lower Ganga basin is under the inundation during the summer monsoon period. The classification of land cover in this region in terms of open water and island is shown in Figure (6.2) for 2007.

6.3 Flood in Kosi sub-basin

The lower catchment of Ganga flows through major parts of Uttar Pradesh, Bihar and West Bengal in India and some parts of Bangladesh. The Kosi sub-basin in lower catchment of Ganga in Bihar region is one of the most flood affected region. The flooding in this region has become an annual feature. Kale [1997] has shown that this region has suffered the highest number of flood events in past few decades compared to other part of India. According **to** Flood Management Information System of Bihar (FMIS, Water Resource Department of Bihar, http://fmis.bih.nic.in), about 73% of the Bihar area is under the reoccurring flood during monsoon period every year.

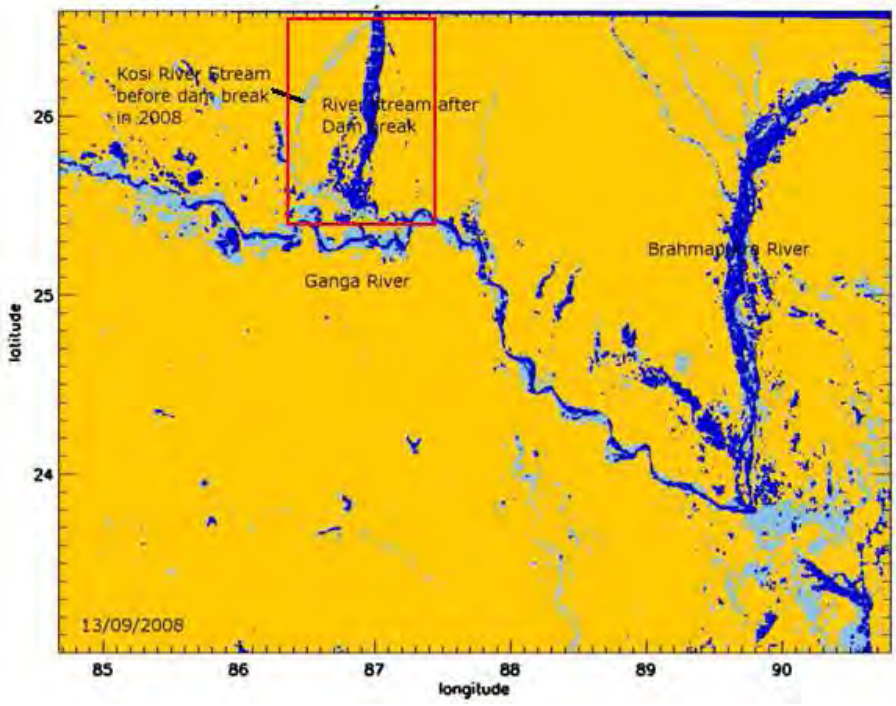

Figure 6.3: Flood in Kosi basin in 2008 within red rectangular box: open water (dark blue) and land covered by water (light blue) with yellow background.

The morphological setup of the Kosi is unique and has upland-to-plain area ratio as 5.25, highest among the modest-size river [Sinha and Friend, 1994]. Kale [2008] argued that plain area in Kosi basin, which is $1/5^{th}$ of total basin area, does not accommodate the enormous runoff (52 x 109 m^3) generated by 84% of the catchment area which leads

to flooding in the region during the monsoon period. The river after flowing in mountainous terrain exits in plain of North Bihar and form one of the world's largest flat alluvial fan [Agarwal and Bhoj, 1992]. The Kosi channel, downstream of the exit-point is very wide, shallow and highly braided. The river carries high sediment along with its flow [Sinha, 2009] and with passage of time the active channel is silted up and takes a new course. This area is also affected by discharge variation because of the occurrence of heavy rainfall as result of 'monsoon breaks': a unique meteorological phenomenon of the Indian monsoon, over the Himalaya and foothills regions [Kale, 2008]. All these factors for Kosi River create unfortunate favourable condition to produce severe flood in lower part of Kosi in plains of Bihar.

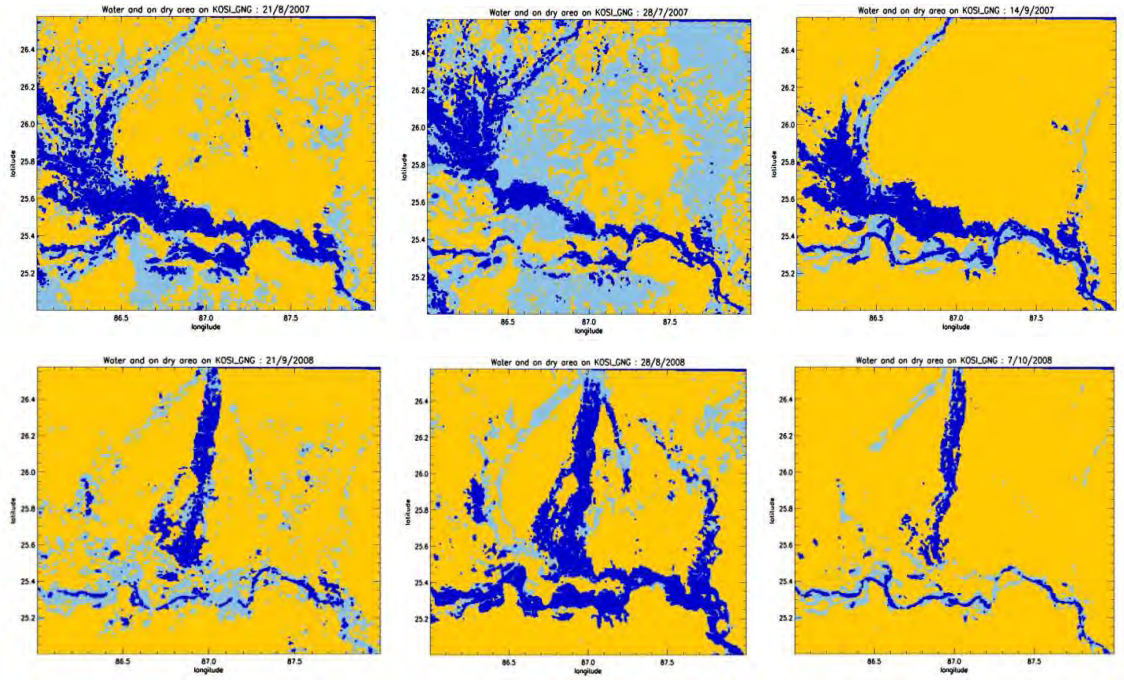

Figure 6.4: Flood in Kosi region: upper row is representing the flood in 2007 whereas the lower is same in year 2008. Blue is open water and light blue is land area covered by water with yellow as background.

The analysis of MODIS images show that during the year 2007 and 2008 a large part of lower Kosi basin is under large flood. The basic differences between these two floods are that in 2007 the flood water was spill in the area along the river course whereas the flood is 2008 was triggered by the breach of levee on eastern embankment of the Kosi. But both the floods have occurred during the monsoon period. Figure (6.4) shows the flood water (blue colour) in these two years. The 2007 flood (upper row in

Figure 6.4) water was spilled over the area located between in Kosi and Ganga whereas the 2008 flood (lower row in Figure 6.4) was in the alluvial fan of Kosi.

6.4 Kosi Flood in 2008

Normally the floods in Kosi basin occurs along the river channel but in year 2008, the north Bihar in this region (red box in Figure 6.3) has suffered a severe flood triggered by the breach of a levee on the Kosi River. The levee was breached on 18th August, 2008 near Kusaha in Nepal; 12 km upstream on eastern embankment and the river water took a straight path midway in Kosi alluvial fan. A Study on this event is presented here from a suite of space based observations from radar altimetry, MODIS images and TRMM precipitation, together with in-situ monthly precipitation with main emphasis on the results from altimetry and MODIS data using the methodology discussed in section (4.2.2). This study discusses the forcing factors of flood and evaluates the surface water extension and water height over water longed area. This study is submitted in International Journal of Remote Sensing (IJRS).

*"**R. K. Pandey**, J. F. Crétaux, M. Bergé-Nguyen, V. M. Tiwari, V. Drolon, F. Papa and S. Calmant, (2014). Water Level Estimation by Remote Sensing for 2008 Flood of Kosi. International Journal of Remote Sensing, 35(2): 424-440, doi: 10.1080/01431161.2013.870678"*

6.4.1 Study Area and Methodology

The study area, lower Kosi basin, is located between 86.5° E to 87.5° E longitude and 25.3° N to 26.6° N latitude and spreads within many districts that fully or partly fall within the study area. The study area is shown in Figure (6.4) illustrating the altimetry tracks over the Kosi basin and districts of Bihar. Snow data over the upper catchment of Kosi basin which lies within Himalaya between 85° E to 90° E longitude and 26° N to 30° N latitude is also used during the flood analysis. The methodology used in this study to evaluate the dynamics of the flood has been presented elsewhere in thesis manuscript in chapter 4.

6.4.2 Datasets

6.4.2.1 Altimetry Data

The plain area of Kosi river basin is crossed by three ENVISAT (green line in Figure 6.4) and one JASON – T/P (red line in Figure 6.5) tracks but only track 696 and

track 967 of ENVISAT mission cross the flood plain. Therefore, the result derived from these two ENVISAT tracks is presented in here.

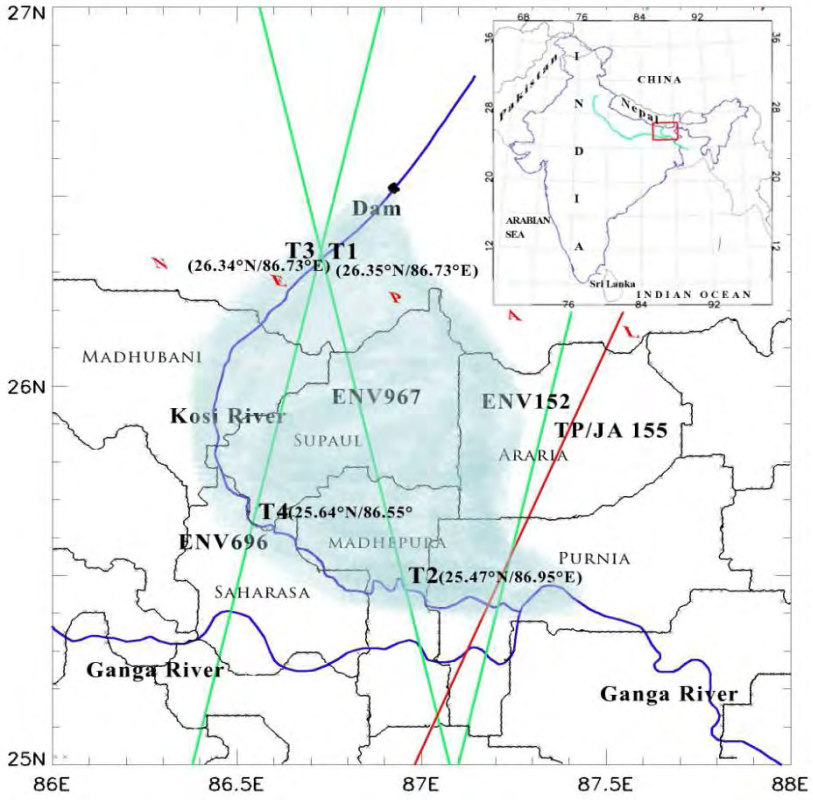

Figure 6.5: Schematic location map of study region: Area within red rectangle, in inset, is the study area. Blue shaded area approximately represents lower Kosi Basin. District boundary is presented by Black lines; Green lines represent ENVISAT ground tracks whereas red line represents T/P or JASON track. Point T1 and T2 for track 967 and T3 and T4 for track 696 are the crossing point (VS) of ground tracks over Kosi River (thick blue line) where water levels are calculated.

Following the results given in Frappart et al. (2006a) and Santos da Silva et al. (2010), the high frequency (20Hz) ranges derived from the ICE-1 algorithm is used in this study. At the intersection of ENVISAT mission over river bed at points marked by T1 and T2 for track 967 and points at T3 and T4 for track 696, the water height variations are calculated using the VALS tool. Water height variations from altimeter data at these locations are shown in Figure (6.6) and are in order of 3m to 7m from upper to lower reach of river. A high water is observed in mid-August or early September whereas the low water is in May/June. Because of internal instrumentation correction onboard the ENVISAT satellite, there is a data gap for the descending tracks between mid-2004 to start of 2007. Therefore, no water level is available for this period

for track 696 at VS T3 and T4. The water height in 2008 is highlighted by red colour in time series.

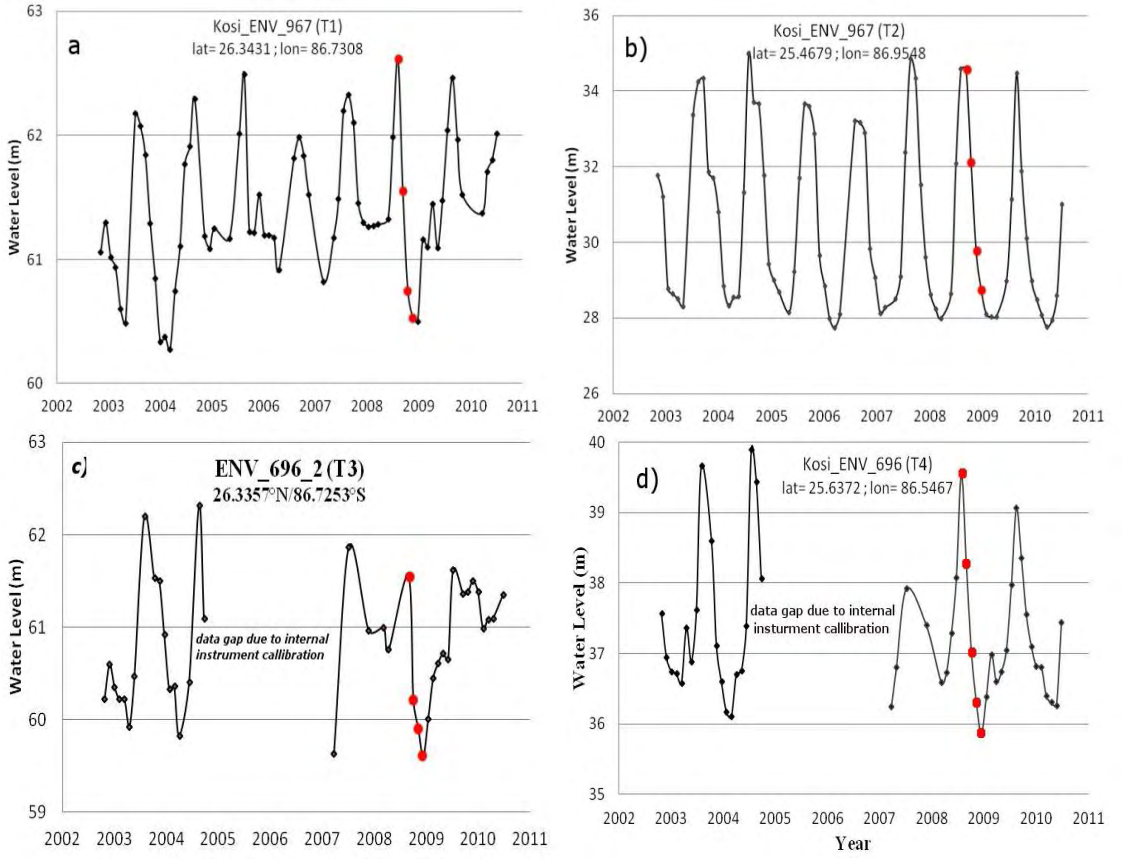

Figure 6.6: Altimetry derived water stage (with ref. to EGM2008) for track 696 and 967 of ENVISAT. Red points highlight ENVISAT measurements acquired after the breach of upper Kosi levee in 2008.

There is a sharp decrease of water level at VS T1 (ENV_967_2: 26.35°N/86.73°E) and T3 (ENV_696_2: 26.34°N/86.73°E) after the breach in levee in 2008 in upper reach of river. For example, the amplitude of annual water level variation is dropped by about 70% in consecutive observations at T1 during the month of August and September in 2008. Similarly on track 696 at T3, there is also a sharp decrease in two consecutive observations. A decreasing pattern is observed downstream, at VS. But there is no abnormal change in water level variation at T2 on the lower part of river, compared to other years. This is because the flood water joined the river bed back again after flowing though the flood plain (Figure 6.3).

6.4.2.2 MODIS Data

The water covered pixels classification, from MODIS images, is performed over the study area (Figure 6.6). The blue colour is water covered area in study region during

the 2008 flood. The morphological study of the Kosi basin shows that there is a gradual decrease in elevation in the lower part (Kale, 2008). This gradient variation from 22 cm per km near the Indo-Nepal Boundary to 7.5 cm per km near the confluence of Ganga River (Report, 2010) favours the rapid spill of the flood water over the plain area. There is very rapid increase in area under water from 20th August and 28th August and the maximum area under water continues in September. This period corresponds to the sharp decrease in water level in Kosi River (Figure 6.6). The maximum area under water found is ~2900 km^2 on 5th September. The flood water regression starts after mid-September but continues for longer time period (Figure 6.8(b)) and, in the analysis of MODIS images, a small area under water has been found till December, 2008.

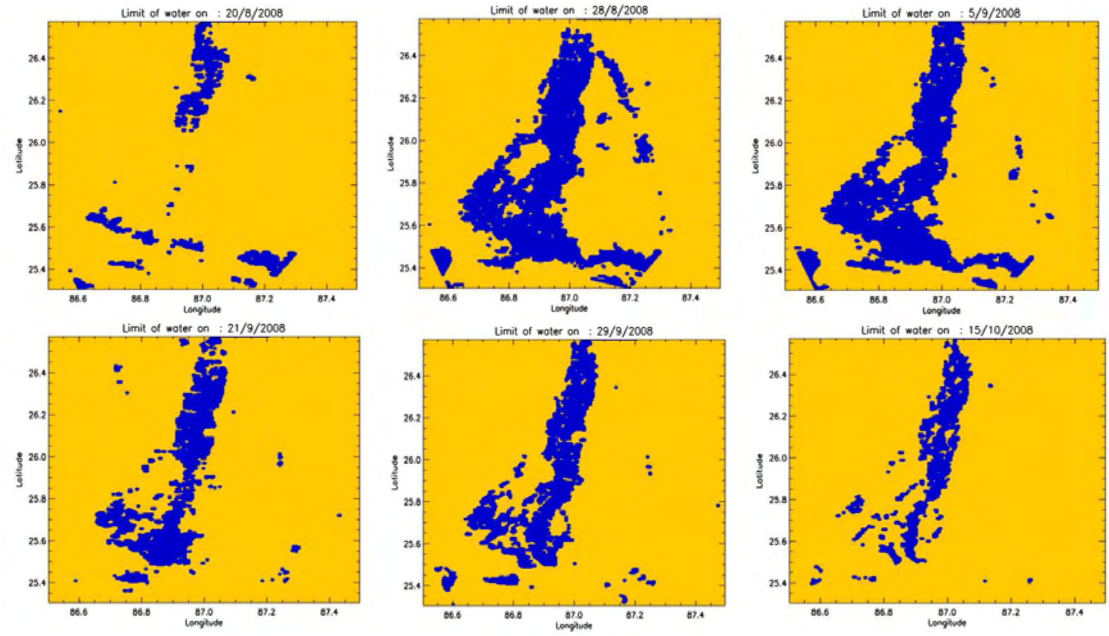

Figure 6.7: Progression and regression of flood water in lower Kosi Basin. Water spillage starts after breach in levee on 20th August. Maximum spillage is around 2900 km^2 on 28 August.

The long term time series shown in Figure 6.8(a) generated from the MODIS observations reveals that the flood is larger in 2008 in comparison to the recent flood events. The observations from MODIS sensor may not be very accurate during cloudy condition as there is less visibility at that time but it provides a fair amount of data sets for flood analysis. The water covered area obtained in this study is less compared to the observation made by Singh et al. (2011) from RADARSAT data. It can be noted that the inundated area is almost double from previous years flood. Figure 6.8(b) shows that the monthly variations of water extent (red line) for 2008 flood during the monsoon period

is larger and last longer compared to mean flooded area (blue line) for last 10 years during the same period. We also show in Figure 6.7 that there is rapid increase of water logged areas in the first 10 days. There is also a small high peak of inundation area, in the 2008 flood as well as in the mean for the last decade, which can be an effect of high precipitations in early monsoon in small part of the catchment (Figure 6.9).

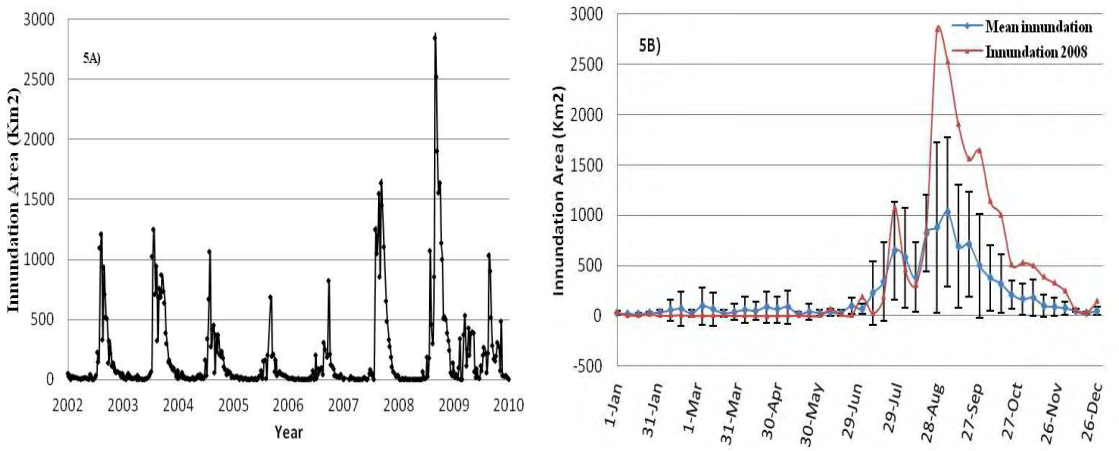

Figure 6.8. Inundation area variation from MODIS obeservations in the lower Kosi basin (a). Water covered area during flood period (b). Monthly variations of inundated area. Red line represents the 2008 flood event. Blue line represents average of inundated surface in past decade, with standard deviation error bars.

6.4.2.3 SPOT-Vegetation Data

The water from snow melting is one of the sources of water to the Himalayan Rivers. Kosi is one such river that is affected by the snow melting in mountains along with rainfall in upper catchment. In order to study the flood of Kosi in north Bihar, the snow data in the upper catchment of Kosi is processed to see the impact of water from melting of snow on the flood water. The snow data, VGT-S10 products, is obtained from SOPT-VEGETATION (http://free.vgt.vito.be/) mission from two satellite sensors VGT 1 (onboard SPOT 4) and VGT 2 (onboard SPOT 5) for hydrological year 1998-1999 to 2010-2011. The VGT-PS-10's products in this study are computed from all the passes on each location acquired during 10 day periods. The VGT-S10 product is built on the Maximum Value Composite principle that allows selecting the pixels for which the reflectance of the date has maximum Normalized Difference Vegetation Index (NDVI) which reduces the interference of cloud cover on observations (Xiao et al, 2002). This data set has a 1Km x 1Km spatial resolution.

The Normalized Difference Snow Index (NDSI) and Near Infrared (NIR) channel value of SPOT-VGT are used jointly to identify the snow covered pixels. NDSI is directly linked to area percentage of snow in kilometre. A threshold value of 0.35 for NDSI, which is smaller compared to NDSI value used by Xiao et al (2002), is used to identify the snow-covered pixels. The smaller threshold value of NDSI minimizes the error in determining the snow cover area in start of hydrological year i.e. June. A value of 0.17 is set to threshold value for NIR to eliminate the wet snow and aloft lakes. The NDSI is calculated using B0 (red), B2 (blue) and NIR bands.

$$\mathrm{NDSI} = \frac{\frac{\rho_{B0}+\rho_{B2}}{2}-\rho_{NIR}}{\frac{\rho_{B0}+\rho_{B2}}{2}+\rho_{NIR}} \qquad \text{Eq. (6.1)}$$

The NDSI variation, i.e. snow cover area variation, in upper catchment of Kosi for period of 2002 to 2010 is shown in Figure (6.9).

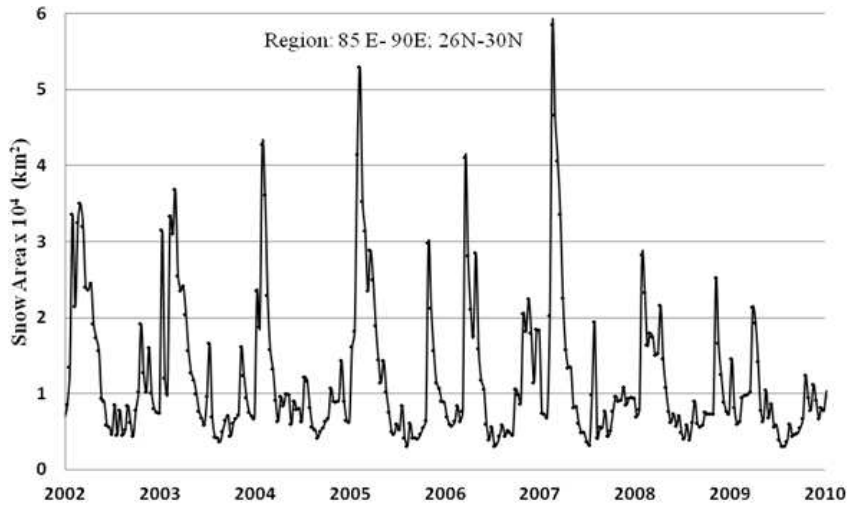

Figure 6.9: Snow covered area in upper catchment of Kosi basin laying in Himalayan.

This analysis of snow cover observation from SPOT- VEGETATION shows that there are no anomalous variations in snow covered area in 2008. This indicates that there is no evidence of excess of snowfall happened during the winter preceding and therefore it has no significant contribution into the water fed to dam and subsequent to the flood.

6.4.2.4 Precipitation Data

Precipitation from Tropical Rainfall Measuring Mission (TRMM) and in-situ precipitation data are used in this study to complement the results obtained from

MODIS and Altimetry observations. The daily TRMM precipitation (product name: 3B42 v7 derived) data over the lower and upper Kosi basin is analysed using web based analysis tool TOVAS (TRMM Online Visualization and Analysis System) from Giovanni application which is developed and maintained by Data and Information Services Centre of Goddard Earth Sciences of NASA (http://disc.sci.gsfc.nasa.gov/precipitation/tovas/). The monthly district wise in-situ rainfall data for a period of 6-years from 2006-2011 is obtained from India Metrological Department (IMD, http://www.imd.gov.in/section/hydro/distrainfall/bihar.html). These in-situ data are arithmetic average of precipitation from a number of rain gauges available in respective districts. This dataset is not very consistent throughout the year but it is available for June to October. The rainfall data which is considered for the analysis has been taken for the Supaul, Araria, Madhepura and Saharasa districts (which were the area most affected by the flood in 2008) and the Khagaria districts in Bihar (Figure 6.5).

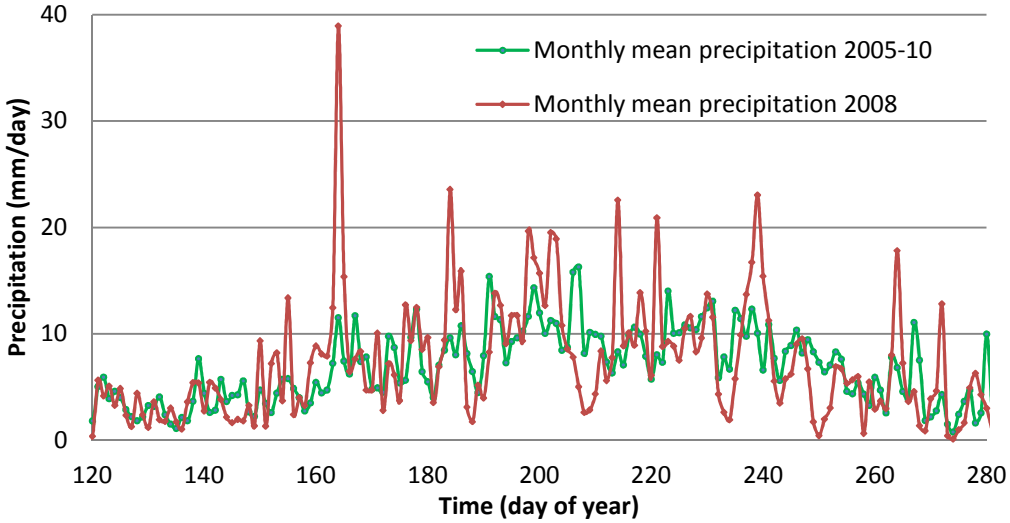

Figure 6.10: Monthly average precipitation in the upper-Kosi Basin in 2008 (green line) compared with average precipitation for 2005-2010 (red line). Comparison shows there are no significant changes in precipitation pattern in 2008 compared to average precipitation in last five years.

The daily TRMM mean precipitation in the upper Kosi basin is shown in Figure (6.10). In 2008, these daily precipitations (red line) are similar to the average daily precipitations between 2005 and 2010 (green line) with few days of high precipitation. Although the spatial resolution of TRMM data is not that good in resolving the spatial variability but it can provide a reasonable estimate of the temporal variations.

Combining the result from snow covered area (Figure 6.9) and rainfall in upper catchment one can conclude that there is no excess precipitation or snow melting which contributed to the breach of the dam. This implies that the flood which followed the breach in the levee is not due to any anomaly in the melting of snow or abnormal high rainfall in the upper catchment of the Kosi basin.

The district wise in-situ rainfall and TRMM rainfall analysis in lower Kosi basin is presented in Figure (6.11) and Figure (6.12) respectively. The in-situ rainfall analysis shows that the 5-years mean precipitations in the individual districts are higher than the mean precipitation over the same period in the combined area. The combined monthly precipitation (red dotted line in Figure 6.11) of all the districts (weighted according to the surface within study area) in 2008 is ~10% higher in July than the 5-years average precipitation (red solid line in Figure 6.11) but lesser than individual district wise rainfall for the same period. The daily TRMM precipitation time series (Figure 6.12) in the lower Kosi basin (Latitude: 86°E-87°E/Longitude: 25°N-26°N), shows that the daily mean precipitation (red line) in 2008 is higher for many days compared to the daily mean precipitation (green line) over the 2005 to 2010 period.

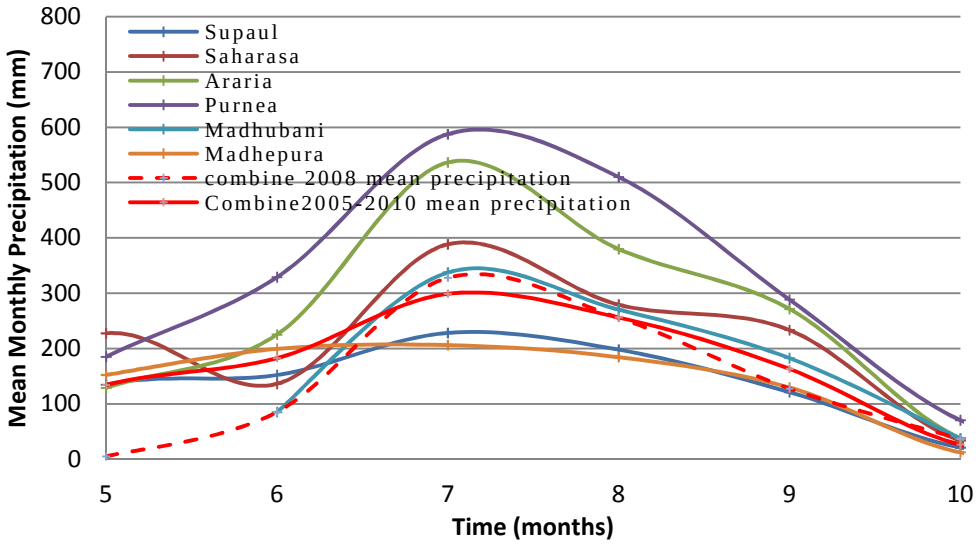

Figure 6.11: Average monthly in-situ precipitations for 2006-2011 in different districts (fully or partly lying in study area) of Bihar. Red dotted and red solid lines represent precipitation in study area (weighted area for partly lying in study region). Average precipitation for study area in 2008 is slightly (~10%) higher than average precipitation during 2006-2011.

The rainfall analysis from these two precipitation datasets, it can be interpreted that the region has received a considerable high amount of water from nearby catchment along with fair amount of precipitation inside the study region. In this region, there had been a higher precipitation in previous years too but the precipitation in 2008 in the lower Kosi basin along with water released because of levee breach lead to a massive flood for longer time duration as seen in Figure (6.8b).

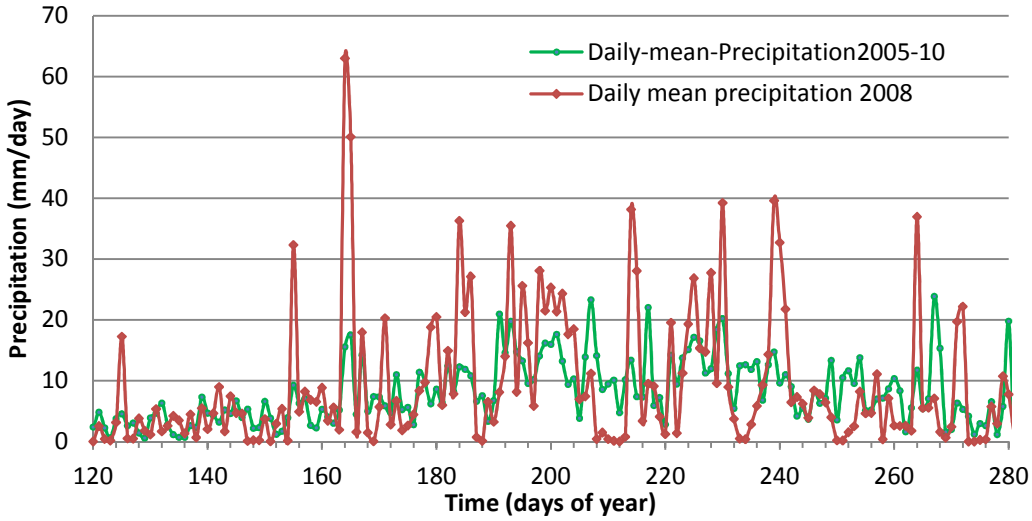

Figure 6.12: Daily mean-precipitation in lower Kosi Basin. Daily average precipitation for 2005-2010 (red line) compared with 2008 daily precipitation (green line).

6.4.3 Surface Water extension and water Height Evaluation

After reviewing the background and the dynamics of the flood event, in this section we will discuss the water height evaluation over flood region. The water level is calculated from MODIS and ENVISAT products using the algorithm discussed earlier, over water logged region i.e. region of interest (ROI). First of all, the water pixel profiling is performed along the ENVISAT track 696 and 967 with data derived from MODIS for selecting the altimetry observations for water stage calculation. The water pixel (dark blue) profiling along track 967 is shown in Figure (6.13). The dark blue colour represents open water pixels and light blue colour represent mix of water and dry land with yellow colour as the background. From profiling of water pixel along these two tracks it has been established that track 967 has more continuous water pixels than track 696 but across both the tracks the water pixel counts are not uniform.

Radar altimetry has, however, a number of limitations over land because radar waveforms (e.g., raw radar altimetry echoes reflected from the ground) are complex and multi-peaked due to interfering reflections from water, vegetation canopy and rough topography. As result, it can be less valid data than those over oceans. Impact on precision is also depending on the type of surface which is surrounding the water body. Thus the monitoring of floodplain over Kosi, in regards of above points, has imposed us to select the data from the footprint size of the radar echo. We relied on the MODIS images analysis for this purpose, considering valid altimetry measurements for altimeter beam in a zone of at least 5 km by 5 km fully covered by water as inferred from MODIS.

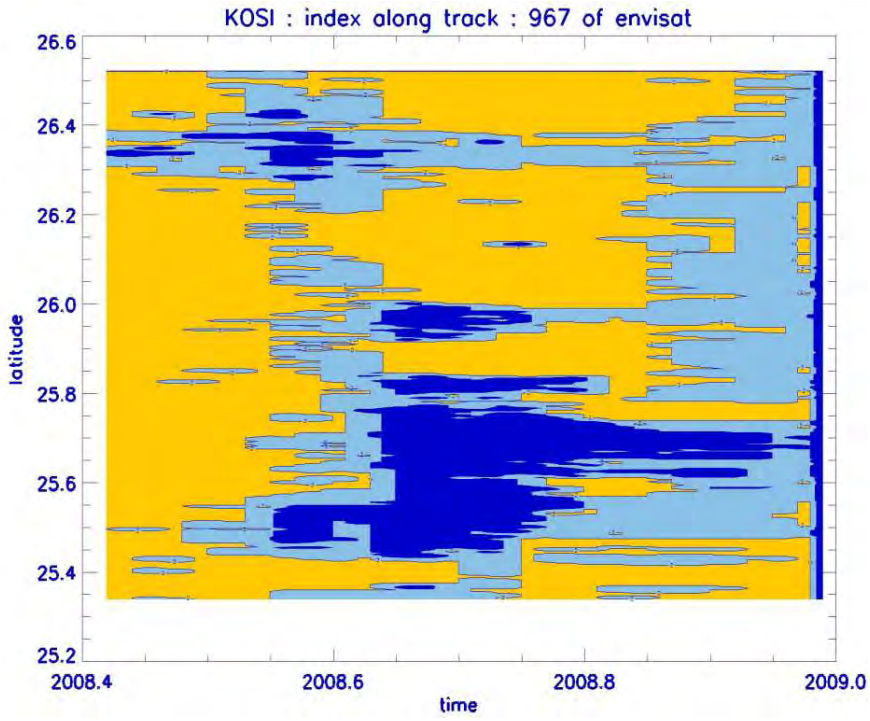

Figure 6.13: Interpolations of MODIS data along the ENVISAT track 967 during the flood period in 2008. Blue colour represents open water pixel, light blue is pixel covered by mix of water and dry land and yellow is non-water pixel.

Due to the slope of water along the satellite track, an average water level is calculated at every 5 km for each pass of ENVISAT if MODIS classification indicated presence of water. The difference of water level from the lowest value at the beginning of the inundation and the highest level when the inundation was at maximum gave us the column water thickness of each of the small section of 5 km long. Median of these

observations is used to produce the averaged water column thickness (and the associated RMS error) along the floodplains for the inundation of 2008.

The high frequency (20 Hz) ENVISAT data along the track 967 is used to calculate the water level over flooded region. Since there is no continuous water pixel along this track, the water level calculation is done in patches over area defined by dark blue colour in Figure (6.13). The obtained water column thickness is in order of 1.2 meters with a 20 cm RMS error. Due to the ENVISAT time sampling, we found only 3 or 4 observations for the period of flood from altimetry data over flooded region. Using the result of water covered area obtained from MODIS image analysis along with altimeter water column thickness, the water volume at peak can be summarized as around 4000 million cubic metres. Since this flood was rapid (2-3 months), due to time sampling of altimetry observations (35 day with ENVISAT), the water level calculation was done in patches. Therefore it is highly impossible to produce precise water level time series over the region of interest.

Conclusion

This chapter has discussed the use of MODIS data for analysis of land cover classification with emphasis on the flood analysis in lower Ganga catchment. The analysis of MODIS images for almost a decade from 2002 to 2010 shows that there has been a large part of this region under the reoccurring floods which have consequences over the agriculture and agriculture based sector. Kosi basin, a small area in this region has received high inundation during 2007 and 2008. An evaluation of 2008 Kosi flood is presented using the proposed methodology in chapter 4 from the altimeter and MODIS data.

Chapter 7

GRACE Data Analysis

Introduction

The surface water in lakes and rivers, groundwater, snow and ice over hilly region, soil moisture, and water contain in canopy are the constituent of hydrological cycle on continents. Although they constitute about 2.5% of the total water in the hydrological cycle but their influence on climate and life on the earth is significant [Chahine, 1992; Rodell and Famiglietti, 1999]. The interaction of water between continent, ocean and atmosphere is shown in Figure (7.1).

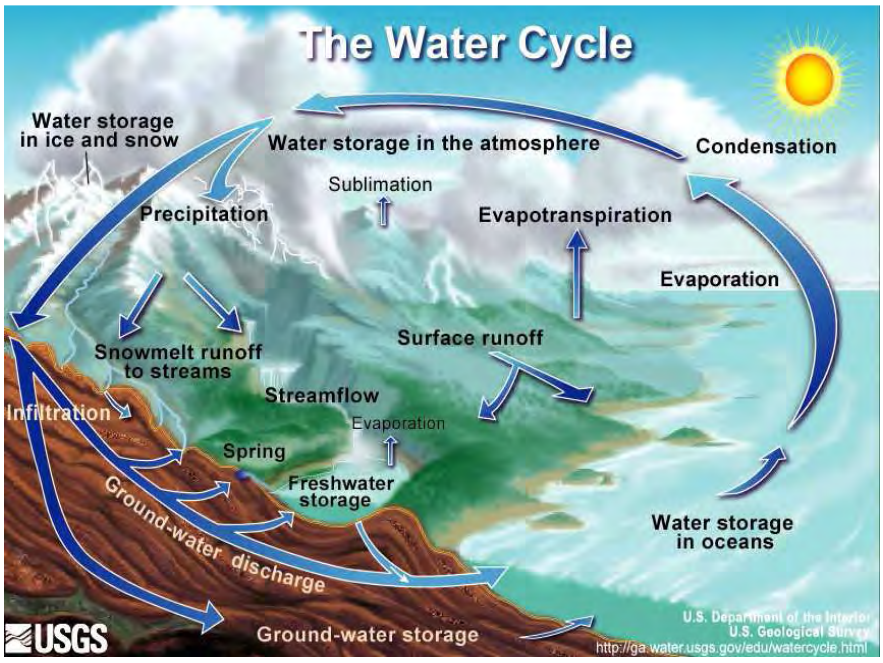

Figure 7.1: Interchange of water between continent, ocean and atmosphere. [Credit: USGS].

The water balance at regional or global scale can be determined by estimation of the volume of water in the different compartments. The quantification of the different constituent of hydrological cycle, at any scale of time and space, is one of the major

concerns to the hydrologists. For a given time interval and spatial scale such as basin, the hydrological balance can be expressed as

$$\frac{dS}{dt} = P - E - R \qquad \text{Eq. (7.1)}$$

where dS/dt is the change in the water stock variation, P is total precipitation (sum of rain and snow fall) , E is evapo-transpiration and R is surface runoff.

The water storage is usually expressed in equivalent water height (in mm for example). This equation simply expresses the difference between the volume of water entering and leaving a particular entity, such as a watershed, which is equal to the volume variation in stored water. On seasonal to monthly time scales, the assessment of the different constituents of the hydrological cycle on a global to continental extent is limited by the lack of sophisticated measuring methods [Trenberth et al. 2007] and particularly by the low spatial density of measuring networks.

7.1 Spatio-Temporal Evaluation of Total Water Storage (TWS)

Until the launch of GRACE, the spatio-temporal variations of water storage at regional or global scale were estimated by Land Surface Models [Döll et al., 2004; Swenson et al., 2003; Wahr et al., 1998]. Some of the commonly applied land surface models are Land Dynamics Model [LaD, Milly and Shmakin, 2002], Water GAP Hydrology Model [Hunger and Döll, 2007; WGHM, Döll et al. 2003], Organising Carbon and Hydrology in Dynamic Ecosystems (ORCHID) [Verant et al., 2004, Krinner et al., 2005], and Global Land Data Assimilation System [GLDAS, Rodell et al, 2004]. These models generally combine climate data with physiographic data (including soil and vegetation) in hydrological studies.

The global applicability of these models is limited, for example, some of these models do not include all relevant storage compartments such as surface water bodies and groundwater. Very few models take into account the impact of human action, in particular of dams and water withdrawals. The GRACE mission observations are providing the spatio-temporal variations in mass distribution [Cazenave and Chen, 2010; Ramillien et al., 2005; Tapley et al., 2004a; 2004b; Wahr et al., 2004] used GRACE as independent source for validation of the output of Land Surface Models

[Cazenave and Chen, 2010; Werth and Güntner, 2010; Guentner, 2008] and in hydrological studies [Fersch et al., 2012; Güntner et al., 2008; Schmidt et al., 2005; Shiklomanov et al., 2002; Rodell and Famiglietti, 1999].

7.2 TWS variation in Indian Subcontinent

India is facing a serious problem of natural resource scarcity especially water because of high demand from agriculture sector, industry sector and more importantly, the rapid population growth [CGWB, 2011, 2006; Garg and Hassan, 2007]. An extensive discussion on the water resources in India is presented by Kumar et al. [2005]. Tiwari et al. [2009] and Rodell et al. [2009] have argued that Northern India is water stress region.

7.2.1 Dataset and Methodology

In this section, the analysis of the water stock variations in Indian sub-continental basin from GRACE data, 10 days (1°x1° grid) equivalent water height (EWH) differences (in meter) for a period of July, 2002 to December, 2010, is discussed. The spatial mean, ΔTWS, is calculated considering the spherical shape of Earth and hence it is depending upon the spatial location i.e. longitude (θ) and latitude (λ):

$$\Delta TWS(t) = \frac{\sum_{i=1}^{n} TWS(\theta_i, \lambda_i, t) \cos \lambda_i}{\sum_{1}^{n} \cos \lambda_i} \qquad \text{Eq. (7.2)}$$

The Climate effect is considered as the difference of 'monthly mean' value of EWH and EWH value at each pixel. The monthly mean is calculated as the mean of EWH value of all the observations in an individual month for period of 2002 to 2010. For example, the average of EWH values for January is obtained as the average of all the EWH value in month of January from each year for above mentioned period. The difference of monthly mean value and EWH value is termed as residual EWH.

7.2.2 TWS variation in Ganga basin

The spatial mean of total water variation (hereafter raw EWH mean) in Ganga-Brahmaputra basin before and after removing the seasonal signal (hereafter residual EWH mean) is shown in Figure (7.2).

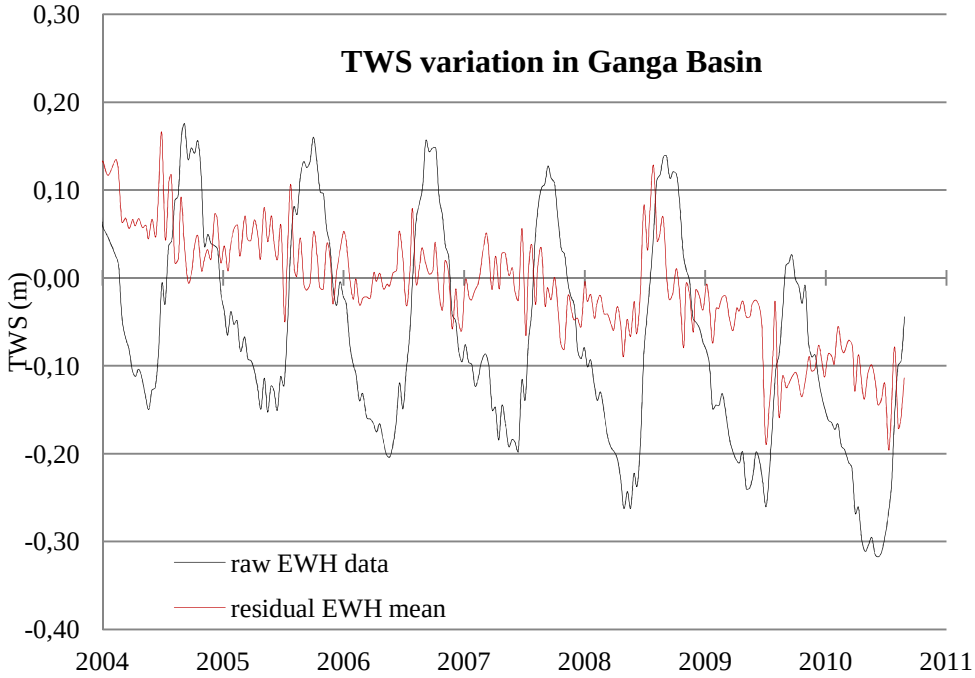

Figure 7.2: TWS in Ganga basin. Black line is TWS variation without considering the seasonal signal and red curve after removing the seasonal signal.

Since there is data gap in early months of 2003 and 2004 therefore the time series is presented for 2004 to 2011for Ganga Basin. The raw EWH mean (black line) shows annual peak to peak similarity in water storage with a decreasing trend of 5.9 mm/year. The residual EWH mean time series (red line) shows high negative trend but positive jump in water storage in the basin in 2008. Drawing an inference from MODIS images analysis in lower Ganga (chapter 6) it can be argued that because of inundation there has been water on surface for longer time which could have generated the more infiltration of water and hence that leads to high water storage. We see a negative shift in residual water storage post 2009 followed by maximum water storage more or less equal to the low water storage in previous year. Because of limited data at the time of analysis it is difficult to say whether there are any decadal variations in water storage. This is matter of investigation but a broad conclusion can be given that there might be low rainfall in 2009 and subsequently high with drawl of ground water during this period.

The spatial trend of TWS variations and residual TWS variations in the Ganga are shown in Figure (7.3). Both spatial trend maps show a negative trend in large part of basin. Tiwari et al. [2009] and Rodell et al. [2009] have also presented the negative

water storage variation in this region. Spatial trend in both the cases show high depression in north-western part of basin compared with other parts of the basin. The depression value is larger after the removal of seasonal signal.

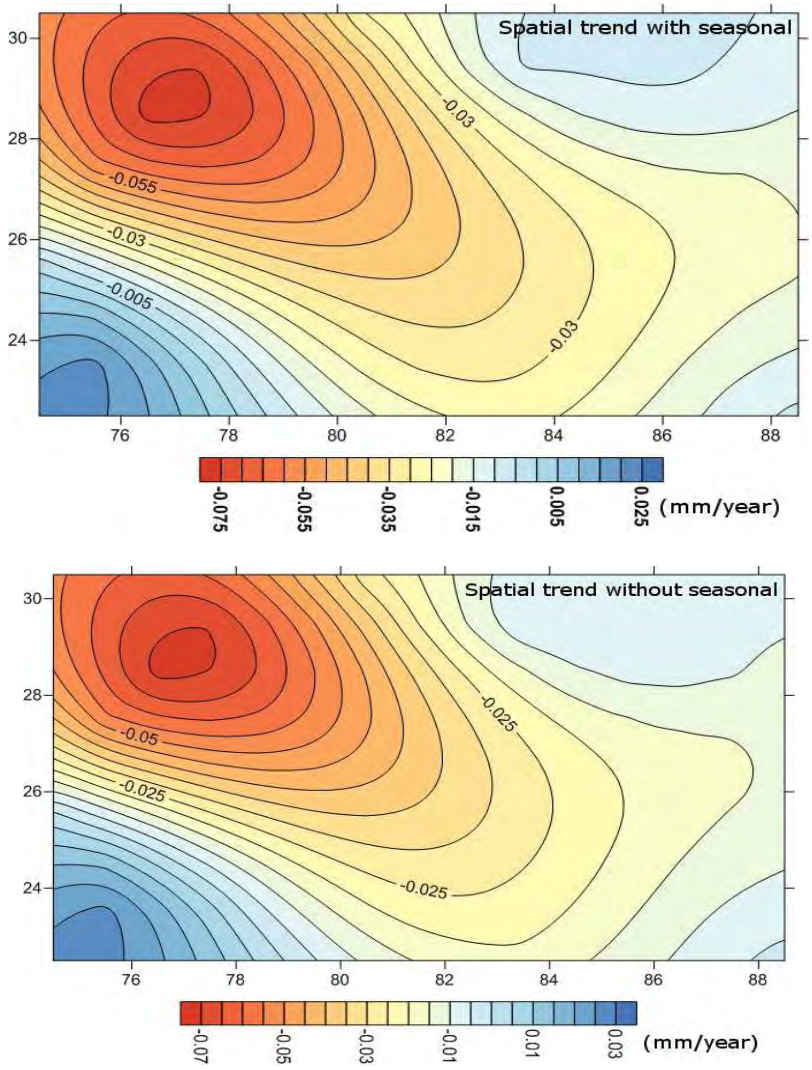

Figure 7.3: Spatial trend of TWS and residual TWS in Ganga basin in mm.

The study of Central Ground Water Board [CGWB, 2011 and 2006] of India concludes a high extraction of groundwater in this basin. The groundwater recharge occurs mainly through the infiltration during the monsoon period and water spill in case of flooding. It is indeed well known that the lower Ganga is drained by many rivers compared to upper catchment and is affected by frequent floods. One can draw an inference that due to frequent flooding in lower part of basin extend the infiltration time and results as a positive trend in lower part of Ganga. The high extraction of groundwater for day-to-day activity, agricultural purpose and industrial use in upper

part of basin leads to decrease in TWS. The GRACE based study of Tiwari et al. [2009] concludes a very high groundwater extraction rate during the period of 2002 to mid-2008 compared to the CGWB estimate in mid-1990's.

The total water storage variation of the basin is also analyzed with EOFs method. The decomposition of TWS is carried out on the residual EWH data (unit: mm). The decomposition of residual TWS in Ganga is shown in Figure (7.4).

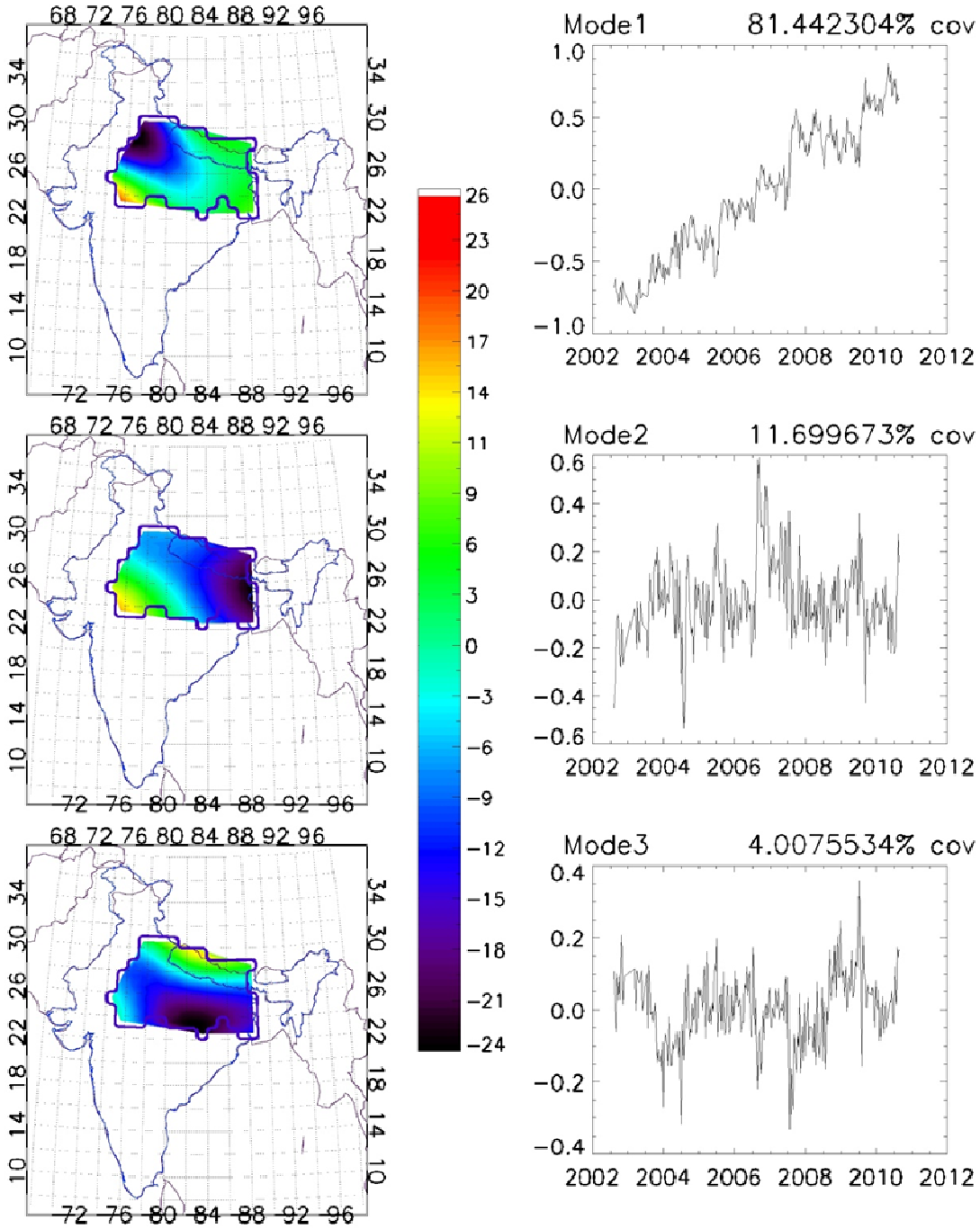

Figure 7.4: Decomposition of residual TWS (1st three modes) in Ganga Basin by EOFs.

The decomposition of residual TWS shows that the majority of the variations are confined in first mode with a variation of 81.4% flowed by 11.7% and 4% for second and third mode. The spatial trend in 1st mode shows that trend is dominated by the signal from north-western part of basin. The principle component of 1st mode shows the decreasing trend considering that time mean is not removed from data before EOF analysis. First two modes could not be correlated with the rainfall but the third mode shows a good correlation.

Year 2004 and 2008 had received high rainfall (more than normal average) which is quite visible in third mode. Further 2009 is quit dry year in India. This event is recorded well in 3rd mode of EOF analysis. Spatial trend in second and third mode is dominated by signal from eastern and southern part of basin respectively. In general, it can be say that depletion in Ganga Basin is compelled by the huge extraction of ground water for agriculture and other livelihood of large population residing in the basin.

7.3 Precipitation Variation in Ganga Basin

The rainfall is important contributor to the total water variation. Subsurface and ground water is recharged by prolonged precipitation and resulting runoff. The Ganga basin receives huge amount of rainfall which provides large contribution in TWS variations in the basin. At small time and spatial scales, the inundation changes TWS. Therefore, it is important to study the temporal and spatial variation of rainfall in study region.

7.3.1 TRMM Rainfall Data

The monthly TRMM data, for period of 1998 to 2010, is used in the present manuscript to analyze the spatio-temporal variation in Ganga basin. This data is analyzed by EOF method (Appendix A2).

7.3.2 Analysis of TRMM Rainfall Data

The spatial trend of rainfall in Ganga basin for 1998 to 2010 is shown in Figure (7.5). The spatial trend shows that the large part of basin has positive trend. A small part of basin shows high positive trend (shown in dark red colour). Since data has a spatial resolution of 1°x1° and rainfall in the basin varies largely, both in space and time

domain (see chapter 3), Mann-Kendall test (Figure 7.6) is performed to see the significance of spatial tendency variations (Appendix A3). The Mann-Kendall test shows that spatial tendency of rainfall from TRMM data is significant in only certain part of the basin (red and blue colour in Figure 7.6)

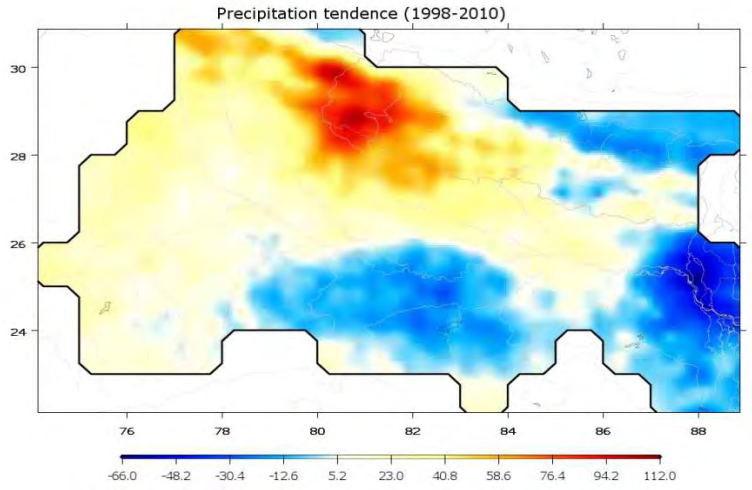

Figure 7.5: Spatial trend of rainfall in Ganga basin from TRMM data

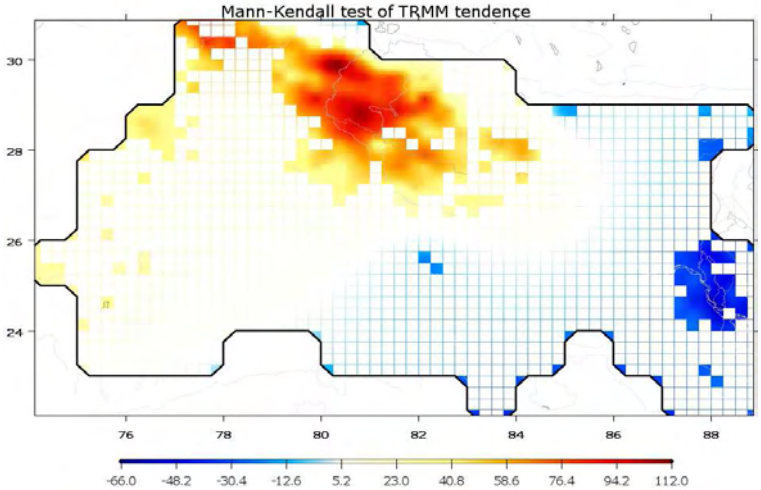

Figure 7.6: Mann-Kendall test for significance tendency of TRMM data

Although the significance of TRMM data tendency in Ganga is limited in certain part of basin, EOF analysis of these datasets has been performed. A majority of the variation, about 43%, is confined in first mode. Variation in second, third and fourth modes are 15%, 9%, and 7% respectively. The first two modes of EOF analysis of TRMM rainfall in Ganga basin is shown in Figure (7.7).

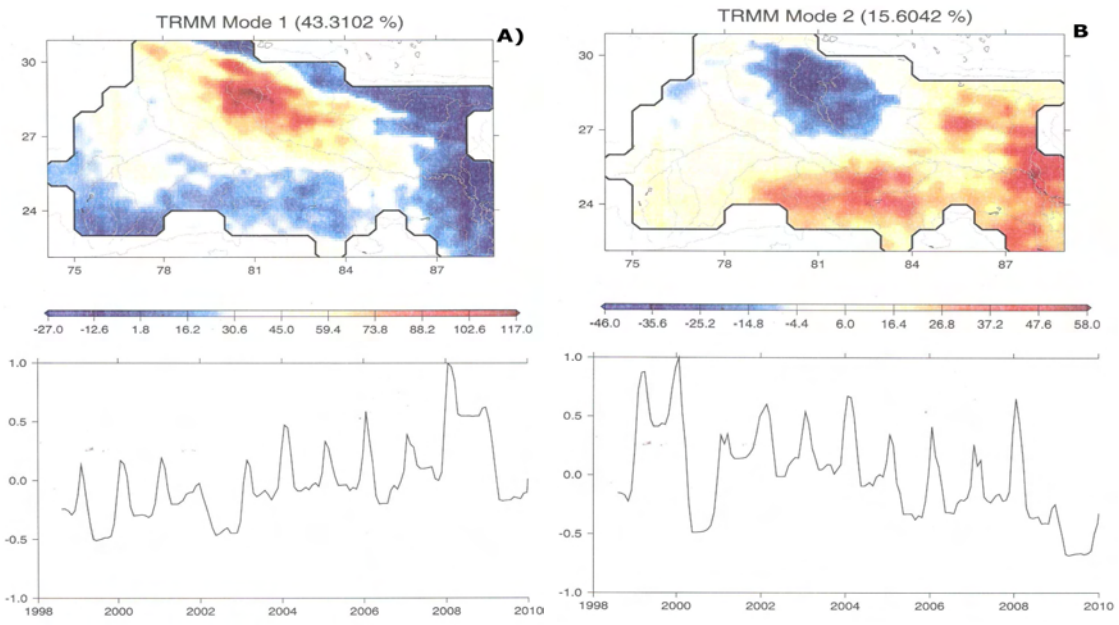

Figure 7.7: EOF analysis of TRMM rainfall data in Ganga Basin.

The first mode shows the high rainfall concentration in upper central part of basin (shown in red colour in Figure 7.7 a), which is the region where the Mann-Kendall test has predicted the significance of spatial trend variation in rainfall where as the second mode (Figure 7.7b) shows high rainfall in the lower part or more specifically in plain of Ganga. The first mode may be governed by the South-west monsoon whereas the second mode may be due to the rainfall in winter season.

The temporal series of EOF analysis in both, mode 1 and mode 2, are showing high rainfall in 2008. The GRACE data analysis shows that during this time period there is positive TWS variation in last one decade. This can be interpreted as high rainfall which lead to large percolation and hence resulted as increase in subsurface and ground water.

Conclusion (in English)

Monitoring of inland water variation is essential for the better understanding of the water cycle at regional and global scale. The tracking of these variations from in-situ measurements are very difficult because of their scarce and inhomogeneous coverage. Remote sensing has emerged as an alternative to the conventional in-situ measurements. Remote sensing techniques, particularly satellite Radar Altimetry represent a major contribution to hydrological studies. Although the Radar Altimetry was initially developed and optimized for the study of oceans, but it has also been adopted for the studying of continental water bodies too. The use of satellite altimetry over continental water bodies is more complicated than over oceans and requires precautions in the processing of the altimetry water level measurement. Indeed, the characteristics of waveforms over inland water surfaces are different from those over ocean surfaces.

Despite the various limitations in the altimeter measurements over inland water bodies, this technique has been successfully used in studies of continental hydrology. The altimetry observation provides an alternative to in-situ measurements and allows the creation of hydrological networks for water level measurements with dense spatio-temporal coverage. The satellite altimetry provides the access to the regions which has an important role in hydrological cycle but difficult to measure hydrological parameters by conventional methods. The results derived from altimetry observations are used in various hydrological studies such as flood monitoring, calculation of changes in volume of lakes and estimation of river discharges.

An example of utilization of this technique to inland water bodies is presented in this PhD thesis. The results obtained for the altimeter measurements for ICE-1 algorithm retracked data from ENVISAT mission over the Indian rivers (Ganga and its tributaries, Krishna, and Godavari) are presented in Chapter 5 and Appendix A1. The altimeter observations from T/P and JASON 2 are also processed for these rivers to derive the water stage. Although, the dam and other artificially constructed reservoirs over these rivers are regulating the stream, the water level variations, in most of cases, follow the similar peak to peak pattern and show the seasonal and inter annual

variations. A JASON 2 altimeter derived water stage along with in-situ measurement in Ganga and Brahmaputra rivers is used for estimating a rating curve. This rating curve is then used to calculate the monthly discharge of these rivers into the Bay of Bengal for the period of 2008 to 2011. The altimeter derived discharges are well within the acceptable range and extent the monthly discharge calculated by Papa et al. [2010] from ERS and ENVISAT missions for these rivers.

The surface water extent and water volume in flooded region can be estimated form the synergy between satellite radar altimetry and imagery. In the present work, since the main focus was to understand the Ganga River Basin, especially in lower Ganga basin, satellite images from MODIS/TERRA are processed to analyze the inundation in this region. The spatio-temporal evolution of floods in the lower Ganga basin and its sub-basin, Kosi, for the period 2002-2010 is presented in this study. The spatio-temporal analysis results can be used to estimate the seasonal volume variation of surface water.

The radar altimetry and MODIS images, together, are used to study the flood dynamics of Kosi, a sub-basin in Ganga basin, which is actually affected by flood almost every year. The analysis of MODIS images for lower Ganga basin for 2002 to 2010 shows that year 2007 and 2008 have large area under water. During the year 2008, Kosi basin was severely hit by flood water release from the breach in levee. An analysis of this flood is carried-out using the methodology described in Chapter 5 by integrating radar altimetry and MODIS observations. The result of MODIS images analysis and surface water and water volume variation in Kosi is presented in Chapter 6.

The surface water information is obtained by the radar altimetry and imagery. Another major constituent of continental water, i.e. groundwater, is also monitored by remote sensing technique: space Gravimetry, particularly GRACE mission which measures the changes in gravitational field of Earth caused by the variation in mass redistribution. The gravitational field variations over continents are assumed to correspond to changes in variations of continental water supplies in absence of any abrupt change in lithosphere.. Therefore the GRACE mission provides the information of water mass variation on time scale of months to years.

The GRACE data have been analyzed to study the variations in total water storage in Ganga river basin and other river basins, Brahmaputra, Krishna, and Godavari in

Indian subcontinent. An analysis of storage variation in Ganga basin is presented in Chapter 7.

In this thesis work different type of remote sensing observations (altimetry, space imagery and satellite Gravimetry) are processed to derive the hydrological parameters and their application in continental hydrological domain. It can be concluded that the remote sensing is playing a vital role in understanding the continental hydrology.

There is a scope of extending the present study for evaluating the ground water storage by removing the various components such as surface water derived from imagery and subsurface water (soil moisture) from the satellite missions or similar other data sets.

Conclusion (in French)

La surveillance de la variation des eaux continentales est essentielle pour une meilleure compréhension du cycle de l'eau à l'échelle régionale et mondiale. L'accessibilité de ces variations par de mesures in situ est difficile en raison de leur disponibilité et de leur couverture. La télédétection est apparue comme une alternative aux mesures in-situ classiques.

L'altimétrie radar en particulier, apporte une contribution majeure à l'hydrologie. Bien que l'altimétrie radar aie été initialement développée et optimisée pour l'étude des océans, elle a été adoptée pour l'étude des plans d'eau continentaux. Dans ce cas elle est plus délicate que sur les océans et nécessite des précautions en matière de mesure du niveau d'eau. En effet, les caractéristiques des formes d'onde sur des lacs ou des rivières sont différentes de celles sur la surface des océans.

Malgré les diverses limitations des mesures altimétriques sur les eaux continentales, cette technique a été utilisée avec succès pour l'hydrologie. L'observation altimétrique offre ainsi une alternative aux mesures in-situ et permet la création de réseaux hydrologiques virtuels avec une couverture spatio-temporelle dense. L'altimétrie satellitaire offre l'accès à des régions qui ont un rôle important dans le cycle hydrologique, mais délicat à suivre par des méthodes conventionnelles. Associés à d'autres techniques, les résultats obtenus à partir des observations altimétriques sont utilisées dans diverses études hydrologiques telles que la surveillance des inondations, le calcul de l'évolution du volume des lacs et l'estimation des débits fluviaux.

Un exemple d'utilisation de cette technique pour les eaux intérieures est présenté dans cette thèse. Les résultats obtenus avec les mesures altimétriques pour la mission ENVISAT sur les rivières indiennes (Ganga et ses affluents, Krishna et Godavari) sont présentés dans le chapitre 5 et l'annexe A1. Les observations altimétriques de T /P et JASON 2 sont également traitées pour ces cours d'eau. Malgré la présence de barrages et réservoirs artificiels, les variations de niveaux dans la plupart des cas est bien mesurée en termes de variations annuelles et interannuels. Les variations de niveau d'eau sur deux stations virtuelles sur le Gange et le Brahmapoutre ont été utilisées par

ailleurs pour d »river une courbe d'étalonnage niveau / débit aussi appelée courbe de tarage. Cette courbe de tarage est ensuite utilisée pour calculer le débit mensuel de ces rivières dans la baie du Bengale pour les périodes pour lesquelles aucunes données in situ ne sont disponibles. La précision des mesures altimétriques est suffisante dans ce cas pour obtenir des mesures dérivées du débit dans le golfe du Bengale qui ont pu être par la suite assimilés dans des modèles de circulation océanique faisant intervenir les entrants d'eau douce dans le golfe.

Une autre partie du travail a consisté à mesurer les variations d'étendue et de volume d'eau (par synergie entre l'altimétrie et l'imagerie satellitaire) dans des régions inondées le long du Gange. L'objectif principal était de comprendre la dynamique des inondations dans le bassin inférieur du Gange et plus particulièrement le long d'un de ses principaux affluents (la rivière Kosi). L'évolution spatio-temporelle de niveaux, surface et volume dans la plaine d'inondation étudiée est présentée au cours de l'étude pour la période 2002-2010. Les images radar altimétrique et l'imagerie MODIS ont ainsi permis de reconstituer des évènements récents d'inondation dans la partie aval de la rivière Kosi et leur dynamique. Nous avons pu en particulier mettre en évidence une inondation exceptionnelle en 2008 due à une rupture de digue en amont du fleuve. Ces résultats sont présentés dans le Chapitre 6.

L'information sur les eaux de surface est obtenue par l'altimétrie radar et l'imagerie satellitaire. Un autre constituant majeur de l'eau continental, (les eaux souterraines), est également surveillé GRACE à la télédétection par l'utilisation de la mission GRACE qui mesure les variations dans le champ gravitationnel de la Terre causées par les redistributions de masse en son sein. En effet, les variations du champ gravitationnel sur les continents sont supposées correspondre à des changements dans les variations des réserves d'eau continentaux en l'absence de tout changement brusque dans la lithosphère tels que la tectonique des plaques des glissements de terrain de grande amplitude. Les données de GRACE ont été analysées pour étudier les variations de la capacité totale de stockage d'eau dans des bassins fluviaux du sous-continent indien : Gange Brahmapoutre, Krishna et Godavari. Ces résultats et analyses sont présentés dans le Chapitre 7.

Dans cette thèse, le travail a consisté à combiner différentes techniques satellites (altimétrie radar, imagerie et gravimétrie) pour en retirer des informations cruciale sur

les stocks d’eau dans les grands bassins fluviaux indiens et leur dynamique spatio-temporelle. Cela nous a permis de conclure que la télédétection joue et jouera de plus en plus un rôle essentiel dans la compréhension de l'hydrologie continentale.

Appendix A1

ENVISAT Derived Water Level over Ganga River:

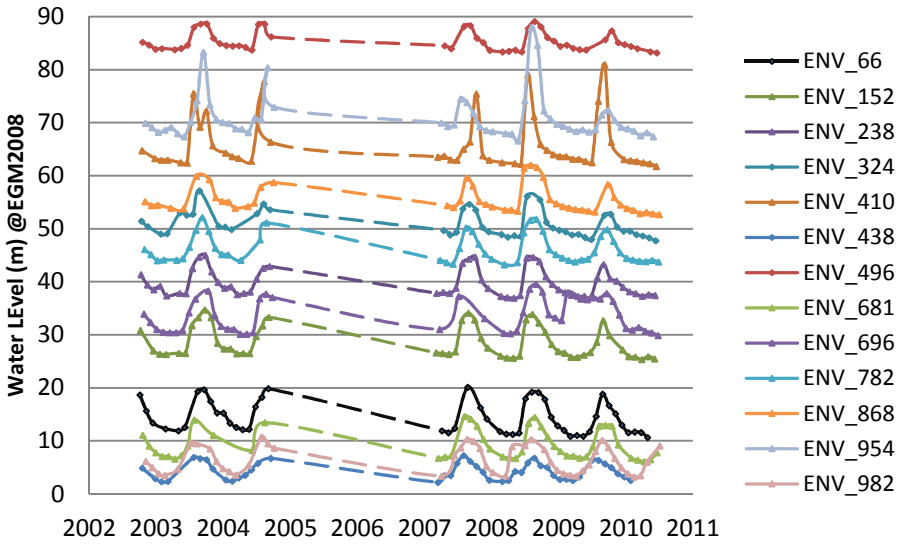

Figure A1.Water level variation over Ganga River for descending tracks of Envisat mission.

ENVISAT Mission derived water level over Krishna River:

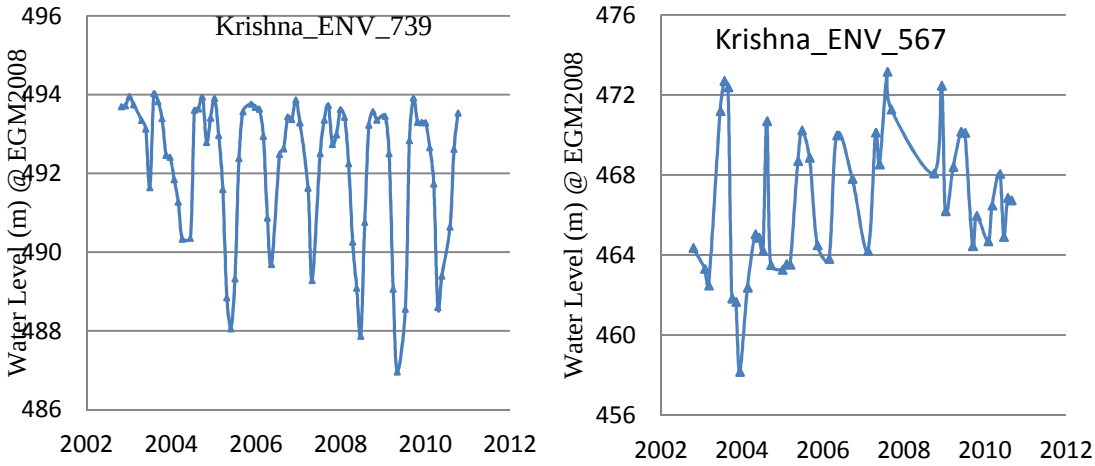

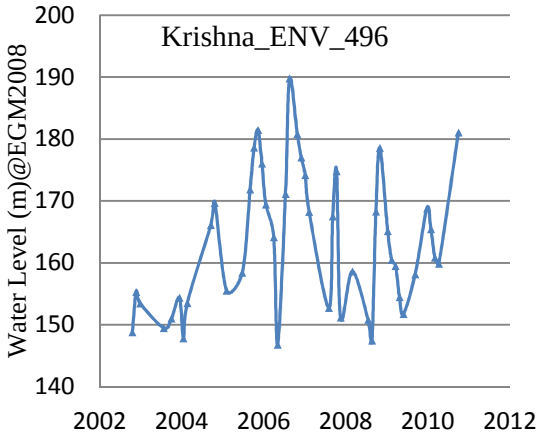
Krishna_ENV_496
Water Level (m)@EGM2008
200
190
180
170
160
150
140
2002
2004
2006
2008
2010
2012

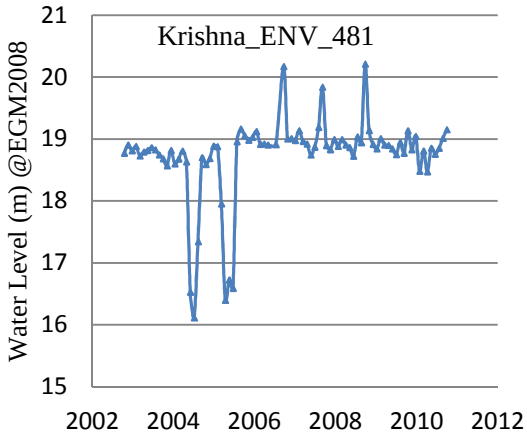
Krishna_ENV_481
Water Level (m) @EGM2008
21
20
19
18
17
16
15
2002
2004
2006
2008
2010
2012

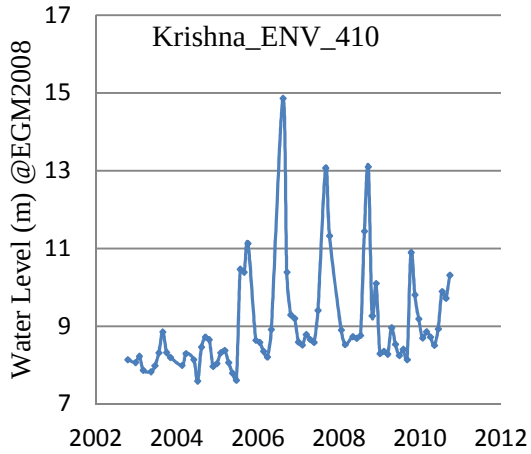
Krishna_ENV_410
Water Level (m) @EGM2008
17
15
13
11
9
7
2002
2004
2006
2008
2010
2012

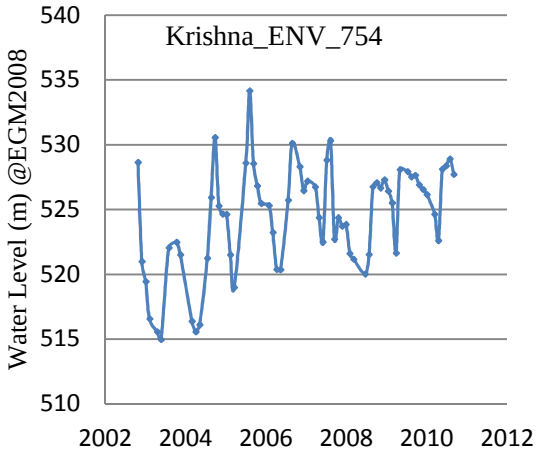
Krishna_ENV_754
Water Level (m) @EGM2008
540
535
530
525
520
515
510
2002
2004
2006
2008
2010
2012

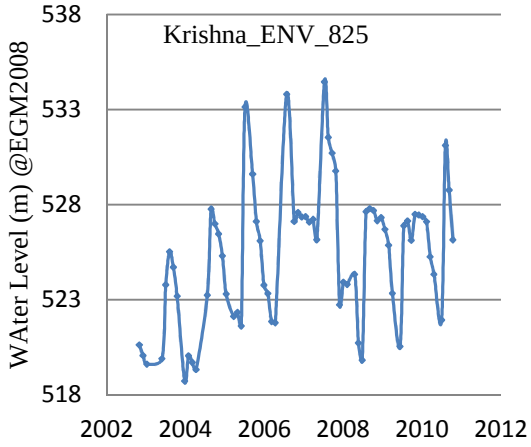
Krishna_ENV_825
WAter Level (m) @EGM2008
538
533
528
523
518
2002
2004
2006
2008
2010
2012

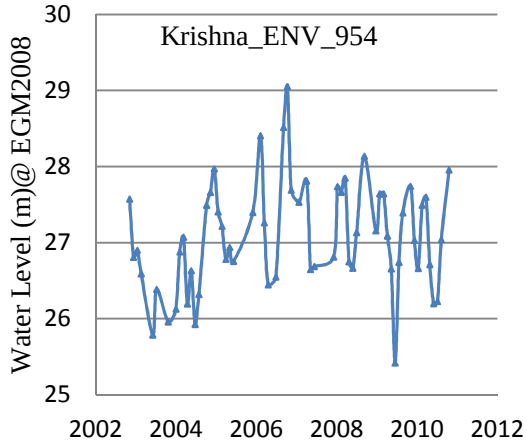
Krishna_ENV_954
Water Level (m)@ EGM2008
30
29
28
27
26
25
2002
2004
2006
2008
2010
2012

ENVISAT Derived Water Level over Godavari River

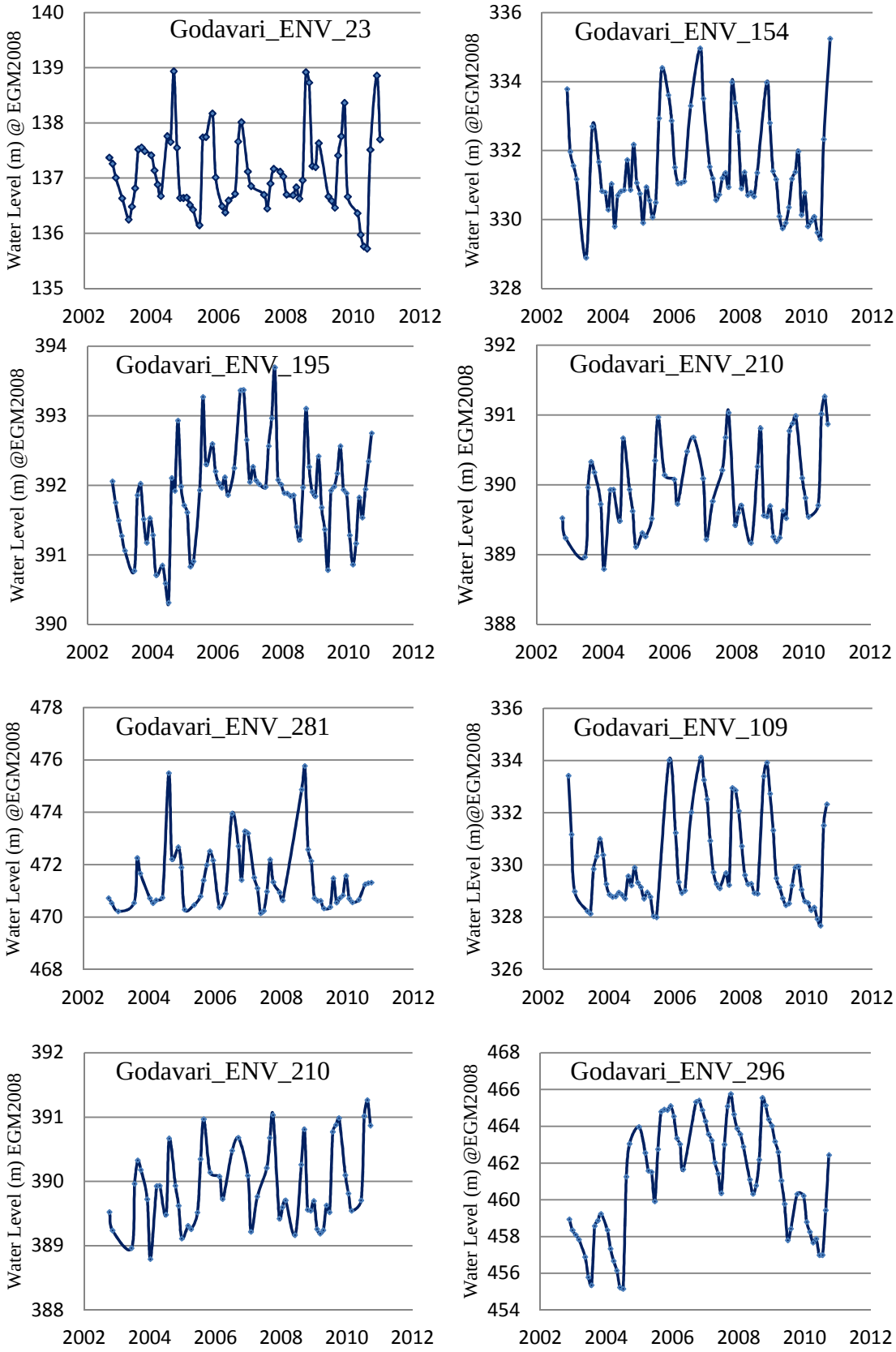

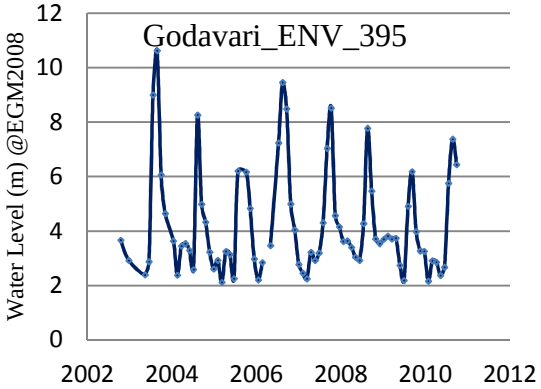
Godavari_ENV_395
Water Level (m) @EGM2008
12
10
8
6
4
2
0
2002
2004
2006
2008
2010
2012

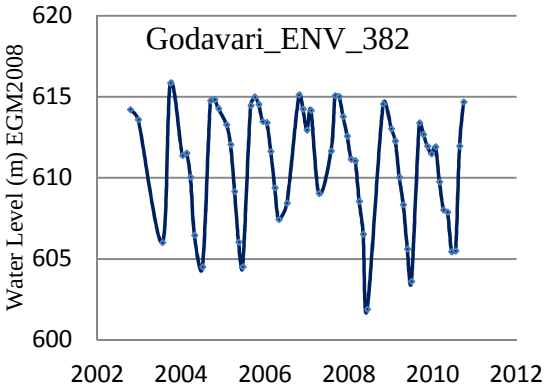
Godavari_ENV_382
Water Level (m) EGM2008
620
615
610
605
600
2002
2004
2006
2008
2010
2012

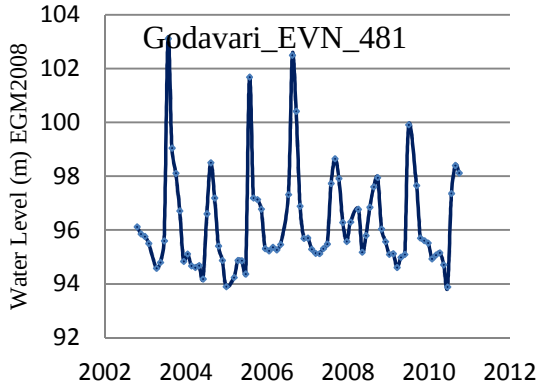
Godavari_EVN_481
Water Level (m) EGM2008
104
102
100
98
96
94
92
2002
2004
2006
2008
2010
2012

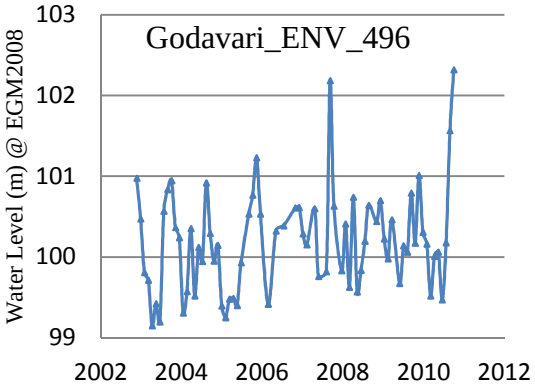
Godavari_ENV_496
Water Level (m) @ EGM2008
103
102
101
100
99
2002
2004
2006
2008
2010
2012

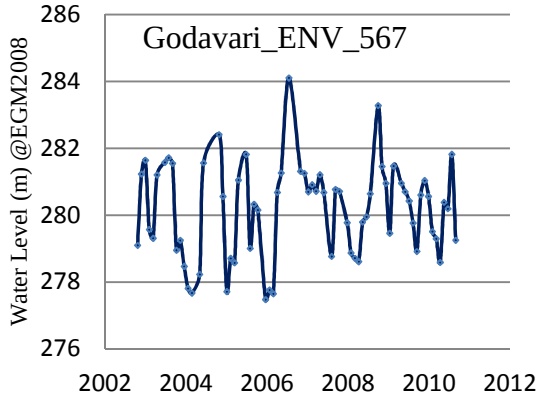
Godavari_ENV_567
Water Level (m) @EGM2008
286
284
282
280
278
276
2002
2004
2006
2008
2010
2012

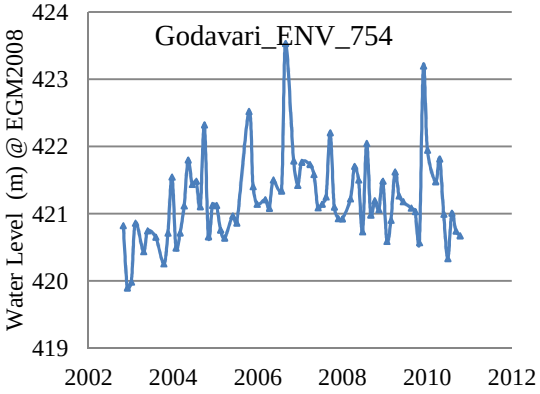
Godavari_ENV_754
Water Level (m) @ EGM2008
424
423
422
421
420
419
2002
2004
2006
2008
2010
2012

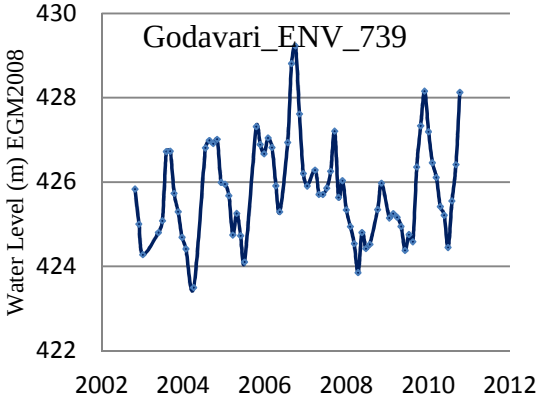
Godavari_ENV_739
Water Level (m) EGM2008
430
428
426
424
422
2002
2004
2006
2008
2010
2012

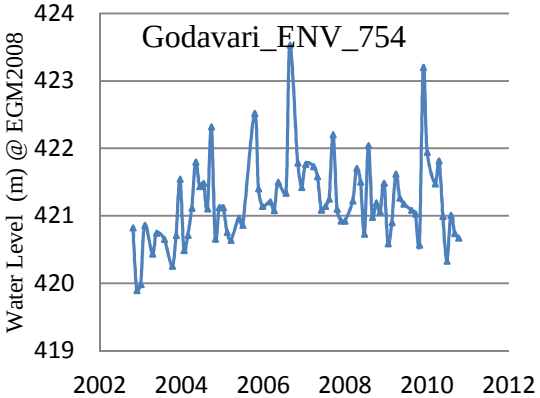
Godavari_ENV_754
Water Level (m) @ EGM2008
424
423
422
421
420
419
2002
2004
2006
2008
2010
2012

T/P-Jason2 Derived Water Level over Ganga River

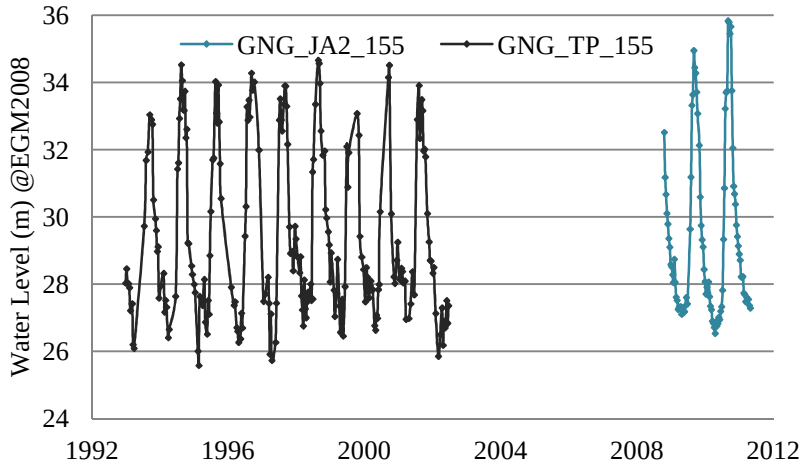

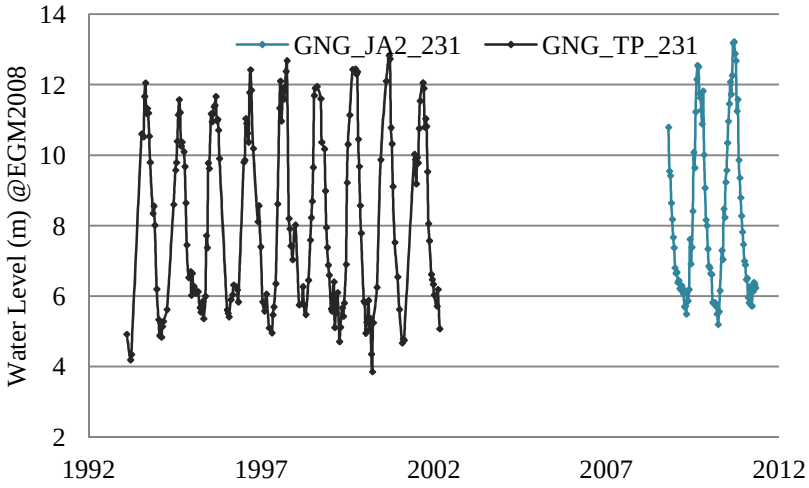

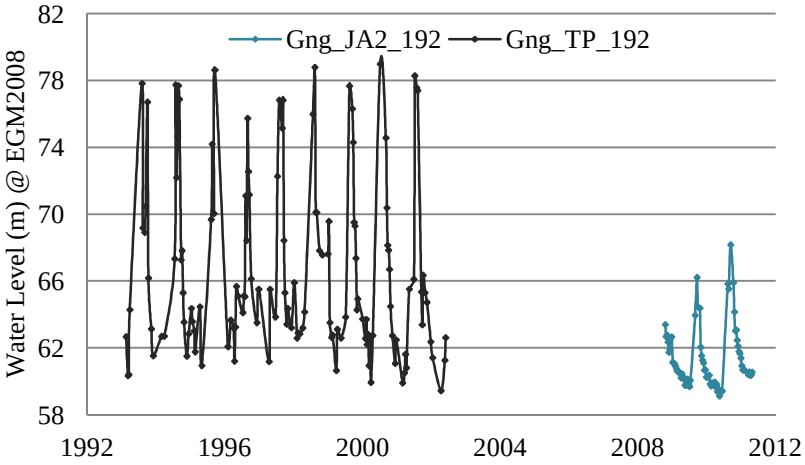

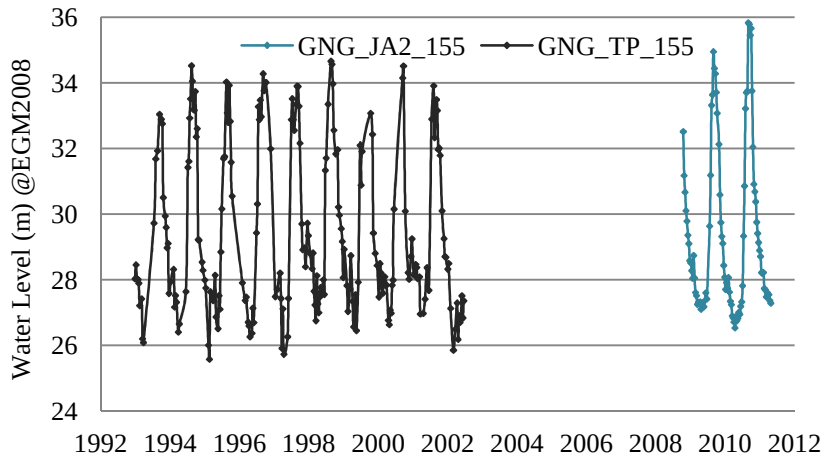
GNG_JA2_155
GNG_TP_155
Water Level (m) @EGM2008
36
34
32
30
28
26
24
1992
1994
1996
1998
2000
2002
2004
2006
2008
2010
2012

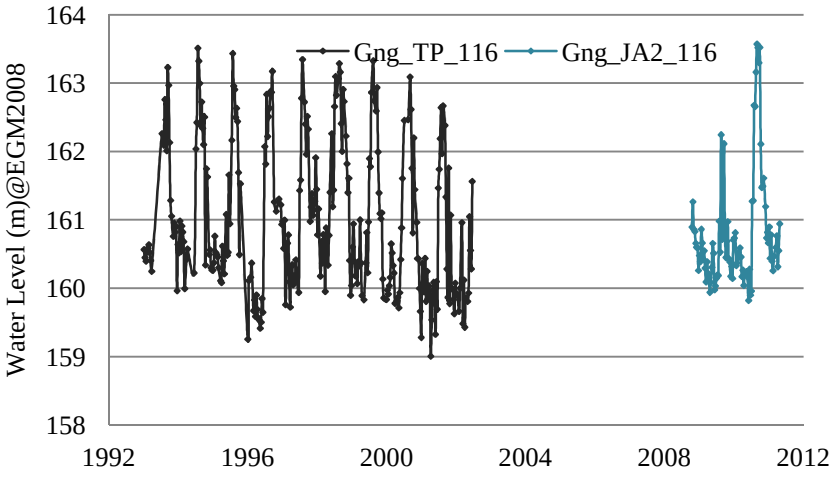
Gng_TP_116
Gng_JA2_116
Water Level (m)@EGM2008
164
163
162
161
160
159
158
1992
1996
2000
2004
2008
2012

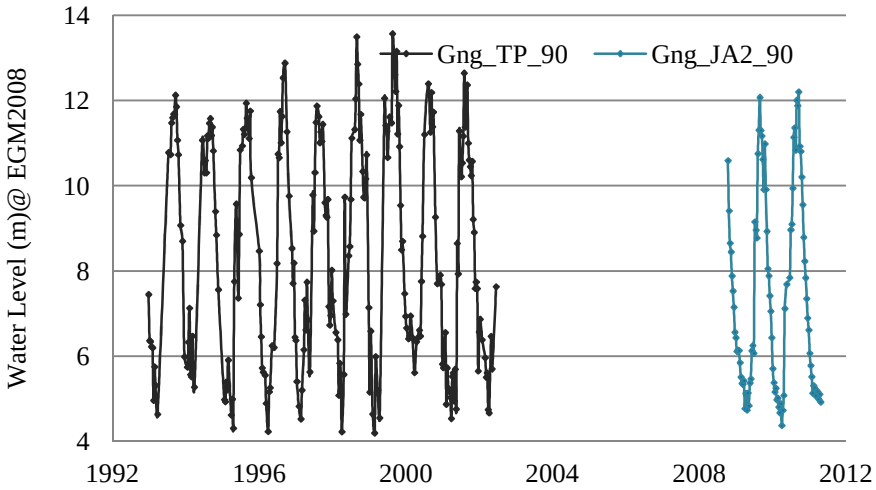
Gng_TP_90
Gng_JA2_90
Water Level (m)@ EGM2008
14
12
10
8
6
4
1992
1996
2000
2004
2008
2012

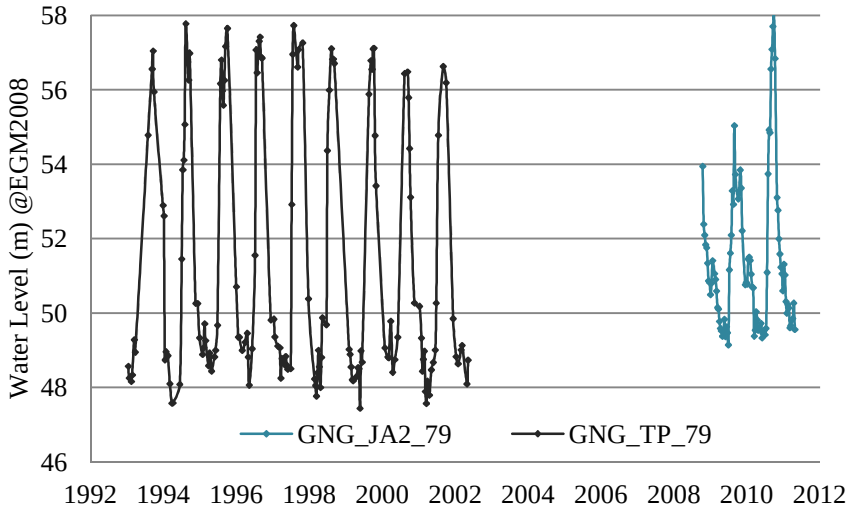
Water Level (m) @EGM2008
58
56
54
52
50
48
46
1992 1994 1996 1998 2000 2002 2004 2006 2008 2010 2012
GNG_JA2_79
GNG_TP_79

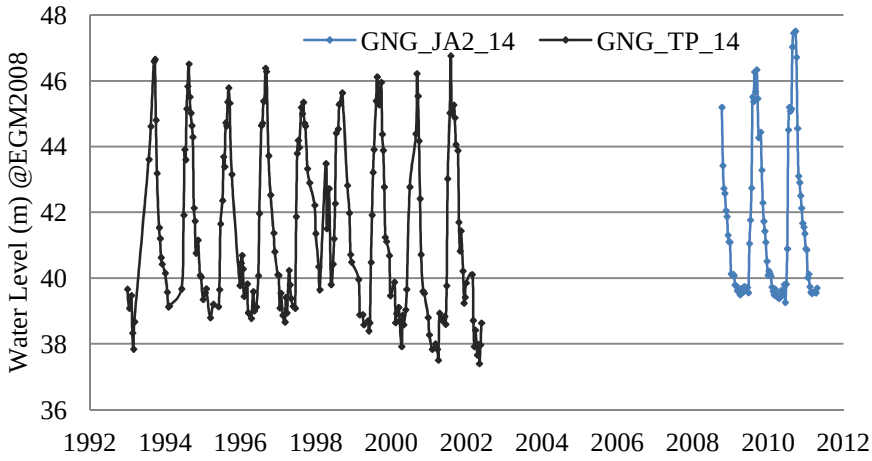
Water Level (m) @EGM2008
48
46
44
42
40
38
36
1992 1994 1996 1998 2000 2002 2004 2006 2008 2010 2012
GNG_JA2_14
GNG_TP_14

Appendix A2

Empirical Orthogonal Functions (EOF)

For the analysis of the variability of large datasets empirical orthogonal function, also known as principle component analysis [Björnsson and Venegas, 1999; Jolliffe, 2002; Hsieh, 2009], is most common approach. The EOF method determines both time series, called EOF time series or principal component time series' and spatial variation. is a linear transformation technique related to factor analysis. For a given set of variables, EOFs/PCA produces a new set of images (called as components) that are uncorrelated with one another and ordered in terms of the amount of variance they explain from the original band set. The first two or three components are explaining the variability in reflectance values for multispectral image and later components are dominated by the noise.

Empirical Orthogonal Functions (EOF) technique, introduced to reduce the large number of variables into few numbers of variables in dataset, is often used for studying the climatic, and oceanographic [Preisendorfer, 1988; Björnsson and Venegas, 1997] and meteorological studies [Lorenz, 1956]. Thompson and Wallace [1998, 2000] have used EOF technique to extract individual modes of variability such as the Arctic Oscillation (AO). This method finds the spatial patterns of variability, their time variation and provides a measure of the 'importance' of each pattern. The physical interpretability of the obtained patterns is a matter of controversy because of the strong constraints satisfied by EOF, namely orthogonality in both space and time [Simmons et al., 1983] that has been incorporated in Extended EOF [Weare and Nasstrom, 1982] technique.

The EOF technique is finds both time series and spatial patterns. The spatial patterns are known as EOFs most popularly but it is also termed as 'Principle component loading factor'. The time series are referred to as 'EOF time series', 'expansion coefficient', principle component time series' or just 'principle component'.

Data matrix

The analysis of dataset with many variable or gridded data is convenient in matrix form. Let's assume a signal F (λ, θ, t) of three dimensions, two-dimensional in space and one dimension in time. The signal is function of time (t), latitude (θ) and longitude (λ). For computation purpose we transfer this three dimensional data into two dimensional matrix. Now the data X(s, t) is in space time filed. X(s, t) represents value of Signal X at time t and spatial position s. The value of the field at discrete time ti and grid point sj is noted xij for i = 1… n and j = 1… p = p1p2. The observed filed can be represented by data matrix:

$$X = \begin{pmatrix} x_{11} & \cdots & x_{1p} \\ \vdots & \ddots & \vdots \\ x_{n1} & \cdots & x_{np} \end{pmatrix} \qquad \text{Eq. (A1)}$$

The departure from the climatology or anomalous field at (t, s), x'_{ts}, is obtained by removing the average at individual space point $\bar{x}_{.j}$.

$$x'_{ts} = x_{ts} - \bar{x}_{.s} \qquad \text{Eq. (A2)}$$

The time average of the field free from the seasonal affect at j^{th} grid point:

$$\bar{x}_{.j} = \frac{1}{n}\sum_{i=1}^{n} x_{ij} \qquad \text{Eq. (A3)}$$

Derivation of EOFs

First step in deriving the EOFs is defining the covariance matrix. For a signal W(φ, t) where φ represents co-coordinate (latitude(θ) and longitude (λ)), the covariance matrix 'C' can be written as:

$$C = \frac{1}{M}\begin{bmatrix} var(\omega 1) & cov(\omega 1, \omega 2) & \cdots & cov(\omega 1, \omega N) \\ \vdots & \ddots & & \vdots \\ cov((\omega N, \omega 1) & Cov(\omega N, \omega 2) & \cdots & var(\omega N) \end{bmatrix} = Q^t Q$$

Eq. (A4)

The Matrix C is a scalar time product and is a real and positive symmetric matrix therefore The Eigen values of C will be real and positive ranging from $\lambda_1, \lambda_2 \ldots \lambda_N$. The

associated Eigen values i.e. EOFs, represent the spatial map. Since the EOFs are orthogonal hence the spatial term can be written as

$$\langle X, Y \rangle = \sum_1^N X_i Y_j \qquad \text{Eq. (A5)}$$

where x and y are positive real values. Hence

$$\langle E_m E_n \rangle = \delta_{,mn} \qquad \text{Eq. (A6)}$$

Now the principle component of W derived from the decomposition of signal at time t_j can be written as:

$$w^j = \sum_{n=1}^N \langle w^j E_n \rangle E_n \text{ With } \langle w^j E_n \rangle = P_n^j \qquad \text{Eq. (A7)}$$

Since the principle components are orthogonal hence

$$\overline{P_n, P_m} = \lambda_n \delta_{n,m} \qquad \text{Eq. (A8)}$$

The orthogonal property leads to equality between the sum of λ_n and hence the total variance of signal in percentage associated with EOFs can be obtained as:

$$\sigma^2 = \langle \overline{w, w} \rangle$$

$$= \sum_{n=1}^{N} \overline{P_n E_n, P_n E_n}$$

$$= \sum_{n=1}^{N} \langle E_n E_n \rangle \overline{P_n P_n}$$

$$= \sum_{n=1}^{N} \lambda_n$$

Singular value decomposition and EOF method

The method for calculating the EOFs consists of the decomposition of signal, says ω (Lat, Lon, time), into singular values is known as Singular Value Decomposition (SVD) method. The decomposition of signal ω can be written as:

$$\omega = USV \qquad \text{Eq. (A9)}$$

where U and V are the orthogonal matrices and S is a diagonal matrix whose coefficients are the singular values of ω. Transpose of V defines the spatial variation of signal whereas the US defines the temporal variation.

Appendix A3

Mann-Kendall (M-K) Test

Mann-Kendall test is a statistical test and widely used for climatologic and hydrologic trend analysis [Motiee, H. and E. McBean, 2009; Yue, S.and C. Wan, 2004; Mavromatis T. and D. Stathis, 2011]. This test is preferred because it is a non parametric test and does not require the data to be distributed normally. Also the test is less sensitive for data gap. According to this test, the null hypothesis H_0 assumes that there is no trend, i.e. data is independent and randomly distributed, and is tested for alternative hypothesis H_1 which assumes that there is a trend.

The computational procedure, the M-K test considers a time series of n data points with x_i and x_j as two subset of data where i = 1, 2, 3 ……, (n-1) and j = i+1, i+2……, n. The data value is evaluated as an ordered time series and is each data value is compared with all subsequent data values. The statistic S is incremented or decremented by 1for data value is higher or lower from its previous data value respectively. The net result of increments and decrements provides the final value of S. The M-K statistic S is computed as [Drapela, K., and I. Drapelova, 2011; Trend Analysis-ETH, DR Helsel]

$$S = \sum_{i<j} \text{sign}\,(x_j - x_i)$$

$$\text{sign}(x) = \begin{cases} 1 & x > 0 \\ 0 & x = 0 \\ -1 & x < 0 \end{cases}$$

Where x_i and x_j are the annual values in years j and i, j > i. [10].

If values of n are less than 10, the value of |S| can be compared to the theoretical distribution of S derived by Mann and Kendall. At certain probability level H_0 is rejected in favor of H_1 if the |S| equals or exceeds a specific value $S_{\alpha/2}$. $S_{\alpha/2}$ is the smallest S having probability less than α/2 and appear in case of no trend. Positive (negative) value of S indicates upward (downward) trend.

Null Distribution

For large data sample (n >10), S is normally distributed with

$$E(S) = 0$$

$$var(S) = \sigma^2 = \frac{n.(n-1).(2n+5) - \sum t_i(i)(i+1)(2i+5)}{18}$$

where t_i represents the number of ties to extent i. The summation term in the numerator is included only if there is tied value in data series. In practice, standard test statistic Z is computed and compared with normal distribution. The Statistic Z is computed as:

$$Z_S = \begin{cases} \frac{S-1}{\sigma} & \text{for } S > 0 \\ 0 & \text{for } S = 0 \\ \frac{S+1}{\sigma} & \text{for } S < 0 \end{cases}$$

The statistic Z_s is used to measure the significance of trend. In fact, this test is used for null hypothesis H_0 test. If $|Z_S|$ is greater than $Z_{\alpha/2}$ where α is chosen significance level, the null hypothesis is invalid implying that the trend is significant.

References

Abarca-Del-Rio, R., J-F. Crétaux, M. Berge-Nguyen and P. Maisongrande, (2012). Does Lake Titicaca still control the Lake Poopó system water levels? An investigation using satellite altimetry and MODIS data (2000–2009). Remote Sensing Letters, 3(8), 707-714

Ad Hoc Work Group on Global Water Datasets. (2001). Global water data: An endangered species. EOS Transactions American Geophysical Union. 82:54– 58.

Agarwal, R.P. and R. Bhoj, (1992). Evolution of Kosi river fan, India: structural implications and geomorphic significance. International Journal of Remote Sensing. 13(10), 1891-1901

Aladin, N., Crétaux, J.-F., Plotnikov, I. S., Kourave, A. V., Smurov, A. O., Cazenave, A., Egorov, A. N. and Papa, F. (2005). Modern hydro-biological state of the small aral sea. Environmetrics, 16, 375–392.

Alsdorf, D. E., J. M. Melack, T. Dunne, L.A.K. Mertes, L.L. Hess, L. and C. Smith, (2000). Interferometric radar measurements of water level changes on the Amazon floodplain. Nature, 404, 174– 177.

Alsdorf, D., Birkett, C., Dunne, T., Melack, J. and Hess, L. (2001). Water level changes in a large Amazon lake measured with space borne radar interferometry and altimetry. Geophys. Res. Lett., 28(14), 2671–2674.

Alsdorf, D.E., and Lettenmaier D.P., (2003). Tracking fresh water from space. Science, 301, 1485-1488.

Alsdorf D.E., Rodriguez E., and Lettenmaier D. (2007), Measuring surface water from Space, Review of Geophysics, 45.

Amarasinghe, U.A, B.R.Sharma, N. Aloysius, C. Scott, Smakhtin, V., Fraiture, C.D., Sinha, A.K., Shukla, A.K. (2005). Spatial variation in water supply and demand across river basins of India. Research Report 83, Colombo, Sri Lanka: International Water Management Institute.

Amarasinghe, U.A,, T. Shah, H. Turral and B.K. Anand. (2007), India's water future to 2025 – 2050: Business-as-usual scenario and deviations, IWMI Res. Rep. 123, p47, Int. Water Manage. Inst., Colombo- Sri Lanka.

Arogyaswamy, R.N.P. 1971. "Some geological factors influencing the behavior of the Kosi." Records of Geological Survey of India, 96, 42–52.

Bartsch A., Pathe, C., K. Scipal, K., and Wagner, W., (2008).Detection of permanent open water surfaces in central Siberia with ENVISAT ASAR wide swath data with special emphasis on the estimation of methane fluxes from tundra wetlands, Hydrology Research, 39(2), 89-100.

Bercher N, P. Kosuth and J. Bruniquel (2006). Quality of river water level time series issued from satellite radar altimetry: influence of river hydrology and satellite measurement accuracy and frequency. Presented at EGU General Assembly, Vienna, April 2006 Berry PAM, Garlick JD, Freeman JA, Mathers EL (cross ref in calmant et al, 2008).

Bercher N, P (2008). Précision de L'altimétrie Satellitaire Radar sur les cours d »eau: Dévzlopement d'une méthode standard de quantification de la qualité des produits alti-hydrologique et applications. Thesis.

Berry, P. A. M,, J. D. Garlick, J. A. Freeman, and E. L. Mathers (2005) Global inland water monitoring from multi-mission altimetry. Geophysical Research Letter, 32. L16401, doi:10.1029/2005GL022814

Bettadpur S (2007). GRACE Product Specification Document, Rev. 4.5. Technical Report GRACE 327-720 (CSR-GR-03-02), Center for Space Research, University of Texas at Austin. http://podaac.jpl.nasa.gov/grace/documentation.html.

Biggs, T.W., A. Gaur, C.A. Scott, P. Thenkabail, P. G. Rao, M. K. Gumma, S.Acharya and H. Turral. (2007).Closing of the Krishna Basin: Irrigation, Streamflow Depletion and Macroscale Hydrology. Research Report 111. International Water Management Institute. Sri Lanka.

Birkett, C. (1995). The contribution of topex/poseidon to the global monitoring of climatically sensitive lakes. Journal of Geophysical Research, 100 (C12).

Birkett C. and Mason, I. M. (1995). A new global lakes database for remote sensing programme studying climatically sensitive large lakes. Journal of Great Lakes Research. 21(3).

Birkett C. (1998). Contribution of the topex nasa radar altimeter to the global monitoring of large rivers and wetlands. Water Resources Research, 34.

Birkett C. (2000). Synergistic remote sensing of Lake Chad: variability of basin inundation. Remote Sensing Environnement, 72.

Birkett, C. M., (1994). Radar altimetry: A new concept in monitoring lake level changes, Eos Trans. AGU, 75, 274–276

Birkett, C.M. (1998). Contribution of the TOPEX NASA radar altimeter to the global monitoring of large rivers and wetlands. Water Resources Research, 34(5), 1223–1239.

Birkett C. M., Mertes, L. A. K., Dunne, T. and Costa, M. H. and Jasinski, M. J. (2002). Surface water dynamics in the Amazon basin : Application of satellite altimetry. Journal of Geophysical Research,107 (D20), 8059, doi :10.1029/2001JD000609

Biswas, A. K. and Uitto, J. I. (2001). Management of International Rivers. In Sustainable Development of the Ganges–Brahmaputra–Meghna Basins, eds. Asit K. Biswas and Juha I. Uitto. New York: United Nations University Press. (cross ref in Rahman, 2005).

Björsson, H and S.A. Venegas. (1997). A Manual for EOF and SVD analysis of Climate Data. C^2GCR report. 97-1.

Brenner A., H. Frey, J. DiMarzio and L. Tsaoussi. (1997). Topography over South America from ERS altimetry. Earth Resources and Remote Sensing. Proceedings of the 3rd ERS Symposium on Space at the Service of Our Environment, volume 1; Volume 1; 409-414; (ESA-SP-414-Vol-1).

Brown G.S. (1977). The average impulse response of a rough surface and is applications. IEEE Transactions: Antennas and Propagations, 25 (1): 67-74.

Bruinsma S., J-M. Lemoine, R. Biancale and N. Valès, (2010). CNES/GRGS 10-day gravity field models (release 2) and their evaluation. Advances in Space Research, 45: 587–601. doi:10.1016/j.asr.2009.10.012.

Callède, J., P. Kosuth, and E. De Oliveira, (2001). Establishment of the stage-discharge relationship of the River Amazon at Óbidos: “ormal difference in level” method using “variable geometry”. Hydrological Science Journal, 46(3): 451–463, doi:10.1080/02626660109492838.

Calmant, S. and F. Seyler, (2006). Continental Surface waters from satellite altimetry. Comptes Rendus Geosciences. 338(14-15): 1113-1122, doi: 10.1016/j.crte.2006 .08.002.

Calmant, S., F. Seyler, and J-F. Crétaux, (2008). Monitoring Continental Surface Waters by Satellite Altimetry. Survey in Geophysics. 29(4-5): 1573-0956. doi:10.1007/10712-008-9051-1

Cazenave, A., P. Bonnefond, and K. DoMinh. (1997). Caspian Sea level from Topex/Poseidon altimetry: level now falling. Geophysical Research Letters. 24: 881–884.

Cazenave, A., and J. Chen, (2010). Time-variable gravity from space and present-day mass redistribution in the Earth system. Earth and Planetary Sciences Letters. doi:10.1016/j.epsl.2010.07.035.

Central Ground Water Board of India (CGWB), (2011). Dynamic groundwater resources of India (as on 31 March, 2009), Central Ground Water Board of India, New Delhi.

Chahine M.T. (1992). The hydrological cycle and its influence on climate. Nature, 359: 373-380.

Chao, B.F. and W.P. O’Connor. (1988). Global surface-water-induced seasonal variation in the Earth’s rotation and gravitational field. Geophysical Journal, 94: 263-270

Chelton, D. B., E. J Walsh, and J. L. MacArthur. (1989). Pulse compression and sea level tracking in satellite altimetry. Journal of Atmospheric and Oceanic Technology. 6: 407-438.

Chelton, D., J. Ries, B. Haines, L.-L. Fu, and P. Callahan, (2001). Chapter 1: Satellite Altimetry in “Satellite altimetry and Earth sciences” (ed. by L.-L. Fu and A. Cazenave). International geophysics. 69: 1-131. Academic press.

Chen, J.L., C.R. Wilson and B.D. Tapley, (2006a). Satellite gravity measurements confirm accelerated melting of Greenland ice sheet. Science, 313. doi:10.1126/science.1129007.

Chen, J.L., C.R. Wilson, D.D. Blankenship and B.D. Tapley, (2006b). Antarctic mass rates from GRACE. Geophysical Research Letters. 33, L11502. doi:10.1029/2006GL026369.

Chowdhury, M. R., and N. Ward (2004). Hydro-meteorological variability in the greater Ganges-Brahmaputra-Meghna Basins. International Journal of Climatology. 24, 1495–1508, doi:10.1002/joc.1076.

Çizmeli, A and D.K.San (2008). Principle of remote sensing. METU GGIT. Online access, http://ocw.metu.edu.tr/course/view.php?id=36.

Coe, M. T., and C. M. Birkett (2004). Calculation of river discharge and prediction of lake height from satellite radar altimetry: Example for the Lake Chad Basin. Water Resources Research. 40, W10205, doi:10.1029/ 2003WR002543.

Committee on Global Change Research, National Research Council (1999). Global Environmental Change: Research Pathways for the Next Decade. National Academy Press, Washington, DC.

Crétaux J.F., A.V Kouraev., F. Papa, M. Bergé-Nguyen, A. Cazenave, N. Aladin, and I.S Plotnikov. (2005). Evolution of sea level of the big Aral Sea from satellite altimetry and its implications for water balance. Journal of Great Lakes Research. 31: 520-534.

Crétaux, J-F and C. Birkett (2006). Lake studies from satellite altimetry. Comptes Rendus Geosciences. doi:10.1016/J.cre.2006.08.002

Crétaux, J-F., M. Bergé-Nguyen, M. Leblanc, R. Abarca Del Rio, F. Delclaux, N. Mognard, C. Lion, R-K. Pandey, S. Tweed, S. Calmant, and P. Maisongrande. (2011a). Flood mapping inferred from remote sensing data. International Water Technology Journal. 1(1): 48-62

Crétaux, J-F. , W. Jelinski, S. Calmant, A. Kouraev, V. Vuglinski, M. Bergé Nguyen, M-C. Gennero, F. Nino, R. Abarca Del Rio , A. Cazenave and P. Maisongrande. (2011b). SOLS: A Lake database to monitor in Near Real Time water level and

storage variations from remote sensing data. Journal of Advanced Space Research. doi:10.1016/j.asr.2011.01.004

Crétaux J-F, S. Calmant, R. Abarca Del Rio, A. Kouraev, M. Bergé-Nguyen and P. Maisongrande, (2011c). Lakes studies from satellite altimetry. Chap. 19 in Coastal altimetry. 509-534. Springer.

CWC (Central Water Commission). (2010). Water and related statistics. New Delhi: Water Planning and Projects Wing, Central Water Commission.

CWC (Central Water commission) http://www.cwc.nic.in/main/webpages/statistics.html

Central Ground Water Board of India (CGWB) (2006), Dynamic groundwater resources of India (as on March, 2004), Cent. Ground Water Board of India, New Delhi.

Dai, A. and K. E. Trenberth, (2002). Estimates of freshwater discharge from continents: Latitudinal and seasonal variations. Journal of Hydrometeorology. 3: 660–687.

Dai, A., T. Qian, K. E. Trenberth, and J. D. Milliman, (2009). Changes in continental freshwater discharge from 1948 to 2004. Journal of Climate. 22(10): 2773–2792, doi:10.1175/2008JCLI2592.1.

Davis, F.W. and D.S. Simonett. GIS and Remote Sensing (Chapter 14). online access www.wiley.com/legacy/wileychi/gis/.../BB1v1_ch14.pdf

Campos De-Oliveira, I., Mercier, F., Maheu, C., Cochenneau, G., Kosuth, P., Blitzkow, D. and A. Cazenove. (2001). Temporal variations of river basin waters from topex/poseidon satellite altimetry application to the Amazon basin. Earth and Planetary Sciences, 333 (10): 633-643.

Deering, D.W. (1978). Rangeland reflectance characteristics measured by aircraft and spacecraft sensors. PhD Dissetation, Texax A&M University, College Station. TX, 338

Döll P., F. Kaspar and B. Lehner, (2003). A global hydrological model for deriving water availability indicators: model tuning and validation. Journal of Hydrology. 270, 105-134.

DR Helsel, Trend Analysis (Chapter 12). pubs.usgs.gov/twri/twri4a3/pdf/chapter12.pdf (online access).

Drapela, K., and I. Drapelova (2011). Application of Mann-Kendall test and the Sen's slope estimates for trend detection in deposition data from Bílý Kříž (Beskydy Mts.,the Czech Republic) 1997 – 2010. Beskdy Mendel University in Brno 4 (2): 133–146

Dunn, C., W. Bertiger, Y. Bar-Sever, S. Desai, B. Haines, D. Kuang, G. Franklin et al. (2003). Instrument of Grace: GPS Augments Gravity Measurements, GPS World, 14(2): 16-28.

Durand, F., D. Shankar, C. de Boyer Montégut, S. S. C. Shenoi, B. Blanke, and G. Madec. (2007). Modelling the barrier-layer formation in the south-eastern Arabian Sea. Journal of Climate. 20(10): 2109–2120, doi:10.1175/ JCLI4112.1.

Eicker, A., 2008. Gravity field refinement by radial basis functions from in-situ satellite data. Dissertation, Institut für Geodäsie und Geoinformation der Universität Bonn.

Fekete B., C.J. Vörösmarty, and W. Grabs. (1999). Global, Composite Runoff Fields Based on Observed River Discharge and Simulated Water Balance. Koblenz, Germany: WMO-GRDC.

Fekete, B. M., C. J. Vörösmarty, and W. Grabs (2000). Global composite runoff fields based on observed river discharge and simulated water balances: Documentation for UNH-GRDC Composite Runoff Fields. v.1.0, Rep. 22, Global Runoff Data Canter, Koblenz, Germany.

Fersch, B., H. Kunstmann, A. Bardossy, B. Devaraju and N Sneeuw, (2012). Continental scale basin water storage variation from global and dynamically downscaled atmospheric water budgets in comparison with GRACE-derived observations. American Meteorological Society. doi: 10.1175/JHM-D-11-0143.1

Frappart, F., K. Dominh, J. Lhermitte, G, Ramilllien, A., Cazenave, and T. LeToan, (2006a). Water volume change in the lower Mekong Basin from satellite altimetry and imagery data. Geophysical Journal International. 167: 570-584.

Frappart F., F. Seyler, J-M. Martinez, J. Leon J. and A. Cazenave (2005). Determination of the water volume in the Negro River sub basin by combination of satellite and in situ data. Remote Sensing of Environment, 99: 387- 399.

Frazier P., K. Pag, J. Louis, S. Briggs and A.I. Robertson. (2003). Relating wetland inundation to river flow using Landsat TM data. International Journal of Remote Sensing, 24(19): 3755-3770.

Fu, L.L., and A. Cazenave (2001). Satellite Altimetry and Earth Sciences: A Handbook of techniques and application. International Geophysical series. vol 69, Academic Press

Gole, C.V. and S.V. Chitale. (1966). Inland delta building activity of Kosi River. Journal of the Hydraulics Division, American Society of Civil Engineers, 92: 111-126.

Garg, NK, and Q. Hassan, (2007). Alarming scaricity of water in India. Current Science. 93(7): 932-941

Gupta, S. K. and R. D. Deshpande, (2004). Water for India in 2050: first-order assessment of available options. Current Science, 86(9): 1216-1224.

Guzkowska M.A.J., C.G. Rapley and I.M. Mason, (1986). Satellite altimeter measurements over land and inland water. Proceedings of IGARSS' 86 Symposiums, Zürich, 8-11 Sept. 1986, Ref. ESA SP-254:1563-1568.

Guzkowska, M.A.J., C.G. Rapley, J.K. Ridley, W. Cudlip, C.M. Birkett and Scott, R.F., 1990. Developments in Inland Water and Land Altimetry, ESA CR-7839/88/F/FL.

Güntner, A. (2008). Improvement of global hydrological models using GRACE data. Survey in Geophysics, 29(4-5): 375-397.

Gruber T., S.V. Bettadpur and M.M. Watkins (2000a). GRACE Science Data System Development Status, Eos Transactions, American Geophysical Union, 81 (48), Fall Meeting Supplement.

Gruber T., A. Bode, C. Reigber, P. Schwintzer, G. Balmin, R. Biancale and J.M. Lemoine. (2000b). GRIM5-C1: Combination Solution of the Global Gravity Field to Degree and Order 120, Geophysical Research Letters, 27: 4005-4008

GRDC: Global Runoff Data Centre. (1993). Federal Institute of Hydrology, Koblenz-Germany.

Hamilton, S. K., S.J. Sippel and J.M. Melack,(2002). Comparison of inundation patterns among major South American floodplains. Journal of Geophysical Research, 107(D20), 10.129–10.143.

Han, S.-C C.K. Shum, C. Jekeli, C.-Y. Kuo, C. Wilson, and K.-W. Seo, (2005). Non-isotropic filtering of GRACE temporal gravity for geophysical signal enhancement. Geophysical Journal International, 163:18–25. doi:10.1111/j.1365-246X.2005.02756.x.

Henry, J-B., P. Chastanet, K. Fellah and Y-L. Desnos, (2006). ENVISAT Multi-Polarised ASAR data for flood mapping. International Journal of Remote Sensing, 27 (10): 1921-1929.

Hess, L. L., J. M. Melack, S. Filoso, and Y. Wang. (1995). Delineation of inundated area and vegetation along the Amazon floodplain with SIR-C synthetic aperture radar. IEEE Transactions: Geoscience and Remote Sensing. 33: 896– 904.

Hess, L. L., J. M. Melack, E.M.L.M. Novo, C. C. F. Barbosa, and M. Gastil. (2003). Dual-season mapping of wetland inundation and vegetation for the central Amazon basin. Remote Sensing of Environment, 87(4): 404-428

Hsieh, W.W., (2009). Nonlinear Principle Component Analysis. Ch. 8 (eds. S.E. Haupt et al.) Artificial Intelligence Methods in the Environmental Sciences. Springer. Berlin.

Hunger, M. and P. Döll. (2008). Value of river discharge data for global-scale hydrological modelling. Hydrology and Earth System: Science Discussion. 4:4125-4173.

India-WRIS webGIS. Water resources information system of India. (http://www.india-wris.nrsc.gov.in/)

Jackson, T.J. and T.J. Schmugge, (1989). Passive microwave remote sensing system for soil moisture: Some supporting research. IEEE Transactions: Geosciences and Remote Sensing. 27: 225-35

Jackson, RD, and AR Heute, (1991). Interpreting vegetation indices. Preventive Veterinary Medicine. 11: 185-200.

Jain, S.K., P.K Agarwal, and VP, Singh (2007). Hydrology and Water resources of India. Water Science and Technology Library, vol. 57, ISBN: 978-1-4020-5180-7.

Jain, S. K., N. S. R. K. Reddy and U. C. Chaube (2009). Analysis of a large inter-basin water transfer system in India. Hydrological Sciences Journal. 50(1). doi:10.1623/hysj.50.1.125.56336

Jagannathan, P., (1968). Rainfall of India. Forecasting Manual Part-V. India Meteorological Department-Poona, India.

Jiang, Z., A.R. Huete, K. Didan, and T. Miura. (2008). Development of a two-band enhanced vegetation index without a blue band. Remote Sensing of Environment. 112: 3833–3845

Jolliffe, I. T. (2002). Principal component analysis Springer, 2nd Ed. New York.

Jordan, C.F. (1969). Derivation of leaf area index from quality of light on the forest floor. Ecology. 50: 663-666.

Justice, C.O., J.R.G. Townshend, E.F. Vermote, E. Masuoka, R.E. Wolfe, N. Saleousn, D.P. Roy and J.T. Moristte. (2002). An overview of MODIS Land data processing and product status. Remote Sensing of Environment. 83: 3-15.

Justice, C.O., E. Vermote, J.R.G. Townshend, R. Defries, D.P. Roy, D.K. Hall, and V.V. Salomonson, et al. (1998). The moderate resolution imaging spectroradiometer (MODIS): Land remote sensing for global change research. IEEE Transactions: Geosciences and Remote Sensing. 36(4): 1228–1249.

Kale, V.S. (1997). Flood studies in India: A brief review. Journal of the Geological Society of India. 49, 359-370.

Kale, V.S. (2008). Himalayan Catastrophe that Engulfed North Bihar. Journal Geological Society of India. 72: 713-719.

Klees, R., E.A. Zapreeva, H.C. Winsemiusand H.H.G. Savenije. (2007). The bias in GRACE estimates of continental water storage variations. Hydrology and Earth System Sciences. 11: 1227-1241.

Koblinsky, C. J., R.T. Clarke, A.C. Brenner, and H. Frey. (1993). Measurement of river level variations with satellite altimetry. Water Resources Research. 29: 1839-1848.

Kosuth, P., Blitzkov, D. and Cochonneau, G. (2006). Establishment of an altimetric reference network over the amazon basin using satellite radar altimetry (topex/poseidon). In Venice 2006 Symposium "15 years of progress in radar altimetry".

Kouraev, A. V., E. A. Zakharova, O. Samain, N. M. Mognard, and A. Cazennave (2004). Ob' river discharge from TOPEX-Poseidon satellite altimetry (1992–2002), Remote Sensing of Environment, 93: 238–245, doi:10.1016/j.rse.2004.07.007.

Kouraev A.V., J-F Crétaux, S.A. Lebedev, A.G. Kostianoy, A.I. Ginzburg, N.A. Sheremet, R. Mamedov, E.A. Zhakharova, L. Roblou, F. Lyard, S. Calmant, M. Bergé-Nguyen. (2011). The Caspian Sea, Handbook on Coastal altimetry, chap. 13: 331-366, Springer.

Kuoa, C-Y. and H-C. Kaoa (2011), Retracked Jason-2 Altimetry over Small Water Bodies: Case Study of Bajhang River, Taiwan. Marine Geodesy, 34: 382-392, doi: 10.1080/01490419.2011.584830.

Kumar, Rakesh, R.D. Singh and K.D. Sharma, (2005). Water Resources of India. Current Science, 89(5): 794-811.

Krinner G., N. Viovy, N. De Noblet-Ducoudré, J. Ogée, J. Polcher, P. Friedlingstein, P. Ciais, S. Sitch and C., Prentice. (2005). A dynamic global vegetation model for studies of the coupled atmosphere-biosphere system. Global Change Biology. 19, GB1015, doi: 10.1029/2003GB002199.

Lal, M., (2001), Climate change – Implications for India's water resources. Journal of Indian Water Resources Society. 21: 101–119.

Laxon S. (1994). Sea ice altimeter processing scheme at the EODC. International Journal of Remote Sensing, 15 (4): 915-924.

Le Traon, P.Y., P. Gaspar, F. Bouyssel, and H. Makhmara (1995). Using Topex/Poseidon data to enhance ERS-1 data. Journal of Atmospheric and Oceanic Technology. 12: 161-170.

Lemoine, F.G., S.C. Kenyon, J.K. Factor, R.G. Trimmer, N.K. Pavlis, D.S. Chinn, C.M. Cox et al. (1998). The Development of the Joint NASA GSFC and the National Imagery and Mapping Agency (NIMA) Geopotential Model EGM96. NASA Technical Paper NASA/TP-1998-206861, Goddard Space Flight Center, Greenbelt.

Lemoine, J.M., S Bruinsma, S. Loyer, R. Biancale, J.C. Marty, F. Perosanz, and G. Balmino (2007). Temporal gravity field models inferred from GRACE data. Advanced Space Research. 39(10): 1620–1629.

Leblanc, M., Lemoalle, J., Bader, J-C., Tweed, S., and Mofor, L. (2011), 15 years of inundation patterns for Lake Chad: new observations during a drought period from satellite thermal data. Journal of Hydrology, 404: 87-92.

Legrésy B., and F. Rémy. (1997). Surface characteristics of the Antarctic ice sheet and altimetric observations. Journal of Glaciology. 43(144): 265-275.

Lillesand, T. M., R. W. Kiefer and J. Chipman, (2007). Remote sensing and image interpretation. ISBN: 978-0-470-05245-7

Lu, D., and Q. Weng. (2007). A survey of image classification methods and techniques for improving classification performance. International Journal of Remote Sensing. 28(5): 823–870

Lanfear, K. J. and R. M. Hirsch, (1999). USGS study reveals a decline in long-record stream gauges. AGU Eos Transactions 80: 605–607.

Legrésy, B., F. Papa, F. Remy, G. Vinay, G., M. Van Den Bosch and O-Z. Zanife, (2005). Envisat radar altimeter measurements over continental surfaces and ice caps using the ICE-2 retracking algorithm. Remote Sensing of Environment. 95: 150-163.

Lee, H., C.K. Shum, Tseng, J-Y. Guo, and C-Y Kuo (2011). Present-Day Lake level Variation from Envisat Altimetry over the North-eastern Qinghai-Tibetan Plateau:

Links with precipitation and temperature. Terrestrial Atmospheric and Oceanic Sciences. 22(2): 169-175, doi 0.3319/TAO.2010.08.09.01(TibXS)

Leon, J. G., S. Calmant, F. Seyler, M. P. Bonnet, M. Cauhopé, and F. Frappart (2006). Rating curves and average water depth at the upper Negro River from satellite altimetry and modelled discharges. Journal of Hydrology. 328(3–4): 481–496, doi:10.1016/j.jhydrol.2005.12.006.

Liu, X. (2008). Global gravity field recovery from satellite-to-satellite track data with the acceleration approach. PhD thesis, Delft, University of Technology, Optima,Graphical Communication, the Netherlands.

Maheu, C. and A. Cazenave (2003). Water level fluctuations in the Plata basin (South America) from Topex/Poseidon satellite altimetry. Geophysical Research Letters, 30(3).

Mason IM, CG Rapley, FA Street-Perrott and M. Guzkowska (1985) ERS-1 observations of lakes for climate research. Proceedings of the EARSeL/ESA symposium on European remote sensing opportunities Strasbourg, 31 March-3 April 1985.

Mavromatis T. and D. Stathis (2011). Response of the water balance in Greece to temperature and precipitation trends. Theoretical and Applied Climatology, 104:13-24. doi:10.1007/s00704-010-0320-9

Mercier, F. (2001). Altimétrie spatiale sur les eaux continentales : apport des missions TOPEX/POSEIDON et ERS1&2 à l'étude des lacs, mers intérieures et bassins fluviaux. Thèse de doctorat, Université Toulouse III - Paul Sabatier.

Mercier, F. and O.Z. Zanife. (2006). Improvement of the topex/poseidon altimetric data processing for hydrological purposes (cash project). In Venice 2006 Symposium "15 years of progress in radar altimetry".

Mertes, L.A.K. (2002). Remote sensing of riverine landscapes. Freshwater Biology. 47: 799-816.

Mertes, L. A. K., D.L. Daniel, J.M. Melack, B. Nelson, L.A. Martinelli, and B.R. Forsberg, (1995). Spatial patterns of Hydrology, geomorphology, and vegetation

on the floodplain of the Amazon River in Brazil from remote sensing perspective. Geomorphology, *13*, 215– 232.

Milly P. C. D. and A. B. Shmakin, (2002). Global modelling of land water and energy balances. Part-1: The Land Dynamics (LaD) model, Journal of Hydrometeorology. 3: 283-299.

Misra, A.K. (2011). Impact of urbanization on the hydrology of Ganga Basin (India). Water Resources Management, 25: 705-719, doi: 10.1007/s11269-010-9722-9.

Mirza, M. M. (2003). The Choice of Stage-Discharge Relationship for the Ganges and Brahmaputra Rivers in Bangladesh, Nordic Hydrology, 34(4): 321–342, doi:10.2166/nh.2003.019

MOEF: Ministry of Environment and Forest–India (2009). Status Paper on river Ganga

Morris, S. M. and S.K. Gill, (1994a). Evaluation of the topex/poseidon altimeter system over the great lakes. Journal of Geophysical Research, 99 (C12), 24: 527–539.

Morris, S. M. and Gill, S. K. (1994b). Variation of great lakes water levels derived from Geosat altimetry. Water Resources Research, 30(4): 1009–1017.

Motiee, H. and E. McBean (2009). An assessment of long-term trends in hydrologic components and implications for water levels in Lake Superior. Hydrology Research, 40(6): 564-579, doi:10.2166/nh.2009.061

MOWR, (1999). Integrated water resource development – a plan for action. Report of the National Commission for Integrated Water Resources Development Plan, Ministry of Water Resources, Govt. of India.

MRT Manual (2002). MODIS Reprojection Tool User's Manual, release 3.0, Department of Mathematics and Computer Science USGS EROS data Center. South Dakota School of Mines and Technology.

Pandey, R.K., J.F. Crétaux, M. Berge-Nguyen, V.M. Tiwari, V. Drolon, F. Papa, and S Calmant. (2013). Water Level Estimation by Remote Sensing for 2008 Flood of Kosi River. International Journal of Remote Sensing.

Papa, F., C. Prigent, F. Durand, and W.B. Rossow. (2006). Wetland dynamics using a suite of satellite observations: A case study of application and evaluation for the

Indian Subcontinent. Geophysical Research Letters, 33. L08401. doi: 10.1029/2006GL025767.

Papa, F., F. Durand, W. B. Rossow, A. Rahman, and S. K. Bala, (2010a). Satellite altimeter□derived monthly discharge of the Ganga-Brahmaputra River and its seasonal to interannual variations from 1993 to 2008, Journal of Geophysical Research. 115, C12013, doi:10.1029/2009JC006075

Papa, F., S. K. Bala, R. K. Pandey, F. Durand, V. V. Gopalakrishna, A. Rahman, and W. B. Rossow (2012). Ganga-Brahmaputra river discharge from Jason-2 radar altimetry: An update to the long-term satellite-derived estimates of continental freshwater forcing flux into the Bay of Bengal. Journal of Geophysical Research. 117, C11021. doi:10.1029/2012JC008158

Pavlis, N. K., S. A. Holmes, S. C. Kenyon, and J. K. Factor (2012). The development and evaluation of the Earth Gravitational Model 2008 (EGM2008), Journal of Geophysical Research. 117 (B04406), doi:10.1029/2011JB008916.

Peng, D.Z., L. Xiong, S. Guo, and N. Shu (2005). Study of Dongting Lake area variation and its influence on water level using MODIS data. Hydrological Sciences, 50(1): 31-44.

Preisendorfer , R.W. and C.D. Mobley. (1988). Principal component analysis in meteorology and oceanography. Elsevier.

Prigent, C., Matthews, E., Aires, F., and Rossow, W.B. (2001), Remote sensing of global wetland dynamics with multiple satellite datasets. Geophysical Research Letters, 28: 4631-4634.

Rahaman, M.M., (2005a). Integrated water resources management in the Ganges Basin: Constraints and opportunities. (Thesis) Helsinki University of Technology, Laboratory Water Resources-Finland.

Rahaman, M.M., (2006). The Ganges water conflict: A comparative analysis of 1977 Agreement and 1996 Treaty. Asteriskos -Journal of International & Peace Studies, 1/2: 195–208.

Rapley, C., M. Guzkowska, W. Cudlip and I. Mason, (1987). A exploratory study of inland water and land altimetry using Seasat data. ESA Contract Report 6483/85/NL/BI.

Rao, Y.P., (1976). Southwest monsoon, Meterological Monograph Synoptic Meterology No. 1/1976, IMD – New Delhi.

Ramillien, G., F. Frappart, A.Cazenave and A. Güntner (2005). Time variations of land water storage from an inversion of 2years of GRACE geoids. Earth and Planetary Science Letters. 235: 283-301

Ramillien, G., F. Frappart, A. Güntner, T. Ngo-Duc, A. Cazenave and K. Laval (2006). Time variations of the regional evapotranspiration rate from Gravity Recovery And Climate Experiment GRACE satellite gravimetry. Water Resources Research. 42, W10403.

Ramillien, G., A. Cazenave, and O. Brunau (2004), Global time variations of hydrological signals from GRACE satellite gravimetry. Geophysical. Journal International, 158(3) : 813–826, doi:10.1111/j.1365-246X.2004.02328.x.

Rantz, S. E. and others, (1982), Measurement and computation of streamflow: Volume 2. Computation of discharge. USGS Water Supply Paper-2175, 285–631.

Rapley, C. G., (1990). Satellite radar altimeters in Microwave Remote Sensing for Oceanographic and Marine Weather-Forecast Models, (ed. by R. A. Vaughan), pp. 45– 63, Kluwer Acad., Norwell, Mass.

Report: Bihar Kosi Flood Recovery Project, June (2010). www.ssvk.org/koshi/bihar_kosi_kflood_recovery_project_2010.pdf.

Report NIH (1998-99), Hydrological inventory of river basins in Eastern Uttar Pradesh. National Institute of Hydrology, Jal Vigyan Bhavan Roorkee.

Rees, W. G. (2001). Physical principle of remote sensing, Cambridge university press, UK. ISBN 0-521-66948-0 (pb).

Richey, J. E., C. Nobre, and C. Deser. (1989). Amazon River discharge and climate variability: 1903 to 1985. Science, 246: 101– 102.

Ridley J.K. and KC. Partington (1988). A model of satellite radar altimeter return from ice sheets. International Journal of Remote Sensing, 9(4): 601-624.

Rodell M. and Famiglietti J.S. (1999). Detectability of variations in continental water storage from satellite observations of the time dependent gravity field, Water Resources Research. 35 (9): 2705-2723.

Rodell, M., J. S. Famiglietti, J. Chen, S. I. Seneviratne, P. Viterbo, S. Holl, et al. (2004). Basin scale estimates of evapotranspiration using GRACE and other observations. Geophysical Research Letters. 31, L20504.

Rodell, M., I. Velicogna, and J. S. Famiglietti, (2009). Satellite-based estimates of groundwater depletion in India. Nature. 462: 999–1002.

Rodda, G. C., S. A. Pieyns, N. S. Sehmi, and G. Matthews (1993). Towards a world hydrological cycle observing system, Hydrol. Sci., 38, 373–378

Roux E, M. Cauhope, M-P. Bonnet, S. Calmant and F. Seyler, (2008). Daily water stage estimated from satellite altimetric data for large river basin monitoring. Hydrological Sciences Journal, 53(1): 81–99.

Rowlands, D.D., R.D. Ray, D.S. Chinn and F.G. Lemoine. (2002). Short-arc analysis of inter-satellite tracking data in a gravity mapping mission. Journal of Geodesy, 76: 307–316, doi:10.1007/s00190-002-0255-8.

Saatchi, S. S., B. Nelson, E. Podest, and J. Holt. (2000). Mapping Land-cover types in the Amazon Basin using 1 km JERS-1 mosaic. International Journal of Remote Sensing, 21(6-7):1201–1234.

Santos da Silva, J., S. Calmant, F. Seyler, O.C.R. Filho, G. Cochonneau,and W.J. Mansur, (2010). Water levels in the Amazon basin derived from the ERS 2 and ENVISAT radar altimetry missions. Remote Sensing of Environment, 114: 2160–2181, doi:10.1016/j.rse.2010.04.020

Sarma, A A L N, T V Lakshmi Kumar and K Koteswara Rao (2010). Extreme value analysis of summer monsoon rainfall over Andhra Pradesh. Indian Journal of Radio and Space Physics, 39: 32-38

Schmidt R., F. Flechtner, C. Reigber, P. Schwintzer, A. Güntner, P. Döll, G. Ramillien A.Cazenave, S. Petrovic, H. Jochman and J. Wunsch, (2006). GRACE

observations of changes in continental water storage. Global and Planetary Change. 50 (1-2): 112-126

Schmidt R, F. Flechtner, U. Meyer, K-H. Neumayer, C. Dahle, R. König and J. Kusche (2008). Hydrological signals observed by the GRACE satellites. Surveys in Geophysics, 29: 319–334.

Schmugge, T.J. and T.J. Jackson (1994). Mapping surface soil moisture with microwave radiometers. Meteorology and Atmospheric Physics, 54: 213-223.

Schmugge, T.J. W.P Kustas, J.C. Ritchie, T.J. Jackson and A. Rango (2002). Remote sensing in hydrology. Advances in Water Resources. 25:1367-1385.

Sengupta, D., G. N. Bharath Raj, and S. S. C. Shenoi (2006), Surface freshwater from Bay of Bengal runoff and Indonesian Throughflow in the tropical Indian Ocean. Geophysical Research Letters, 33, L22609, doi:10.1029/2006GL027573.

Seyler, F., M-P Bonnet, S. Calmant et al. (2006). Online altimetry service for hydrology: The Cash Project. ESA conference: 15 Years of Progress in Radar Altimetry, Venis-Italy.

Shah, T., U.A. Amarasinghe, P.G. McCornick (2008). India's River Linking Project: The state of the debate. IWMI-CPWF Project on Strategic Analyses of India's National River-Linking Project. International Water Management Institute, Colombo, Sri Lanka.

Sakamoto T., N.V. Nguyen, A. Kotera, H. Ohno, N. Ishitsuka, and M. Yokozawa, (2007). Detecting temporal changes in the extent of annual flooding within the Cambodia and the Vietnamese Mekong Delta from MODIS time series imagery, Remote Sensing of Environment, 109(3), 295-313, doi:10.1016/j.rse.2007.01.011.

Shiklomanov, A. I., R.B. Lammers and C.J. Vörösmarty (2002). Widespread decline of hydrological monitoring threatens Pan-arctic research, Eos Trans. AGU, 83(2): 13-16.

Singh, S.K., A.K. Pandey and M.S. Nathawa. (2011). Rainfall variability and spatio temporal dynamics of flood inundation during the 2008 Kosi Flood in Bihar State, India. Asian Journal of Earth Sciences 4(1): 9-19.

Sinha, R., G.V. Bapalu, L.K. Singh, and B. Rath, (2008). Flood risk analysis in the Kosi river basin, north Bihar using multiparametric approach of Analytical Hierarchy Process (AHP), J. Indian Soc. Remote Sens. 36, 293–307.

Sinha, R. (2009). The Great avulsion of kosi on 18August 2008. Current Science. 97: 429-433.

Sinha, R. and P.F. Friend. (1994). River systems and their sediment flux, Indo-Gangetic plains, Northern Bihar, India. Sedimentology. 41: 825-45.

Siqueira, P., Chapman, B., & McGarragh, G. (2003). The co-registration, calibration, and interpretation of multisession JERS-1 SAR data over South America. Remote Sensing of Environment, 87: 389–403.

Smith, L. C. (1997). Satellite remote sensing of river inundation area, stage, and discharge: A review. Hydrological Processes, 11(10):1427–1439.

Swenson, S. C., and J. Wahr (2006). Post-processing removal of correlated errors in GRACE data, Geophysical Research Letters, 33, L08402, doi:10.1029/ 2005GL025285.

Swenson, S. C. and J. Wahr. (2002). Methods for inferring regional surface-mass anomalies from Gravity Recovery and Climate Experiment (GRACE) measurements of timevariable gravity. Journal of Geophysical Research, 107(B9), 2193.

Swenson, S., J. Wahr, and P. C. D. Milly (2003). Estimated accuracies of regional water storage variations inferred from the Gravity Recovery and Climate Experiment (GRACE). Water Resources Research, 39(8), 1223, doi:10.1029/2002WR001808.

Tapley B.D., G.H. Born and M.E. Parke (1982). The Seasat altimeter data and its accuracy assessment, Journal of Geophysical Research, 87: 3179-3188.

Tapley B.D., Bettadpur S., Watkins M., Reigber C. (2004a). The Gravity Recovery and Climate Experiment : Mission overview and early results. Geophysical Research Letters, 31, L09607, doi:10.1029/2004GL019920.

Tapley B.D., S. Bettadpur, J.C. Ries, P.F. Thompson and M. Watkins, (2004b). GRACE measurements of mass variability in the Earth system. Science, 305: 503-505.

Tapley, BD., and C. Reigber. (2003). GRACE: Gravity Recovery And Climate Experiment, An Earth System Science Pathfinder (ESSP) Mission. http://www.csr.utexas.edu/grace/publications/presentations/HPC2001.html). Online access on May, 2013,

Tapley, B. D., S. Bettadpur, J.C. Ries, P.E. Thompson, and M.M. Watkins, (2004).GRACE measurements of mass variability in the earth system. Science, 305: 503-505.

Tiwari, V. M., J. M. Wahr,. and S. Swenson, (2009). Dwindling groundwater resources in northern India, from satellite gravity observations. Geophysical Research Letters, 36, L18401 , doi: 10.1029/2009GL039401

Tiwari, V. M., J. M. Wahr, S. Swenson and B. Singh. (2011). Land Water Storage Variation over Southern India from Space Gravimetry. Current Science, 101: 536-540.

Touboul P.E., E. Willemenot, B. Foulon and V. Josselin. (1999). Accelerometers for CHAMP, GRACE and GOCE space missions: synergy and evolution, Bollettino di Geofisica Teorica e Applicata, 40(3-4): 321-327.

Touboul, P., (2001). Space Accelerometer: Present Status. (eds. C. Lammerzahl, C.W.F. Francis, and F.W. Hehl) LNP 562: 273–291, Springer-Verlag Berlin Heidelberg

Toshihiro, S., N V. Nguyen, A. Kotera, H Ohno, N Ishitsuku and M Yokozawa (2007). Detecting temporal changes in the extent of annual flooding within the Cambodia and the Vietnamese Mekong Delta from MODIS time series imagery. Remote Sensing of Environment. 109(3): 295-313.

Töyrä, J., A. Pietroniro, and L.W. Martz (2001). Multisensor Hydrologic Assessment of a Freshwater Wetland, Remote Sensing of Environment, 75(2), 162-173.

Töyrä, J., and A. Pietroniro (2005). Towards operational monitoring of a northern wetland using geomatics-based techniques, Remote Sensing of Environment, 97, 174-191.

Trenberth, K. E, L. Smith, T. Qian, A. Dai, and J. Fasullo, (2007). Estimates of the global water budget and its annual cycle using observational and model data. Journal of Hydrometeorology, 8: 758–769.

Trend Analysis - ETH (2013). Analysis *of Climate and Weather Data.* www.iac.ethz.ch/edu/courses/master/electives/acwd/Trend.pdf

Tucker, C.J. (1979). Red and photographic infrared linear combinations for monitoring vegetation. Remote Sensing Environment. 8:127-150.

Velicogna, I., and J. Wahr (2006). Measurements of time-variable gravity show mass loss in Antarctica. Science, 311: 1754-1756.

Venot, J.P., B.R. Sharma and K.V.G.K. Rao, (2008). The lower Krishna basin trajectory: relationships between basin development and downstream environmental degradation. International Water Management Institute, Colombo, Sri Lanka. RR 125.

Vermote, E.F., N.Z. ElSaleous, C.O. Justice, Y. J. Kaufman, J. L. Privette, L. Remer, J.C. Roger., and D. Tanre, (1997). Atmospheric correction of visible to middle-infrared EOS-MODIS data over land surfaces: background, operational algorithm and validation. Journal of Geophysical Research, 102, D14, 17131-17141. doi:10.1029/97JD00201

Vermote, E. F. and A. Vermeulen. (1999).Atmospheric correction algorithm: Spectral reflectances (MOD09). Algorithm Technical Background Document, ver. 4.0. NASA contract NAS5-96062

Vermote, E.F, S.Y. Kotchenova and J.P. Ray. (2011). MODIS Surface Reflectance User's Guide.

Verant S., K. Laval, J. Polcher and M. Castro, (2004). Sensitivity of the continental hydrological cycle to spatial resolution over the Iberian Peninsula, Journal of Hydrometeorology, 5(2): 267-285.

Vinayachandran, P. N., and J. Kurian (2007), Hydrographic observations and model simulation of the Bay of Bengal freshwater plume. Deep Sea Research, Part I, 54: 471–486, doi:10.1016/j.dsr.2007.01.007.

Vörösmarty C.J., C.J. Willmott, B.J. Choudhury, A.L. Schloss, T.K. Stearns, S.M. Robeson and T.J. Dorman, (1996). Analyzing the discharge regime of a large tropical river through remote sensing, ground-based climatic data, and modelling, Water Resources Research, 32, 3137-3150.

Vörösmarty, C., A. Askew, W. Grabs, R. G. Barry, C. Birkett, P. Döll, B. Goodison, A. Hall, R. Jenne, L. Kitaev, J. Landwehr, M. Keeler, G. Leavesley, J. Schaake, K. Strzepek, S. S. Sundarvel, K. Takeuchi and F. Webster (2001). Global water data: A newly endangered species. Eos Trans. AGU, 82(5), doi:10.1029/01EO00031.

Wahr J. And M. Molenaar (1998). Time variability of the Earth's gravity field: Hydrological and oceanic effects and their possible detection using GRACE. Journal of Geophysical Research, 103 (B12), 30: 205-229.

Wehr T. and Attema E. (2001). Geophysical validation of ENVISAT data products. Advances in Space Research, 28(1): 83-91.

Wahr J. (1985). Deformation of the Earth induced by polar motion. Journal of. Geophysical Research. 90(B11), 9363-9368.

Wahr, J., S.C. Swenson, V. Zlotnicki, and I. Velicogna (2004). Time-variable gravity from GRACE: first results. Geophysical Research Letters, 31, L11501.

Wahr, J., S.C. Swenson, and I. Velicogna. (2006). Accuracy of GRACE mass estimates. Geophysical Research Letters, 33, L06401.

Wang Y., L.L.Hess, S. Filoso and J.M. Melack, (1995). Understanding the radar backscattering from flooded and non-flooded Amazonian forests: Results from canopy backscatter modelling, Remote Sensing of Environment, 54: 324-332.

Wells, N. A. and J. A. Dorr (1987), Shifting of the Kosi River, northern India. Geology, 15: 204-207.

Weare, B. C., and J. S. Nasstrom, (1982). Examples of extended empirical orthogonal function analysis. Monthly Weather Review, 110: 481-485.

Werth, S., A. G¨untner, S. Petrovic, and R. Schmidt, (2009). Integration of GRACE mass variations into a global hydrological model. Earth and Planetary Science Letters, 277(1-2): 166-173.

Wingham D.J., C.G Rapley. and H. Griffiths, (1986). New techniques in satellite altimeter tracking systems, Proceedings of IGARSS'86 Symposium, Zürich, 8-11 Sept. 1986, Ref. ESA SP-254, 1339-1344.

Winsemius, H.C., (2009). Satellite data as complementary information for hydrological modeling. (PhD thesis), Water Resources Section, Faculty of Civil Engineering andGeosciences, Delft University of Technology. Netherlands.

Witter, D. L. and D. B. Chelton (1991), A Geosat altimeter wind speed algorithm and a method for altimeter wind speed algorithm development. Journal of Geophysical Research, 96(C5), 8853-8860.

World Climate Research Programme, Scientific plan for the GEWEX Continental Scale International Project (GCIP. (1992). WCRP-67 WMO/TD 461.

World Meteorological Organization/United Nations Educational, Scientific, and Cultural Organization, (WMO/UNESCO), (1991). Report on Water Resources Assessment, Progress in the Implementation of the Mar del Plata Action Plan and a Strategy for the 1990s, UN Water Conference, Argentina, U. N. Educ., Sci., and Cult. Org., Paris.

Xiao, X., B. Moore, X. Qin, Z. Shen, and S. Boles. (2002). Large-scale observations of alpine snow and ice cover in Asia: Using multi-temporal VEGETATION sensor data. International Journal of Remote Sensing. 22(11): 2213-2228.

Xiao XM, Q. Zhang, B. Braswell, et al. (2004). Modeling gross primary production of temperate deciduous broadleaf forest using satellite images and climate data. Remote Sensing of Environment, 91: 256–270.

Xie, Y., Z. Sha and M. Yu (2008). Remote sensing imagery in vegetation mapping: a review. Journal of Plant Ecology, 1(1): 9–23.

Yue, S.and C. Wan (2004). The Mann-Kendall Test Modified by Effective Sample Size to Detect Trend in Serially Correlated Hydrological Series. Water Resources Management. 18: 201–218.

Zeng, N., J.-H. Yoon, J.A. Marengo, A. Subramaniam, C.A. Nobre, A. Mariotti, and J. D. Neelin, (2008). Causes and impacts of the 2005 Amazon drought. Environmental Research Letters, 3, 014002, doi:10.1088/1748-9326/3/1/014002.

Zakharova, E. A., A. V. Kouraev, A. Cazenave, and F. Seyler, (2006). Amazon River discharge estimated from TOPEX/Poseidon altimetry. Comptes. Rendus Geoscience, 338: 188–196.

Zaprowski, B.J. (2005). Climatic influences on profile concavity and river incision. Journal of Geophysical Research. 110, F03004. doi:10.1029/2004JF000138.

Zhan, X, R.A. Sohlberg, JRG Townshend, C DiMiceli, ML Carroll and JC Eastman, (2002). Detection of land cover change usinf MODIS 250m data. Remote Sensing of Environment. 83: 336-350.

Zhang G., H. Xie, S. Duan, M. Tian, and D. Yi (2011), Water level variation of Lake Qinghaifrom satellite and in situ measurements under climate change. Journal of. Applied Remote Sensing. 5(1), doi:10.1117/1.3601363

Résume (en Anglais)

Remote sensing is considered as an important tool to study continental hydrology. Remote sensing observations are used for estimating water level variations in rivers, lakes and flood plains, for mapping of inundation and wetlands and monitoring the spatio-temporal variation of water masses on regional (i.e. at basins scale) to global scale. The objective of this thesis is to analyze observations from various types of satellite missions: radar altimetry, satellite imagery and satellite gravimetry. Satellite Altimetry is used for water stage estimation over inland water bodies. The derived water stage can be used for river discharge estimation, and deriving the river slopes. Altimetry observation combined with satellite imagery is used for determination of surface water volume in flooded zones.

In this thesis, altimetry observations are used to derive the water stages in major Indian rivers. Discharge of Ganga and Brahmaputra rivers into Bay of Bengal is also derived. Satellite imagery is used to analyze the flooding in Ganga basin. Altimetry derived result and MODIS imagery are used together in North Bihar in Ganga basin to study the flood dynamics of Kosi. GRACE observations are also used to study the variation of total water storage in the Ganga river basin.

Key Words: Remote sensing, Satellite altimetry, Satellite imagery, Gravimetry, Continental hydrology, Indian River basins

Résumé (en Français)

La télédétection est considérée comme un outil important pour étudier l'hydrologie continentale. Elle est utilisée pour estimer les variations de niveau d'eau dans les rivières, les lacs et les plaines inondables, aussi que pour la cartographie des inondations et des zones humides et le suivi de la variation spatio-temporelle des masses d'eau à l'échelle mondiale. L'objectif de cette thèse est d'analyser l'observation de différents types de missions satellitaires: l'altimétrie radar, l'imagerie et la gravimétrie. L'altimétrie satellitaire est couramment utilisée pour l'estimation des niveaux d'eau des lacs, des rivières, et des zones inondées. L'altimétrie, combinée à des données in situ permet de calculer les débits des rivières, et combinées à de l'imagerie permet de déterminer des variations de volume d'eau dans les zones inondées ou les lacs.

Dans cette thèse, l'altimétrie a été utilisée sur les grands fleuves indiens, et a en particulier permis de calculer les débits dans le delta du Gange et du Brahmapoutre dans la baie du Bengale. Par ailleurs nous avons analysé la dynamique des inondations dans le bassin du Gange et plus précisément dans le nord de l'état de Bihār le long de la rivière Kosi (affluent du Gange) en utilisant des données d'imagerie et d'altimétrie combinées. Enfin les observations de la mission gravimétrique GRACE ont également été utilisées pour étudier la variation de stock d'eau dans les bassins du Gange.

Mots Clés: Remote sensing, Satellite altimetry, Satellite imagery, Gravimetry, Continental hydrology, Indian River basin.